

Investigations of Global Chemistry-Climate Interactions and Organic Aerosol Using Atmospheric Modeling

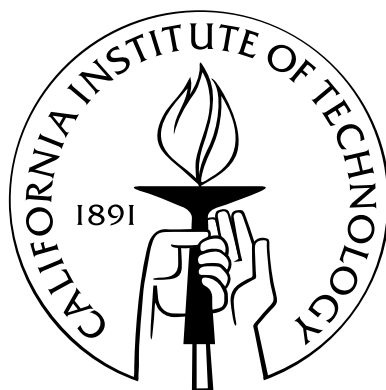
Thesis by

Havala Olson Taylor Pye

In Partial Fulfillment of the Requirements

for the Degree of

Doctor of Philosophy



California Institute of Technology

Pasadena, California

2011

(Defended August 13, 2010)

© 2011

Havala Olson Taylor Pye

All Rights Reserved

To Nick

Acknowledgements

A number of people have helped me throughout my journey at Caltech and have enabled me to accomplish the work contained in this thesis. I would like to start by thanking my advisor, Dr. John Seinfeld, whose professionalism, support, trust, and expertise has been invaluable. I also owe a lot of thanks to the GEOS-Chem user community and support team especially Bob Yantosca, Claire Carouge, and Philippe Le Sager and my collaborators Loretta Mickely, Shiliang Wu, and Daniel Jacob for their help with science questions and coding practice.

Many of the people I have worked with are not only excellent scientists but great friends as well. I would like to thank my first-year chemical engineering colleagues for all their help with classes and studying. My fellow Seinfeld first-years, Arthur Chan, Andrew Metcalf, and Puneet Chhabra, have been great for discussing science, hanging out at a holiday party, and even going camping. Daven Henze, Hong Liao, and Fabien Paulot have been invaluable resources when it comes to questions about GEOS-Chem, aerosols, and chemistry. The current modelers, Jean Chen, Joey Ensberg, Zach Lebo, and Andi Zuend, as well as the current and former roof labbers, Beth Kautzman, Alan Kwan, Christine Loza, Shane Murphy, Sally Ng, Jason Surratt, and Lindsay Yee, have been a pleasure to get to know and work with. I would also like to thank ManNin Chan, Anne Chen, Jill Craven, Tristan Day, Andy Downard, Nathan Eddingsaas, Amir Hakami, Jason Gamba, Mandy Grantz, Scott Hersey, Jesse Kroll, Xerxes Lopez-Yglesias, Philip Stier, Dr. Paul Wennberg, Dr. Yuk Yung, and Dr. Richard Flagan for the casual conversations, scientific feedback, and general company.

The support of the chemical engineering staff, especially Suresh Gupta, Kathy Bubash, and Yvette Grant, has been instrumental in making the day-to-day experience of graduate school easier. Suresh has ordered countless hard-drives and set up numerous back-up systems to make sure I could

get my work done. Kathy has been helpful with logistics since before I started at Caltech, and Yvette has been a general go-to for things ranging from travel reservations to file folders.

I would also like to thank my friends and family. My graduate school experience has been made richer by the friends I have met here, including Kathleen Spencer, Diana Smirnova, Mary Louie, and Yvonne Chen who have inspired me and kept me company. My first Southern California friends were at Eaton Canyon and I will always remember my time spent at the canyon. In addition, thanks must go to my Mom, Wade, Poppa, Granbev, Christine, Rob, Sally, and Nick for their support and encouragement.

I did not get to Caltech without having some great teachers throughout my life. I would like to thank Mrs. Mayfield, Mr. Goldstein, Mrs. Doker, Mrs. Stephens, Ms. Coulter, and Mr. Fannin for encouraging me in math and science. I would also like to thank Dr. Pedro Arce, Dr. C.-Y. Wu, and Dr. Jean Andino for the opportunities they have provided to me.

To everyone who has helped me in the past five years and throughout my education, thank you.

Abstract

Aerosol, or particulate matter (PM), is an important component of the atmosphere responsible for negative health impacts, environmental degradation, reductions in visibility, and climate change. In this work, the global chemical transport model, GEOS-Chem, is used as a tool to examine chemistry-climate interactions and organic aerosols.

GEOS-Chem is used to simulate present-day (year 2000) and future (year 2050) sulfate, nitrate, and ammonium aerosols and investigate the potential effects of changes in climate and emissions on global budgets and U.S. air quality. Changes in a number of meteorological parameters, such as temperature and precipitation, are potentially important for aerosols and could lead to increases or decreases in PM concentrations. Although projected changes in sulfate and nitrate precursor emissions favor lower PM concentrations over the U.S., projected increases in ammonia emissions could result in higher nitrate concentrations.

The organic aerosol simulation in GEOS-Chem is updated to include aerosol from primary semivolatile organic compounds (SVOCs), intermediate volatility compounds (IVOCs), NO_x dependent terpene aerosol, and aerosol from isoprene + NO_3 reaction. SVOCs are identified as the largest global source of organic aerosol even though their atmospheric transformation is highly uncertain and emissions are probably underestimated. As a result of significant nighttime terpene emissions, fast reaction of monoterpenes with the nitrate radical, and high aerosol yields from NO_3 oxidation, biogenic hydrocarbons reacting with the nitrate radical are expected to be a major contributor to surface level aerosol concentrations in anthropogenically influenced areas such as the United States. Globally, 69 to 88 Tg/yr of aerosol is predicted to be produced annually, approximately 22 to 24 Tg/yr of which is from biogenic hydrocarbons.

Contents

Acknowledgements	iv
Abstract	vi
1 Introduction	1
2 Effect of changes in climate and emissions on future sulfate-nitrate-ammonium aerosol levels in the United States	6
2.1 Abstract	7
2.2 Introduction	7
2.3 Methods	10
2.3.1 GEOS-Chem/GISS Model Set-up	10
2.3.2 Emissions	11
2.3.3 Inorganic Aerosol Model	13
2.4 Present-day Predictions	13
2.4.1 Sulfate	13
2.4.2 Nitrate	14
2.4.3 Ammonium	15
2.4.4 Comparison to Measurements	15
2.5 Predictions of Future Inorganic Aerosol Levels Over the U.S.	18
2.5.1 Effect of Changes in Climate Alone	18
2.5.2 Climate Penalty vs. Climate Benefit	25

2.5.3	Effect of Changes in Anthropogenic Emissions Alone	26
2.5.4	Effect of Changes in Both Climate and Anthropogenic Emissions	27
2.6	Global Budgets of Sulfate, Nitrate, and Ammonium	28
2.6.1	Present-day Budgets	28
2.6.2	Effect of Changes in Climate Alone	29
2.6.3	Effect of Changes in Anthropogenic Emissions Alone	30
2.6.4	Effect of Changes in Both Climate and Anthropogenic Emissions	31
2.7	Implications for Eastern U.S. Outflow	32
2.8	Conclusions	33
2.9	Acknowledgements	34
3	A global perspective on aerosol from low-volatility organic compounds	60
3.1	Abstract	61
3.2	Introduction	61
3.3	Model Description	64
3.3.1	Global Model	64
3.3.2	Absorptive Partitioning	65
3.3.3	SOA from Traditional Precursors	66
3.3.4	Aerosol from SVOCs	67
3.3.5	Aerosol from IVOCs	71
3.3.6	Additional Model Parameters and Specifications	75
3.3.7	Aerosol Aging	76
3.4	Results and Discussion	77
3.4.1	OA from SVOCs and IVOCs	77
3.4.2	Global Budgets	78
3.4.3	United States Organic Aerosol	80
3.4.4	Sensitivity Tests	82
3.4.5	Modern vs. Fossil Carbon	86

3.5	Model Uncertainties	88
3.5.1	IVOC Behavior	88
3.5.2	SVOC Volatility	90
3.5.3	Horizontal Resolution and Inter-annual Variability	91
3.6	Conclusions	91
3.7	Appendix 3.A: Effect of meteorology and grid resolution on global OA budget	94
3.8	Acknowledgements	95
4	Global modeling of organic aerosol: The importance of reactive nitrogen	127
4.1	Abstract	128
4.2	Introduction	128
4.3	Model Description	130
4.3.1	Global Model	130
4.3.2	Emissions	131
4.3.3	SOA Parameterization	133
4.4	Results and Discussion	137
4.4.1	Emissions	137
4.4.2	Global Budget	138
4.4.3	Surface Level Aerosol Over the United States	140
4.5	Considerations	143
4.5.1	Dependence of SOA Formation on NO _x Level	143
4.5.2	Modeled Importance of Nitrate Aerosol	144
4.5.3	Uncertainties in Isoprene Chemistry	146
4.5.4	Extrapolation of Chamber Studies	147
4.6	Conclusions	148
4.7	Acknowledgements	150
5	Future Work	169

A Secondary organic aerosol (SOA) formation from reaction of isoprene with nitrate radicals (NO_3)	172
B Supplement to: A global perspective on aerosol from low-volatility organic compounds	197
C Supplement to: Global modeling of organic aerosol: The importance of reactive nitrogen	203

List of Tables

2.1	Present-day and 2050 predicted emissions	44
2.2	Predicted changes in natural emissions due to climate change	45
2.3	Implications of changes in meteorological parameters for inorganic aerosol	46
2.4	Global sulfate budget	47
2.5	Global budgets of nitrate and ammonium aerosol	48
2.6	Annually averaged and wintertime outflow in kgS/s of SO_x	49
3.1	Low-volatility organic compounds	106
3.2	Emissions of primary low-volatility organic compounds	107
3.3	Parameters for SVOC oxidation	108
3.4	Rate constants for IVOC oxidation	109
3.5	Global OA budget	110
3.6	Sensitivity tests	111
3.7	Mean bias for the sensitivity simulations	112
3.8	Effect of model resolution and meteorology on global OA budget	113
3.9	Traditional (non-volatile POA) simulation	114
4.1	SOA Yield Parameterizations at 298 K	159
4.2	SOA precursor emissions	160
4.3	Global net production of SOA	161

List of Figures

2.1	Present-day predictions of surface-level aerosols for the U.S.	50
2.2	Present-day predictions of aerosols compared to observations	51
2.3	Predicted change in U.S. surface temperature	52
2.4	Predicted change in precipitation and afternoon planetary boundary layer depth . . .	53
2.5	Predicted level 1 zonal wind	54
2.6	Predicted change in aerosol concentrations due to changes in climate alone	55
2.7	Predicted changes in aerosol concentrations due to climate change with present-day and future emissions	56
2.8	Predicted changes in U.S. surface-level aerosol concentrations due to changes in an- thropogenic emissions only	57
2.9	Predicted changes in U.S. surface-level aerosol concentrations due to changes in an- thropogenic emissions and climate	58
2.10	Annual change in SO_x ($SO_2 + SO_4^{2-}$) outflow from the U.S.	59
3.1	Emissions of SVOCs and IVOCs	115
3.2	Predicted concentration of aerosol from SVOCs and IVOCs	116
3.3	Fraction of primary semivolatile material in aerosol phase as POA	117
3.4	SVOC budget	118
3.5	Emission, oxidation, and aerosol formation from aromatics and IVOCs	119
3.6	Total OA and contribution of each component	120
3.7	Winter surface total OC concentration	121
3.8	DJF surface total OC concentration relative to non-volatile POA simulation	122

3.9	Effect of enthalpy of vaporization	123
3.10	Change in global OA net source	124
3.11	Fraction of SVOC emissions from modern carbon	125
3.12	Fraction of IVOC emissions from modern carbon	126
4.1	Schematic of SOA model	162
4.2	Fraction of each parent hydrocarbon reacting and contribution to SOA	163
4.3	Fraction of peroxy radical species reacting with NO	164
4.4	Fraction of semivolatile mass that partitions to the aerosol phase but later evaporates	165
4.5	Surface level organic aerosol in a traditional, non-volatile POA simulation during Au- gust 2000	166
4.6	The change in surface concentration of total OA due to a change in β	167
4.7	Enhancement in surface-level aerosol due to the nitrate oxidation pathway	168

Chapter 1

Introduction

Particulate matter (PM) poses a health risk for people living in both developed and developing countries. For regulatory purposes, PM is usually classified as PM₁₀ (particles less than 10 μm in diameter) and PM_{2.5} (particles less than 2.5 μm in diameter). The fine particles (PM_{2.5}) are able to travel deeply into the human respiratory system and have been linked to irritation, reduced lung function, irregular heartbeat, heart attacks, and premature death (USEPA, 2004). PM_{2.5} can also cause reductions in visibility, environmental damage such as lake or stream acidification, and visual damage to structures. Although there is no safe particulate matter level, the World Health Organization (WHO) air quality guidelines recommend that the PM_{2.5} level not exceed 10 $\mu\text{g}/\text{m}^3$ annually averaged and 25 $\mu\text{g}/\text{m}^3$ daily averaged (WHO, 2006). In the United States, the Environmental Protection Agency (EPA), under the authority of the Clean Air Act, sets standards for acceptable levels of particulate matter to protect human health and welfare. These standards are known as the National Ambient Air Quality Standards (NAAQS). The current NAAQS for PM_{2.5} is 15 $\mu\text{g}/\text{m}^3$ as an annual average and 35 $\mu\text{g}/\text{m}^3$ as a 24-hour average.

On a global scale, particulate matter influences the Earth's radiation budget and therefore can lead to climate change. Aerosols can directly affect climate by scattering and absorption of solar radiation. Indirect effects include increased cloud droplet number concentration, drizzle suppression, increased cloud height, and increased cloud lifetime (IPCC, 2007).

Regulation of particulate matter is complicated by that fact that aerosols contain many species and come from both natural and anthropogenic sources. Sulfate, nitrate, ammonium, and organics can be directly emitted to the atmosphere or form from gas-to-particle conversion in situ. Some components of aerosol may also result from the synergistic effect of natural and anthropogenic emissions such as the oxidation of a biogenic hydrocarbon, like isoprene, by anthropogenic oxidants, like NO_2 (Surratt et al., 2010).

Chemical transport models can be used to assess the impact of air quality management strategies as well as our understanding of the governing processes for aerosol formation. Modeling studies are complementary to laboratory and field campaigns for developing a complete picture of the atmospheric transformation of a species. For example, modeling work can highlight a deficiency in

current understanding when the modeled and observed concentrations do not agree, and laboratory experiments can identify a new species or formation pathway to include in a model. A well developed model can then be used to diagnose how projected changes in emissions or climate may influence pollutant concentrations.

GEOS-Chem (<http://acmg.seas.harvard.edu/geos/>) is a global 3-dimensional chemical transport model managed at Harvard University that simulates fully coupled ozone-NO_x-hydrocarbon chemistry (Bey et al., 2001). The model typically runs with assimilated meteorology from the Goddard Earth Observing System (GEOS) but can also use meteorology from the Goddard Institute for Space Studies (GISS) general circulation model (Wu et al., 2007). In addition to gas-phase chemistry, GEOS-Chem currently simulates a wide variety of aerosols including sulfate, nitrate, ammonium, sea salt, dust, and organic aerosol.

Chapter 2 of this thesis combines meteorology from the GISS model with GEOS-Chem to examine the impacts of changes in emissions and climate on future sulfate, nitrate, and ammonium aerosol levels. The thermodynamic partitioning model, ISORROPIA II (Fountoukis and Nenes., 2007), is implemented to describe the formation of nitrate and ammonium aerosol, and GEOS-Chem is used to simulate present-day (approximately year 2000) and future (approximately year 2050) aerosol levels. Results are presented in terms of global budgets as well as surface layer concentrations over the U.S.

Organic aerosol is a major constituent of atmospheric aerosol (Zhang et al., 2007) and accurately simulating organic aerosol in global and regional models continues to be challenging. Organic aerosol forms from direct emissions of low-volatility compounds that partition to the aerosol phase and higher volatility compounds that are oxidized in the atmosphere. Organic aerosol has traditionally been classified as either primary or secondary as a result of this distinction. Primary organic aerosol (POA) is aerosol that partitions directly to the aerosol phase without any chemical transformation, while secondary organic aerosol (SOA) is formed in the atmosphere by the reaction of gas-phase species. Significant amounts of organic aerosol, including primary organic aerosol, is semivolatile to some extent (Robinson et al., 2007) and can be modeled using absorptive partitioning theory

(Pankow, 1994). Chapters 3 and 4 focus on improving the organic aerosol simulation in GEOS-Chem. In Chapter 3, traditional, nonvolatile POA from biomass, biofuel, and fossil fuel burning is replaced with a pool of semivolatile organic compounds (SVOCs) that partition directly between the gas and aerosol phases. Aging of the SVOCs in the gas-phase is represented using a simple parameterization. SOA from intermediate volatility compounds, which are much lower in volatility than traditional SOA precursors but still volatile enough to be emitted almost entirely in the gas-phase, are also introduced in GEOS-Chem. Chapter 4 focuses on aerosol that forms from biogenic hydrocarbons emitted by plants. Major biogenic SOA precursors include isoprene, monoterpenes, and sesquiterpenes. Using a new model framework, Chapter 4 details some important interactions between anthropogenic emissions and the biogenic hydrocarbons.

Bibliography

- Bey, I., Jacob, D. J., Yantosca, R. M., Logan, J. A., Field, B. D., Fiore, A. M., Li, Q. B., Liu, H. G. Y., Mickley, L. J., and Schultz, M. G.: Global modeling of tropospheric chemistry with assimilated meteorology: Model description and evaluation, *J. Geophys. Res.*, 106, 23073–23095, 2001.
- Foutoukis, C. and Nenes, A.: ISORROPIA II: A computationally efficient thermodynamic equilibrium model for K^+ - Ca^{2+} - Mg^{2+} - NH_4^+ - Na^+ - SO_4^{2-} - NO_3^- - Cl^- - H_2O aerosols, *Atmos. Chem. Phys.*, 7, 4639–4659, 2007.
- Intergovernmental Panel on Climate Change (IPCC): *Climate Change 2007: The Physical Science Basis*, Cambridge Univ. Press, Cambridge, United Kingdom, 2007.
- Pankow, J. F.: An absorption-model of gas-particle partitioning of organic-compounds in the atmosphere, *Atmos. Environ.*, 28, 185–188, 1994.
- Robinson, A. L., Donahue, N. M., Shrivastava, M. K., Weitkamp, E. A., Sage, A. M., Grieshop, A. P., Lane, T. E., Pierce, J. R., and Pandis, S. N.: Rethinking organic aerosols: Semivolatile emissions and photochemical aging, *Science*, 315, 1259–1262, doi:10.1126/SCIENCE.1133061, 2007.

Surratt, J. D., Chan, A. W. H., Eddingsaas, N. C., Chan, M. N., Loza, C. L., Kwan, A. J., Hersey, S. P., Flagan, R. C., Wennberg, P. O., and Seinfeld, J. H.: Reactive intermediates revealed in secondary organic aerosol formation from isoprene, *Proc. Natl. Acad. Sci. U. S. A.*, 107, 6640–6645, doi:10.1073/Pnas.0911114107, 2010.

United States Environmental Protection Agency (USEPA): Air Quality Criteria for Particulate Matter (Final Report, Oct 2004), Environmental Protection Agency, Washington, DC, EPA 600/P-99/002aF-bF, 2004.

World Health Organization (WHO): WHO Air quality guidelines for particulate matter, ozone, nitrogen dioxide and sulfur dioxide: Global update 2005, Summary of risk assessment, WHO Press, Geneva, Switzerland, 2006.

Wu, S. L., Mickley, L. J., Jacob, D. J., Logan, J. A., Yantosca, R. M., and Rind, D.: Why are there large differences between models in global budgets of tropospheric ozone?, *J. Geophys. Res.*, 112, D05302, doi:10.1029/2006JD007801, 2007.

Zhang, Q., Jimenez, J. L., Canagaratna, M. R., Allan, J. D., Coe, H., Ulbrich, I., Alfarra, M. R., Takami, A., Middlebrook, A. M., Sun, Y. L., Dzepina, K., Dunlea, E., Docherty, K., DeCarlo, P. F., Salcedo, D., Onasch, T., Jayne, J. T., Miyoshi, T., Shimojo, A., Hatakeyama, S., Takegawa, N., Kondo, Y., Schneider, J., Drewnick, F., Borrmann, S., Weimer, S., Demerjian, K., Williams, P., Bower, K., Bahreini, R., Cottrell, L., Griffin, R. J., Rautiainen, J., Sun, J. Y., Zhang, Y. M., and Worsnop, D. R.: Ubiquity and dominance of oxygenated species in organic aerosols in anthropogenically-influenced Northern Hemisphere midlatitudes, *Geophys. Res. Lett.*, 34, L13801, doi:10.1029/2007GL029979, 2007.

Chapter 2

Effect of changes in climate and emissions on future sulfate-nitrate-ammonium aerosol levels in the United States *

*Reproduced by permission of American Geophysical Union from "Effect of changes in climate and emissions on future sulfate-nitrate-ammonium aerosol levels in the United States" by H. O. T. Pye, H. Liao, S. Wu, L. J. Mickley, D. J. Jacob, D. K. Henze, and J. H. Seinfeld, *Journal of Geophysical Research*, 114, D01205, doi:10.1029/2008JD010701. Copyright 2009 by the American Geophysical Union.

2.1 Abstract

Global simulations of sulfate, nitrate, and ammonium aerosols are performed for the present-day and 2050 using the chemical transport model GEOS-Chem. Changes in climate and emissions projected by the IPCC A1B scenario are imposed separately and together with the primary focus of the work on future inorganic aerosol levels over the United States. Climate change alone is predicted to lead to decreases in levels of sulfate and ammonium in the southeast U.S. but increases in the midwest and northeast U.S. Nitrate concentrations are projected to decrease across the U.S. as a result of climate change alone. In the U.S., climate change alone can cause changes in annually averaged sulfate-nitrate-ammonium of up to $0.61 \mu\text{g}/\text{m}^3$, with seasonal changes often being much larger in magnitude. When changes in anthropogenic emissions are considered (with or without changes in climate), domestic sulfate concentrations are projected to decrease due to sulfur dioxide emission reductions, and nitrate concentrations are predicted to generally increase due to higher ammonia emissions combined with decreases in sulfate despite reductions in emissions of nitrogen oxides. The ammonium burden is projected to increase from 0.24 Tg to 0.36 Tg, and the sulfate burden to increase from 0.28 Tg S to 0.40 Tg S as a result of globally higher ammonia and sulfate emissions in the future. The global nitrate burden is predicted to remain essentially constant at 0.35 Tg with changes in both emissions and climate as a result of the competing effects of higher precursor emissions and increased temperature.

2.2 Introduction

Particulate matter is an important constituent of the atmosphere responsible for negative health impacts [e.g., *Dockery et al.*, 1993], reductions in visibility, and changes in climate (*IPCC*, 2007). Atmospheric concentrations of aerosols will change in the future as climate and aerosol precursor emissions change. Nitrate (NO_3^-), ammonium (NH_4^+), and sulfate (SO_4^{2-}) are significant constituents of particulate matter (PM), forming mainly from gas-phase precursors.

In the absence of changes in aerosol precursor emissions, changes in climate alone will influence

future aerosol levels. For example, alterations in wind speed, precipitation, and boundary layer height can translate into changes in stagnation and ventilation (*Leung and Gustafson, 2005*). *Mickley et al.* (2004) showed that a decrease in the number of cyclones tracking over southern Canada has important implications for increased stagnation in the midwest and northeast U.S. during summer. *Dawson et al.* (2007) demonstrated that perturbations to present-day temperature, wind speed, absolute humidity, mixing height, and precipitation can all significantly affect PM_{2.5} (particulate matter with diameter <2.5 μm).

Surface temperatures are generally projected to be higher in the future with particularly strong warming over continents (*IPCC, 2007*). Temperature influences PM_{2.5} concentrations through its effect on precursor emissions rates, chemical reaction rates, and gas-aerosol partitioning of semi-volatile species. For example, increasing temperature can lead to a reduction in nitrate aerosol mass as a result of ammonium and nitrate partitioning to the gas-phase (*Dawson et al., 2007*). Changes in gas-aerosol partitioning of nitrate/nitric acid will also affect total nitrate (nitrate aerosol and nitric acid) as a result of the different wet and dry deposition rates of the two species (*Aw and Kleeman, 2003*). In contrast, higher temperatures can result in increased gas-phase reaction rates and oxidant concentrations, which can lead to higher sulfate concentrations (*Dawson et al., 2007; Liao et al., 2006; Rae et al., 2007*). *Jacob and Winner* (2008) present a review of studies examining the effect of changes in climate on ozone and PM.

Future PM concentrations in the U.S. will be influenced not only by changes in domestic emissions but by changes in other regions as well. Transpacific transport of Asian pollution has been shown to contribute to sulfate in the U.S. (*Benkovitz et al., 2006; Heald et al., 2006; Park et al., 2006; Chin et al., 2007; Koch et al., 2007; Liu et al., 2008*), and the preferential export of sulfur dioxide (SO₂) from Asia over ammonia/ammonium leads to slight decreases in U.S. nitrate (*Park et al., 2004*).

This study is a companion study to the work of *Wu et al.* (2008), which investigated the effects of projected climate and emissions changes on tropospheric ozone. This work investigates the potential effects of projected climate and emission changes on sulfate-nitrate-ammonium aerosol levels, with a focus on the United States. Future climate, for year 2050, is simulated with the Goddard Institute

for Space Studies (GISS) general circulation model (GCM) version III (*Rind et al.*, 2007). IPCC emission scenario A1B (*Nakicenovic and Swart*, 2000) is adopted. Eventually, multiple emissions scenarios will be tested with the GISS/GEOS-Chem framework. Warming under A1B is generally predicted to be more pronounced than under B1 and less pronounced than under A2 since A1B represents rapid growth with balanced energy use. However, for year 2050, A1B was found to have the highest multi-model mean surface warming (compared to B1 and A2) in the IPCC Fourth Assessment Report (*IPCC*, 2007).

The global meteorological fields from the GISS model provide the conditions for input into the atmospheric chemical transport model GEOS-Chem for both present-day (1999-2001) and years 2049-2050. Effects of climate change alone, emission changes alone, and both climate and emissions changes in concert on sulfate-nitrate-ammonium levels are simulated. While the focus is on a specific future emission scenario, the mechanistic understanding of the magnitudes and directions of the projected changes will allow for extrapolation of the effects to other potential emissions scenarios such as mitigation strategies for air quality attainment. Due to the nonlinear nature of secondary inorganic aerosol formation, particularly for nitrate, the change in sulfate concentrations due to changes in sulfur dioxide emissions is likely to be the most robust and generally applicable sensitivity.

Secondary organic aerosol (SOA) is another important component of atmospheric aerosol and should be included in an examination of PM_{2.5}. GEOS-Chem currently has the capability to treat SOA from biogenics (*Chung and Seinfeld*, 2002; *Henze and Seinfeld*, 2006) and aromatics (*Henze et al.*, 2008a). Studies indicate the amount of SOA predicted by models severely underestimates the actual amount present in the atmosphere (*de Gouw et al.*, 2005; *Heald et al.*, 2005; *Volkamer et al.*, 2006; *de Gouw et al.*, 2008). The treatment of SOA will be part of a future work that focuses on improving the underlying SOA model in addition to examining the effects of changes in climate and emissions on future organic aerosol levels.

The methods and model set-up used to examine sulfate, nitrate, and ammonium aerosols are discussed in Section 2.3 followed by present-day predictions of those aerosols (Section 2.4). Section 2.5 presents predictions for future inorganic aerosol levels over the U.S. due to changes in climate

alone, emission changes alone, and combined climate and emission changes. Global budgets for the present-day and future can be found in Section 2.6, and Section 2.7 discusses some implications of changes in climate and emissions for sulfur outflow from the U.S.

2.3 Methods

2.3.1 GEOS-Chem/GISS Model Set-up

The atmospheric chemical transport model, GEOS-Chem v.7-4-11 (<http://www-as.harvard.edu/chemistry/trop/geos>), is employed with GISS GCM III (*Rind et al.*, 2007) meteorological data. The models use 23 hybrid sigma-pressure levels with the lowest layers extending up to 200, 500, and 900 m for a surface pressure of 1010 hPa. A comparison of present-day GISS Model E (similar to Model III) predictions of precipitation, specific humidity, temperature, and other meteorological variables to observations can be found in the work of *Schmidt et al.* (2006), and *Rind et al.* (2007) compares Model E and Model III meteorology using several tracers. The analysis of (*Rind et al.*, 2007) includes the use of a radon tracer as a diagnostic of precipitation. The interface between GEOS-Chem and the GISS meteorological fields is described by *Wu et al.* (2007), and the same meteorology as used in the work of *Wu et al.* (2008) is used here. Present-day meteorological conditions in the GISS GCM are simulated with greenhouse gas levels corresponding to years 1999-2001. Year 2049-2051 climate is obtained from a dynamic GCM simulation in which CO₂ and other greenhouse gases follow the IPCC A1B scenario. Although changes in aerosols and ozone could have significant influences on climate by the end of the 21st century (*Levy et al.*, 2008), those effects are not considered here in the GISS simulations. CO₂ is calculated to reach 522 ppm by 2050. The GISS GCM yields a global mean surface temperature increase of 1.6 K and an increase of 8% in annual mean precipitation for 2000-2050 (*Wu et al.*, 2008).

The GEOS-Chem simulations use a global resolution of 4° latitude by 5° longitude with 23 vertical layers and include coupled ozone-NO_x-hydrocarbon and aerosol chemistry (*Bey et al.*, 2001; *Park et al.*, 2004; *Liao et al.*, 2007) with all tracers listed by *Liao et al.* (2007). Changes in ozone

and aerosol precursor emissions are considered for both present-day and future (2050) scenarios. SO_2 is both directly emitted and produced by atmospheric oxidation of dimethyl sulfide (DMS); SO_2 reacts in either gas or aqueous phases to form sulfate. A minor sulfate formation pathway on fine sea salt aerosol as a result of SO_2 reacting with ozone is also considered (*Alexander et al.*, 2005). The global burden of sulfate on coarse sea salt aerosol is expected to be small and its lifetime short (*Alexander et al.*, 2005), so the production of sulfate on coarse sea salt is neglected in the analysis. Ammonium nitrate aerosol forms from gas-aerosol partitioning of ammonia and nitric acid (*Seinfeld and Pandis*, 2006). Ammonia is emitted directly and does not participate in gas-phase chemistry, although it is removed by wet and dry deposition. Nitric acid is formed from gas-phase nitrogen oxides (NO_x), which are mostly of anthropogenic origin but have important natural sources, including lightning and soils. In addition to its daytime photooxidation source, nitric acid (HNO_3) is produced in heterogeneous nighttime reactions involving N_2O_5 , NO_3 , and NO_2 (*Jacob*, 2000; *Martin et al.*, 2003; *Evans and Jacob*, 2005). In addition to these heterogeneous reactions, aerosols may influence the gas phase by modifying photolysis rates (*Martin et al.*, 2003). Nitric acid, sulfate, nitrate, and ammonium are assumed to be completely soluble in the cloud condensate phase in convective updrafts and rainout and washout. The representation of dry deposition follows a resistance in series scheme (*Wesely*, 1989), with the surface resistances for sulfate, nitrate, and ammonium aerosols following the work of *Zhang et al.* (2001).

2.3.2 Emissions

Present-day emissions of ozone and aerosol precursors in GEOS-Chem generally follow *Wu et al.* (2007) with fossil fuel emissions outside the U.S. updated to 1998. The present-day ammonia emission inventory is based on the work of *Bouwman et al.* (1997), as implemented by *Park et al.* (2004). Most ammonia is anthropogenic in origin and results from domesticated animals and agricultural operations (*Park et al.*, 2004). Ammonia emissions are not calculated on-line as a function of temperature in this model, but do have an imposed seasonality that was determined as a function of temperature for one base year (*Park et al.*, 2004). Sulfur emission sources from the Global Emission

Inventory Activity (GEIA) are also described by *Park et al.* (2004) and now include emissions from ships (*Corbett et al.*, 1999). *Bey et al.* (2001) and references therein provide information on the anthropogenic NO_x emission inventories. Present-day methane levels in the model are based on observations and are set to 1750 ppb with a 5% inter-hemispheric gradient (*Wu et al.*, 2008). Future emissions follow the Integrated Model to Assess the Greenhouse Effect (IMAGE) model for IPCC scenario A1B (*Streets et al.*, 2004) and are implemented using prescribed growth factors for different regions, species, and sources. Table 2.1 shows anthropogenic emissions for the present-day and year 2050 (following IPCC A1B). The future (2049-2051) methane level in GEOS-Chem is set to 2400 ppb for simulations in which changes in anthropogenic emissions are considered.

Natural emissions of DMS, NO_x from lightning and soils, sea salt, and biogenic hydrocarbons depend on meteorology and are computed online in the model. Natural emissions predicted for both the present-day and future climate are given in Table 2.2. DMS emissions (*Saltzman et al.*, 1993; *Nightingale et al.*, 2000) are treated as a function of wind speed, and present-day climatological sea surface temperatures and DMS ocean concentrations are used. Lightning NO_x emissions are parameterized based on convective cloud-top height (*Price and Rind*, 1992; *Wang et al.*, 1998) and are distributed according to *Pickering et al.* (1998). Lightning NO_x emissions are scaled to produce 4.8 Tg N for year 2000. Soil NO_x emissions are calculated as described by *Wang et al.* (1998) considering changes in temperature, wind speed, and precipitation (*Yienger and Levy*, 1995). Sea salt is emitted in both fine and coarse sizes as a function of wind speed (*Alexander et al.*, 2005; *Monahan et al.*, 1986). Biogenic hydrocarbon emissions include those from isoprene (*Guenther et al.*, 1995), monoterpenes (*Guenther et al.*, 1995), acetone (*Jacob et al.*, 2002), and other alkenes (scaled to isoprene). Due to the relatively coarse resolution of surface wind speed and the particularly strong dependence of dust emissions on wind speed, emissions of dust are not included. Changes in land use and biomass burning due to climate change are also not considered.

2.3.3 Inorganic Aerosol Model

ISORROPIA II (*Fountoukis and Nenes, 2007*) is implemented in GEOS-Chem to compute gas-aerosol equilibrium partitioning of nitric acid and ammonia. Particles in this study are not size-resolved; however, they can be generally assumed to represent PM_{2.5} since formation of sulfate-nitrate-ammonium on coarse mode sea salt and dust is excluded. Submicrometer-sized particles are likely to reach gas-aerosol equilibrium on time-scales less than the 1 hour computational time step used here (*Meng and Seinfeld, 1996*).

Accumulation mode sea salt sodium and chloride are considered in the gas-aerosol equilibrium along with sulfate, nitrate, and ammonium. Calcium, magnesium, and potassium concentrations are not considered in the present study due to the issues with dust emissions previously mentioned. All inorganic aerosols are assumed to exist on the upper, metastable branch of the hygroscopic hysteresis curve. Although this assumption may not hold at higher altitudes in the free troposphere (*Wang et al., 2008*), since the focus of this study is mainly on surface-level concentrations, where humidities reach high values on a daily basis, the metastable assumption is acceptable.

2.4 Present-day Predictions

2.4.1 Sulfate

Present-day sulfate concentrations across the United States vary seasonally (Figure 2.1), as governed by changes in photochemistry and wet removal with influences from transport. SO₂ emissions exhibit little seasonality with the highest emissions in the eastern United States. Sulfate concentrations are lowest in December-January-February (DJF) when oxidants/photochemistry are lowest. In March-April-May (MAM), higher levels of photochemistry lead to enhanced levels of sulfate compared to those in DJF, but increased precipitation and transport keep sulfate concentrations at moderate levels. In-cloud sulfate production near the surface via reaction with H₂O₂ is highest in MAM due to slightly more cloud cover than in JJA, but aqueous production is still significantly less than production from gas-phase OH reaction. The most active photochemistry occurs during June-

July-August (JJA), the season when precipitation is particularly intense in the Southeast for the meteorology used here. As a result, sulfate concentrations are significant but tend to be more localized than in MAM. September-October-November (SON) is characterized by intermediate, but still significant, oxidant levels. While production rates of sulfate in MAM and SON are similar, as a result of low precipitation, sulfate concentrations are actually higher in SON than JJA or MAM for some locations like the Southeast.

2.4.2 Nitrate

Anthropogenic NO_x emissions, like anthropogenic SO_2 , exhibit little seasonal variation and are highest in the eastern United States. Soil NO_x emissions peak in JJA over the middle of the United States. Soil NO_x is potentially more important in the western United States where anthropogenic NO_x emissions are lower.

Nitrate aerosol concentrations (Figure 2.1) can be explained by the combined effects of temperature, precipitation, and photochemistry. Oxidant levels and wet deposition determine the amount of total nitrate ($\text{HNO}_3 + \text{NO}_3^-$) available. Since HNO_3 undergoes efficient dry deposition when compared to that for particles, gas-aerosol partitioning also influences total nitrate levels. Maximum predicted nitrate aerosol surface concentrations in the United States lie north and west of the main anthropogenic NO_x source region in the Northeast, reflecting the role of ammonia emissions in the Midwest. As a result, nitrate formation in the Midwest tends to be nitric acid-limited (*Park et al.*, 2004) as diagnosed by the gas ratio (*Ansari and Pandis*, 1998) which is the free ammonia ($[\text{NH}_3] + [\text{NH}_4^+] - 2 \times [\text{SO}_4^{2-}]$) divided by total nitrate ($[\text{HNO}_3] + [\text{NO}_3^-]$) expressed in molar concentration units. The Northeast tends to be ammonia-limited due to higher sulfate concentrations and lower ammonia emissions.

The highest nitrate aerosol (NO_3^-) concentrations are predicted to occur in winter due to low temperatures and low sulfate concentrations. Total (gas + aerosol) nitrate is high in JJA, but both high temperatures and precipitation lead to the lowest nitrate aerosol concentrations in this season. Like MAM, SON is characterized by both intermediate photochemistry and temperatures. Because

precipitation in SON is relatively low, which reduces loss of total nitrate by wet deposition, SON nitrate aerosol concentrations are significant but not as high as those in DJF.

2.4.3 Ammonium

Unlike NO_x and SO_2 , anthropogenic ammonia emissions, mostly from domesticated animals and fertilizer use, exhibit pronounced seasonality with the highest and lowest emissions occurring in JJA and DJF, respectively. NH_3 emissions from sources such as crops and soils are also largest in JJA and smallest in DJF. Spatially, emissions are highest in the eastern U.S., but also significant in the West. Ammonium aerosol concentrations (Figure 2.1) follow those of sulfate and nitrate, with which they are chemically linked.

2.4.4 Comparison to Measurements

To evaluate the predictions of present-day concentrations of sulfate, nitrate, and ammonium, simulations are compared to the Clean Air Status and Trends Network (CASTNET, <http://www.epa.gov/castnet/>) measurements (Figure 2.2). CASTNET provides concentrations of sulfate, nitrate, nitric acid, and ammonium as well as estimates of dry deposition velocities and fluxes. While some GEOS-Chem grid cells do not contain any CASTNET sites, a number of grid cells have 5 or more CASTNET sites each over the eastern United States. Seasonal CASTNET averages are created from monthly data from years 1998-2001 to represent a climatological mean. For the purposes of analysis, an arbitrary division between eastern and western United States is made at 92.5° W longitude which runs from Minnesota to Louisiana. The Interagency Monitoring of Protected Visual Environments (IMPROVE) network also provides sulfate and nitrate concentration measurements, and *Liao et al.* (2007) present a comparison of sulfate concentrations predicted by GEOS-Chem to IMPROVE observations. CASTNET measurements are chosen here for comparison because of their more complete spatial coverage over the eastern U. S. where the highest sulfate and nitrate aerosol concentrations occur.

Inorganic aerosol concentrations are generally under-predicted over the entire United States.

However, nitrate is typically over-predicted in the eastern U.S. (e.g. JJA). The normalized mean bias for the entire U.S. ($\text{NMB} = \sum_{i=1}^N (P_i - O_i) / \sum_{i=1}^N (O_i) * 100\%$, where P_i is the prediction and O_i is the observation) ranges from -50% in JJA to -17% in SON for sulfate and -41% in MAM to -6% in DJF for nitrate. The normalized mean bias for ammonium ranges from -32% in JJA to +5% in SON. The correlation between nitrate observations and predictions is the weakest of the inorganic aerosols with the poorest correlation in JJA. Nitrate aerosol concentrations in the western U.S. in JJA are significantly under-predicted.

Some under-prediction could result from coarse ($>2.5 \mu\text{m}$ diameter) material being captured in the CASTNET samples. However, *Morris et al.* (2005) estimate that most secondary nitrate ($>90\%$) can be assumed to be present in fine particles in the rural West, although exceptions can occur. In addition, nitrate may volatilize from the Teflon filters used in CASTNET (*Ames and Malm, 2001*). As a result, CASTNET sites may under-report or over-report $\text{PM}_{2.5}$ depending on the amount of coarse aerosol present and the extent of nitrate volatilization.

Examining data from five individual CASTNET sites in the western United States (mostly Southern California) reveals that both gas-phase nitric acid and total nitrate are under-predicted, which could be a result of (1) insufficient formation of HNO_3 in the gas phase or (2) insufficient partitioning of HNO_3 to particulate nitrate resulting in total nitrate being preferentially lost via efficient dry deposition of HNO_3 . Dry deposition velocities predicted by the model at these 5 western sites in JJA have a normalized mean bias of +88% compared to the CASTNET data. A sensitivity study, performed in the West for JJA in which the dry deposition velocity of HNO_3 was capped at 1.5 cm/s, however, did not produce a significant improvement in nitrate aerosol predictions, indicating that under-prediction of nitrate aerosol is not a result of HNO_3 dry deposition alone.

Other studies using different global chemical transport models and different thermodynamic models for inorganic aerosols also reveal significant underestimates in fine mode nitrate in Southern California (*Mhyre et al., 2006; Bauer et al., 2007*). GEOS-Chem simulations with an inorganic aerosol model based on MARS-A and GEOS assimilated meteorology at a finer resolution also exhibit an underestimate (*Park et al., 2006*). Some models predict significant coarse-mode nitrate

in Southern California, but the IMPROVE sites show significant fine-mode nitrate (on the order of $1 \mu\text{g}/\text{m}^3$ or more) is present in the vicinity of Southern California (*Liao et al.*, 2007).

Nitrate aerosol formation is particularly sensitive to ammonia emissions [e.g., *Bauer et al.*, 2007], suggesting that inaccuracy in the NH_3 inventory may be a factor in model under-predictions. *Yu et al.* (2005) found that total nitrate, total ammonia ($\text{NH}_3 + \text{NH}_4^+$), and sulfate strongly influence nitrate predictions and that errors in total ammonia were more influential in this regard than errors in sulfate. Also, *Karydis et al.* (2007) noted that modest errors in ammonium concentrations can be associated with significant errors in nitrate predictions. The *Bowman et al.* (1997) NH_3 emissions inventory used here reports a global uncertainty of $\pm 25\%$, and individual seasonal and regional uncertainties may be considerably higher. Some studies examining the validity of ammonia emissions inventories have focused mainly on the eastern United States (*Mendoza-Dominguez and Russell*, 2001; *Gilliland et al.*, 2003; *Pinder et al.*, 2006). *Gilliland et al.* (2006) investigated seasonal allocations of the EPA National Emission Inventory (NEI) 2001 inventory and indicated that summer NH_3 emissions are likely underestimated to a greater extent in the West than the East.

Additional box model calculations were performed here using conditions representative of summer in Southern California to determine the extent to which errors in predicted total ammonia and total nitrate could be responsible for under-predictions in nitrate aerosol. The analysis indicates that both total nitrate and total ammonia would have to be more than a factor of five higher than current model predictions to obtain nitrate levels consistent with CASTNET data. It is unlikely that emissions inventories of ammonia and NO_x in Southern California during the summer are low by this much. If total nitrate levels produced by the model were correct, then total NH_3 (and probably ammonia inventories) would have to be more than a factor of 10 higher than current predictions, to produce simulations consistent with CASTNET observations in Southern California. The EPA NEI for ammonia has been shown to be too high for use in GEOS-Chem (*Gilliland et al.*, 2003; *Henze et al.*, 2008b), and errors in the ammonia inventory are probably not the primary reason for inaccuracies in nitrate predictions based on the sensitivity analysis performed. Nitrate under-prediction may result, at least in part, from a lack of representation of some processes in the

model such as interaction with dust and organics (*Ansari and Pandis, 2000*). Since regional models can capture the high nitrate concentrations in the Los Angeles basin (*Kleeman and Cass, 2001*), a global model, even at 1° by 1° resolution (*Park et al., 2006*), may be too coarse to represent nitrate formation in Southern California.

Since this work is primarily directed toward examining changes in aerosol concentrations as a result of future climate change, the underestimate in present-day nitrate in the western U.S. does not compromise conclusions regarding the direction in which inorganic aerosol levels are likely to change in the future, but is an important issue to address in future work.

2.5 Predictions of Future Inorganic Aerosol Levels Over the U.S.

Changes in sulfate, nitrate, and ammonium aerosol concentrations due to changes in climate and emissions are now examined. Section 2.5.1 addresses how projected changes in meteorology from 2000 to 2050 are predicted to affect sulfate, nitrate, and ammonium aerosol levels with anthropogenic emissions held at present-day values. Section 2.5.2 discusses the effect of climate change with anthropogenic emissions at future levels. Section 2.5.3 describes effects of changes in anthropogenic emissions with climate held at present-day conditions, and changes in climate and emissions together are addressed in Section 2.5.4.

2.5.1 Effect of Changes in Climate Alone

Climate change alone will influence future aerosol concentrations through modifications of gas-phase chemistry, transport, removal, and natural emissions. Most predicted changes in natural emissions over the 50-year period considered here are relatively modest (Table 2.2), except for lightning NO_x and biogenic hydrocarbons, both of which influence gas-phase tropospheric chemistry. Note that natural ammonia emissions are assumed to be independent of meteorological conditions.

Meteorology influences aerosol concentrations through changes in temperature, precipitation,

planetary boundary layer depth (PBL depth), transport, humidity, and oxidant levels. In some seasons, certain effects appear to dominate, but generally, changes in concentrations result from multiple climatic changes. Temperature generally increases 1- 2 K between 2000 and 2050 in all seasons over the U.S. with increases in JJA over Texas being the largest and statistically significant (at the 5% level). All tests of statistical significance were performed using 10 years of present-day (2000) and 10 years of future (2050) meteorology although GEOS-Chem simulations only use 3 years for the present-day and 3 years for the future. About 1 K of cooling is shown for DJF in the southwest U.S. as a result of interannual variability and a relatively cold winter in 2051. The cooling during DJF is not found in the trend using 10 years of present-day and future data and is not statistically significant. Although the warming in DJF and JJA over the U.S. is generally statistically significant, the warming in MAM and SON is not statistically significant (at 5%). Higher specific humidities are predicted over the U.S. in the future as relative humidity is expected to remain roughly constant (*Held and Soden, 2000*).

Precipitation trends shown in Figure 2.4 for three years of the present-day and future are generally consistent with the trends using 10 years of present-day and future GISS meteorology. However, not all changes in precipitation are significant at the 5% level. Predicting future rainfall over mid-latitudes is difficult, as it involves two competing factors: 1) increased specific humidity in a warmer climate, which increases rainfall and 2) increased atmospheric stability due to heating aloft which decreases rainfall. Precipitation is predicted to generally increase (Figure 2.4), especially for DJF and MAM over the eastern U.S., reflecting changes in both large-scale and convective precipitation. DJF and MAM precipitation increases are roughly on the order of 1 mm/day which is more than a 50% increase in DJF and about a 20-30% increase in MAM. The increase in precipitation over the Midwest in DJF is consistent with the trend using 10 years of present-day and 10 years of future GISS meteorology and statistically significant (at 5%). Convective precipitation is largest in JJA and usually highest in the Southeast during all seasons. Changes in convective precipitation may be more important than changes in large-scale precipitation as convective storms are generally short-lived and do not necessarily completely wash out aerosols and their precursors (*Dawson et al.,*

2007). Increases in precipitation in the west during JJA are generally small in magnitude (<0.2 mm/day) despite large percentage changes ($>50\%$). The decrease in precipitation over Texas and the increase in the Northeast during JJA are on the order of 30% and are statistically significant (at 5%). Precipitation increases almost 50% in the Southeast in SON and decreases approximately 40% in the Northeast during that same time, but SON precipitation changes are generally not statistically significant (at 5%). Models reviewed by the *IPCC* (2007) generally predict increased precipitation over North America, with a warming climate (A1B), except for the Southwest, with increases in the Northeast and decreases in the Southwest more certain. Regional projected precipitation changes have large uncertainty, indicated by the fact that about half of the 21 models in the work of the *IPCC* (2007) predict increases in precipitation and about half predict decreases in precipitation across most of the U.S. for JJA.

The boundary layer depth over the U.S. is predicted to generally decrease from present-day to 2050 (Figure 2.4). In contrast, there is a particularly strong increase in the afternoon PBL depth of about 30% over Texas during JJA associated with the northeastward movement of the Bermuda high and the associated drying and warming of Texas (*Wu et al.*, 2008). Increases and decreases in the PBL depth are generally less than 20% . Note that decreases in the PBL depth (favoring higher aerosol concentrations) are generally associated with increases in precipitation (favoring lower aerosol concentrations), and these two changes will generally have opposite effects on aerosol concentrations.

The DJF and SON seasons are predicted to experience particularly strong changes in the zonal winds in the lowest model level across the U.S. (Figure 2.5) with westerlies doubling in strength during SON. During DJF, the westerlies are predicted to decrease in strength, while during SON, both the westerlies and easterlies increase in strength. The increase in westerly wind strength in SON is consistent with the ensemble of models examined by *IPCC* (2007) that show a strengthening and northward shift in mid-latitude westerlies particularly in autumn and winter for 2100 under A1B projections (although the meteorology here shows a weakening of the westerlies in DJF in 2050). The DJF trend in zonal winds is consistent with trends using 10 years of present-day and future GISS meteorology although the decrease is only significant in the Midwest (at 25%). The SON trend

of weakening easterlies in the south and strengthening westerlies in the north is reflected in trends using 10 years of GISS zonal winds at level 1 (at surface) and level 7 (at approximately 5 km) and significant at the 25% level near the east coast. Additional changes in meteorology will be discussed in relation to predicted changes in aerosol levels during each season.

Figure 2.6 shows the predicted change in surface concentrations of inorganic aerosols from the present-day to 2050 as a result of predicted changes in meteorology alone. Table 2.3 summarizes the climatic parameters important for explaining the changes in concentrations of sulfate, nitrate, and ammonium aerosols. Each season will be discussed in the following sections since different meteorological changes are influential during different times of the year.

2.5.1.1 DJF Season

In winter, SO_2 , total nitrate, SO_4^{2-} , and NH_4^+ are predicted to show similar trends between 2000 and 2050, with increased concentrations over the Midwest but decreased concentrations over the northeast U.S. (Figure 2.6). Changes in aerosol-phase nitrate are generally correlated with changes in total nitrate except for the southeast U.S., where changes reflect additional processes including the influence of higher temperatures. The largest change in nitrate for the southeast U.S. is predicted to occur in a present-day ammonia-limited regime according to the gas ratio (<1), so increased sulfate levels may result in less ammonia being available for nitrate. Additional factors may be influential in the Southeast such as decreased dry deposition as a result of weaker westerlies and changes in vertical transport. Future predicted changes in the planetary boundary layer (PBL) also play a role determining concentration changes in the Midwest and Southeast, since the boundary layer is generally lower leading to higher surface concentrations. Changes in precipitation and convective flux do not appear to contribute significantly to changes in DJF concentrations.

Since many species, including carbon monoxide and black carbon, follow a trend similar to the inorganic aerosols, changes in transport must be a major determining factor for changes in concentrations. Predicted changes in the strength of the wintertime westerly winds and meridional winds across the United States are expected to play a major role in determining changes in inorganic aerosol

concentrations. The westerly winds in the lower 2.5 km of the atmosphere decrease in strength over most of the U.S., especially in the Midwest and Northeast where the wind strength decreases by as much as 70% at 0.9 km in altitude. A lower PBL and weaker westerlies imply slower transport of aerosols away from regions in the Midwest and higher inorganic concentrations. Weaker westerlies also reduce the transport of aerosols and their precursors to the Northeast. Increased precipitation in the Midwest may further reduce the amount of aerosols transported eastward. Present-day meridional winds generally flow south to north in the eastern U.S. during DJF. With climate change, the winds in the northeast U.S. are actually predicted to change direction and flow more intensely from north to south. As a result, aerosols and their precursors are transported more quickly away from the northeast U.S. and concentrations decrease.

2.5.1.2 MAM Season

In spring, sulfate concentrations are predicted to increase in the Midwest and Northeast and decrease in the Southeast (Figure 2.6). Nitrate, total nitrate, and ammonium concentrations generally decrease. Increased wet deposition of gaseous HNO_3 in addition to higher temperature causes decreased nitrate concentrations. Gas phase sulfate production generally decreases in the future as a result of lower OH concentrations due to climate change, but the increases in aqueous-phase oxidation are generally of larger magnitude than the changes in gas-phase production for the lowest 4 levels (approximately 1.5 km) of the atmosphere. Although higher specific humidities are expected to increase HO_x ($\text{HO}_x = \text{OH} + \text{HO}_2$) production, higher temperatures and higher biogenic emissions can result in decreasing OH and increasing HO_2 over the U.S. In the future springtime, H_2O_2 increases 20% to 40% due to higher temperatures and increased water vapor producing more HO_x (with perhaps a minor effect of water fostering the $\text{HO}_2 + \text{HO}_2$ reaction). In the work of *Liao et al.* (2006), annually increased sulfate levels in the future in the eastern U.S. were attributed to higher oxidant concentrations.

2.5.1.3 JJA Season

Predicted changes in concentrations during summer do not appear to be the result of a single dominant factor. *Wu et al.* (2008) examined changes in ozone concentrations during JJA with the same meteorology as used here. Ozone was predicted to increase in the Midwest and Northeast as a result of increased isoprene emissions, lower peroxyacetyl nitrate stability, a more shallow PBL, reduced convective ventilation, and more frequent stagnation. Ozone in the Southeast was found to be insensitive to climate change as a result of the competing effects of isoprene emissions and meteorology. For aerosols, a lower PBL, reduced convective ventilation, and more frequent stagnation could lead to higher concentrations, and sulfate concentrations generally increase over the Midwest (Figure 2.6). Along the East Coast and somewhat inland, higher H_2O_2 levels and a lower PBL are predicted to lead to more in-cloud H_2O_2 production of SO_4^{2-} . More precipitation adjacent to the East Coast acts to reduce sulfate. A deeper PBL over Texas and part of the Southeast contributes to sulfate and ammonium decreases in those regions. Changes in nitrate aerosol generally follow changes in total nitrate. Dry deposition of nitric acid can act as a positive feedback by reducing total nitrate when aerosol nitrate evaporates at higher temperatures (*Aw and Kleeman*, 2003).

2.5.1.4 SON Season

Multiple species (total nitrate, SO_4^{2-} , SO_2 , and NH_4^+) show a similar trend during SON with decreasing concentrations in the southeast U.S. and increasing concentrations in the northeast U.S. (Figure 2.6). The increasing westerly zonal wind speed across the northern U.S. transports aerosols and their precursors away from the Midwest more quickly and transports nitrate to the Northeast where temperature increases are larger and sulfate increases are substantial. Thus, despite increases on the order of 0.4 to 1 ppb (about 1 to 2.8 $\mu\text{g}/\text{m}^3$ at standard temperature and pressure, STP) in total nitrate, aerosol nitrate shows relatively small increases in the Northeast. The Northeast may also see slightly less transport in the future during SON as meridional winds are predicted to decrease in strength in the Northeast and along the East Coast. In the northeast U.S., precipitation is predicted to decrease by as much as 40% and convective fluxes around 1.4 km in altitude decrease,

both of which contribute to higher concentrations.

For the Southeast, changes in vertical transport and precipitation play a role in determining future inorganic aerosol concentrations. Precipitation is predicted to increase by as much as 50% in the Southeast. Black carbon was used as a surrogate species to examine the effects of changes in precipitation. Hydrophobic black carbon concentrations generally increase in the Southeast unlike hydrophilic black carbon which shows a pattern similar to sulfate. Thus, increased wet removal must be the primary reason for decreases in the Southeast during SON with changes in transport playing a minor role.

2.5.1.5 Annual changes

On an annual basis, sulfate concentrations are predicted to decrease over the Southeast and southern United States by up to $0.34 \mu\text{g}/\text{m}^3$, whereas sulfate increases over the Midwest and Northeast by up to $0.32 \mu\text{g}/\text{m}^3$. In the work of *Tagaris et al. (2007)*, sulfate concentrations in 2050 for scenario A1B are generally predicted to increase in the U.S. due to climate change alone in the Midwest, Northeast, and Southeast as a result of increases in climate sensitive SO_2 emissions which increase by 4% in their study. The increases in sulfate concentration in the Midwest and Northeast (>10%) were larger (relatively) than the changes in the Southeast (<1%) (*Tagaris et al., 2007*).

Due to higher temperatures, future nitrate aerosol concentrations are expected to be lower, and on an annual basis, nitrate aerosol is predicted to decrease across almost the entire eastern U.S. with a maximum decrease of $0.24 \mu\text{g}/\text{m}^3$. Projected changes in nitrate aerosol are not purely a result of temperature increases, as total nitrate can increase or decrease in individual seasons (as discussed in the preceding sections). Higher absolute humidity can favor nitrate partitioning to the aerosol phase (*Dawson et al., 2007*), but this effect is not pronounced in the annual changes in this study.

Ammonium changes reflect those of sulfate and nitrate. The largest annually averaged ammonium decrease of about $0.16 \mu\text{g}/\text{m}^3$ is predicted to occur over the South where both nitrate aerosol and sulfate decrease. Annual increases of ammonium do not exceed $0.09 \mu\text{g}/\text{m}^3$ over the Midwest where sulfate increases.

The annually averaged decrease in sulfate in the southeast U.S. (bottom row of Figure 2.6, first column of Figure 2.7) results from changes during SON. *Racherla and Adams* (2006) and *Liao et al.* (2006) found that sulfate concentrations near the surface over the eastern U.S. generally increase between the present-day and future (2050 and 2100, scenario A2), consistent with the results shown here for the Midwest and Northeast. *Racherla and Adams* (2006) also predict that the largest seasonal decrease in sulfate burden between the present-day and 2050 for the eastern U.S. will occur during SON as a result of increased precipitation. Predictions of regional changes in precipitation for the U.S. between the present-day and future are not necessarily robust model results (*IPCC*, 2007), and studies may continue to give different predictions for changes in sulfate for the Southeast unless projected precipitation changes are consistent in both magnitude and direction.

2.5.2 Climate Penalty vs. Climate Benefit

As discussed in Section 2.5.1, aerosol levels will change due to changes in climate alone. *Wu et al.* (2008) discussed the concept of a “climate change penalty” in which more aggressive emission controls may be necessary to meet ozone air quality goals in the future as a result of climate change. For sulfate-nitrate-ammonium aerosols, particulate air quality may benefit from climate change. In this section, the effect of climate change on aerosols is further explored with anthropogenic emissions at future levels. Figure 2.7 shows how alterations in climate alone are predicted to affect inorganic aerosol concentrations with either (a) present-day or (b) future anthropogenic emission levels. Both columns represent the effect of climate change, but anthropogenic emissions are held at either present-day (column (a)) or future (column (b)) levels. For present-day emissions, column (a), the annually-averaged change in ammonium closely resembles that of sulfate, and most ammonium would likely be in the form of ammonium sulfate. At future emission levels, column (b), the absolute changes in sulfate are predicted to be muted as concentrations of sulfate are generally predicted to be lower. The relative change in sulfate for most of the Midwest and Southeast with either present-day or future anthropogenic emissions is on the order of 10% to 15%. However, with future emissions, the sulfate change in the Southwest becomes a larger relative amount at about 17%. With future

anthropogenic emissions ammonium changes more closely follow those of nitrate aerosol, and more ammonium is expected to be in the form of ammonium nitrate. With present-day emissions, nitrate decreases due to climate change are largest in the Midwest where nitrate concentrations are generally highest with present-day emissions. However, with future emissions, the largest magnitude decreases occur in the Southeast. Due to higher nitrate concentrations in the Southeast using future anthropogenic emissions, changes in nitrate are still roughly 25% in the Southeast near Texas for present-day or future emissions.

With either set of emissions, the Southeast is predicted to experience decreases in inorganic aerosol levels as a result of the climate change scenario considered here. With present-day emissions and climate change, the Midwest and Northeast would experience degraded air quality. With future emissions, air quality improvements in the Southeast that would occur solely as a result of climate change are reduced, but air quality degradation in the Midwest and Northeast is also reduced.

2.5.3 Effect of Changes in Anthropogenic Emissions Alone

This section addresses the extent to which changes in anthropogenic emissions of aerosol precursors between the present-day and 2050 would influence inorganic aerosol concentrations with present-day climate. Under the A1B scenario, anthropogenic NO_x emissions are predicted to increase 78% globally compared to the present-day but decrease approximately 35% in the United States (Table 2.1). Ammonia emissions are predicted to increase globally and domestically by 32% and 40%, respectively. SO_2 emissions are predicted to increase 31% globally but decrease 74% in the United States.

Sulfate concentrations in the U.S. are predicted to decrease in all seasons due to domestic reductions in SO_2 emissions (Figure 2.8). The largest decreases are predicted to occur in JJA and SON. Annually-averaged sulfate concentrations are predicted to decrease by as much as $3.25 \mu\text{g}/\text{m}^3$ in the Northeast. In contrast, global SO_2 emissions are projected to increase, which may have important implications for background aerosol levels in the U.S. and the EPA Regional Haze Rule.

Unlike sulfate, future nitrate aerosol concentrations are predicted to exhibit both increases and

decreases (Figure 2.8). Lower domestic NO_x emissions lead to a general decrease of total nitrate in the United States. The largest reductions in total nitrate are predicted to occur in JJA, with decreases up to 1.43 ppb (about $3.6 \mu\text{g}/\text{m}^3$ nitrate at STP). However, decreased sulfate levels coupled with increased ammonia emissions result in more ammonia available to react with nitrate. Total ammonia increases by as much as 1.9 ppb (about $1.3 \mu\text{g}/\text{m}^3 \text{NH}_3$ at STP) in JJA. As a result of higher total ammonia and reduced sulfate, nitrate aerosol concentrations can more than double. In some locations, the gas ratio increases from <1 (indicating ammonia-limited) to values >1 (nitric acid-limited). Nitrate aerosol decreases in the Midwest occur where the gas ratio indicates a present-day nitric acid-limited regime. Ammonium concentrations follow the trend in sulfate, except where ammonium reacts predominately with nitrate (DJF). In general, considering only emissions changes, U.S. levels of inorganic aerosols are predicted to be lower in the future than in the present-day. An exception occurs in winter when an increase in the total sulfate-nitrate-ammonium inorganic aerosol concentration on the order of $1 \mu\text{g}/\text{m}^3$ is predicted in some locations.

2.5.4 Effect of Changes in Both Climate and Anthropogenic Emissions

Predicted sulfate, nitrate, and ammonium concentration changes considering both future emissions and climate change (Figure 2.9) are similar to those due to emissions changes alone. For 2050 conditions, annual U.S. sulfate concentrations are predicted to decrease by up to $3.2 \mu\text{g}/\text{m}^3$, and ammonium decreases by up to $0.79 \mu\text{g}/\text{m}^3$. The percent decrease in sulfate, as high as 77%, is similar to the percent decrease in SO_2 emissions (74% in the U.S.). Ammonium decreases up to 61% in the Southeast which is higher than the percent increase in ammonia emissions (40% in the U.S.).

Nitrate increases in some areas by up to $1.67 \mu\text{g}/\text{m}^3$ and decreases in others by up to $0.43 \mu\text{g}/\text{m}^3$. Climate change slightly mitigates the effects of changes in anthropogenic emissions on nitrate levels.

Bauer et al. (2007) predicted nitrate aerosol levels for 2030 under the A1B scenario. The emission projections used by *Bauer et al.* (2007) involve a decrease in SO_2 and NO_x , as in the present study. Changes in nitrate aerosol concentrations in the U.S. predicted in that study are somewhat similar to those presented here, with a decrease in the Midwest and an increase in the Northeast. The

predictions differ in the southern U.S. where *Bauer et al.* (2007) predict a decrease in nitrate, whereas the present study predicts a slight increase.

2.6 Global Budgets of Sulfate, Nitrate, and Ammonium

2.6.1 Present-day Budgets

Table 2.4 shows the present-day global budget for sulfate aerosol. The present-day global burden of sulfate aerosol is predicted to be 0.28 Tg S. This estimate is at the lower end of predicted present-day sulfate burdens, as summarized by *Tsigaridis et al.* (2006), and slightly outside the range of burdens reported in AeroCom Experiment A [*Textor et al.*, 2006]. The effective wet deposition rate coefficient for this work is high compared to coefficients for the AeroCom models (but still within range), which contributes to the lower burden seen here. Differences in sulfate predictions can also result from different representations of precursor gas removal, chemical production, atmospheric transport, etc. [*Textor et al.*, 2006]. The sulfate lifetime predicted here (against total deposition) is within the range of those from AeroCom Experiment A. Under present-day conditions in this work, the global sulfate source is 32 Tg S/yr. The largest contribution, about 62% globally and annually averaged, is in-cloud oxidation of SO₂ by hydrogen peroxide (H₂O₂). In-cloud oxidation by ozone contributes 5% of the global source, gas-phase SO₂ oxidation is 26%, and sulfate production on submicrometer sea salt is 1%. Direct emission of sulfate aerosol represents 6% of global sulfate sources.

Nitrate and ammonium production listed in Table 2.5 represents the net production from gas-aerosol equilibrium partitioning. Aerosol nitrate is predicted to have a present-day global burden of 0.35 Tg and a lifetime of 7.6 days (against wet and dry deposition). The ammonium burden is 0.24 Tg with a lifetime of 3.7 days. The predicted nitrate burden compares well with previous GEOS-Chem simulations using assimilated meteorology, but sulfate and ammonium burdens are slightly lower than those in the work of *Park et al.* (2004) as a result of a shorter lifetime against deposition. Wet deposition is the dominant loss process for sulfate, nitrate, and ammonium, with over 80% of each species lost through wet processes.

The ammonium lifetime is shorter than that of nitrate since ammonium is associated with both sulfate and nitrate. Sulfate has a shorter lifetime than nitrate, which reflects the spatial distribution of its production in relation to removal by precipitation. Sulfate produced in-cloud is expected to have a much shorter lifetime than sulfate produced in the gas-phase (*Koch et al.*, 2003). Note that in GEOS-Chem, SO_2 dissolved in precipitation is converted to SO_4^{2-} when evaporation of that precipitation occurs. This source is included in the wet deposition row in Table 2.4; thus wet deposition represents the net wet removal as a result of rainout, washout, and scavenging in convective updrafts.

2.6.2 Effect of Changes in Climate Alone

Global burdens and budgets of sulfate, nitrate, and ammonium aerosol for future climate are presented in Tables 2.4 and 2.5. As in the study of *Mahowald et al.* (2006), the global sea salt source and burden are found to be relatively insensitive to climate change since sea salt emission and the global burden increase by less than 2%. The sulfate budget also changes imperceptibly with climate. In the work of *Liao et al.* (2006), simulating equilibrium climate under the A2 scenario in 2100 produced larger changes than those in this study, presumably as a result of more pronounced changes in climate. Gas-phase production of sulfate decreased while in-cloud formation increased by 5% in the work of *Liao et al.* (2006). Both *Liao et al.* (2006) and *Racherla and Adams* (2006) showed decreased sulfate burdens in the future due to climate change alone of 14% and 8% for 2100 and 2050 (A2 scenario), respectively.

The nitrate aerosol burden is predicted to decrease by about 21% between the present-day and future climate. This decrease is most likely a consequence of higher temperatures and increased partitioning to the gas phase. The lifetime of nitrate aerosol is also predicted to decrease to 6.6 days due to changes in wet removal. The decrease in nitrate burden compares well with that of other models using the A2 scenario which predict decreases in nitrate due to climate change alone varying from 13% to 47% (*Liao et al.*, 2006; *Racherla and Adams*, 2006). *Racherla and Adams* (2006) attribute the decrease in burdens and lifetimes of many PM species to increased wet deposition in

the future. *Liao et al.* (2006) found that more nitrate remains in the gas phase. In the present study, wet deposition of nitrate is predicted to decrease by about 11% in the future, and most of the future reduced nitrate burden results from less nitrate partitioning into the aerosol phase. However, increased precipitation in the future can play a role in reducing the lifetime of nitrate against deposition.

Changes in nitrate will influence ammonium. The burden, wet deposition, and production of ammonium are predicted to decrease by 5% to 6% in this study. Changes in ammonium here are milder than those predicted by *Racherla and Adams* (2006) and likely reflect the fact that the sulfate burden is relatively insensitive to climate change under the A1B scenario. The slight decrease in ammonium production may reflect the reduced nitrate burden. Both studies (this one and *Racherla and Adams* (2006)) predict a decrease in the global ammonium burden in the future.

2.6.3 Effect of Changes in Anthropogenic Emissions Alone

Sulfate, nitrate, and ammonium global burdens are predicted to change significantly in response to predicted changes in anthropogenic emissions (under present-day climate, Tables 2.4 and 2.5). The sulfate burden increases 39% to 0.39 Tg S as a result of higher global SO₂ emissions. Gas-phase formation of SO₄²⁻ increases 79% and represents 35% of sulfate production (compared to 26% in the present-day). Sulfate production by aqueous H₂O₂ reaction also increases by about 21%, but O₃ aqueous production decreases almost 59%. *Liao et al.* (2006) also indicate that with future emissions, in-cloud production from reaction with O₃ will decrease. Present-day in-cloud production by reaction with O₃ is largest over North America and Europe and these regions are projected to have lower SO₂ emissions in the future. Despite increases in both wet and dry deposition of sulfate, the sulfate lifetime increases slightly compared to the present-day to 3.4 days. Globally, higher NO_x and ammonia emissions lead to the nitrate aerosol burden increasing 28% compared to the present-day. Both nitrate production and wet deposition increase in magnitude, and the nitrate lifetime decreases from 7.6 to 5.8 days. The ammonium burden increases 53% to 0.37 Tg, but the ammonium lifetime remains relatively constant at 3.7 days. All source and loss processes increase

in magnitude for ammonium and nitrate aerosol.

2.6.4 Effect of Changes in Both Climate and Anthropogenic Emissions

Most studies show the future sulfate burden following the global change in SO₂ emissions (*Liao et al.*, 2006; *Bauer et al.*, 2007; *Shindell et al.*, 2007). In contrast, for the B1 scenario in 2030, *Unger et al.* (2006) calculated an increased sulfate burden despite decreased global SO₂ emissions; this effect was attributed to emissions shifting to subtropical regions with higher oxidation rates and lower wet deposition. The predicted sulfate burden change in the present study is larger for changes in both climate and emissions together than for either change alone (Table 2.4). Changes in the sulfate production and loss processes are dominated by the effects of changes in SO₂ emissions alone, but the effects of climate change and emissions together on gas-phase production of sulfate are not additive. The sulfate lifetime increases slightly over the control case by 0.3 days.

The aerosol nitrate burden is predicted to remain relatively constant at 0.35 Tg considering combined changes in climate and emissions (Table 2.5). However, the nitrate lifetime decreases significantly to 5.1 days. Formation increases due to higher precursor (NO_x and NH₃) emissions but decreases due to higher temperatures; the two effects effectively compensate for each other in terms of the global burden. For other scenarios or models, one effect may dominate over the other (*Liao et al.*, 2006; *Bauer et al.*, 2007). *Shindell et al.* (2007) calculated that the nitrate burden (excluding nitrate on dust) was approximately the same in 2030 and 2050 but slightly lower than that in the present-day under A1B despite increasing global NO_x and NH₃ emissions. The assumed increase in NH₃ emissions was much smaller in the work of *Shindell et al.* (2007) than in other studies (*Adams et al.*, 2001; *Liao and Seinfeld*, 2005; *Liao et al.*, 2006; *Bauer et al.*, 2007). *Bauer et al.* (2007) (A1B 2030) determined that future nitrate depends most strongly on changes in ammonia emissions between the present and 2030. Studies that consider only emissions changes and not the effects of climate change on future nitrate levels show a quadrupling of the nitrate global burden in 2100 under the A2 scenario (*Adams et al.*, 2001; *Liao and Seinfeld*, 2005). The current study highlights the need to consider the effect of climate change when predicting future aerosol levels.

For ammonium, the global burden increase under both climate and emission changes is primarily due to increased anthropogenic NH_3 emissions with some dampening from climate change. The lifetime of ammonium is predicted to remain relatively constant due to an increased burden and an increased rate of production.

2.7 Implications for Eastern U.S. Outflow

In this section, the effect of changes in climate and emissions on sulfur outflow from the U.S. East Coast are examined. SO_2 and SO_4^{2-} in U.S. outflow were chosen for further examination since pollution transport has been shown to affect sulfate concentrations over the Atlantic Ocean and on different continents (*Park et al.*, 2004; *Benkovitz et al.*, 2006; *Heald et al.*, 2006; *Chin et al.*, 2007; *Koch et al.*, 2007; *Liu et al.*, 2008). The effect of long-range transport on nitrate concentrations (*Park et al.*, 2004) is less well known. To quantify the outflow of sulfur from the U.S., the rate of transport of sulfur is obtained at 67.5° W from 26° to 50° N (Figure 2.10). Note that some pollution from Canada will also be included in this outflow. For the present-day simulations performed here, the largest seasonal SO_x ($\text{SO}_x = \text{SO}_2 + \text{SO}_4^{2-}$) outflow rate across this plane occurs during DJF followed by MAM. Exported SO_x tends to have significant contributions of SO_4^{2-} and SO_2 although SO_2 usually dominates in winter and SO_4^{2-} can dominate in summer reflecting the shift in photochemistry and SO_4^{2-} production in the U.S. DJF also experiences particularly strong westerlies (Figure 2.5), which can lead to higher rates of export than in other seasons.

Table 2.6 shows the annually averaged and DJF seasonal transport rates of SO_2 , SO_4^{2-} , and SO_x across 67.5° W from 26° to 50° N for the present-day and future. The table also shows how the transport is predicted to change in the future due to changes in climate and emissions combined. Outflow of SO_2 and SO_4^{2-} decreases in the future annually as well as during DJF as a result of lower SO_2 emissions and weaker DJF westerlies. The changes in SO_x outflow are substantial; export is reduced 45% on an annual basis and 49% during DJF.

2.8 Conclusions

Changes in both climate and emissions will influence future inorganic aerosol (sulfate, nitrate, and ammonium) concentrations. The atmospheric chemical transport model, GEOS-Chem, driven by meteorology from the GISS GCM, allows for the separation of the effects of changes in climate from those in emissions. The GEOS-Chem/GISS framework with the inorganic gas-aerosol equilibrium model, ISORROPIA II, generally provides a good representation of present-day sulfate, nitrate, and ammonium levels in the United States; an exception is the under-prediction of nitrate in the western United States. Ammonia inventories represent a significant source of uncertainty for nitrate aerosol predictions, but sensitivity tests indicate that changes to the NH_3 inventory alone will likely not correct nitrate estimates in the West.

Future changes in meteorological parameters such as precipitation are somewhat uncertain. This work is intended to give an indication of how sulfate, nitrate, and ammonium aerosols may respond to future climate for the A1B scenario in 2050 and some meteorological changes that may be important for aerosols in this, and other scenarios. Climate change alone is predicted to impact aerosol concentrations with different climatic changes being important in different seasons. In some seasons, like winter, many different species show a similar pattern and one meteorological change appears to dominate changes in aerosol concentrations, whereas in other seasons, like summer, a single controlling factor cannot be isolated. Although aerosols are particularly sensitive to changes in precipitation, changes in precipitation are not always the governing factor for changes in concentrations.

Simulations based on projected future emissions indicate that higher PM levels may occur in winter (DJF) due to increased nitrate aerosol, but domestic SO_2 emission reductions will have benefits in all seasons. This study highlights the important role of ammonia emissions in determining inorganic aerosol levels. Allowing ammonia to increase while reducing sulfate partially negates some advantages of SO_2 controls.

Studies summarized by the *IPCC* (2007) indicate that extreme meteorological events can be expected to become more prevalent in the future. Although the study here focuses on seasonally and annually averaged concentrations, the effects of climate change on short-term, high concentration

events merits examination. High concentration events may show trends different from those examined here as they are likely to reflect changes in episodic events. In addition, under the emission scenario considered here (A1B) domestic emissions of NO_x and SO_2 are predicted to decrease while global emissions increase. The result of domestic SO_2 emissions reductions will have benefits for the North Atlantic and other regions that receive U.S. pollution outflow. The implications of climate and emissions changes on intercontinental transport should be further examined.

2.9 Acknowledgements

This work was supported by the U.S. Environmental Protection Agency's STAR Program (grants RD830959 and RD833370). Havala Pye was supported by a National Science Foundation Graduate Research Fellowship. Hong Liao acknowledges the support from National Natural Science Foundation of China (grant 40775083). We would like to acknowledge the Clean Air Status and Trends Network (CASTNET). Discussions with Becky Alexander, Athanasios Nenes, Yang Zhang, and Donald Dabdub are greatly appreciated.

Bibliography

- Adams, P. J., J. H. Seinfeld, D. Koch, L. Mickley, and D. Jacob (2001), General circulation model assessment of direct radiative forcing by the sulfate-nitrate-ammonium-water inorganic aerosol system, *J. Geophys. Res.*, *106*(D1), 1097–1111.
- Alexander, B., R. J. Park, D. J. Jacob, Q. B. Li, R. M. Yantosca, J. Savarino, C. C. W. Lee, and M. H. Thiemens (2005), Sulfate formation in sea-salt aerosols: Constraints from oxygen isotopes, *J. Geophys. Res.*, *110*, D10307, doi:10.1029/2004JD005659.
- Ames, R. B., and W. C. Malm (2001), Comparison of sulfate and nitrate particle mass concentrations measured by IMPROVE and the CDN, *Atmos. Environ.*, *35*(5), 905–916, doi:10.1016/S1352-2310(00)00369-1.

- Ansari, A. S., and S. N. Pandis (1998), Response of inorganic PM to precursor concentrations, *Environ. Sci. Technol.*, *32*(18), 2706–2714.
- Ansari, A. S., and S. N. Pandis (2000), Water absorption by secondary organic aerosol and its effect on inorganic aerosol behavior, *Environ. Sci. Technol.*, *34*(1), 71–77.
- Aw, J., and M. J. Kleeman (2003), Evaluating the first-order effect of intraannual temperature variability on urban air pollution, *J. Geophys. Res.*, *108*(D12), 4365, doi:10.1029/2002JD002688.
- Bauer, S. E., D. Koch, N. Unger, S. M. Metzger, D. T. Shindell, and D. G. Streets (2007), Nitrate aerosols today and in 2030: A global simulation including aerosols and tropospheric ozone, *Atmos. Chem. Phys.*, *7*(19), 5043–5059.
- Benkovitz, C. M., S. E. Schwartz, M. P. Jensen, and M. A. Miller (2006), Attribution of modeled atmospheric sulfate and SO₂ in the Northern Hemisphere for June–July 1997, *Atmos. Chem. Phys.*, *6*, 4723–4738.
- Bey, I., D. J. Jacob, R. M. Yantosca, J. A. Logan, B. D. Field, A. M. Fiore, Q. B. Li, H. G. Y. Liu, L. J. Mickley, and M. G. Schultz (2001), Global modeling of tropospheric chemistry with assimilated meteorology: Model description and evaluation, *J. Geophys. Res.*, *106*(D19), 23,073–23,095.
- Bouwman, A. F., D. S. Lee, W. A. H. Asman, F. J. Dentener, K. W. VanderHoek, and J. G. J. Olivier (1997), A global high-resolution emission inventory for ammonia, *Global Biogeochem. Cycles*, *11*(4), 561–587.
- Chin, M., T. Diehl, P. Ginoux, and W. Malm (2007), Intercontinental transport of pollution and dust aerosols: Implications for regional air quality, *Atmos. Chem. Phys.*, *7*(21), 5501–5517.
- Chung, S. H., and J. H. Seinfeld (2002), Global distribution and climate forcing of carbonaceous aerosols, *J. Geophys. Res.*, *107*(D19), 4407, doi:10.1029/2001JD001397.
- Corbett, J. J., P. S. Fischbeck, and S. N. Pandis (1999), Global nitrogen and sulfur inventories for oceangoing ships, *J. Geophys. Res.*, *104*(D3), 3457–3470.

- Dawson, J. P., P. J. Adams, and S. N. Pandis (2007), Sensitivity of $\text{PM}_{2.5}$ to climate in the eastern U.S.: a modeling case study, *Atmos. Chem. Phys.*, *7*(16), 4295–4309.
- de Gouw, J. A., et al. (2005), Budget of organic carbon in a polluted atmosphere: Results from the New England Air Quality Study in 2002, *J. Geophys. Res.*, *110*, D16305, doi:10.1029/2004JD005623.
- de Gouw, J. A., et al. (2008), Sources of particulate matter in the northeastern United States in summer: 1. Direct emissions and secondary formation of organic matter in urban plumes, *J. Geophys. Res.*, *113*, D08301, doi:10.1029/2007JD009243.
- Dockery, C., A. Pope, X. Xu, J. D. Spengler, J. H. Ware, M. E. Fay, B. G. Ferris, and F. E. Speizer (1993), An association between air pollution and mortality in six U.S. cities, *N. Engl. J. Med.*, *329*(24), 1753–1759.
- Evans, M. J., and D. J. Jacob (2005), Impact of new laboratory studies of N_2O_5 hydrolysis on global model budgets of tropospheric nitrogen oxides, ozone, and OH, *Geophys. Res. Lett.*, *32*, L09813, doi:10.1029/2005GL022469.
- Fountoukis, C., and A. Nenes (2007), ISORROPIA II: A computationally efficient thermodynamic equilibrium model for K^+ - Ca^{2+} - Mg^{2+} - NH_4^+ - Na^+ - SO_4^{2-} - NO_3^- - Cl^- - H_2O aerosols, *Atmos. Chem. Phys.*, *7*(17), 4639–4659.
- Gilliland, A. B., R. L. Dennis, S. J. Roselle, and T. E. Pierce (2003), Seasonal NH_3 emission estimates for the eastern United States based on ammonium wet concentrations and an inverse modeling method, *J. Geophys. Res.*, *108*(D15), 4477, doi:10.1029/2002JD003063.
- Gilliland, A. B., K. W. Appel, R. W. Pinder, and R. L. Dennis (2006), Seasonal NH_3 emissions for the continental United States: Inverse model estimation and evaluation, *Atmos. Environ.*, *40*(26), 4986–4998, doi:10.1016/J.ATMOSENV.2005.12.066.
- Guenther, A., C. N. Hewitt, D. Erickson, R. Fall, C. Geron, T. Graedel, P. Harley, L. Klinger, M. Lerdau, W. A. McKay, T. Pierce, B. Scholes, R. Steinbrecher, R. Tallamraju, J. Taylor, and

- P. Zimmerman (1995), A global-model of natural volatile organic-compound emissions, *J. Geophys. Res.*, *100*(D5), 8873–8892.
- Heald, C. L., D. J. Jacob, R. J. Park, L. M. Russell, B. J. Huebert, J. H. Seinfeld, H. Liao, and R. J. Weber (2005), A large organic aerosol source in the free troposphere missing from current models, *Geophys. Res. Lett.*, *32*, L18809, doi:10.1029/2005GL023831.
- Heald, C. L., D. J. Jacob, R. J. Park, B. Alexander, T. D. Fairlie, R. M. Yantosca, and D. A. Chu (2006), Transpacific transport of Asian anthropogenic aerosols and its impact on surface air quality in the United States, *J. Geophys. Res.*, *111*, D14310, doi:10.1029/2005JD006847.
- Held, I. M., and B. J. Soden (2000), Water vapor feedback and global warming, *Annu. Rev. Energy Environ.*, *25*, 441–475, doi:10.1146/ANNUREV.ENERGY.25.1.441.
- Henze, D. K., and J. H. Seinfeld (2006), Global secondary organic aerosol from isoprene oxidation, *Geophys. Res. Lett.*, *33*, L09812, doi:10.1029/2006GL025976.
- Henze, D. K., J. H. Seinfeld, N. L. Ng, J. H. Kroll, T. M. Fu, D. J. Jacob, and C. L. Heald (2008a), Global modeling of secondary organic aerosol formation from aromatic hydrocarbons: High- vs. low-yield pathways, *Atmos. Chem. Phys.*, *8*(9), 2405–2420.
- Henze, D. K., J. H. Seinfeld, and D. Shindell (2008b), Inverse modeling and mapping US air quality influences of inorganic PM_{2.5} precursor emissions using the adjoint of GEOS-Chem, *Atmos. Chem. Phys. Discuss.*, *8*(4), 15,031–15,099.
- Intergovernmental Panel on Climate Change (IPCC) (2007), *Climate Change 2007: The Physical Science Basis*, Cambridge Univ. Press, Cambridge, UK.
- Jacob, D. J. (2000), Heterogeneous chemistry and tropospheric ozone, *Atmos. Environ.*, *34*(12-14), 2131–2159, doi:10.1016/S1352-2310(99)00462-8.
- Jacob, D. J., B. D. Field, E. M. Jin, I. Bey, Q. B. Li, J. A. Logan, R. M. Yantosca, and H. B. Singh (2002), Atmospheric budget of acetone, *J. Geophys. Res.*, *107*(D10), 4100, doi:10.1029/2001JD000694.

- Jacob, D. J., and D. A. Winner (2008), Effect of climate change on air quality, *Atmos. Environ.*, submitted.
- Karydis, V. A., A. P. Tsimpidi, and S. N. Pandis (2007), Evaluation of a three-dimensional chemical transport model (PMCAMx) in the eastern United States for all four seasons, *J. Geophys. Res.*, *112*, D14211, doi:10.1029/2006JD007890.
- Kleeman, M. J., and G. R. Cass (2001), A 3D Eulerian source-oriented model for an externally mixed aerosol, *Environ. Sci. Technol.*, *35*(24), 4834–4848, doi:10.1021/ES010996m.
- Koch, D., J. Park, and A. Del Genio (2003), Clouds and sulfate are anticorrelated: A new diagnostic for global sulfur models, *J. Geophys. Res.*, *108*(D24), 4781, doi:10.1029/2003JD003621.
- Koch, D., T. C. Bond, D. Streets, N. Unger, and G. R. van der Werf (2007), Global impacts of aerosols from particular source regions and sectors, *J. Geophys. Res.*, *112*, D02205, doi:10.1029/2005JD007024.
- Leung, L. R., and W. I. Gustafson (2005), Potential regional climate change and implications to U.S. air quality, *Geophys. Res. Lett.*, *32*, L16711, doi:10.1029/2005GL022911.
- Levy, H., M. D. Schwarzkopf, L. Horowitz, V. Ramaswamy, and K. L. Findell (2008), Strong sensitivity of late 21st century climate to projected changes in short-lived air pollutants, *J. Geophys. Res.*, *113*, D06102, doi:10.1029/2007JD009176.
- Liao, H., and J. H. Seinfeld (2005), Global impacts of gas-phase chemistry-aerosol interactions on direct radiative forcing by anthropogenic aerosols and ozone, *J. Geophys. Res.*, *110*, D18208, doi:10.1029/2005JD005907.
- Liao, H., W. T. Chen, and J. H. Seinfeld (2006), Role of climate change in global predictions of future tropospheric ozone and aerosols, *J. Geophys. Res.*, *111*, D12304, doi:10.1029/2005JD006852.
- Liao, H., D. K. Henze, J. H. Seinfeld, S. L. Wu, and L. J. Mickley (2007), Biogenic secondary organic aerosol over the United States: Comparison of climatological simulations with observations, *J. Geophys. Res.*, *112*, D06201, doi:10.1029/2006JD007813.

- Liu, J., D. L. Mauzerall, and L. W. Horowitz (2008), Source-receptor relationships between East Asian sulfur dioxide emissions and Northern Hemisphere sulfate concentrations, *Atmos. Chem. Phys.*, *8*(14), 3721–3733.
- Mahowald, N. M., J. F. Lamarque, X. X. Tie, and E. Wolff (2006), Sea-salt aerosol response to climate change: Last Glacial Maximum, preindustrial, and doubled carbon dioxide climates, *J. Geophys. Res.*, *111*, D05303, doi:10.1029/2005JD006459.
- Martin, R. V., D. J. Jacob, R. M. Yantosca, M. Chin, and P. Ginoux (2003), Global and regional decreases in tropospheric oxidants from photochemical effects of aerosols, *J. Geophys. Res.*, *108*(D3), 4097, doi:10.1029/2002JD002622.
- Mendoza-Dominguez, A., and A. G. Russell (2001), Emission strength validation using four-dimensional data assimilation: Application to primary aerosol and precursors to ozone and secondary aerosol, *J. Air Waste Manage. Assoc.*, *51*(11), 1538–1550.
- Meng, Z. Y., and J. H. Seinfeld (1996), Time scales to achieve atmospheric gas-aerosol equilibrium for volatile species, *Atmos. Environ.*, *30*(16), 2889–2900, doi:10.1016/1352-2310(95)00493-9.
- Mhyre, G., A. Grini, and S. Metzger (2006), Modelling of nitrate and ammonium-containing aerosols in presence of sea salt, *Atmos. Chem. Phys.*, *6*(12), 4809–4821.
- Mickley, L. J., D. J. Jacob, B. D. Field, and D. Rind (2004), Effects of future climate change on regional air pollution episodes in the United States, *Geophys. Res. Lett.*, *31*, L24103, doi:10.1029/2004GL021216.
- Monahan, E. C., D. E. Spiel, and K. L. Davidson (1986), *Oceanic Whitecaps and Their Role in Air-Sea Exchange Processes*, A model of marine aerosol generation via whitecaps and wave disruption, edited by E. C. Monahan and G. M. Niocaill, pp.167-174, D. Riedel, Norwall, Mass.
- Morris, R., B. Koo, and G. Yarwood (2005), Evaluation of multisectional and two-section particulate matter photochemical grid models in the western United States, *J. Air Waste Manage. Assoc.*, *55*(11), 1683–1693.

- Nakicenovic, N., and R. Swart (2000), *Special Report on Emissions Scenarios*, Cambridge Univ. Press, Cambridge, UK.
- Nightingale, P. D., P. S. Liss, and P. Schlosser (2000), Measurements of air-sea gas transfer during an open ocean algal bloom., *Geophys. Res. Lett.*, *27*(14), 2117–2120.
- Park, R. J., D. J. Jacob, B. D. Field, R. M. Yantosca, and M. Chin (2004), Natural and transboundary pollution influences on sulfate-nitrate-ammonium aerosols in the United States: Implications for policy, *J. Geophys. Res.*, *109*, D15204, doi:10.1029/2003JD004473.
- Park, R. J., D. J. Jacob, N. Kumar, and R. M. Yantosca (2006), Regional visibility statistics in the United States: Natural and transboundary pollution influences, and implications for the Regional Haze Rule, *Atmos. Environ.*, *40*(28), 5405–5423, doi:10.1016/J.ATMOSENV.2006.04.059.
- Pickering, K. E., Y. Wang, W.-K. Tao, C. Price, and J. F. Muller (1998), Vertical distributions of lightning NO_x for use in regional and global chemical transport models, *J. Geophys. Res.*, *103*(D23), 31,203–31,216.
- Pinder, R. W., P. J. Adams, S. N. Pandis, and A. B. Gilliland (2006), Temporally resolved ammonia emission inventories: Current estimates, evaluation tools, and measurement needs, *J. Geophys. Res.*, *111*, D16310, doi:10.1029/2005JD006603.
- Price, C., and D. Rind (1992), A simple lightning parameterization for calculating global lightning distributions, *J. Geophys. Res.*, *97*(D9), 9919–9933.
- Racherla, P. N., and P. J. Adams (2006), Sensitivity of global tropospheric ozone and fine particulate matter concentrations to climate change, *J. Geophys. Res.*, *111*, D24103, doi:10.1029/2005JD006939.
- Rae, J. G. L., C. E. Johnson, N. Bellouin, O. Boucher, J. M. Haywood, and A. Jones (2007), Sensitivity of global sulphate aerosol production to changes in oxidant concentrations and climate, *J. Geophys. Res.*, *112*, D10312, doi:10.1029/2006JD007826.

- Rind, D., J. Lerner, J. Jonas, and C. McLinden (2007), Effects of resolution and model physics on tracer transports in the NASA Goddard Institute for Space Studies general circulation models, *J. Geophys. Res.*, *112*, D09315, doi:10.1029/2006JD007476.
- Saltzman, E. S., D. B. King, K. Holmen, and C. Leck (1993), Experimental-determination of the diffusion-coefficient of dimethylsulfide in water, *J. Geophys. Res.*, *98*(C9), 16,481–16,486.
- Schmidt, G. A., et al. (2006), Present-day atmospheric simulations using GISS ModelE: Comparison to in situ, satellite, and reanalysis data, *J. Climate*, *19*(2), 153–192.
- Seinfeld, J. H., and S. N. Pandis (2006), *Atmospheric Chemistry and Physics: From Air Pollution to Climate Change*, 2nd Edition, John Wiley and Sons, Inc., New York, NY.
- Shindell, D. T., G. Faluvegi, S. E. Bauer, D. M. Koch, N. Unger, S. Menon, R. L. Miller, G. A. Schmidt, and D. G. Streets (2007), Climate response to projected changes in short-lived species under an A1B scenario from 2000-2050 in the GISS climate model, *J. Geophys. Res.*, *112*, D20103, doi:10.1029/2007JD008753.
- Streets, D. G., T. C. Bond, T. Lee, and C. Jang (2004), On the future of carbonaceous aerosol emissions, *J. Geophys. Res.*, *109*, D24212, doi:10.1029/2004JD004902.
- Tagaris, E., K. Manomaiphiboon, K. J. Liao, L. R. Leung, J. H. Woo, S. He, P. Amar, and A. G. Russell (2007), Impacts of global climate change and emissions on regional ozone and fine particulate matter concentrations over the United States, *J. Geophys. Res.*, *112*, D14312, doi:10.1029/2006JD008262.
- Textor, C., et al. (2006), Analysis and quantification of the diversities of aerosol life cycles within AeroCom, *Atmos. Chem. Phys.*, *6*, 1777–1813.
- Tsigaridis, K., M. Krol, F. J. Dentener, Y. Balkanski, J. Lathiere, S. Metzger, D. A. Hauglustaine, and M. Kanakidou (2006), Change in global aerosol composition since preindustrial times, *Atmos. Chem. Phys.*, *6*, 5143–5162.

- Unger, N., D. T. Shindell, D. M. Koch, M. Amann, J. Cofala, and D. G. Streets (2006), Influences of man-made emissions and climate changes on tropospheric ozone, methane, and sulfate at 2030 from a broad range of possible futures, *J. Geophys. Res.*, *111*, D12313, doi:10.1029/2005JD006518.
- Volkamer, R., J. L. Jimenez, F. San Martini, K. Dzepina, Q. Zhang, D. Salcedo, L. T. Molina, D. R. Worsnop, and M. J. Molina (2006), Secondary organic aerosol formation from anthropogenic air pollution: Rapid and higher than expected, *Geophys. Res. Lett.*, *33*, L17811, doi:10.1029/2006GL026899.
- Wang, J., A. A. Hoffman, R. J. Park, D. Jacob, and S. T. Martin (2008), Global distribution of solid and aqueous sulfate aerosols: Effect of the hysteresis of particle phase transitions, *J. Geophys. Res.*, *113*, D11206, doi:10.1029/2007JD009367.
- Wang, Y. H., D. J. Jacob, and J. A. Logan (1998), Global simulation of tropospheric O₃-NO_x-hydrocarbon chemistry 1. Model formulation, *J. Geophys. Res.*, *103*(D9), 10,713–10,725.
- Wesely, M. L. (1989), Parameterization of surface resistances to gaseous dry deposition in regional-scale numerical-models, *Atmos. Environ.*, *23*(6), 1293–1304, doi:10.1016/0004-6981(89)90153-4.
- Wu, S. L., L. J. Mickley, D. J. Jacob, J. A. Logan, R. M. Yantosca, and D. Rind (2007), Why are there large differences between models in global budgets of tropospheric ozone?, *J. Geophys. Res.*, *112*(D5), D05302, doi:10.1029/2006JD007801.
- Wu, S. L., L. J. Mickley, E. M. Leibensperger, D. J. Jacob, D. Rind, and D. G. Streets (2008), Effects of 2000-2050 global change on ozone air quality in the United States, *J. Geophys. Res.*, *113*, D06302, doi:10.1029/2007JD008917.
- Yienger, J. J., and H. Levy (1995), Empirical-model of global soil-biogenic NO_x emissions, *J. Geophys. Res.*, *100*(D6), 11,447–11,464.
- Yu, S. C., R. Dennis, S. Roselle, A. Nenes, J. Walker, B. Eder, K. Schere, J. Swall, and W. Rorabarge (2005), An assessment of the ability of three-dimensional air quality models with current

thermodynamic equilibrium models to predict aerosol NO_3^- , *J. Geophys. Res.*, *110*, D07S13, doi:10.1029/2004JD004718.

Zhang, L. M., S. L. Gong, J. Padro, and L. Barrie (2001), A size-segregated particle dry deposition scheme for an atmospheric aerosol module, *Atmos. Environ.*, *35*(3), 549–560, doi:10.1016/S1352-2310(00)00326-5.

Table 2.1: Present-day and 2050 predicted (IPCC A1B scenario) emissions of aerosol precursors.

Species	Global		U.S. ^a	
	2000	2050	2000	2050
NO _x (Tg N/yr)				
aircraft	0.5	0.5	0.11	0.11
anthropogenic	23.7	47.9	6.11	3.88
biomass burning	6.5	8.1	0.05	0.08
biofuel	2.2	2.1	0.01	0.01
fertilizer	0.5	0.9	0.05	0.06
NH ₃ (Tg N/yr)				
anthropogenic	33.3	50.5	2.11	3.31
biomass burning	5.9	6.1	0.05	0.05
biofuel	1.6	1.7	0.18	0.16
natural	14.2	14.2	0.58	0.58
SO ₂ (Tg S/yr)				
aircraft	0.1	0.1	0.02	0.02
anthropogenic	61.2	81.8	9.24	2.35
biomass burning	1.2	2.0	0.01	0.03
biofuel	0.3	0.3	<0.01	<0.01
volcanos	5.5	5.5	0.07	0.07
ships	4.2	5.4	–	–
SO ₄ ²⁻ (Tg S/yr)				
anthropogenic	2.0	2.6	0.16	0.04

^aU.S. emissions are for the contiguous states only.

Table 2.2: Predicted changes in natural emissions due to predicted climate change (IPCC A1B scenario).

Species	Global		U.S. ^a	
	2000	2050	2000	2050
DMS (Tg S/yr)	16.0	16.0	–	–
NO _x (Tg N/yr)				
lightning	4.7	5.6	0.08	0.09
soil	5.9	6.4	0.36	0.40
Seasalt (Tg/yr)				
accumulation	71.5	72.5	–	–
coarse	5322.0	5395.3	–	–
Biogenic HCs ^b (Tg C/yr)	631.9	778.2	42.37	52.06

^aU.S. emissions are for the contiguous states only.

^bIsoprene, monoterpenes, acetone, other alkenes

Table 2.3: Implications of changes in meteorological parameters from 2000 to 2050 for inorganic aerosol concentrations over the United States.

Season	Meteorological parameter	Major implications for aerosols ^a
DJF	Precipitation	Increased wet deposition of species over MW and SE ^b
	Temperature	Nitrate decreases (noticeably in SE) as it partitions to nitric acid
	Zonal wind	Slower transport in MW leads to increased concentrations in MW; reduced transport of aerosols and precursors to the NE
	Meridional wind PBL	Faster transport away from NE and concentrations decrease Concentrations increase in MW and SE
MAM	Precipitation	Increased wet deposition of aerosols and/or soluble precursor gases and decreased aerosol concentrations
JJA	Temperature	Nitrate decreases as it partitions to nitric acid, higher biogenic emissions influence HO _x
	Humidity	Favors higher HO _x production, catalyzes H ₂ O ₂ formation and leads to more sulfate formation
	PBL	Indicates reduced surface ventilation but effect does not appear to be dominant
	Precipitation	Reduces concentrations along east coast
SON	Temperature	Nitrate decreases as it partitions to nitric acid
	Humidity	Leads to more sulfate formation
	PBL	Concentrations in MW and NE increase due to reduced ventilation, sulfate decreases in SE
	Cyclone frequency	More frequent stagnation (<i>Wu et al.</i> , 2008) suspected to lead to increased concentrations in MW
	Convective flux	Decreased ventilation favors increased concentrations; important for sulfate
	Precipitation	Contributing factor for concentration decreases in the SE and increases in the NE
SON	Temperature	Nitrate decreases as it partitions to gas phase
	Zonal wind	Faster transport away from Midwest, aerosols and precursors transported to the NE
	Convective flux/vertical transport	Contributing factor for concentration decreases in the SE and increases in the NE

^aSee Figure 2.6 for predicted changes in aerosol concentrations.^bMW: Midwest, SE: Southeast, NE: Northeast

Table 2.4: Global sulfate budget.

	2000 Climate 2000 Emissions	2050 Climate 2000 Emissions	2000 Climate 2050 Emissions	2050 Climate 2050 Emissions
Burden (Tg S)	0.28	0.28	0.39	0.40
Emission (Tg S/yr)	2.04	2.04	2.62	2.62
Production (Tg S/yr)				
Gas-phase	8.24	8.15	14.74	14.92
H ₂ O ₂ in-cloud	19.53	19.37	23.70	23.17
O ₃ in-cloud	1.54	1.52	0.63	0.57
On fine sea salt	0.16	0.16	0.16	0.16
Deposition (Tg S/yr)				
Wet	28.72	28.35	37.91	37.31
Dry	2.80	2.89	3.95	4.14
Lifetime (days)	3.2	3.3	3.4	3.5

Table 2.5: Global budgets of nitrate and ammonium aerosol. Budgets are for present-day and future climate (2000C, 2050C) and present-day and future emissions (2000E, 2050E).

	Nitrate				Ammonium			
	2000C	2050C	2000C	2050C	2000C	2050C	2000C	2050C
	2000E	2000E	2050E	2050E	2000E	2000E	2050E	2050E
Burden (Tg)	0.35	0.27	0.44	0.35	0.24	0.23	0.37	0.36
Production (Tg/yr)	16.8	15.1	28.0	24.8	24.3	23.1	37.0	35.4
Wet deposition (Tg/yr)	13.7	12.2	23.1	20.3	21.1	19.9	32.2	30.5
Dry deposition (Tg/yr)	3.1	2.9	5.0	4.6	3.2	3.2	4.8	4.9
Lifetime (days)	7.6	6.6	5.8	5.1	3.7	3.6	3.7	3.7

Table 2.6: Annually averaged and wintertime outflow in kgS/s of SO_x from the Eastern U.S. (location depicted in Figure 2.10) for the present-day (1999-2001) and future (2049-2050) considering both changes in climate and emissions. The percent change (in %) between the present-day and future is shown in right column.

	Present-day	Future	Percent Change
Annual (kgS/s)			
SO_2	38	19	-51%
SO_4^{2-}	27	17	-37%
SO_x	65	35	-45%
DJF (kgS/s)			
SO_2	78	33	-58%
SO_4^{2-}	36	26	-29%
SO_x	115	59	-49%

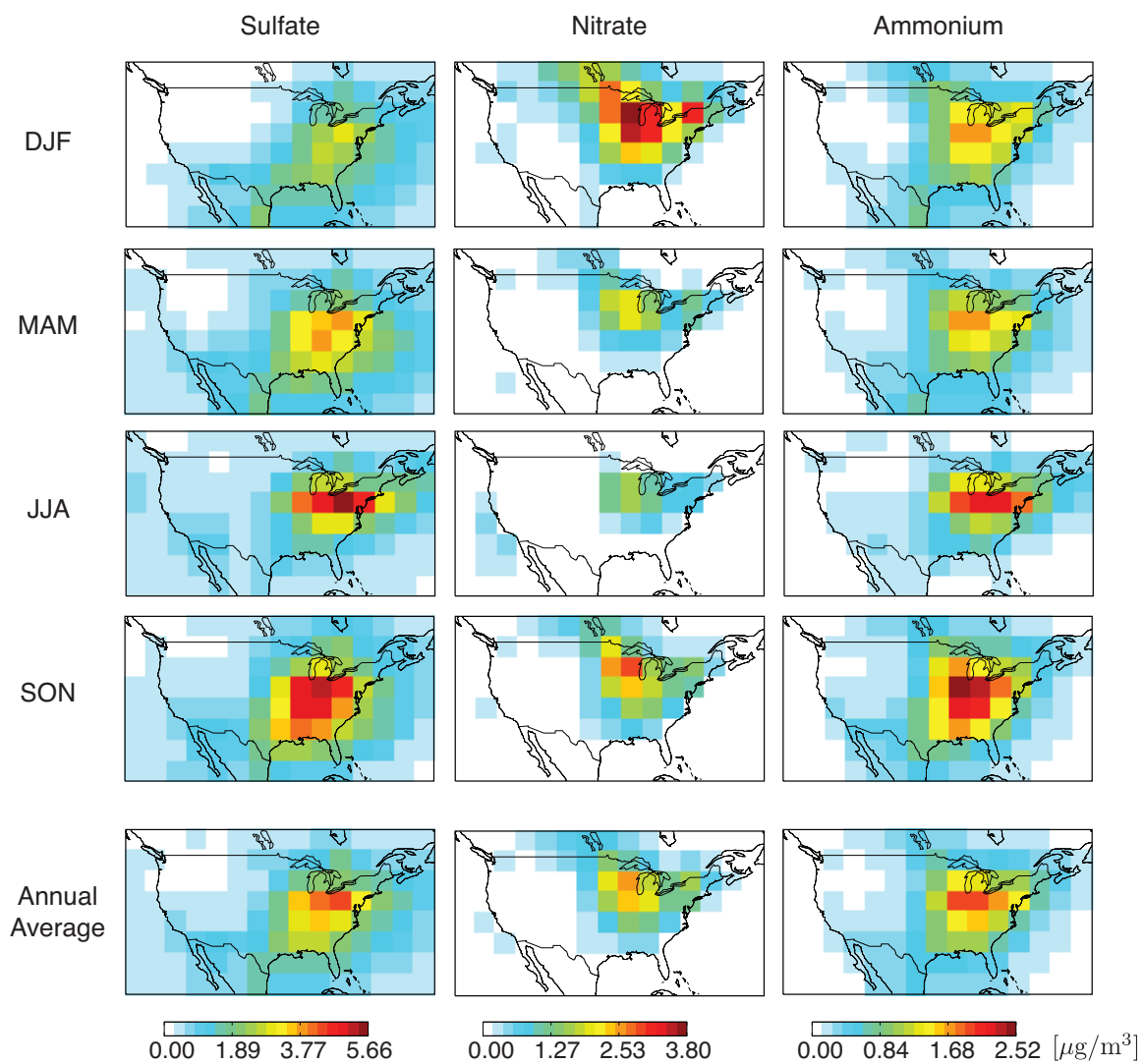


Figure 2.1: Present-day (year 1999-2001 meteorology and emissions) predictions of surface-level sulfate, nitrate, and ammonium aerosols for the United States. Each of the first four rows is a seasonal average (DJF, MAM, JJA, SON) and the bottom row is the annual average over three years.

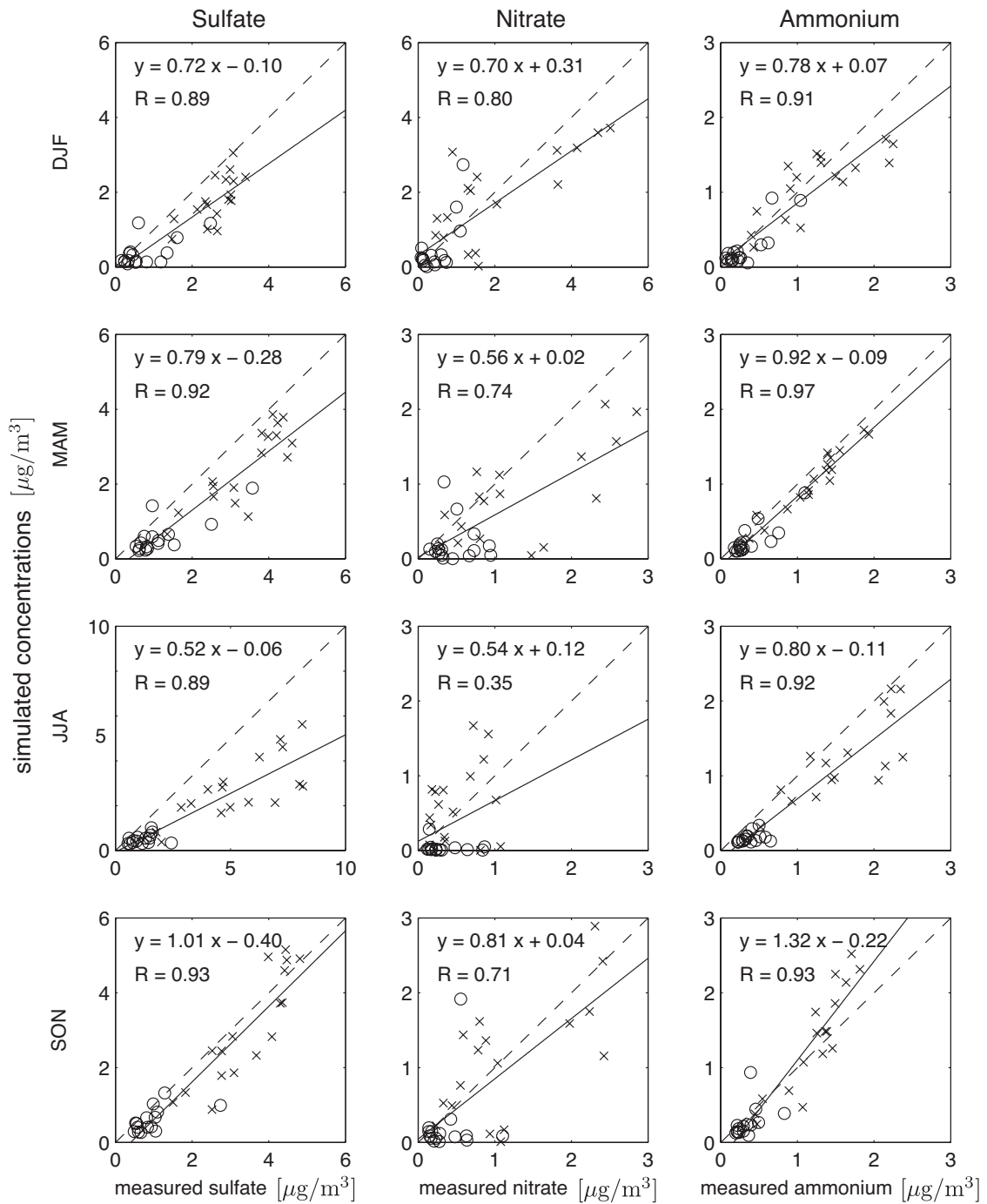


Figure 2.2: Present-day predictions of sulfate, nitrate, and ammonium aerosols compared to CASTNET observations. Simulated values are seasonal averages for the three-year period 1999-2001. CASTNET measured values are converted to model resolution for comparison and are seasonally averaged over 1998-2001. Circles represent western U.S. sites (west of 92.5° W) and crosses represent eastern U.S. sites. Also shown is the 1:1 line (dashed) and linear fit (solid line and equation). R is the correlation coefficient between simulated and measured concentrations.

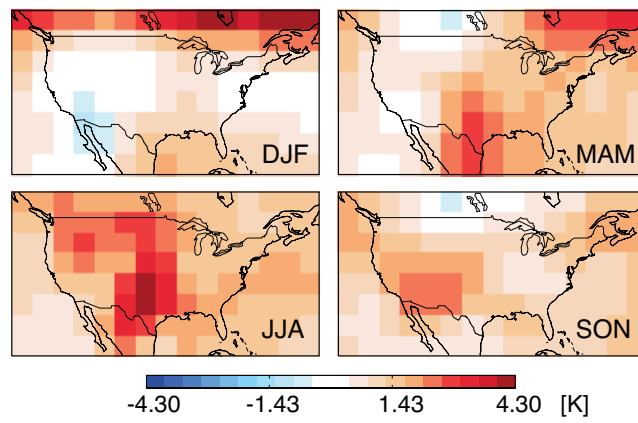


Figure 2.3: Predicted change in U.S. surface temperature from the present-day (1999-2001) to future (249-2051).

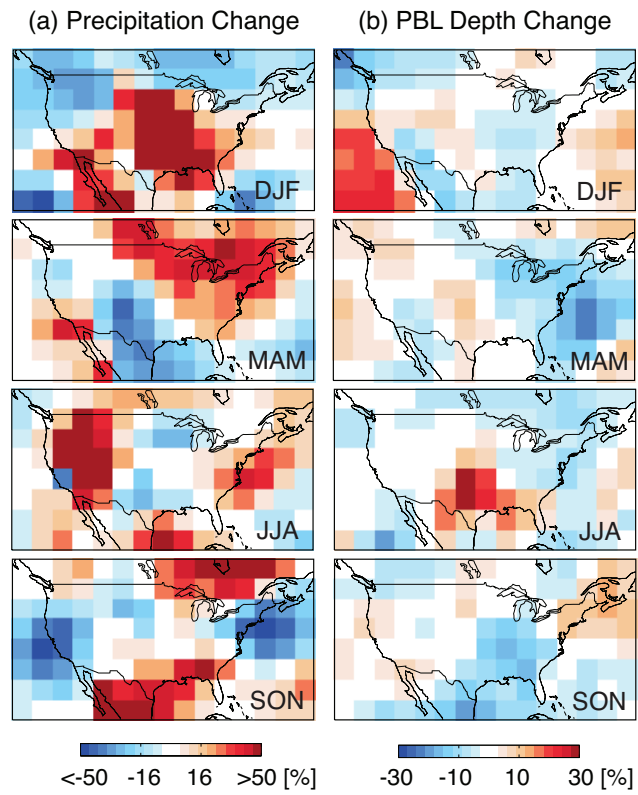


Figure 2.4: Predicted change in precipitation and afternoon planetary boundary layer (PBL) depth between the present-day (1999-2001) and future (2049-2051). The change is expressed as percent change relative to present-day.

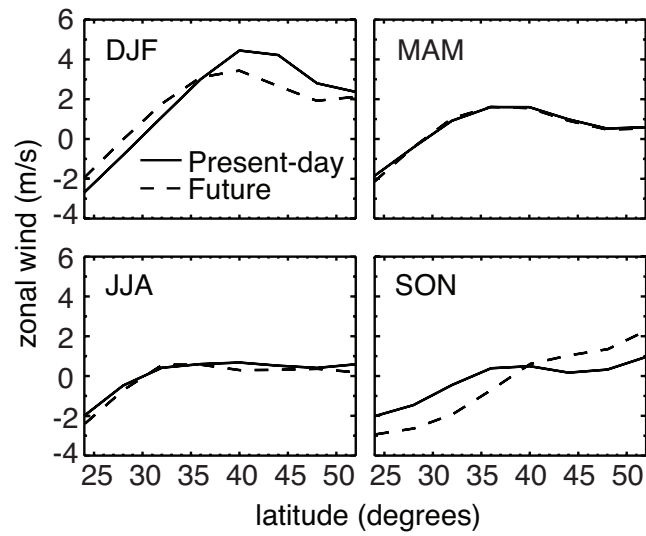


Figure 2.5: Predicted level 1 (approximately 0.13 km) zonal wind for the present-day (1999-2001) and future (2049-2051) over the U.S. (averaged from 120° to 60° W longitude).

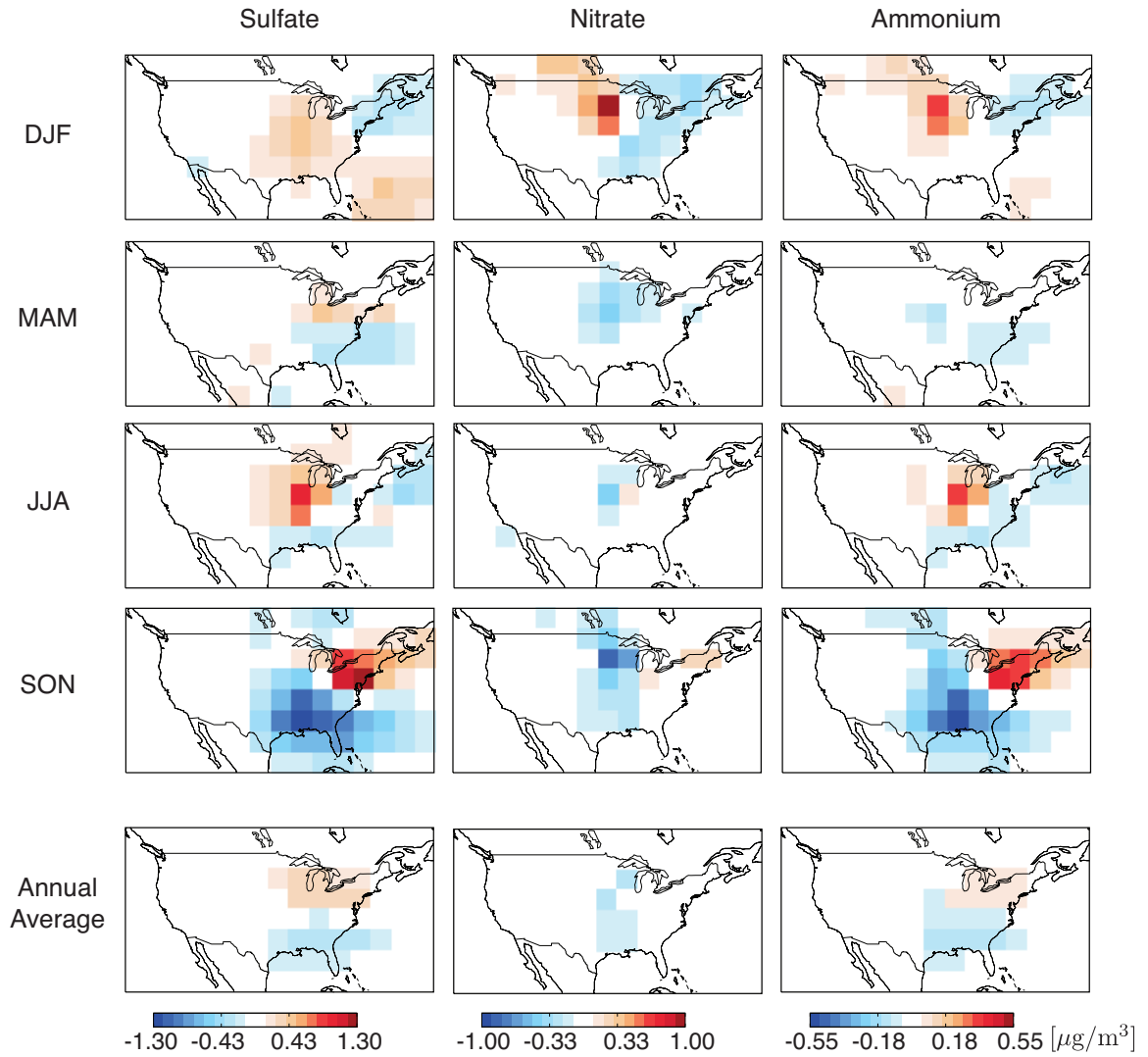


Figure 2.6: Predicted change in U.S. surface-level aerosol concentrations due to changes in climate alone from the present-day (1999-2001) to the future (2049-2051). Greenhouse gases follow the IPCC scenario A1B. Anthropogenic emissions are held at present-day values, but natural emissions may change in response to climate.

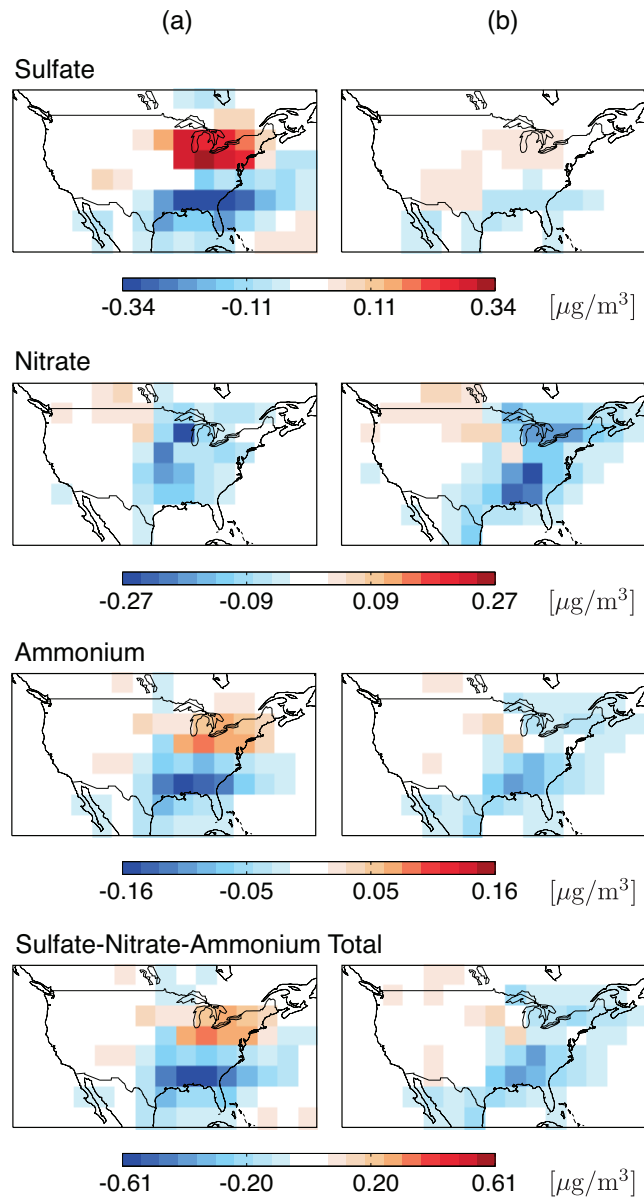


Figure 2.7: Predicted changes in aerosol concentrations due to climate change from the present-day (1999-2001) to the future (2049-2051) with (a) present-day emissions and (b) future emissions (annually averaged). Column (a) is the same as the annual plots in Figure 2.6 except with a different scale. Column (a) represents the difference between simulations of future climate with present-day emissions and present-day climate with present-day emissions. Column (b) represents the difference between future climate with future anthropogenic emissions and present-day climate with future anthropogenic emissions.

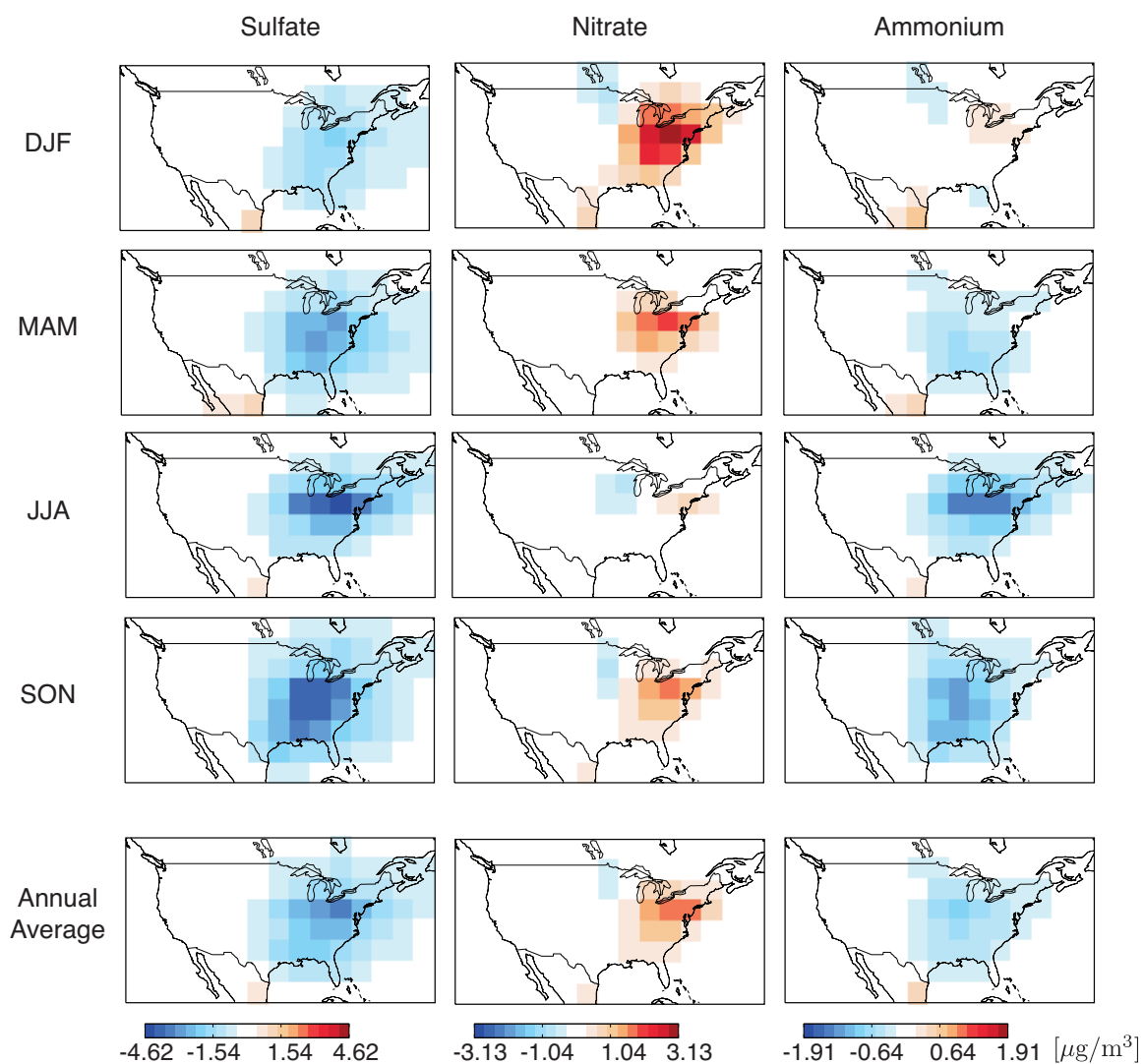


Figure 2.8: Predicted changes in U.S. surface-level aerosol concentrations from the present-day (1999-2001) to the future (2049-2051) due to changes in anthropogenic emissions only (meteorology is held at present-day values). Emissions follow IPCC A1B scenario as described in the text.

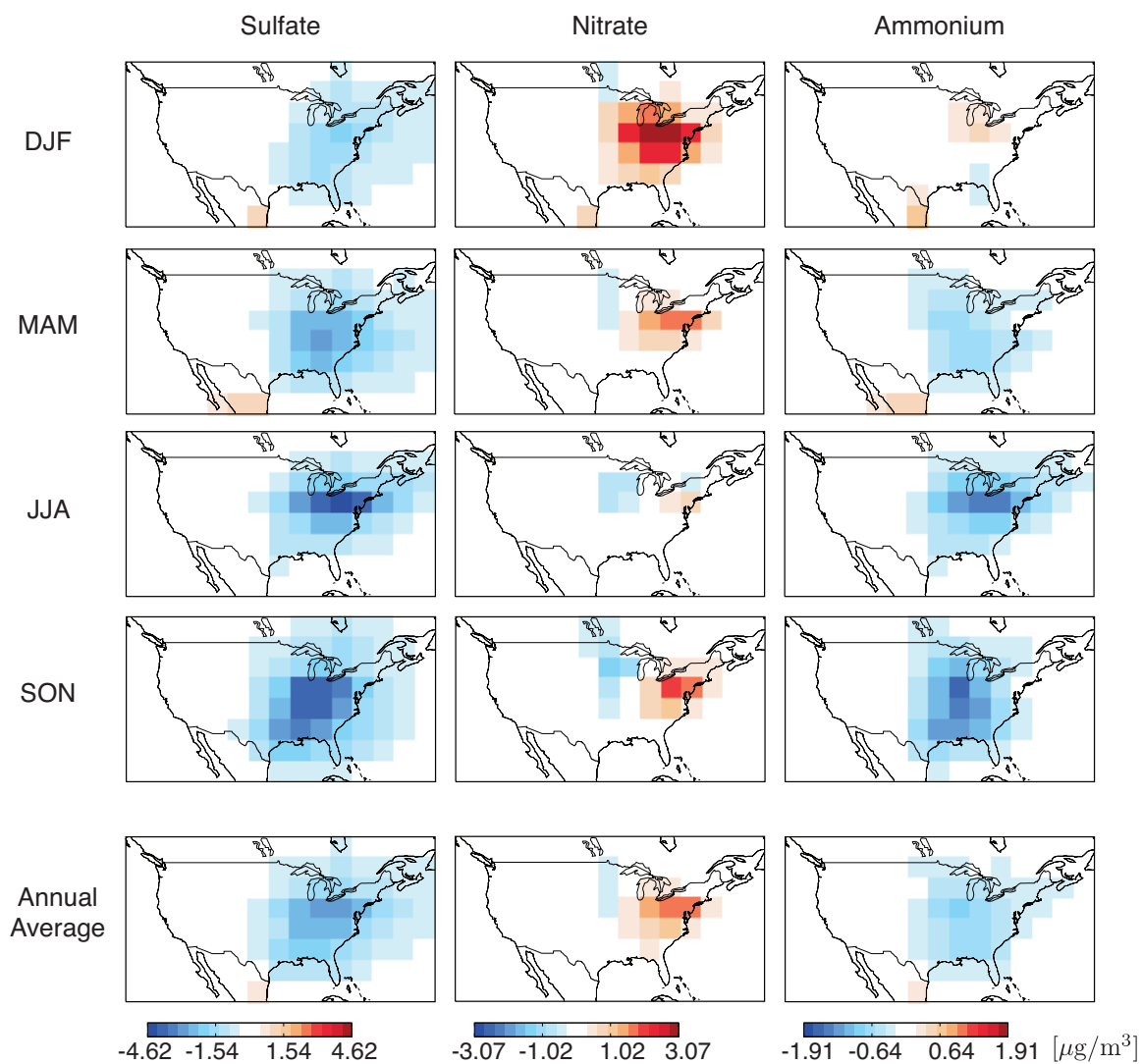


Figure 2.9: Predicted changes in U.S. surface-level aerosol concentrations due to changes in anthropogenic emissions and climate from the present-day (1999-2001) to the future (2049-2051). Emissions follow IPCC A1B scenario as described in text.

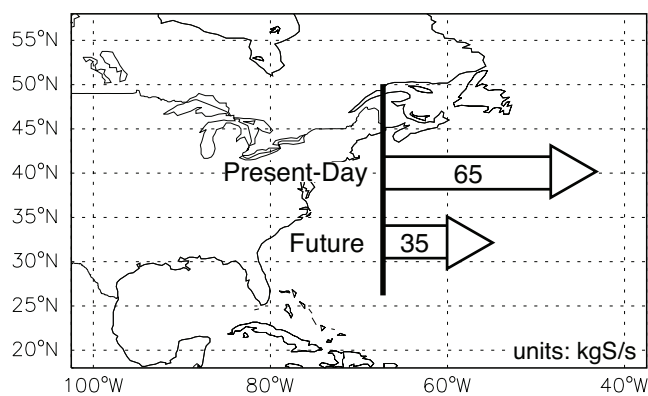


Figure 2.10: Annual change in SO_x ($\text{SO}_2 + \text{SO}_4^{2-}$) outflow from the U.S. due to changes in climate and emissions from present-day to 2050. Transport is calculated through a plane (shown) that runs along 67.5° W from 26° to 50° N. Numbers are averaged over the three present-day years or future years as applicable.

Chapter 3

A global perspective on aerosol from low-volatility organic compounds *

*Reproduced with permission from “A global perspective on aerosol from low-volatility organic compounds” by H. O. T. Pye and J. H. Seinfeld, *Atmospheric Chemistry and Physics*, 10, 4377-4401. Copyright 2010 by the Authors. CC Attribution 3.0 License.

3.1 Abstract

Global production of organic aerosol from primary emissions of semivolatile (SVOCs) and intermediate (IVOCs) volatility organic compounds is estimated using the global chemical transport model, GEOS-Chem. SVOC oxidation is predicted to be a larger global source of net aerosol production than oxidation of traditional parent hydrocarbons (terpenes, isoprene, and aromatics). Using a prescribed rate constant and reduction in volatility for atmospheric oxidation, the yield of aerosol from SVOCs is predicted to be about 75% on a global, annually-averaged basis. For IVOCs, the use of a naphthalene-like surrogate with different high-NO_x and low-NO_x parameterizations produces a global aerosol yield of about 30%, or roughly 5 Tg/yr of aerosol. Estimates of the total global organic aerosol source presented here range between 60 and 100 Tg/yr. This range reflects uncertainty in the parameters for SVOC volatility, SVOC oxidation, SVOC emissions, and IVOC emissions, as well as wet deposition. The highest estimates result if SVOC emissions are significantly underestimated (by more than a factor of 2) or if wet deposition of the gas-phase semivolatile species is less effective than previous estimates. A significant increase in SVOC emissions, a reduction of the volatility of the SVOC emissions, or an increase in the enthalpy of vaporization of the organic aerosol all lead to an appreciable reduction of prediction/measurement discrepancy. In addition, if current primary organic aerosol (POA) inventories capture only about one-half of the SVOC emission and the Henry's Law coefficient for oxidized semivolatiles is on the order of 10³ M/atm, a global estimate of OA production is not inconsistent with the top-down estimate of 140 Tg/yr by (Goldstein and Galbally, 2007). Additional information is needed to constrain the emissions and treatment of SVOCs and IVOCs, which have traditionally not been included in models.

3.2 Introduction

Organics represent a significant fraction of the aerosol mass in the atmosphere (Zhang et al., 2007). Bottom-up estimates of particulate matter concentrations, such as those that would be used to estimate aerosol radiative forcings, visibility, or implications for public health, must be able to

represent the processes critical for organic aerosol formation. Work by Lipsky and Robinson (2006) and Robinson et al. (2007) as well as others (Huffman et al., 2009a,b) indicates that what has traditionally been considered non-volatile primary organic aerosol (POA) is actually a dynamic system of semivolatile species that partition between the gas and aerosol phases as well as undergo gas-phase oxidation to form species of different volatilities that can condense to form secondary organic aerosol (SOA). We present the first estimates of the contribution of primary semivolatile organic compounds and other low-volatility organic compounds to global aerosol production.

Emissions of low-volatility organic compounds can be subdivided somewhat arbitrarily into two classes based on volatility (Donahue et al., 2006): semivolatile organic compounds (SVOCs) and intermediate volatility organic compounds (IVOCs). Semivolatile organic compounds are those that partition directly between the gas and aerosol phases under ambient conditions and include compounds with saturation concentrations roughly between 0.1 and $10^4 \mu\text{g}/\text{m}^3$. SVOC emissions include traditional POA plus any vapor phase species that are in direct equilibrium with the particle phase. SVOCs include species such as large polycyclic aromatic hydrocarbons (PAHs) (e.g. fluoranthene) and long *n*-alkanes (e.g. *n*-pentacosane).

Intermediate volatility organic compounds (IVOCs) are more volatile than SVOCs and roughly span saturation concentrations from 10^4 to $10^6 \mu\text{g}/\text{m}^3$. Since IVOCs partition appreciably to the aerosol phase only under very high aerosol loadings (loadings that typically exceed those found in urban areas), IVOCs are assumed to be emitted entirely in the gas phase. However, due to their relatively low volatility compared to traditional SOA precursors, IVOCs can be easily converted to lower volatility products that partition to the aerosol phase. Species that would fall in the IVOC range include small PAHs (e.g. naphthalene), intermediate length alkanes (e.g. *n*-hexadecane), and phenols.

Species with saturation concentrations below $0.1 \mu\text{g}/\text{m}^3$ are also emitted. Under most atmospherically relevant conditions, such species partition essentially entirely to the aerosol phase and can be considered non-volatile. They are estimated to comprise less than 5% of traditional POA inventories (Grieshop et al., 2009b).

A major obstacle to representing low-volatility organic compounds in atmospheric models is that the identities of many of the species that fall in the SVOC and IVOC categories are unknown. In addition, current inventories used in atmospheric models may not include many of the IVOC emissions (for example, see the work by Shrivastava et al., 2008). From a modeling perspective, an efficient lumping mechanism must be developed. Since the volatility represents the tendency of a species to be in the particle phase, an effective approach is to lump species based on volatility. Information would then be needed about the volatility of the emissions and how the volatility changes with atmospheric processing. A two-dimensional approach using a volatility basis set combined with carbon oxidation state has also been proposed (Jimenez et al., 2009).

Isothermal chamber dilution (Grieshop et al., 2009b), thermodenuder systems (Grieshop et al., 2009b; Huffman et al., 2009b), and dilution samplers (Lipsky and Robinson, 2006) have been used to constrain the volatility of organic compound emissions. The volatility distribution of SVOC emissions from various sources, such as wood burning and diesel exhaust, show sufficient similarity that they can be represented with a single volatility distribution (Robinson et al., 2007; Shrivastava et al., 2006; Grieshop et al., 2009b). Volatility fits of SVOC emissions have typically been assumed to be directly applicable to existing POA inventories based on the assumption that emission factors tend to be measured at unrealistically high organic loadings and often use filters that collect gas phase emissions as well (Grieshop et al., 2009b). IVOC emissions must typically be estimated as they are not captured by traditional POA sampling techniques. IVOC emissions may also vary considerably from source to source (Shrivastava et al., 2008; Grieshop et al., 2009a).

Aerosol formation from SVOCs, IVOCs, and their oxidation products has been implemented in regional models such as PMCAMx and CHIMERE (Robinson et al., 2007; Shrivastava et al., 2008; Murphy and Pandis, 2009; Hodzic et al., 2010) as well as box models (Dzepina et al., 2009; Grieshop et al., 2009a). The SVOCs, and IVOCs if applicable, are typically represented using the volatility basis set framework (Donahue et al., 2006) and allow for oxidation in the gas phase and formation of lower volatility products. Replacing the traditional non-volatile POA with semivolatile POA in regional models has led to improvements in the urban to regional organic aerosol (OA) concentra-

tion ratio (Robinson et al., 2007; Shrivastava et al., 2008) and predicts an ambient aerosol more dominated by oxygenated species (Shrivastava et al., 2008; Murphy and Pandis, 2009), consistent with observations.

In this work, organic aerosol formation from SVOCs and IVOCs is studied using the global chemical transport model, GEOS-Chem. Section 3.3 describes the global model framework as well as the emissions and atmospheric transformation of SVOCs and IVOCs. Results are presented in Sect. 3.4 in terms of predicted aerosol levels, global budgets, and modern vs. fossil carbon. The paper finishes by addressing model uncertainties (Sect. 3.5) and placing the results in the larger context of top-down vs. bottom-up global aerosol budgets (Conclusions).

3.3 Model Description

3.3.1 Global Model

The global chemical transport model, GEOS-Chem (version 8-01-04, <http://acmg.seas.harvard.edu/geos/>), is used to simulate year 2000 organic aerosol concentrations. Simulations are conducted at 2° latitude by 2.5° longitude horizontal resolution using GEOS-4 assimilated meteorology with 30 vertical layers going up to 0.01 hPa for baseline simulations. For computational speed, and in preparation for climate change-organic aerosol interaction studies, sensitivity tests are performed at 4° latitude by 5° longitude horizontal resolution with 23 vertical levels up to 0.002 hPa using GISS GCM Model III meteorology (Rind et al., 2007; Wu et al., 2007, 2008). All simulations are conducted for year 2000 with a minimum of 11 months of initialization. Simulations include fully coupled ozone-NO_x-hydrocarbon chemistry (Bey et al., 2001), and formation of inorganic (Park et al., 2004; Pye et al., 2009) and organic aerosol (Park et al., 2003, 2006; Henze and Seinfeld, 2006; Liao et al., 2007; Henze et al., 2008).

3.3.2 Absorptive Partitioning

Formation of organic aerosols occurs by absorptive partitioning (Odum et al., 1996), and the partitioning framework used here is based on the work of Chung and Seinfeld (2002). An equilibrium partitioning coefficient, $K_{\text{OM},i}$, describing the partitioning between the gas and aerosol phases of a semivolatile species can be calculated assuming a pseudo-ideal solution and absorptive partitioning theory (Pankow, 1994):

$$K_{\text{OM},i} = \frac{RT}{\tilde{M}_i \gamma_i P_i^{\text{vap}}} \quad (3.1)$$

where R is the gas constant, T is temperature, \tilde{M}_i is the molecular weight, γ_i is the activity coefficient of compound i in the aerosol phase, and P_i^{vap} is the vapor pressure of pure species i at temperature T . Absorptive partitioning can also be described using a saturation concentration, C_i^* , which is the inverse of the equilibrium partitioning coefficient (for a discussion of the difference between C_i^* and $K_{\text{OM},i}$ see the supporting material from Donahue et al., 2006):

$$K_{\text{OM},i} = \frac{1}{C_i^*}. \quad (3.2)$$

In terms of concentrations of the semivolatile i , $[G_i]$ and $[A_i]$, in the gas and aerosol phases, respectively,

$$K_{\text{OM},i} = \frac{[A_i]}{[G_i][M_o]} \quad (3.3)$$

where $[M_o]$ is the concentration of particle-phase absorptive material into which the semivolatile compound can partition. In this study, the partitioning medium includes only the particle-phase organics (inorganic constituents and water included in some studies are not considered here). Primary and secondary organic aerosol is assumed to form a single absorbing phase. When non-volatile POA is present,

$$[M_o] = [\text{POA}] + \sum_i [A_i], \quad (3.4)$$

and if POA is semivolatile, this reduces to,

$$[M_o] = \sum_i [A_i]. \quad (3.5)$$

Combining Eqs. (3.3) and (3.4) or (3.5) as appropriate, along with a mass balance, yields an implicit equation for M_o . Organic aerosol will form only when (i.e. the implicit equation for M_o will only have a solution when) (Chung and Seinfeld, 2002),

$$\sum_i K_{OM,i} ([A_i] + [G_i]) > 1. \quad (3.6)$$

Simulations indicate that this condition is generally satisfied with a few exceptions. Formation of organic aerosol through other means, such as cloud processing or reactive uptake, are not considered in the present study.

3.3.3 SOA from Traditional Precursors

SOA from traditional precursors follows earlier studies for terpenes (Chung and Seinfeld, 2002), isoprene (Henze and Seinfeld, 2006), and aromatics (Henze et al., 2008). Parent hydrocarbons are oxidized in the gas-phase to form a series of semivolatile species,



where $\alpha_1, \alpha_2, \dots$ are mass-based stoichiometric coefficients for products $\text{P}_1, \text{P}_2, \dots$. Sometimes, only one semivolatile or nonvolatile product is necessary to represent chamber data (like for low- NO_x aromatic oxidation (Ng et al., 2007; Chan et al., 2009) or nitrate radical oxidation of terpenes (Chung and Seinfeld, 2002)), but typically two semivolatile products have been used (Odum et al., 1996) with partitioning parameters, α_i and $K_{OM,i}$, determined by fits to laboratory data. Models such as PMCAMx have been used to investigate the possibility of continued aging of the SOA formed from traditional parent hydrocarbons due to continued OH oxidation of the gas-phase semivolatile

species (Lane et al., 2008). In the present work, traditional SOA species are not considered subject to continued oxidation beyond that captured in chamber studies.

3.3.4 Aerosol from SVOCs

POA is defined to be any SVOC that partitions directly to the particle phase after emission without undergoing oxidation. In source regions, there is likely to be net POA production, but as air masses move to more remote regions, POA will be driven out of the particle phase due to dilution and oxidation of the gas-phase species. Oxidation of the primary gas-phase SVOCs can lead to lower volatility products that partition to make SOA.

3.3.4.1 SVOC Emissions

SVOCs from all sources are assumed to be emitted as two semivolatile surrogate species, $SVOC_1$ and $SVOC_2$, in roughly equal fractions of 0.49 and 0.51 based on the work by Shrivastava et al. (2006) and Lipsky and Robinson (2006). Partitioning coefficients for $SVOC_1$ and $SVOC_2$ are given in Table 3.1 and correspond to saturation concentrations of roughly 1600 and 20 $\mu\text{g}/\text{m}^3$. Under most atmospherically relevant conditions, only the lower volatility component is expected to partition appreciably to the aerosol phase.

The SVOC emissions are based on the traditional non-volatile POA emission inventory used in GEOS-Chem (Park et al., 2003, 2006). The non-volatile POA inventory includes contributions from biomass burning, biofuel burning, and anthropogenic sources (Table 3.2 and Fig. 3.1). Monthly biomass burning emissions are based on the Global Fire and Emission Database version 2 (GFEDv2) for year 2000 (van der Werf et al., 2006). Global biofuel and anthropogenic organic carbon emissions are from the technology-based inventory by Bond et al. (2004). Over North America, anthropogenic emissions are superseded with those based on work by Cooke et al. (1999). US biofuel emissions are constructed based on residential and industrial wood fuel consumption, as implemented in the work of Park et al. (2003). The scaling and seasonal distribution of US anthropogenic and biofuel organic carbon (OC) emissions are also detailed in the work of Park et al. (2003).

Providing a global estimate of SVOC emissions is difficult due to the fact that it is unclear what portion of the SVOCs traditional POA represents, and traditional POA emissions themselves are uncertain. Estimates of the traditional POA emission rate in global models has ranged from 17 to 142 Tg/yr as summarized in the work of Farina et al. (2010). Note that since biomass burning is a significant POA contributor, emissions of SVOCs likely vary from year to year as different areas become more or less prone to burning. Part of the uncertainty in global OC emissions, estimated at a factor of two in the work by Bond et al. (2004), is likely due to the fact that traditional POA inventories try to capture organic aerosol emissions over all atmospherically relevant conditions using measurements or observations of emission factors under a single or limited set of conditions in terms of temperature and organic aerosol loadings. For a species that is semivolatile, like POA, one set of conditions will not characterize the emissions well.

Debate continues on whether traditional POA inventories represent most SVOC emissions or a very limited subset. POA emission factors are often obtained under organic concentrations higher than atmospherically relevant, which may force organic vapors that would be in the gas phase under ambient conditions into the particle phase during sampling. Under such conditions, the POA inventory may be a good representation of SVOC emissions. However, an examination of the Schauer et al. (2001) inventory for wood burning, which gives OC emission factors consistent with those used in the GFEDv2 biomass burning inventory, shows individual PAH compounds with saturation concentrations of 12, 100, and $9 \times 10^3 \mu\text{g}/\text{m}^3$ being emitted 91, 56, and 4% in the particle phases. Thus, compounds over the entire SVOC volatility range exhibit appreciable mass in the gas and particle phase. Furthermore, models using non-volatile POA tend to underestimate, not overestimate, ambient organic aerosol concentrations (Heald et al., 2005; Liao et al., 2007). We proceed by assuming traditional non-volatile POA inventories likely represent a subset of SVOC emissions.

The SVOC emission rate in grid cell I, J can be estimated using:

$$E_{\text{SVOC}}(I, J) = \left[1 + \frac{G_{\text{R}}}{\text{POA}_{\text{R}}} \right] E_{\text{NVPOA}}(I, J) \quad (3.8)$$

where E_{SVOC} is the emission rate of SVOCs (Tg C/yr), G_{R} is the emission of the gas-phase SVOC surrogate in a representative study (mg/kg), POA_{R} is the emission of organic aerosol in that same representative study (mg/kg), and E_{NVPOA} is the traditional, non-volatile POA emission rate (Tg C/yr). For unit conversion purposes, the organic matter to organic carbon (OM/OC) ratio is assumed to be the same for G_{R} and POA_{R} in the above equation. Using the work of Schauer et al. (2001) as the representative study, the ratio of gas-phase SVOC surrogates to the particle-phase organics ($G_{\text{R}}/\text{POA}_{\text{R}}$) is about 0.27. The gas-phase SVOC surrogate estimate is based on adding up the gas-phase speciated emissions that were also found in the particle phase. Some of the SVOC emissions could be part of the gas-phase unresolved complex mixture in the work of Schauer et al. (2001) or were misclassified as IVOCs and are not reflected in the 0.27 estimate. Accounting for all the gas-phase species on the PUF sampling train/filter and the entire gas-phase UCM would increase the 0.27 estimate to 0.61. The possibility remains that POA inventories may represent a significantly different fraction of SVOCs than in the study of Schauer et al. (2001), and scaling POA emissions up 27% is likely a fairly conservative estimate, given that the uncertainty in the baseline POA emissions is easily a factor of 2 (Bond et al., 2004). Global emissions of SVOCs are predicted to be 37 Tg C yr^{-1} (Table 3.2 and Fig. 3.1).

Since traditional POA inventories are reported as the mass of carbon emitted, the mass of organic matter that includes any additional oxygen, nitrogen, or other species associated with the carbon must be determined. The range of OM/OC ratios for SVOCs likely ranges from just above 1 for carbon-rich species to above 2 for highly oxygenated species such as those found in wood smoke (Schauer et al., 2001). Simulations here use a value of 1.4, which is only slightly higher than the OM/OC ratio estimated for hydrocarbon like organic aerosol, HOA (OM/OC: 1.2–1.3) (Aiken et al., 2008; Zhang et al., 2005), slightly lower than the OM/OC ratio for primary biomass burning organic aerosol, P-BBOA (OM/OC: 1.6–1.7) (Aiken et al., 2008), and consistent with the wood burning inventory of Schauer et al. (2001) (OM/OC: 1.4–1.7). The OM/OC ratio affects the partitioning of organics since it determines the total SVOC mass available for partitioning.

3.3.4.2 SVOC Oxidation

Primary SVOC emissions age in the gas phase by reaction with OH, based on the wood burning chamber experiments of Grieshop et al. (2009a). An OH rate constant of 2×10^{-11} cm³/molec/s is assumed for the present work. The mass of the parent SVOC is assumed to increase 50% through functionalization, a value slightly larger than, but still consistent with, Grieshop et al. (2009a) for oxidation of wood smoke. The volatility of the SVOC is reduced by a factor of 100 as a result of the OH reaction. This represents a slightly slower rate of oxidation, but a more aggressive addition of oxygen and reduction in volatility, than that used by Robinson et al. (2007) and was found to give better O:C ratio agreement with experiments than the traditional Robinson et al. (2007) parameters in the work of Grieshop et al. (2009a). Table 3.3 summarizes the SVOC oxidation parameters and compares them with the optimized parameters in the work of Grieshop et al. (2009a) and the parameters of Robinson et al. (2007).

The mechanism by which aging of low-volatility organic compounds occurs is not well-constrained. Previous work (Robinson et al., 2007) has suggested that aging occurs as the result of sequential OH oxidation reactions in the gas-phase. The SVOCs in the present study are assumed to undergo only one generation of oxidation. This assumption is made for three main reasons. First, chamber studies, which are the source of oxidation data, tend to access only initial reactions. Secondly, since the model assumes that oxidation leads only to functionalization of the molecule and therefore a reduction in volatility, it is likely to be less valid for later generations of oxidation in which molecular fragmentation becomes more important (Kroll et al., 2009). Lastly, for a 50% (or 40% as used by Grieshop et al., 2009a) increase in mass per generation, a parent SVOC with an initial OM/OC of 1.4 would require only 1 generation of oxidation to reach a final OM/OC of about 2, consistent with the observed OM/OC of aged aerosol in the experiment on which the parameters are based (Grieshop et al., 2009a), with the OM/OC of oxygenated organic aerosol, OOA (OM/OC: 1.8–2.4, 2.2) (Aiken et al., 2008; Zhang et al., 2005), and with other estimates of the OM/OC of oxidized regional aerosol (OM/OC: 2.1) (Turpin and Lim, 2001).

3.3.5 Aerosol from IVOCs

IVOCs are emitted entirely in the gas phase and form aerosol only upon oxidation. Since naphthalene is predicted to be a major SOA precursor in the oxidation of wood burning and diesel combustion exhaust (Chan et al., 2009), here, IVOCs are represented as a naphthalene-like surrogate that forms aerosol according to the chamber studies of Chan et al. (2009).

In addition to naphthalene, other important classes of speciated IVOCs include alkanes and phenols (Schauer et al., 2001, 2002). A significant portion of IVOCs likely belongs to the unresolved complex mixture and thus its identity and aerosol yield is not known. Aerosol yield information is available for many alkanes (Jordan et al., 2008) as well as naphthalene and functionalized naphthalene species (Chan et al., 2009). Gasoline combustion likely produces more alkanes than aromatics (Schauer et al., 2002), but wood burning, globally the largest source of POA, likely emits more gas-phase aromatics than alkanes (Schauer et al., 2001; Hays et al., 2002). Approximately 75% of the speciated IVOC surrogate in the wood burning inventory of Schauer et al. (2001) is phenol (C^* about $10^6 \mu\text{g}/\text{m}^3$) or substituted phenol compounds. Due to their ring structures, these phenol compounds are likely to behave more like naphthalene than an alkane in terms of yields under high- NO_x vs. low- NO_x conditions. So, if all IVOCs are to be represented with one surrogate compound, naphthalene is a good choice.

3.3.5.1 IVOC Emissions

Since naphthalene is an important IVOC from many sources including wood combustion and vehicle exhaust (Chan et al., 2009; Schauer et al., 2001, 2002), IVOC emissions are assumed to be spatially distributed like naphthalene. First, a baseline emission inventory of naphthalene (NAP) is created. For biomass and biofuel burning, this is done using an emission ratio to CO. An emission factor of 0.025 g NAP/kg dry matter burned is used along with CO emission factors (Andreae and Merlet, 2001) to produce emission ratios of 0.0602 and 0.0701 mmol NAP/mol CO for biomass and biofuel burning, respectively. The emission factor presented by Andreae and Merlet (2001) is consistent with that of naphthalene presented by Hays et al. (2002) for the burning of foliar fuels, but about a

factor of 10 lower than the value in the work of Schauer et al. (2001). Anthropogenic naphthalene emissions, from sources such as traffic oil combustion, consumer products, and industrial sources (Zhang and Tao, 2009), are spatially distributed like benzene from the EDGAR2 inventory and are aseasonal. Emissions given for 1990 are scaled to year 2000 based on CO₂ emissions from liquid fossil fuel usage (Bey et al., 2001; Fu et al., 2008). The magnitude of non-biomass and biofuel burning emissions of naphthalene is estimated based on Zhang and Tao (2009) to be about 0.09 Tg C/yr. The baseline naphthalene emission inventory from all sources constructed here is approximately 0.22 Tg C/yr (Table 3.2).

As is the case for SVOCs, the magnitude of total IVOC emissions is uncertain. To estimate total IVOC emissions, the naphthalene emission inventory is scaled up. This assumes that the relative contributions of biomass burning vs. biofuel burning vs. anthropogenic sources to IVOC emissions are consistent with those of naphthalene. The emission rate of IVOCs in grid cell I, J (E_{IVOC}) is determined by scaling the naphthalene emission (E_{NAP}),

$$E_{IVOC}(I, J) = \beta E_{NAP}(I, J) \quad (3.9)$$

where, the scaling factor, β , is estimated from,

$$\beta = E_{NVPOA, BB+BF} \left(\frac{E_{IVOC, BB+BF}}{E_{NVPOA, BB+BF}} \right)_{R_1} \left(\frac{E_{IVOC, TOT}}{E_{IVOC, BB+BF}} \right)_{R_2} \left(\frac{1}{E_{NAP, TOT}} \right) \quad (3.10)$$

$E_{A,B}$ are the global emissions of species A (IVOC, NVPOA: traditional POA, or NAP: naphthalene) from source type B (BB: biomass burning, BF: biofuel burning, or TOT: total). Subscripts R_1 and R_2 are used to label the two ratios for further discussion.

The first ratio in Eq. 3.10, R_1 , is estimated based on the Schauer et al. (2001) inventory for pine wood burning. $E_{IVOC, BB+BF}$ is approximated as any species collected on the filter/polyurethane foam (PUF) sampling train with only a gas-phase emission reported plus the entire gas-phase unresolved complex mixture (UCM). The gas-phase UCM in the work of Schauer et al. (2001) for pine wood burning represents roughly 10% of the total non-methane organic carbon (gas+aerosol) mass

emitted. The two contributions (PUF gases and UCM gases) to IVOC emissions are roughly equal. Using the organic aerosol emission rate ($E_{\text{NVPOA, BB+BF}}$) from the work of Schauer et al. (2001) as well, R_1 is estimated as,

$$\frac{E_{\text{IVOC, BB+BF}}}{E_{\text{NVPOA, BB+BF}}} \approx 0.34. \quad (3.11)$$

Since the IVOC is spatially distributed like naphthalene, R_2 can be replaced by:

$$\frac{E_{\text{IVOC, TOT}}}{E_{\text{IVOC, BB+BF}}} = \frac{E_{\text{NAP, TOT}}}{E_{\text{NAP, BB+BF}}} \quad (3.12)$$

and consequently, only $E_{\text{NAP, BB+BF}}$ is needed to complete the scaling factor.

Thus, our scaling incorporates two ideas: IVOCs are spatially distributed like naphthalene and the ratio of IVOCs to traditional POA for wood burning sources is 0.34 as in the work of Schauer et al. (2001). As a result, the predicted scaling factor, β , is 66 and yields a global IVOC emission rate of about 15 Tg C/yr (Table 3.2 and Fig. 3.1). The large value of the scaling factor, β , means that naphthalene itself is actually a relatively small (<2%) contribution to global IVOC emissions.

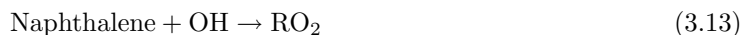
The IVOC emissions are not linked to the POA emission inventory within each grid cell; rather, they are spatially distributed like naphthalene. On a global basis, the present work predicts IVOC emissions of roughly 0.5×POA in magnitude. As a result of the separation of POA and IVOC emissions, the ratio of IVOC:traditional POA emissions is roughly 2.1 for anthropogenic sources and 0.34 for biomass and biofuel sources combined. These ratios are consistent with the discussion by Shrivastava et al. (2008) and box model studies by Grieshop et al. (2009a), indicating that diesel combustion (an anthropogenic source) may produce relatively more IVOCs than wood burning.

3.3.5.2 IVOC Oxidation

IVOC aging behavior is based on the chamber studies of Chan et al. (2009) and Kautzman et al. (2010) examining the oxidation of naphthalene under high- and low- NO_x conditions. Similar to light aromatic oxidation (Ng et al., 2007), naphthalene oxidation under high- NO_x conditions was found to produce semivolatile SOA while oxidation under low- NO_x conditions was found to produce

essentially non-volatile SOA. The yield of aerosol ranged from 13 to 30% for the high-NO_x oxidation and was constant at 73% for low-NO_x oxidation. For naphthalene, the results indicate that the first oxidation step is rate-limiting for SOA formation. Calculations using diesel engine and wood burning emission profiles indicate that naphthalene and other PAHs are responsible for substantially more SOA than light aromatics on short timescales (about 12 h) (Chan et al., 2009), and ambient aerosol contains compounds indicative of naphthalene oxidation (Kautzman et al., 2010).

Formation of aerosol from IVOC oxidation is modeled similar to the aerosol from aromatic oxidation in the work of Henze et al. (2008). Reaction of the parent hydrocarbon with OH in the presence of oxygen results in the formation of a peroxy radical species,



Under high-NO_x conditions, reaction of the RO₂ radical with NO likely dominates over reaction of RO₂ with HO₂ or RO₂ and thus SOA can be assumed to form from the following channel:



where the two semivolatile products are described using parameters by Chan et al. (2009). Under low-NO_x conditions, the RO₂ radical is expected to react predominantly with HO₂ and lead to one essentially non-volatile product (Chan et al., 2009; Kautzman et al., 2010):



In practice, the non-volatile SOA product is represented in GEOS-Chem using a partitioning coefficient, K_{OM} , of $10^4 \text{ m}^3/\mu\text{g}$. Values for the partitioning coefficients and mass-based stoichiometric coefficients of all the products are given in Table 3.1, and Table 3.4 contains the gas-phase rate constants.

3.3.6 Additional Model Parameters and Specifications

In the current version of GEOS-Chem, the semivolatile products of parent hydrocarbon oxidation are lumped together into several gas-phase and aerosol-phase tracers (Henze and Seinfeld, 2006; Liao et al., 2007; Henze et al., 2008). Since the identity of each individual species is not preserved during transport, some artificial migration of mass between the volatilities may occur. In the present work, for the SVOC related species, separate tracers are used for each phase (gas and aerosol) as well as each volatility for a total of 4 tracers related to primary SVOC emissions and 4 tracers for SVOC oxidation products. The use of separate tracers prevents migration between the different volatilities during transport which was found to be significant at $4^\circ \times 5^\circ$ resolution using a lumped tracer. For IVOC oxidation, the effects of lumping were found to be less significant, but in order to obtain the best estimate of IVOC aerosol produced under high- NO_x conditions, separate tracers for each of the IVOC oxidation products are used. Each species with a saturation concentration below $10^5 \mu\text{g}/\text{m}^3$ in Table 3.1 has a separate gas and aerosol phase tracer. The IVOC has a gas-phase tracer only for a total of 15 additional tracers for the low-volatility organic aerosol simulation. A list of GEOS-Chem tracers for a standard full-chemistry SOA simulation can be found in Table 2 in the work of Liao et al. (2007).

Emitted SVOCs, aged SVOCs, and aged IVOCs in the gas and aerosol phases are subject to wet and dry deposition. The IVOC surrogate gas is not deposited. Dry deposition is represented by a resistance in series method (Wesely, 1989), with the surface resistances for aerosols following the work of Zhang et al. (2001). SVOCs that partition directly to the aerosol phase to form POA are treated as hydrophobic and are assumed insoluble. Gas-phase SVOC emissions are treated as relatively hydrophobic with an effective Henry's law coefficient of $9.5 \text{ M}/\text{atm}$ and a heat of dissolution, $\Delta H/R$ of -4700 K based on phenanthrene (Sander, 1999). Other SVOC species, such as long-chain alkanes, are more hydrophobic with Henry's law coefficients of $10^{-4} \text{ M}/\text{atm}$ to $0.3 \text{ M}/\text{atm}$. However, SVOCs such as functionalized phenols or oxygenated species, will likely be more soluble than phenanthrene. The SVOC and IVOC oxidation products are treated like the traditional SOA species and are hydrophilic (Henry's law coefficient of $10^5 \text{ M}/\text{atm}$ for all gas-phase semivolatiles), and all SOA is

scavenged with an 80% efficiency (Chung and Seinfeld, 2002). The effect of a lower Henry's law coefficient will be examined in sensitivity studies.

The equilibrium partitioning coefficients of all species are adjusted for temperature based on the Clausius-Clapeyron equation. As in previous studies using GEOS-Chem, the enthalpy of vaporization is assumed to be 42 kJ/mol for all organic species (Chung and Seinfeld, 2002). However, a discrepancy exists in the predicted enthalpy of vaporization for semivolatile organic aerosol estimated for complex SOA systems (around 10–40 kJ/mol, Offenberg et al. (2006)) and based on theory or single component systems (around 100 kJ/mol, Epstein et al. (2010)). The enthalpy of vaporization is examined in Sect. 3.4.4.1.

3.3.7 Aerosol Aging

Modeling efforts are still limited in their ability to represent aging that occurs on timescales longer than a few days, as these conditions are not readily accessed in chamber experiments (Jimenez et al., 2009). On long timescales, compounds may continue to functionalize and form more aerosol or may fragment and reduce aerosol formation. Chamber experiments tend to produce aerosol that resembles semivolatile oxygenated OA, SV-OOA, which is higher in volatility and lower in O:C than that observed in the atmosphere which tends to be dominated by low-volatility oxygenated OA, LV-OOA, with high O:C (Ng et al., 2009). Lane et al. (2008), Murphy and Pandis (2009), Jimenez et al. (2009), and Farina et al. (2010) have postulated that the semivolatiles formed from traditional precursors such as isoprene, terpenes, and aromatics continue to oxidize in the atmosphere in the gas phase. However, the analysis of Chhabra et al. (2010) indicates that the chamber oxidation of several parent hydrocarbons, including toluene, xylene, and naphthalene, does approach LV-OOA type aerosol with high O:C. In the work presented here, chemical reaction and aerosol formation from all parent hydrocarbons (traditional, SVOCs, and IVOCs) is limited to the behavior that is currently captured in chamber experiments.

3.4 Results and Discussion

3.4.1 OA from SVOCs and IVOCs

Figure 3.2 shows the amount of organic aerosol predicted to form from direct partitioning of SVOC emissions (POA), oxidation of SVOCs, and oxidation of IVOCs. Concentrations are shown for the winter and summer at the surface. The highest POA concentrations (Fig. 3.2a, b) reflect biomass burning source regions, but anthropogenic source regions such as the US and East Asia also have high POA concentrations. Compared to POA, the SOA formed from SVOC oxidation is more regionally distributed (Fig. 3.2c, d). SOA from IVOC oxidation has a similar spatial distribution to SOA from SVOCs, but in general, concentrations are lower (Fig. 3.2e, f).

Compared to the traditional simulation with non-volatile POA and no IVOCs, generally less total organic aerosol is predicted at the surface in the revised simulation with semivolatile POA, primary SVOC aging in the gas phase, and SOA from IVOCs (see Fig. S1 in supplement located in Appendix B, note that both traditional and revised simulations form aerosol from traditional SOA precursors such as biogenic hydrocarbons and light aromatics). The largest decreases in total organic aerosol are over the biomass burning and isoprene source regions. Small increases of up to $0.2 \mu\text{g}/\text{m}^3$ in organic aerosol are predicted at northern high latitudes in DJF (December-January-February). The largest surface level, seasonally averaged increase ($0.4 \mu\text{g}/\text{m}^3$) occurs during SON (September-October-November) over Eastern Russia near a biomass burning source region as a result of IVOC oxidation.

While the revised simulation generally predicts lower total OA concentrations near the surface, starting at roughly 4 km (model level 7) OA concentrations tend to be higher in the revised simulation (Fig. S1). Not all regional changes necessarily transition from decreases to increases at 4 km though. Concentrations over the US during JJA (June-July-August) tend to be lower than the traditional simulation predicts up until about 7 km. Biomass burning outflow (JJA Africa), South American outflow (JJA and SON), and Asian outflow regions are among the first locations other than high latitudes at which increases in total OA occur as altitude increases.

Several factors influence the change in organic aerosol concentration between the traditional and revised simulations. With semivolatile POA, concentrations will tend to decrease, as a large portion of the POA is predicted to evaporate. The SVOC emission rate is higher (27%) than the standard POA emission rate, but not high enough to compensate for POA evaporation. This shift to the gas phase is reflected in Fig. 3.3, which displays the fraction of primary SVOCs in the particle phase as POA in the revised simulation. During DJF over the eastern US, about 20% and as much as 27% of the primary SVOC is partitioned to the aerosol phase. (At 270 K, a typical wintertime temperature in the Northeast US, the saturation concentration of SVOC₂ is about 3 µg/m³.) In JJA, 10 to 20% of the SVOC is in the aerosol phase. In the western US as much as 36% is in the particle phase due to high biomass burning emissions. In addition to the effect of evaporation, the OM/OC ratio for POA decreases from 2.1 in the traditional simulation to 1.4 in the revised simulation, which affects the amount of aerosol available for partitioning.

Concentrations of total OA could also increase for a number of reasons. Since SVOCs are oxidized in the gas phase, OA will tend to be shifted toward more remote or downwind areas relative to source regions. Also, changes in wet deposition (SVOCs and oxidized SVOCs are less aggressively wet deposited than hydrophilic traditional POA) allow further transport of some SVOC emissions. The introduction of IVOCs adds another source of OA. Oxidation of the IVOC through the RO₂+HO₂ route (which is more dominant than the RO₂+NO route in remote regions, Henze et al., 2008) produces non-volatile aerosol at a high yield. Still, even with the introduction of IVOCs, surface OA levels are lower than those in the traditional model (Fig. S1 in supplement).

3.4.2 Global Budgets

Despite the fact that the revised simulation, with the new SVOC and IVOC inventories, has a larger pool of organics with the potential to form OA, global production of OA decreases 23% in the revised simulation compared to the traditional simulation. Table 3.5 shows the global OA budget for each simulation. In the traditional simulation, traditional SOA and non-volatile POA represent a global OA source of 87 Tg/yr. In the revised simulation, the net OA source decreases

to 67 Tg/yr. The formation of traditional SOA decreases as well (although only 11%), likely as a result of a reduced partitioning medium into which the SOA may absorb. The tropospheric lifetime of OA against deposition (defined as the tropospheric burden divided by the sum of wet and dry deposition) increases in the revised simulation. In the traditional simulation, POA is assumed to be emitted as 50% hydrophobic and 50% hydrophilic and converted from hydrophobic to hydrophilic forms with an e-folding lifetime of 1.15 days. In the revised simulation, the hydrophobic nature of POA leads to a much longer POA lifetime (17 days against deposition). In addition, production of aerosol is shifted to higher altitudes where it is less subject to wet or dry deposition and thus has a longer lifetime. By coincidence, the global tropospheric burden of organic aerosol is roughly the same in the traditional and revised simulations.

As shown in Fig. 3.4, only about 50% of the carbon emitted as an SVOC leads to net aerosol production. The rest is wet or dry deposited in the gas phase. Of the 37 Tg C/yr emitted, only 0.5 Tg C/yr are predicted to lead to net POA formation, most of which (97%) is due to the lower volatility SVOC (SVOC₂). 95% of the emitted SVOC carbon reacts in the gas phase with OH to form an oxidized SVOC (O-SVOC). The O-SVOC is fairly effectively wet and dry deposited (it is treated like traditional gas-phase SOA products with a Henry's law coefficient of 10^5 M/atm) and a significant fraction is lost to deposition in the gas phase. Only 18 Tg C/yr forms net SOA. Roughly 80% of the SOA from SVOCs is from the lower volatility product ($C^* = 0.2 \mu\text{g}/\text{m}^3$) while 20% is from the higher volatility product ($C^* = 16 \mu\text{g}/\text{m}^3$). Ultimately, the OA from SVOCs is lost to wet and dry deposition with wet deposition being dominant. The yield of OA from SVOCs is about 50% on a carbon basis (mass of carbon in aerosol/ mass of carbon emitted) and about 75% in terms of total mass of SVOC aerosol produced divided by total mass of SVOC emitted. Figure 3.4 also shows the relative rates of formation of aerosol from each source in the pie chart (in Tg C/yr). More than half of the global aerosol carbon is predicted to come from primary SVOC oxidation products. The second largest contribution is from traditional SOA followed by SOA from IVOCs and POA.

Figure 3.5 shows the emission, oxidation, and SOA formation predicted for light aromatics and IVOCs. Because of where they are emitted, most of the parent hydrocarbons react following the

high-NO_x RO₂+NO pathway. As shown by Henze et al. (2008), aromatics that react faster with OH will have a greater tendency to follow the RO₂+NO pathway since biofuel and fossil fuel burning emissions tend to be colocated with anthropogenic NO_x sources, and the parent hydrocarbon is more likely to be oxidized in the source region. The IVOC surrogate, naphthalene, reacts faster with OH than benzene or toluene, but similar in rate to xylene. For both naphthalene and xylene, the amount of oxidation through the high-NO_x pathway is about twice that through the low-NO_x pathway. Benzene, with the slowest OH rate constant, reacts slightly more through the RO₂+HO₂ than the RO₂+NO pathway. The high-NO_x IVOC oxidation pathway results in about 1 Tg/yr of SOA and the low-NO_x pathway results in about 4 Tg/yr, leading to an overall yield of aerosol from IVOCs of about 30%.

3.4.3 United States Organic Aerosol

Figure 3.6 shows the predicted concentration of total OA over the United States for the winter and summer and the contributions of different OA types to that total. The contribution of light aromatics to total OA is not shown but is similar in magnitude to that from IVOCs. The highest concentrations in the winter are predicted to be located in the Southeast US as a result of a biomass burning event and high SVOC emissions. During the winter, POA is a significant contributor to total OA concentrations. POA contributions are highest in the Northeast where temperatures are lower and partitioning to the aerosol phase is favored. Anthropogenic and biofuel burning emissions also tend to be highest in the Northeast (Fig. 3.1). Despite significant POA contributions, SOA from SVOCs is the dominant wintertime OA component, generally contributing 50% or more to surface concentrations. In the summer, the highest OA also occurs in the Southeast, but is due primarily to biogenic SOA. The highest POA contributions in summer reflect biomass burning sources. Outside of the biomass burning locations, POA is generally lower in the summer than in the winter. Despite the significant contribution of biogenic SOA, SOA from SVOCs remains an important contributor to total OA, representing up to 50% of the OA in the Northeast and 50% or more in the Western US.

Since the winter organic aerosol is dominated by SVOC aerosol, further examination of wintertime concentrations allows us to assess the model performance while minimizing uncertainties in the biogenic aerosol parameterization as a source of discrepancy. Figure 3.7 shows winter (December-January-February 2000) simulated and observed aerosol OC concentrations over the US. Surface measurements of total OC from the Interagency Monitoring of Protected Visual Environments (IMPROVE) network (<http://vista.cira.colostate.edu/improve/>) are overlaid in circles on top of the simulated OC concentrations. Since the IMPROVE network observations are reported as mass of carbon rather than the mass of total organic aerosol, converting model values, which tend to be in total organic mass, to organic carbon mass is an additional source of potential discrepancy. Since the aerosol from SVOCs is tracked in GEOS-Chem as the mass of carbon and OM/OC ratios of 1.4 for POA and 2.1 for SOA are applied in the partitioning routines, focusing on the wintertime, where aerosol is dominated by SVOC sources with a model imposed OM/OC ratio, can reduce the effect of the OM/OC ratio which must be specified for traditional and IVOC SOA. To convert traditional and IVOC SOA to OC, an OM/OC ratio of 2.1 is used and is roughly consistent with chamber data with the notable exception of α -pinene SOA (Chhabra et al., 2010). Comparisons to the IMPROVE network by Liao et al. (2007) indicate that GEOS-Chem underpredicts annual OA levels by about $0.56 \mu\text{g}/\text{m}^3$ (mean bias) or 34% (normalized mean bias) with the bias being larger in magnitude in the western US and lower in magnitude in the eastern US. A comparison of simulated and observed OC levels for the US during DJF 2000 in this work, indicate that GEOS-Chem underestimates OC by $0.20 \mu\text{gC}/\text{m}^3$ (21%) for the $2^\circ \times 2.5^\circ$ simulations and $0.37 \mu\text{gC}/\text{m}^3$ (39%) for the $4^\circ \times 5^\circ$ simulation. The bias for the $4^\circ \times 5^\circ$ simulation is likely larger as a result of the coarser model resolution and the fact that a climatological meteorology has been used as opposed to the assimilated, year-specific meteorology used by $2^\circ \times 2.5^\circ$ simulations. Compared to the semivolatile simulation (Fig. 3.7 bottom), the traditional simulation (Fig. 3.7 top) is more consistent with the IMPROVE observations. Sensitivity tests will be used to determine the factors that allow model performance to be brought closer to observations.

3.4.4 Sensitivity Tests

A number of key inputs and parameters involved in the global simulation of organic aerosol are uncertain; this fact suggests that sensitivity simulations will be useful in understanding the extent to which these uncertainties influence the predictions. The quantities examined in the sensitivity tests are listed in Table 3.6. For computational efficiency, the sensitivity tests are performed at $4^\circ \times 5^\circ$ resolution with GISS GCM meteorology. The effect of changes in meteorology and grid resolution on the global OA budget are examined in appendix (3.A) in this chapter. Although both the resolution and meteorology differ from those in the simulations discussed in the previous section, since the sensitivity tests address relative changes, the conclusions should be robust and relatively independent of the meteorology used (a discussion of interannual variability and resolution appears in Sect. 3.5.3). A *Traditional* (non-volatile POA and traditional SOA only) simulation is performed for comparison purposes. Even though the *Revised* simulation better represents the current scientific understanding of low-volatility organic compounds, the predicted concentration of OC over the US is low compared to observations (see Fig. 3.7). Due to the sparse nature of the IMPROVE network data for year 2000 DJF and the fact that the revised simulation predicts such low OC values, sensitivity simulations are compared to the *Traditional* simulation as well as observations. A traditional GEOS-Chem simulation has also been extensively evaluated against observations in the work of Liao et al. (2007).

Table 3.6 lists the additional simulations performed. The *Revised* simulation with semivolatile POA, oxidation of SVOCs, IVOC aerosol, and traditional SOA is described in previous sections. Two sensitivity tests are performed to examine the effects of changes in emissions. IVOC emissions are highly uncertain, and in the $2*IVOC$ simulation, the IVOC emissions are doubled. For the $2*SVOC$ simulation, the traditional POA inventory is doubled to obtain SVOC emissions ($G_R/POA_R=1$). Two simulations are also performed to address uncertainties in the SVOC and O-SVOC partitioning coefficients. In *SVOC K*10*, the SVOC emissions are a factor of 10 less volatile than in the *Revised* simulation, having saturation concentrations ($1/K_{OM}$) of 2 and $160 \mu\text{g}/\text{m}^3$. The $100\times$ decrease in saturation concentration is maintained so that the corresponding O-SVOCs have satura-

tion concentrations of 0.02 and 1.6 $\mu\text{g}/\text{m}^3$. For *O-SVOC K*10*, the SVOCs have the same saturation concentration as in the *Revised* simulation, but the SVOC oxidation products are a factor of 1000 times less volatile than their parent and thus have saturation concentrations of 0.02 and 1.6 $\mu\text{g}/\text{m}^3$ (the same as in the *SVOC K*10* simulation). An additional simulation, *H-Law/100*, reduces the effective Henry's Law coefficient relevant for scavenging of the secondary gas-phase semivolatile species to $10^3 \text{ M}/\text{atm}$. ΔH^*2 , in which the enthalpy of vaporization is doubled to 83 kJ/mol for all semivolatiles, is performed to examine wintertime surface concentrations as well. Parameters not listed in Table 3.6, such as biogenic hydrocarbon emissions, remain the same as in the base case.

3.4.4.1 Winter US Concentrations

As mentioned previously, wintertime OA concentrations are dominated by contributions from POA and SOA from SVOCs and offer an opportunity to examine model performance while minimizing the effect of errors in the parameterization of biogenic SOA. Figures 3.8 and 3.9 show the response of wintertime surface concentrations to the sensitivity tests in Table 3.6 relative to the *Traditional* simulation. Table 3.7 shows the mean bias and normalized mean bias for the sensitivity simulations compared to the IMPROVE network. Panel (a) of Fig. 3.8 represents the difference in surface concentrations between the *Revised* and *Traditional* simulations and highlights the fact that the *Revised* simulation results in a large decrease in surface concentrations as a result of POA evaporation. By doubling the IVOC emissions, *2*IVOC*, surface concentrations increase slightly, but a significant underestimate still exists as IVOCs contribute generally a small fraction of the wintertime OA. Increasing the SVOC emissions within the uncertainty of traditional POA inventories, *2*SVOC*, brings surface concentrations much closer to the traditional simulation and thus observations, although a slight underestimate persists. The *SVOC K*10* simulation is also effective in reducing the discrepancy between the new and traditional model formulations, since it is essentially making SVOCs more similar to traditional POA. In this simulation, roughly a factor of 6 to 10 more SVOCs with saturation concentrations of 1–2 $\mu\text{g}/\text{m}^3$ are emitted than recommended by Grieshop et al. (2009b). A comparison to the *O-SVOC K*10* simulation shows that the improvement in the *SVOC K*10*

simulation must be primarily a result of greater POA formation, not greater formation of SOA from SVOCs. The *O-SVOC K*10* indicates that reducing the volatility of the SVOC oxidation products alone is not especially effective for bringing the model closer to observations. The *H-Law/100* simulation has only a small effect on winter surface concentrations, but can have a significant effect on the global budget of OA, which will be addressed in the next section. Figure 3.9 shows the change in OC surface concentration for DJF relative to the traditional simulation for the ΔH^*2 simulation. The new enthalpy produces a result similar to that of doubling the POA inventory (*2*SVOC* simulation) in terms of reducing the discrepancy with the traditional simulation and observations. In conclusion, increasing the SVOC emissions, decreasing the SVOC emission volatility, or increasing the enthalpy of vaporization effectively reduce measurement/model discrepancy, although significant underestimates of the seasonal mean OC concentration persist (mean bias of $-0.51 \mu\text{gC}/\text{m}^3$ for *2*SVOC*, $-0.44 \mu\text{gC}/\text{m}^3$ for *SVOC K*10*, and $-0.50 \mu\text{gC}/\text{m}^3$ for ΔH^*2 compared to the IMPROVE observations). The reduction in volatility in *SVOC K*10* may be too extreme, and the higher enthalpy of vaporization may not be appropriate for lumped organics that span a relatively large range of volatility (Donahue et al., 2006). However, the increase in SVOC emissions, *2*SVOC*, lies within the uncertainty of the POA emission inventory in the work of Bond et al. (2004). Tripling the POA emission inventory to obtain SVOC emissions (not shown) results in DJF OC concentrations about $1 \mu\text{gC}/\text{m}^3$ higher than in the traditional simulation. The possibility remains that IVOCs could be underestimated by a substantially larger amount than examined here, or that the doubling of IVOC emissions in combination with doubling the POA emission inventory may provide a good present-day simulation. Additional constraints as well as a correct treatment of SOA temperature dependence are needed to assess the optimal model parameters.

For reference, Fig. S2 (see supplement in Appendix B) shows the effects of the first six sensitivity simulations on surface level June-July-August OC concentrations. The summertime simulations also indicate that increasing the SVOC emissions or decreasing the SVOC emission volatility are effective ways of reducing the discrepancy with the traditional simulation. However, since the summer OA is dominated by contributions from biogenic SOA, future updates to this source of SOA will likely

have significant effects on the summertime predictions.

3.4.4.2 Global Budget Sensitivity

Figure 3.10 shows the effect of the different sensitivity simulations on the global OA production rate compared to the *Traditional* simulation (all simulations use GISS meteorology at $4^\circ \times 5^\circ$ resolution). The *Traditional* simulation (at $4^\circ \times 5^\circ$) predicts 80 Tg/yr of net OA production using an OM/OC ratio of 2.1 for POA. The net OA source for the *Traditional* simulation includes the emission rate of non-volatile POA. As mentioned previously, the *Revised* simulation leads to a decrease of the net global OA source (-26% , see Table 3.5 for $2^\circ \times 2.5^\circ$ simulation results), but an increase of the OA lifetime due to a shift of production away from the surface. Doubling the IVOC emissions ($2*IVOC$) increases the global OA production rate compared to the *Revised* simulation, but not compared to the *Traditional* simulation (-17% compared to *Traditional*). Doubling the POA emission inventory to obtain SVOC emissions ($2*SVOC$), however, leads to an OA source that exceeds the *Traditional* simulation by 12% . The *SVOC K*10* and *O-SVOC K*10* simulations lead to a global production rate slightly larger than in the *Traditional* simulation ($+3\%$ and $+2\%$ respectively). The decrease in effective Henry's Law coefficient significantly increases the OA source ($+12\%$) and lifetime due to less effective wet removal.

Production of organic aerosol in the *Revised* framework at $2^\circ \times 2.5^\circ$ horizontal resolution with GEOS-4 is estimated to be 67 Tg/yr compared to 87 Tg/yr in the *Traditional* framework. The lowest global net production rate out of all simulations (at all resolutions and meteorologies) performed occurs with the *Revised* framework at $4^\circ \times 5^\circ$ horizontal resolution (GISS) and is about 60 Tg/yr. The sensitivity tests at $4^\circ \times 5^\circ$ horizontal resolution indicate that the global production rate could be 12% higher than that predicted in the traditional simulation if SVOC emissions are significantly underestimated or wet deposition of the gas-phase semivolatiles is less effective. The $2*SVOC$ test was repeated using the $2^\circ \times 2.5^\circ$ resolution (with GEOS-4 meteorology, see supplement in Appendix B) and the increase in production over the *Traditional* simulation was confirmed to be roughly the same as in the coarser resolution simulations (13%). Thus, the range of estimates for global OA

production examined here is approximately 60 to 100 Tg/yr.

One additional sensitivity test was performed to examine the effect of the biogenic emission inventory on the OA budget. Using the GEIA biogenic inventory (Guenther et al., 1995) instead of MEGAN (Guenther et al., 2006) results in a modest (about 7%) increase in the global OA production rate. For the $4^\circ \times 5^\circ$ resolution with GISS GCM III meteorology, GEIA estimates global isoprene sources to be 490 Tg/yr which is 24% higher than the MEGAN estimate. Terpene emissions increase by 14% compared to the MEGAN inventory. Isoprene SOA increases to 8 Tg/yr, and terpene SOA increases to 5 Tg/yr. However, the global OA budget (burden, sources, and losses) remains within 10% of the estimate using the MEGAN inventory. Current global chemical transport models and chemical mechanisms are known to have significant issues simulating isoprene and OH levels under low-NO_x conditions like over the Amazon (Lelieveld et al., 2008; Butler et al., 2008; Archibald et al., 2010). Improved isoprene chemistry and/or improved isoprene SOA formation parameterizations could lead to substantial changes in the global estimate of SOA from isoprene.

3.4.5 Modern vs. Fossil Carbon

The fraction of modern vs. fossil aerosol carbon can provide an additional model constraint. The major contributors to US surface OA are predicted to be biogenic hydrocarbons (mainly in summer) and SVOCs followed by IVOCs and aromatics. Slightly more than half of the global aromatic emissions are from fossil fuel sources (Henze et al., 2008). The fraction of modern carbon in POA and SOA formed from SVOCs is not separately tracked but depends on the composition of the SVOC emissions. Figure 3.11 shows the fraction of modern carbon in the SVOC emissions globally and for the US. Biomass and biofuel burning produce modern C while anthropogenic sources are assumed to be 100% fossil. Figure 3.11 indicates that aerosol from SVOCs over the US has a significant and often dominant modern component. The IVOC emissions over the US are dominated by fossil carbon (Fig. 3.12).

The radioisotope, ^{14}C , can be used to distinguish between modern (contemporary) and fossil carbon in ambient samples. ^{14}C is produced in the upper atmosphere by cosmic rays and has a half

life of about 5700 years. Fossil carbon should be depleted in ^{14}C , while modern carbon from sources such as biogenic VOC oxidation or wood burning should be enriched. Carbon isotope measurements have been performed in various locations to determine the contribution of modern and fossil carbon to total aerosol carbon. Carbon isotope measurements in the Southern California air basin in 1987 indicate that 30–40% of the fine particulate carbon was modern (Kaplan and Gordon, 1994). Szidat (2009) found OC was usually more than 50% modern for cities in Switzerland and Sweden, with biogenic OA likely responsible for modern carbon in summer and wood burning responsible in winter. Carbon isotope analysis of individual PAHs in Sweden indicates that residential wood burning is the dominant source of PAHs in the winter (Sheesley et al., 2009). During two field campaigns (2003 and 2006), Mexico City was found to have, on average, 70% modern carbon (Marley et al., 2009). In the analysis of aerosol at 12 US sites by Schichtel et al. (2008), total carbon was found to be about 50% modern in urban, 70–97% modern in near-urban, and 82 to 100% modern in remote areas. In short, the carbonaceous aerosol in a variety of locations exhibits significant amounts of modern carbon, with the fraction of modern carbon increasing with distance from urban centers (Schichtel et al., 2008). These observations lend support to the hypothesis that SVOCs contribute significantly to ambient OA and that scaling up SVOC emissions may be more justified than scaling up IVOC emissions. However, when scaling up the POA emission inventory to obtain SVOC emissions in this work, all sources were scaled up equally. Scaling up the POA emission inventories from all sources equally is supported by the work of Shrivastava et al. (2006) and others that indicate that diesel and wood combustion exhaust have very similar volatility profiles in the SVOC range. Thus, traditional POA inventories may represent the same fraction of SVOC emissions in each case. But, work by Shrivastava et al. (2008) and Grieshop et al. (2009a) indicate that diesel combustion or other anthropogenic sources may produce relatively more IVOCs than wood burning. The volatility at which the wood burning and anthropogenic emission volatility profiles diverge is not known (this work assumes it is about $10^4 \mu\text{g}/\text{m}^3$ based on sources that have been examined), and the fraction of SVOCs captured by diesel exhaust and wood burning POA inventories might differ leading to the need for source specific SVOC scaling factors. SVOCs from anthropogenic sources could be

underestimated to a greater extent by the traditional POA inventory than SVOCs from biomass or biofuel burning sources which means the fossil carbon SVOC emissions may be underestimated.

Using alkanes to obtain the spatial distribution of IVOC emissions would likely lead to large estimates of anthropogenic sources and small estimates of wood burning sources since wood burning is not a large source of intermediate volatility alkanes (approximately C17) (Schauer et al., 2001). Thus, the IVOC composition would be shifted even more toward fossil fuel sources than predicted by the naphthalene spatial distribution. Since ambient data indicate a large modern C component to aerosol, the alkane distribution would further diminish the expected role of IVOCs in ambient organic aerosol formation.

Modern carbon, however, should be distinguished from non-anthropogenic carbon. Biofuel combustion from activities like residential wood burning is a significant anthropogenic source of modern carbon. The high fraction of modern carbon in urban areas, especially compared to rural areas, in the winter suggests substantial contributions of wood burning to aerosol carbon in the US (Bench et al., 2007; Schichtel et al., 2008).

3.5 Model Uncertainties

Modeling organic aerosol production from SVOCs and IVOCs requires extrapolating experimental results obtained under idealized conditions or a from limited set of ambient observations to global conditions. As a result, potential discrepancies between experiments, observations, and the atmosphere must be addressed.

3.5.1 IVOC Behavior

Naphthalene is used as a surrogate to represent SOA formation from the entire set of IVOC emissions. Other important classes of IVOCs include alkanes and phenol type compounds. A significant portion of the IVOCs may also be part of the gas-phase UCM. Naphthalene is expected to be more representative of phenol-type compounds than alkanes would be, but does naphthalene exhibit behavior representative of IVOCs? High-NO_x oxidation of an alkane IVOC surrogate in the work of

Presto et al. (2009) resulted in less volatile SOA than low-NO_x oxidation, opposite of the behavior observed for naphthalene (Chan et al., 2009). However, in terms of yields, the IVOC, heptadecane, is predicted to react slightly faster with OH than naphthalene and result in a slightly lower but similar (20% vs. 26%) yield of SOA under high-NO_x conditions (Chan et al., 2009).

Assuming naphthalene is a good surrogate for IVOCs, is naphthalene behavior accurately captured by the current parameterization? Chamber experiments are likely to be most representative of the atmosphere when aerosol loadings are low and oxidation times are long. Low-NO_x conditions in which the peroxy radical from IVOC oxidation is expected to react with HO₂ is predicted to form a non-volatile aerosol product based on chamber experiments (Chan et al., 2009). However, chamber aerosol studies typically do not access very low organic concentrations, and thus what appears non-volatile in a chamber study may actually be semivolatile under atmospheric conditions. As a result, the dominance of aromatic and IVOC aerosol in remote regions near the surface could be a model artifact. In addition, aerosol from the RO₂+RO₂ pathway, which should be minor, is not accounted for in our model.

Another option for treating SOA from IVOCs is the volatility basis set approach with parameters by Robinson et al. (2007) or Grieshop et al. (2009a). IVOC compounds can be lumped into a series of volatility bins and oxidized with a prescribed reduction in volatility and increase in mass. With multiple generations of oxidation and no fragmentation reactions, this approach can give a very high yield of aerosol from IVOCs which could be on the order of 200% or more (J. Jimenez, personal communication, 2010). The yield is especially high using the parameters introduced by Grieshop et al. (2009a). Modeling for the Mexico City area indicates that the Grieshop et al. (2009a) parameters with multigenerational oxidation tend to overestimate organic aerosol downwind of the city (Hodzic et al., 2010). While the Robinson et al. (2007) parameters may give more realistic predictions of the total OA, the aerosol they produce predicts too low of an O:C ratio (Hodzic et al., 2010). Currently, Robinson et al. (2007) or Grieshop et al. (2009a) frameworks likely cannot be consistent with ambient measurements indicating that OOA is relatively non-volatile (Cappa and Jimenez, 2010) without predicting too much of an increase in mass or too low of an increase in O:C.

Simulations presented in this work obtain a lower net yield of aerosol from IVOCs of about 30% indicating a more minor role of IVOC aerosol. Both the basis set and the naphthalene-like approach used here may be similar in that near-source (i.e. high-NO_x) SOA tends to be semivolatile, while remote (i.e. low-NO_x) SOA tends to be relatively non-volatile. However, the reason for this trend and overall yields are very different in each case. Naphthalene can continue to serve as an IVOC surrogate until more information on IVOC emissions and/or IVOC oxidation behavior is obtained.

3.5.2 SVOC Volatility

The parameterization for SVOC volatility uses two surrogate compounds to represent SVOC emissions, in contrast to the volatility basis set which uses 4 or more volatility classes to represent emissions. Very low-volatility compounds (those with $C^* < 0.1 \mu\text{g}/\text{m}^3$) will be found in the aerosol phase under almost all atmospherically relevant conditions. The lowest volatility SVOC emitted in this work is assumed to have a C^* of $20 \mu\text{g}/\text{m}^3$ (at 300 K), and we likely do not represent SVOCs with saturation concentrations below $1 \mu\text{g}/\text{m}^3$. The volatility basis set approaches of Robinson et al. (2007) and Grieshop et al. (2009b) distribute low-volatility organic compounds with C^* s down to $0.01 \mu\text{g}/\text{m}^3$. Grieshop et al. (2009b) indicate that up to 5% of SVOC emissions may be considered non-volatile under atmospheric conditions since the C^* values are below $1 \mu\text{g}/\text{m}^3$. However, emissions of these very low-volatility compounds are not well constrained. Fits of wood-smoke data tend to diverge at organic concentrations less than about $100 \mu\text{g}/\text{m}^3$ (Shrivastava et al., 2006). Thermodenuder data can provide additional constraints but also show significant variability with somewhere between 80 and 40% of the wood-smoke aerosol evaporating at 50°C (Grieshop et al., 2009b). Grieshop et al. (2009a) included low-volatility compounds in their model of chamber aging and found that including a 9% contribution of C^* 0.1 and 0.01 degraded model performance. The two volatility components used here should roughly capture the partitioning of species with C^* of 1 to $10^4 \mu\text{g}/\text{m}^3$ and thus capture 95% (for wood burning) to 98% (for diesel) of the SVOC mass. If a 5% low-volatility emission were to be included in our simulation, it could account for up to 2 Tg C/yr of net primary organic aerosol formation. This could easily more than quadruple the net

POA source, but would have a small effect on the global aerosol production rate, which is predicted to exceed 60 Tg/yr.

3.5.3 Horizontal Resolution and Inter-annual Variability

Sensitivity tests performed indicate that doubling SVOC emissions leads to more realistic surface-level OC concentrations for the US in winter. This conclusion was reached using sensitivity tests for DJF in year 2000 with GISS meteorology at $4^{\circ} \times 5^{\circ}$ horizontal grid resolution. The same tests were repeated for DJF in year 2001 with GISS meteorology at $4^{\circ} \times 5^{\circ}$ to confirm that this conclusion is not highly sensitive to the choice of meteorological year (see supplement Fig. S3 in Appendix B). Three of the tests in Table 3.6 were also performed for year 2000 DJF using GEOS-4 meteorology at $2^{\circ} \times 2.5^{\circ}$ horizontal grid resolution. Thus, the robustness of the conclusions with respect to meteorological year as well as horizontal grid resolution and meteorology can be determined. GISS tests for year 2000 and 2001 both indicate that doubling SVOC emissions brings concentrations closer to those observed, but still leaves a slight underestimate that may be larger in 2001. Using the GEOS-4 meteorology at $2^{\circ} \times 2.5^{\circ}$ indicates that concentrations might actually be higher compared to the traditional simulation in the northeast when SVOC emissions are doubled (Fig. S4). In conclusion, years 2000 and 2001 are roughly similar in terms of the effects of the sensitivity simulations on DJF surface OC. The GEOS-4 $2^{\circ} \times 2.5^{\circ}$ simulation confirms that doubling SVOC emissions is reasonable. However, these tests and the fact that the $2^{\circ} \times 2.5^{\circ}$ and $4^{\circ} \times 5^{\circ}$ simulations have different mean biases (Table 3.7) illustrate that tuning a model based on one simulation may not produce the same result for other simulations (like the Northeast at $2^{\circ} \times 2.5^{\circ}$ vs. $4^{\circ} \times 5^{\circ}$). Any tuning of the model emissions should be based on multiple constraints and/or a large observational data set.

3.6 Conclusions

In this study, we present a global estimate, using GEOS-Chem, of organic aerosols from primary emissions of gases and aerosols with saturation concentrations of roughly less than $10^6 \mu\text{g}/\text{m}^3$. Sources of these compounds include biomass burning, biofuel burning, and anthropogenic activities. POA,

which has traditionally been considered non-volatile, is replaced by a pool of semivolatile organic compounds, denoted here as SVOCs, that can partition between the gas and aerosol phases and can be oxidized in the gas phase to less volatile species that partition even more effectively to the aerosol phase. In addition, intermediate volatility organic compounds, denoted as IVOCs, which exist entirely in the vapor phase, can undergo oxidation in the gas phase to form lower volatility species that partition to the aerosol phase (based on naphthalene-like behavior). Aerosol that results from the oxidation of any of these gas-phase species is termed secondary organic aerosol (SOA). Globally, biomass burning and anthropogenic sources contribute similar amounts of IVOCs. Over the US, the dominant fraction of IVOCs arises from anthropogenic sources.

Implementation of semivolatile POA generally leads to decreases in predicted surface-level concentrations of organic aerosol due to a portion of the POA evaporating upon emission. US winter organic carbon concentrations from the IMPROVE network are used to assess the accuracy of model predictions under conditions in which the effect of uncertainties in biogenic SOA formation are likely to be at a minimum. Sensitivity tests indicate that uncertainties in the IVOC emissions, the Henry's Law coefficient for scavenging of gas-phase semivolatiles, or the assumed 100x (or 1000x) decrease in volatility upon oxidation of the primary SVOCs are not especially influential in reducing the discrepancy between predictions and observations. However, a significant increase in SVOC emissions, a reduction of the volatility of the SVOC emissions, or an increase in the enthalpy of vaporization to 83 kJ/mol all lead to an appreciable reduction of the prediction/measurement discrepancy. The reduction in SVOC volatility examined is likely too extreme, but scaling up the SVOC emissions by a factor of 2 seems reasonable considering that traditional inventories do not necessarily capture SVOCs emitted in the gas phase. The higher enthalpy of vaporization is also supported by a recent study (Epstein et al., 2010) but may not be appropriate for lumped organics (Donahue et al., 2006).

The range of estimates for global organic aerosol production is 60–100 Tg/yr. Virtually all of this production is SOA, since POA tends to evaporate and oxidize in the gas phase after emission. The sensitivity tests examine uncertainties one parameter at a time, so the range in organic aerosol production could be larger if uncertainties in multiple parameters were to be accounted for

simultaneously. If current traditional POA inventories capture only about one-half of the SVOC emissions and gas-phase semivolatiles are much less aggressively wet removed, this would lead to an estimate of global OA production that is not inconsistent with top-down calculations, such as those by (Goldstein and Galbally, 2007) who estimated SOA production ranging from 140 Tg/yr and up. Much of the increase in SOA shown here compared to previous estimates, like those by Henze et al. (2008), results from reclassification of most of the POA as SOA due to evaporation and subsequent oxidation. Also note that the present estimate of OA production is net production, so a species that partitions to the aerosol, but later evaporates, is not counted in net aerosol. The effects of chemical aging of SOA beyond that reflected in current chamber experiments are not explicitly considered.

SVOC and IVOC emissions are predicted to have different fractions of modern and fossil carbon which can provide constraints on estimates of SVOC and IVOC aerosol. In the US, SVOC emissions have a significant biofuel component which, along with biomass burning emissions, results in a significant fraction of modern C. US IVOC emissions, however, are predicted to be predominantly fossil. The high fraction of modern carbon observed in organic aerosol in the US is consistent with an important contribution of aerosol from SVOCs.

While representing POA as semivolatile is clear progress in modeling of organic aerosol, additional constraints are needed to sharpen estimates. Information in the form of improved SVOC and IVOC emission estimates or data (such as ^{14}C fractions, O:C ratios, AMS PMF components (OOA, HOA), correlation with gas-phase tracers (Weber et al., 2007; de Gouw et al., 2005), or identification of marker compounds (Bhave et al., 2007)) that allow for the determination of sources of OA can help to constrain models.

Supplemental information can be found in Appendix B.

3.7 Appendix 3.A: Effect of meteorology and grid resolution on global OA budget

The effect of changes in meteorology and horizontal grid resolution on the global OA budget are briefly examined. GEOS-Chem with GEOS-4 and GISS GCM III meteorology at $4^{\circ} \times 5^{\circ}$ has been compared previously with a focus on tropospheric ozone budgets (Wu et al., 2007). Wu et al. (2007) found that an important difference between the GEOS assimilated and GISS GCM meteorology is the treatment of wet convection. The GISS model allows for non-precipitating condensed water, and in GEOS-Chem with GISS meteorology, soluble species are not scavenged in shallow convective updrafts below 700 hPa. Differences in clouds can lead to differences in oxidant levels. Boundary layer turbulence is also treated slightly differently in GEOS-Chem with GEOS meteorology versus GEOS-Chem with GISS meteorology (Wu et al., 2007). Although these differences exist between the two meteorologies, organic aerosols have been successfully simulated and compared to observations using GEOS meteorology at $2^{\circ} \times 2.5^{\circ}$ resolution (Park et al., 2003) and $1^{\circ} \times 1^{\circ}$ nested grid resolution (Park et al., 2006) and using GISS meteorology at $4^{\circ} \times 5^{\circ}$ resolution (Liao et al., 2007). Note that the $2^{\circ} \times 2.5^{\circ}$ GEOS and $4^{\circ} \times 5^{\circ}$ GISS simulations should be viewed as 2 different realizations of year 2000 conditions and should not be the same, but show similar responses to changes in parameters.

Table 3.8 shows the effect of changes in meteorology and resolution on precursor emissions, OA net production, aerosol lifetime, and global OH. Natural emissions such as lightning NO_x and biogenic hydrocarbons that are parameterized based on meteorology are predicted to change significantly in some cases. The change to $4^{\circ} \times 5^{\circ}$ GISS meteorology results in 7% higher terpene emissions, but 11% lower isoprene emissions, presumably due to differences in temperature. Except for POA, the net OA production is expected to decrease. The change in global net OA production as a result of the change in resolution is relatively larger for biogenic SOA compared to the change in emissions. For example, although isoprene emissions are 11% lower at the coarser resolution, the production rate of isoprene SOA is 40% lower. Presumably, global OA production decreases as a result of lower isoprene emissions. SOA production could also decrease as a result of more effective deposition of

the gas-phase precursors or semivolatiles. OH levels over the Amazon are generally slightly lower in the GCAP $4^\circ \times 5^\circ$ simulation compared to the $2^\circ \times 2.5^\circ$ simulation which supports lower isoprene SOA formation as well.

To gain further insight into the effects of changes in meteorology and resolution and why POA production may have increased at $4^\circ \times 5^\circ$, the effect of the changes on a traditional non-volatile POA simulation are shown in Table 3.9. Hydrophobic and hydrophilic forms of POA are separated. Hydrophobic POA is similar to the semivolatile POA, in that it is emitted but can be converted to another species (hydrophilic POA for the traditional simulation or SOA in the revised simulation). In the traditional simulation, for $4^\circ \times 5^\circ$ resolution compared to $2^\circ \times 2.5^\circ$, hydrophobic POA is more effectively wet and dry deposited as reflected by the higher deposition rates and shorter tropospheric lifetime against deposition. For production of semivolatile POA to increase at $4^\circ \times 5^\circ$ for the same SVOC emissions, POA must be more quickly lost to wet and dry deposition before it evaporates and reacts with OH. The aerosol deposition velocity over land is generally higher for the $4^\circ \times 5^\circ$ GISS study than $2^\circ \times 2.5^\circ$ GEOS-4 study due to a higher friction velocity over land in the GISS meteorological fields. Thus, OA production can generally decrease as a result of lower isoprene SOA, but POA production can increase due to more aggressive deposition. SOA from SVOCs, IVOCs, and aromatics is only slightly affected by the change in resolution and meteorology.

3.8 Acknowledgements

The numerical simulations for this research were performed on Caltech's Division of Geological and Planetary Sciences Dell cluster. H. O. T. P. acknowledges support by a National Science Foundation Graduate Research Fellowship. This research has been supported by the US Environmental Protection Agency Science to Achieve Results (STAR) agreements RD-833749 and RD-83337001 and by the Office of Science (BER), US Department of Energy Grant No. DE-FG02-05ER63983. Although the research described in the article has been funded in part by the US Environmental Protection Agency's STAR program, it has not been subjected to any EPA review and therefore does not necessarily reflect the views of the Agency, and no official endorsement should be inferred.

The authors would like to thank Arthur Chan, Jose Jimenez, Fabien Paulot, and Paul Wennberg for useful discussions.

Bibliography

- Aiken, A. C., Decarlo, P. F., Kroll, J. H., Worsnop, D. R., Huffman, J. A., Docherty, K. S., Ulbrich, I. M., Mohr, C., Kimmel, J. R., Sueper, D., Sun, Y., Zhang, Q., Trimborn, A., Northway, M., Ziemann, P. J., Canagaratna, M. R., Onasch, T. B., Alfarra, M. R., Prevot, A. S. H., Dommen, J., Duplissy, J., Metzger, A., Baltensperger, U., and Jimenez, J. L.: O/C and OM/OC ratios of primary, secondary, and ambient organic aerosols with high-resolution time-of-flight aerosol mass spectrometry, *Environ. Sci. Technol.*, 42, 4478–4485, doi:10.1021/ES703009q, 2008.
- Andreae, M. O. and Merlet, P.: Emission of trace gases and aerosols from biomass burning, *Global Biogeochem. Cy.*, 15, 955–966, doi:10.1029/2000GB001382, 2001.
- Archibald, A. T., Jenkin, M. E., and Shallcross, D. E.: An isoprene mechanism intercomparison, *Atmos. Environ.*, doi:10.1016/J.ATMOSENV.2009.09.016, in press, 2010.
- Atkinson, R.: Gas-phase tropospheric chemistry of volatile organic compounds: 1. Alkanes and alkenes, *J. Phys. Chem. Ref. Data*, 26, 215–290, 1997.
- Atkinson, R. and Arey, J.: Atmospheric degradation of volatile organic compounds, *Chem. Rev.*, 103, 4605–4638, doi:10.1021/CR0206420, 2003.
- Bench, G., Fallon, S., Schichtel, B., Malm, W., and McDade, C.: Relative contributions of fossil and contemporary carbon sources to PM_{2.5} aerosols at nine Interagency Monitoring for Protection of Visual Environments (IMPROVE) network sites, *J. Geophys. Res.*, 112, D10205, doi:10.1029/2006JD007708, 2007.
- Bey, I., Jacob, D. J., Yantosca, R. M., Logan, J. A., Field, B. D., Fiore, A. M., Li, Q. B., Liu, H. G. Y., Mickley, L. J., and Schultz, M. G.: Global modeling of tropospheric chemistry with

- assimilated meteorology: Model description and evaluation, *J. Geophys. Res.*, 106, 23073–23095, 2001.
- Bhave, P. V., Pouliot, G. A., and Zheng, M.: Diagnostic model evaluation for carbonaceous PM_{2.5} using organic markers measured in the southeastern U.S., *Environ. Sci. Technol.*, 41, 1577–1583, 2007.
- Bond, T. C., Streets, D. G., Yarber, K. F., Nelson, S. M., Woo, J. H., and Klimont, Z.: A technology-based global inventory of black and organic carbon emissions from combustion, *J. Geophys. Res.*, 109, D14203, doi:10.1029/2003JD003697, 2004.
- Butler, T. M., Taraborrelli, D., Brhl, C., Fischer, H., Harder, H., Martinez, M., Williams, J., Lawrence, M. G., and Lelieveld, J.: Improved simulation of isoprene oxidation chemistry with the ECHAM5/MESSy chemistry-climate model: lessons from the GABRIEL airborne field campaign, *Atmos. Chem. Phys.*, 8, 4529–4546, doi:10.5194/acp-8-4529-2008, 2008.
- Cappa, C. D. and Jimenez, J. L.: Quantitative estimates of the volatility of ambient organic aerosol, *Atmos. Chem. Phys. Discuss.*, 10, 1901–1938, doi:10.5194/acpd-10-1901-2010, 2010.
- Chan, A. W. H., Kautzman, K. E., Chhabra, P. S., Surratt, J. D., Chan, M. N., Crounse, J. D., Krten, A., Wennberg, P. O., Flagan, R. C., and Seinfeld, J. H.: Secondary organic aerosol formation from photooxidation of naphthalene and alkylnaphthalenes: implications for oxidation of intermediate volatility organic compounds (IVOCs), *Atmos. Chem. Phys.*, 9, 3049–3060, doi:10.5194/acp-9-3049-2009, 2009.
- Chhabra, P. S., Flagan, R. C., and Seinfeld, J. H.: Elemental analysis of chamber organic aerosol using an aerodyne high-resolution aerosol mass spectrometer, *Atmos. Chem. Phys.*, 10, 4111–4131, doi:10.5194/acp-10-4111-2010, 2010.
- Chung, S. H. and Seinfeld, J. H.: Global distribution and climate forcing of carbonaceous aerosols, *J. Geophys. Res.*, 107, 4407, doi:10.1029/2001JD001397, 2002.

- Cooke, W. F., Lioussse, C., Cachier, H., and Feichter, J.: Construction of a $1^\circ \times 1^\circ$ fossil fuel emission data set for carbonaceous aerosol and implementation and radiative impact in the ECHAM4 model, *J. Geophys. Res.*, 104, 22137–22162, 1999.
- de Gouw, J. A., Middlebrook, A. M., Warneke, C., Goldan, P. D., Kuster, W. C., Roberts, J. M., Fehsenfeld, F. C., Worsnop, D. R., Canagaratna, M. R., Pszenny, A. A. P., Keene, W. C., Marchewka, M., Bertman, S. B., and Bates, T. S.: Budget of organic carbon in a polluted atmosphere: Results from the New England Air Quality Study in 2002, *J. Geophys. Res.*, 110, D16305, doi:10.1029/2004JD005623, 2005.
- Donahue, N. M., Robinson, A. L., Stanier, C. O., and Pandis, S. N.: Coupled partitioning, dilution, and chemical aging of semivolatile organics, *Environ. Sci. Technol.*, 40, 2635–2643, doi:10.1021/ES052297c, 2006.
- Dzepina, K., Volkamer, R. M., Madronich, S., Tulet, P., Ulbrich, I. M., Zhang, Q., Cappa, C. D., Ziemann, P. J., and Jimenez, J. L.: Evaluation of recently-proposed secondary organic aerosol models for a case study in Mexico City, *Atmos. Chem. Phys.*, 9, 5681–5709, doi:10.5194/acp-9-5681-2009, 2009.
- Epstein, S. A., Riipinen, I., and Donahue, N. M.: A semiempirical correlation between enthalpy of vaporization and saturation concentration for organic aerosol, *Environ. Sci. Technol.*, 44, 743–748, doi:10.1021/ES902497z, 2010.
- Farina, S. C., Adams, P. J., and Pandis, S. N.: Modeling global secondary organic aerosol formation and processing with the volatility basis set: implications for anthropogenic SOA, *J. Geophys. Res.*, doi:10.1029/2009JD013046, 115, D09202, doi:10.1029/2009JD013046, 2010.
- Fu, T. M., Jacob, D. J., Wittrock, F., Burrows, J. P., Vrekoussis, M., and Henze, D. K.: Global budgets of atmospheric glyoxal and methylglyoxal, and implications for formation of secondary organic aerosols, *J. Geophys. Res.*, 113, D15303, doi:10.1029/2007JD009505, 2008.

- Goldstein, A. H. and Galbally, I. E.: Known and unexplored organic constituents in the earth's atmosphere, *Environ. Sci. Technol.*, 41, 1514–1521, doi:10.1021/ES072476p, 2007.
- Grieshop, A. P., Logue, J. M., Donahue, N. M., and Robinson, A. L.: Laboratory investigation of photochemical oxidation of organic aerosol from wood fires 1: measurement and simulation of organic aerosol evolution, *Atmos. Chem. Phys.*, 9, 1263–1277, doi:10.5194/acp-9-1263-2009, 2009.
- Grieshop, A. P., Miracolo, M. A., Donahue, N. M., and Robinson, A. L.: Constraining the volatility distribution and gas-particle partitioning of combustion aerosols using isothermal dilution and thermodenuder measurements, *Environ. Sci. Technol.*, 43, 4750–4756, doi:10.1021/ES8032378, 2009b.
- Guenther, A., Hewitt, C. N., Erickson, D., Fall, R., Geron, C., Graedel, T., Harley, P., Klinger, L., Lerdau, M., Mckay, W. A., Pierce, T., Scholes, B., Steinbrecher, R., Tallamraju, R., Taylor, J., and Zimmerman, P.: A global-model of natural volatile organic-compound emissions, *J. Geophys. Res.*, 100, 8873–8892, 1995.
- Guenther, A., Karl, T., Harley, P., Wiedinmyer, C., Palmer, P. I., and Geron, C.: Estimates of global terrestrial isoprene emissions using MEGAN (Model of Emissions of Gases and Aerosols from Nature), *Atmos. Chem. Phys.*, 6, 3181–3210, doi:10.5194/acp-6-3181-2006, 2006.
- Hays, M. D., Geron, C. D., Linna, K. J., Smith, N. D., and Schauer, J. J.: Speciation of gas-phase and fine particle emissions from burning of foliar fuels, *Environ. Sci. Technol.*, 36, 2281–2295, doi:10.1021/ES0111683, 2002.
- Heald, C. L., Jacob, D. J., Park, R. J., Russell, L. M., Huebert, B. J., Seinfeld, J. H., Liao, H., and Weber, R. J.: A large organic aerosol source in the free troposphere missing from current models, *Geophys. Res. Lett.*, 32, L18809, doi:10.1029/2005GL023831, 2005.
- Henze, D. K. and Seinfeld, J. H.: Global secondary organic aerosol from isoprene oxidation, *Geophys. Res. Lett.*, 33, doi:10.1029/2006GL025976, 2006.

- Henze, D. K., Seinfeld, J. H., Ng, N. L., Kroll, J. H., Fu, T.-M., Jacob, D. J., and Heald, C. L.: Global modeling of secondary organic aerosol formation from aromatic hydrocarbons: high- vs. low-yield pathways, *Atmos. Chem. Phys.*, 8, 2405–2420, doi:10.5194/acp-8-2405-2008, 2008.
- Hodzic, A., Jimenez, J. L., Madronich, S., Canagaratna, M. R., DeCarlo, P. F., Kleinman, L., and Fast, J.: Potential contribution of semi-volatile and intermediate volatility primary organic compounds to secondary organic aerosol in the Mexico City region, *Atmos. Chem. Phys. Discuss.*, 10, 657–710, doi:10.5194/acpd-10-657-2010, 2010.
- Huffman, J. A., Docherty, K. S., Aiken, A. C., Cubison, M. J., Ulbrich, I. M., DeCarlo, P. F., Sueper, D., Jayne, J. T., Worsnop, D. R., Ziemann, P. J., and Jimenez, J. L.: Chemically-resolved aerosol volatility measurements from two megacity field studies, *Atmos. Chem. Phys.*, 9, 7161–7182, doi:10.5194/acp-9-7161-2009, 2009a.
- Huffman, J. A., Docherty, K. S., Mohr, C., Cubison, M. J., Ulbrich, I. M., Ziemann, P. J., Onasch, T. B., and Jimenez, J. L.: Chemically-resolved volatility measurements of organic aerosol from different sources, *Environ. Sci. Technol.*, 43, 5351–5357, doi:10.1021/ES803539d, 2009b.
- Jimenez, J. L., Canagaratna, M. R., Donahue, N. M., Prevot, A. S. H., Zhang, Q., Kroll, J. H., DeCarlo, P. F., Allan, J. D., Coe, H., Ng, N. L., Aiken, A. C., Docherty, K. S., Ulbrich, I. M., Grieshop, A. P., Robinson, A. L., Duplissy, J., Smith, J. D., Wilson, K. R., Lanz, V. A., Hueglin, C., Sun, Y. L., Tian, J., Laaksonen, A., Raatikainen, T., Rautiainen, J., Vaattovaara, P., Ehn, M., Kulmala, M., Tomlinson, J. M., Collins, D. R., Cubison, M. J., Dunlea, E. J., Huffman, J. A., Onasch, T. B., Alfarra, M. R., Williams, P. I., Bower, K., Kondo, Y., Schneider, J., Drewnick, F., Borrmann, S., Weimer, S., Demerjian, K., Salcedo, D., Cottrell, L., Griffin, R., Takami, A., Miyoshi, T., Hatakeyama, S., Shimono, A., Sun, J. Y., Zhang, Y. M., Dzepina, K., Kimmel, J. R., Sueper, D., Jayne, J. T., Herndon, S. C., Trimborn, A. M., Williams, L. R., Wood, E. C., Middlebrook, A. M., Kolb, C. E., Baltensperger, U., and Worsnop, D. R.: Evolution of organic aerosols in the atmosphere, *Science*, 326, 1525–1529, doi:10.1126/SCIENCE.1180353, 2009.
- Jordan, C. E., Ziemann, P. J., Griffin, R. J., Lim, Y. B., Atkinson, R., and Arey, J.: Modeling

- SOA formation from OH reactions with C-8-C-17 n-alkanes, *Atmos. Environ.*, 42, 8015–8026, doi:10.1016/J.ATMOSENV.2008.06.017, 2008.
- Kaplan, I. R. and Gordon, R. J.: Non-fossil-fuel fine-particle organic-carbon aerosols in Southern California determined during the Los-Angeles aerosol characterization and source apportionment study, *Aerosol. Sci. Tech.*, 21, 343–359, 1994.
- Kautzman, K. E., Surratt, J., Chan, M. N., Chan, A. W. H., Hersey, S. P., Chhabra, P. S., Dalleska, N. F., Wennberg, P. O., Flagan, R. C., and Seinfeld, J. H.: Chemical composition of gas- and aerosol-phase products from the photooxidation of naphthalene, *J. Phys. Chem. A*, 114, 913–934, 2010.
- Kroll, J. H., Smith, J. D., Che, D. L., Kessler, S. H., Worsnop, D. R., and Wilson, K. R.: Measurement of fragmentation and functionalization pathways in the heterogeneous oxidation of oxidized organic aerosol, *Phys. Chem. Chem. Phys.*, 11, 8005–8014, doi:10.1039/B905289e, 2009.
- Lane, T. E., Donahue, N. M., and Pandis, S. N.: Simulating secondary organic aerosol formation using the volatility basis-set approach in a chemical transport model, *Atmos. Environ.*, 42, 7439–7451, doi:10.1016/J.ATMOSENV.2008.06.026, 2008.
- Lelieveld, J., Butler, T. M., Crowley, J. N., Dillon, T. J., Fischer, H., Ganzeveld, L., Harder, H., Lawrence, M. G., Martinez, M., Taraborrelli, D., and Williams, J.: Atmospheric oxidation capacity sustained by a tropical forest, *Nature*, 452, 737–740, doi:10.1038/NATURE06870, 2008.
- Liao, H., Henze, D. K., Seinfeld, J. H., Wu, S. L., and Mickley, L. J.: Biogenic secondary organic aerosol over the United States: Comparison of climatological simulations with observations, *J. Geophys. Res.*, 112, D06201, doi:10.1029/2006JD007813, 2007.
- Lipsky, E. M. and Robinson, A. L.: Effects of dilution on fine particle mass and partitioning of semivolatile organics in diesel exhaust and wood smoke, *Environ. Sci. Technol.*, 40, 155–162, doi:10.1021/ES050319p, 2006.

- Marley, N. A., Gaffney, J. S., Tackett, M., Sturchio, N. C., Heraty, L., Martinez, N., Hardy, K. D., Marchany-Rivera, A., Guilderson, T., MacMillan, A., and Steelman, K.: The impact of biogenic carbon sources on aerosol absorption in Mexico City, *Atmos. Chem. Phys.*, 9, 1537–1549, doi:10.5194/acp-9-1537-2009, 2009.
- Murphy, B. N. and Pandis, S. N.: Simulating the formation of semivolatile primary and secondary organic aerosol in a regional chemical transport model, *Environ. Sci. Technol.*, 43, 4722–4728, doi:10.1021/ES803168a, 2009.
- Ng, N. L., Kroll, J. H., Chan, A. W. H., Chhabra, P. S., Flagan, R. C., and Seinfeld, J. H.: Secondary organic aerosol formation from m-xylene, toluene, and benzene, *Atmos. Chem. Phys.*, 7, 3909–3922, doi:10.5194/acp-7-3909-2007, 2007.
- Ng, N. L., Canagaratna, M. R., Zhang, Q., Jimenez, J. L., Tian, J., Ulbrich, I. M., Kroll, J. H., Docherty, K. S., Chhabra, P. S., Bahreini, R., Murphy, S. M., Seinfeld, J. H., Hildebrandt, L., DeCarlo, P. F., Lanz, V. A., Prevot, A. S. H., Dinar, E., Rudich, Y., and Worsnop, D. R.: Organic aerosol components observed in worldwide datasets from aerosol mass spectrometry, *Atmos. Chem. Phys. Discuss.*, 9, 27745–27789, doi:10.5194/acpd-9-27745-2009, 2009.
- Odum, J. R., Hoffmann, T., Bowman, F., Collins, D., Flagan, R. C., and Seinfeld, J. H.: Gas/particle partitioning and secondary organic aerosol yields, *Environ. Sci. Technol.*, 30, 2580–2585, 1996.
- Offenberg, J. H., Kleindienst, T. E., Jaoui, M., Lewandowski, M., and Edney, E. O.: Thermal properties of secondary organic aerosols, *Geophys. Res. Lett.*, 33, L03816, doi:10.1029/2005GL024623, 2006.
- Pankow, J. F.: An absorption-model of gas-particle partitioning of organic-compounds in the atmosphere, *Atmos. Environ.*, 28, 185–188, 1994.
- Park, R. J., Jacob, D. J., Chin, M., and Martin, R. V.: Sources of carbonaceous aerosols over the United States and implications for natural visibility, *J. Geophys. Res.*, 108(D12), 4355, doi:10.1029/2002JD003190, 2003.

- Park, R. J., Jacob, D. J., Field, B. D., Yantosca, R. M., and Chin, M.: Natural and transboundary pollution influences on sulfate-nitrate-ammonium aerosols in the United States: Implications for policy, *J. Geophys. Res.*, 109, D15204, doi:10.1029/2003JD004473, 2004.
- Park, R. J., Jacob, D. J., Kumar, N., and Yantosca, R. M.: Regional visibility statistics in the United States: Natural and transboundary pollution influences, and implications for the Regional Haze Rule, *Atmos. Environ.*, 40, 5405–5423, doi:10.1016/J.ATMOENV.2006.04.059, 2006.
- Presto, A. A., Miracolo, M. A., Kroll, J. H., Worsnop, D. R., Robinson, A. L., and Donahue, N. M.: Intermediate-volatility organic compounds: A potential source of ambient oxidized organic aerosol, *Environ. Sci. Technol.*, 43, 4744–4749, doi:10.1021/ES803219q, 2009.
- Pye, H. O. T., Liao, H., Wu, S., Mickley, L. J., Jacob, D. J., Henze, D. K., and Seinfeld, J. H.: Effect of changes in climate and emissions on future sulfate-nitrate-ammonium aerosol levels in the United States, *J. Geophys. Res.*, 114, D01205, doi:10.1029/2008JD010701, 2009.
- Rind, D., Lerner, J., Jonas, J., and McLinden, C.: Effects of resolution and model physics on tracer transports in the NASA Goddard Institute for Space Studies general circulation models, *J. Geophys. Res.*, 112, D09315, doi:10.1029/2006JD007476, 2007.
- Robinson, A. L., Donahue, N. M., Shrivastava, M. K., Weitkamp, E. A., Sage, A. M., Grieshop, A. P., Lane, T. E., Pierce, J. R., and Pandis, S. N.: Rethinking organic aerosols: Semivolatile emissions and photochemical aging, *Science*, 315, 1259–1262, doi:10.1126/SCIENCE.1133061, 2007.
- Sander, R.: Compilation of Henry’s Law constants for inorganic and organic species of potential importance in environmental chemistry (version 3), <http://www.henrys-law.org>, 1999.
- Schauer, J. J., Kleeman, M. J., Cass, G. R., and Simoneit, B. R. T.: Measurement of emissions from air pollution sources. 3. C-1-C-29 organic compounds from fireplace combustion of wood, *Environ. Sci. Technol.*, 35, 1716–1728, doi:10.1021/ES001331e, 2001.
- Schauer, J. J., Kleeman, M. J., Cass, G. R., and Simoneit, B. R. T.: Measurement of emissions

- from air pollution sources. 5. C-1-C-32 organic compounds from gasoline-powered motor vehicles, *Environ. Sci. Technol.*, 36, 1169–1180, doi:10.1021/ES0108077, 2002.
- Schichtel, B. A., Malm, W. C., Bench, G., Fallon, S., McDade, C. E., Chow, J. C., and Watson, J. G.: Fossil and contemporary fine particulate carbon fractions at 12 rural and urban sites in the United States, *J. Geophys. Res.*, 113, D02311, doi:10.1029/2007JD008605, 2008.
- Sheesley, R. J., Kruså, M., Krecl, P., Johansson, C., and Gustafsson, O.: Source apportionment of elevated wintertime PAHs by compound-specific radiocarbon analysis, *Atmos. Chem. Phys.*, 9, 3347–3356, doi:10.5194/acp-9-3347-2009, , 2009.
- Shrivastava, M. K., Lipsky, E. M., Stanier, C. O., and Robinson, A. L.: Modeling semivolatile organic aerosol mass emissions from combustion systems, *Environ. Sci. Technol.*, 40, 2671–2677, doi:10.1021/ES0522231, 2006.
- Shrivastava, M. K., Lane, T. E., Donahue, N. M., Pandis, S. N., and Robinson, A. L.: Effects of gas particle partitioning and aging of primary emissions on urban and regional organic aerosol concentrations, *J. Geophys. Res.*, 113, D18301, doi:10.1029/2007JD009735, 2008.
- Szidat, S.: Radiocarbon analysis of carbonaceous aerosols: Recent developments, *Chimia*, 63, 157–161, doi:10.2533/CHIMIA.2009.157, 2009.
- Turpin, B. J. and Lim, H. J.: Species contributions to PM_{2.5} mass concentrations: Revisiting common assumptions for estimating organic mass, *Aerosol. Sci. Tech.*, 35, 602–610, 2001.
- van der Werf, G. R., Randerson, J. T., Giglio, L., Collatz, G. J., Kasibhatla, P. S., and Arellano Jr., A. F.: Interannual variability in global biomass burning emissions from 1997 to 2004, *Atmos. Chem. Phys.*, 6, 3423–3441, doi:10.5194/acp-6-3423-2006, 2006.
- Weber, R. J., Sullivan, A. P., Peltier, R. E., Russell, A., Yan, B., Zheng, M., de Gouw, J., Warneke, C., Brock, C., Holloway, J. S., Atlas, E. L., and Edgerton, E.: A study of secondary organic aerosol formation in the anthropogenic-influenced southeastern United States, *J. Geophys. Res.*, 112, D13302, doi:10.1029/2007JD008408, 2007.

- Wesely, M. L.: Parameterization of surface resistances to gaseous dry deposition in regional-scale numerical-models, *Atmos. Environ.*, **23**, 1293–1304, 1989.
- Wu, S. L., Mickley, L. J., Jacob, D. J., Logan, J. A., Yantosca, R. M., and Rind, D.: Why are there large differences between models in global budgets of tropospheric ozone?, *J. Geophys. Res.*, **112**, D05302, doi:10.1029/2006JD007801, 2007.
- Wu, S. L., Mickley, L. J., Leibensperger, E. M., Jacob, D. J., Rind, D., and Streets, D. G.: Effects of 2000–2050 global change on ozone air quality in the United States, *J. Geophys. Res.*, **113**, D06302, doi:10.1029/2007JD008917, 2008.
- Zhang, L. M., Gong, S. L., Padro, J., and Barrie, L.: A size-segregated particle dry deposition scheme for an atmospheric aerosol module, *Atmos. Environ.*, **35**, 549–560, 2001.
- Zhang, Q., Worsnop, D. R., Canagaratna, M. R., and Jimenez, J. L.: Hydrocarbon-like and oxygenated organic aerosols in Pittsburgh: insights into sources and processes of organic aerosols, *Atmos. Chem. Phys.*, **5**, 3289–3311, doi:10.5194/acp-5-3289-2005, 2005.
- Zhang, Q., Jimenez, J. L., Canagaratna, M. R., Allan, J. D., Coe, H., Ulbrich, I., Alfarra, M. R., Takami, A., Middlebrook, A. M., Sun, Y. L., Dzepina, K., Dunlea, E., Docherty, K., DeCarlo, P. F., Salcedo, D., Onasch, T., Jayne, J. T., Miyoshi, T., Shimojo, A., Hatakeyama, S., Takegawa, N., Kondo, Y., Schneider, J., Drewnick, F., Borrmann, S., Weimer, S., Demerjian, K., Williams, P., Bower, K., Bahreini, R., Cottrell, L., Griffin, R. J., Rautiainen, J., Sun, J. Y., Zhang, Y. M., and Worsnop, D. R.: Ubiquity and dominance of oxygenated species in organic aerosols in anthropogenically-influenced Northern Hemisphere midlatitudes, *Geophys. Res. Lett.*, **34**, L13801, doi:10.1029/2007GL029979, 2007.
- Zhang, Y. X. and Tao, S.: Global atmospheric emission inventory of polycyclic aromatic hydrocarbons (PAHs) for 2004, *Atmos. Environ.*, **43**, 812–819, doi:10.1016/J.ATMOSENV.2008.10.050, 2009.

Table 3.1: Low-volatility organic compounds.

Species	Description	α^a	K_{OM}^b [m ³ /μg]	C^* [μg/m ³]	Reference
SVOC ₁	primary SVOC emission	0.49 ^c	0.0006	1646	Shrivastava et al. (2006)
SVOC ₂	primary SVOC emission	0.51 ^c	0.05	20	Shrivastava et al. (2006)
O–SVOC ₁	oxidized SVOC ₁	1.5	0.06	16.46	Grieshop et al. (2009a)
O–SVOC ₂	oxidized SVOC ₂	1.5	5.0	0.20	Grieshop et al. (2009a)
IVOC	primary IVOC emission ^d	NA	1×10^{-5}	10^5	
O–IVOC _{N,1}	high NO _x IVOC oxidation product ^d	0.21	0.59	1.69	Chan et al. (2009)
O–IVOC _{N,2}	high NO _x IVOC oxidation product ^d	1.07	0.0037	270	Chan et al. (2009)
O–IVOC _{H,1}	low NO _x IVOC oxidation product ^d	0.73	10 000	0.0001	Chan et al. (2009)

^a See Equation 3.7.

^b Reference temperature for SVOC parameters is 300 K. IVOC SOA reference temperature is 299 K.

^c Fraction of total SVOC emissions.

^d IVOC behavior based on naphthalene.

Table 3.2: Emissions of primary low-volatility organic compounds (year 2000).

Species	Biomass burning [Tg C/yr]	Biofuel burning [Tg C/yr]	Anthropogenic sources ^a [Tg C/yr]	Total [Tg C/yr]
Traditional non-volatile POA	19	7.1	2.7	29
SVOCs	24	9.0	3.4	37
Naphthalene ^b	0.09	0.05	0.09	0.22
IVOC surrogate	5.7	3.2	5.8	15

^a Excluding biomass and biofuel burning.

^b The baseline naphthalene emission inventory is used only to obtain the spatial distribution of IVOC emissions.

Table 3.3: Parameters for SVOC oxidation.

Parameter	This work	Robinson et al. (2007)	Grieshop et al. (2009a)
Gas-phase OH rate constant [$\text{cm}^3 \text{ molec}^{-1} \text{ s}^{-1}$]	2×10^{-11}	4×10^{-11}	2×10^{-11}
Reduction in volatility per reaction	100×	10×	100×
Increase in mass per reaction	50%	7.5%	40%
Number of oxidation reactions per parent hydrocarbon	1	> 1	> 1

Table 3.4: Rate constants for IVOC oxidation. $k=Ae^{B/T}$. Sources: Atkinson and Arey (2003); Henze et al. (2008); Atkinson (1997).

Reaction	A [cm ³ molec ⁻¹ s ⁻¹]	B [K]	k_{298} [cm ³ molec ⁻¹ s ⁻¹]
NAP+OH	1.56×10^{-11}	117	2.3×10^{-11}
RO ₂ +HO ₂	1.4×10^{-12}	700	1.5×10^{-11}
RO ₂ +NO	2.6×10^{-12}	350	8.5×10^{-12}

Table 3.5: Global OA budget for traditional (non-volatile POA) and revised (semivolatile POA, SOA from SVOCs, and SOA from IVOCs) simulations. The OM/OC ratio for traditional, non-volatile POA is 2.1. The OM/OC ratio for semivolatile POA is 1.4. The OM/OC ratio for all SOA is 2.1. Simulations were performed at $2^\circ \times 2.5^\circ$ horizontal resolution with GEOS-4 meteorology.

	Tropospheric burden [Tg]	Net Source ^a [Tg/yr]	Wet Deposition [Tg/yr]	Dry Deposition [Tg/yr]	Lifetime [days]
Traditional Non-volatile POA Simulation					
Traditional POA	0.92	61	53	8.4	5.5
Traditional SOA	0.72	26	23	2.3	10
Total OA	1.64	87	76	11	6.9
Revised Simulation					
Semivolatile POA	0.03	0.70	0.22	0.49	17
SOA from SVOCs	0.81	38	34	4.4	7.7
SOA from IVOCs	0.09	5.2	4.6	0.6	6.5
Traditional SOA	0.71	23	21	2.0	11
Total OA	1.65	67	60	7.4	9.0
Percent Change in OA					
Traditional OA	-1%	-11%	-11%	-15%	12%
Total OA	0%	-23%	-22%	-31%	30%

^a Net Source includes emission for POA in the traditional simulation.

Table 3.6: Sensitivity tests with GCM meteorology at $4^\circ \times 5^\circ$.

Label	I VOC Emissions [Tg C/yr]	SVOC emissions [Tg C/yr]	K_{OM} SVOC [m ³ /μg]	K_{OM} O-SVOC [m ³ /μg]	Henry's Law Coefficient ^c [M/atm]	ΔH_{vap} [kJ/mol]
Traditional ^a	NA	29	large	NA	10^5	42 ^d
Revised ^b	15	37	0.0006, 0.05	0.06, 5.0	Traditional	Traditional
2*I VOC	2×Revised	Revised	Revised	Revised	Traditional	Traditional
2*SVOC	Revised	2×Traditional	Revised	Revised	Traditional	Traditional
SVOC K*10	Revised	Revised	10×Revised	10×Revised	Traditional	Traditional
O-SVOC K*10	Revised	Revised	Revised	10×Revised	Traditional	Traditional
H-Law/100	Revised	Revised	Revised	Revised	10^3	Traditional
ΔH^*2	Revised	Revised	Revised	Revised	Traditional	83

^a Traditional simulation with non-volatile POA and SOA from traditional precursors.

^b Revised simulation uses semivolatile POA, oxidation of SVOCs, SOA from IVOCs, and SOA from traditional precursors.

^c For wet removal of gas-phase semivolatiles.

^d Implemented using a value of 41.6 kJ/mol.

Table 3.7: Mean bias (MB) in $\mu\text{gC}/\text{m}^3$ and normalized mean bias (NMB) in percent (%) for the sensitivity simulations for DJF 2000 ($MB = \frac{1}{N} \sum_{i=1}^N (P_i - O_i)$, $NMB = 100\% * \sum_{i=1}^N (P_i - O_i) / \sum_{i=1}^N (O_i)$), where P_i are the model predictions and O_i are the IMPROVE observations at N locations). IMPROVE observations are shown in Fig. 3.7. Sensitivity simulations are outlined in Table 6. $2^\circ \times 2.5^\circ$ simulations use GEOS4 meteorology. $4^\circ \times 5^\circ$ simulations use GISS GCM meteorology.

Simulation	MB [$\mu\text{gC}/\text{m}^3$]	NMB [%]
$2^\circ \times 2.5^\circ$ Traditional	-0.20	-22
$2^\circ \times 2.5^\circ$ Revised	-0.59	-63
$4^\circ \times 5^\circ$ Traditional	-0.37	-39
$4^\circ \times 5^\circ$ Revised	-0.70	-75
$4^\circ \times 5^\circ$ 2*IVOC	-0.68	-73
$4^\circ \times 5^\circ$ 2*SVOC	-0.51	-55
$4^\circ \times 5^\circ$ SVOC K*10	-0.44	-47
$4^\circ \times 5^\circ$ O-SVOC K*10	-0.60	-64
$4^\circ \times 5^\circ$ H-Law/100	-0.67	-71
$4^\circ \times 5^\circ$ ΔH^*2	-0.50	-54

Table 3.8: Effect of model resolution and meteorology on global OA budget. $2^\circ \times 2.5^\circ$ simulations are performed with GEOS-4 assimilated meteorology. $4^\circ \times 5^\circ$ simulations were performed with GISS GCM Model 3 meteorology. Both simulations use revised framework (semivolatile POA, SOA from SVOCs, and SOA from IVOCs). To convert POA to Tg C, divide by 1.4. To convert SOA to Tg C, divide by 2.1.

Process	$2^\circ \times 2.5^\circ$ Assimilated Meteorology	$4^\circ \times 5^\circ$ GCM Meteorology	Difference (%)
Precursor Emissions [Tg/yr]			
SVOCs	52	52	0%
IVOCs	16	16	0%
terpenes	115	123	7%
alcohols	38	38	1%
sesquiterpenes	15	15	0%
isoprene	446	396	-11%
aromatics	18	18	0%
OA Net Production by Parent Hydrocarbon Class [Tg/yr]			
SVOC (POA)	0.7	1.1	56%
SVOC (SOA)	38.3	37.0	-3%
IVOCs	5.2	5.1	-2%
terpenes	5.6	4.1	-26%
alcohols	1.1	0.8	-32%
sesquiterpenes	1.5	1.0	-35%
isoprene	11.2	6.7	-40%
aromatics	3.5	3.3	-6%
Total OA Production	67	59	-12%
Tropospheric Lifetime Against Deposition [days]			
POA	17.4	9.5	-45%
SVOC SOA	7.7	5.3	-31%
IVOC SOA	6.5	4.4	-31%
Traditional SOA	11.4	9.1	-20%
Mass weighted OH Concentration [molec cm^{-3}]			
[OH]	1.07×10^6	1.03×10^6	-4%

Table 3.9: Traditional (non-volatile POA) simulation for $2^\circ \times 2.5^\circ$ and $4^\circ \times 5^\circ$ grid resolution. $2^\circ \times 2.5^\circ$ simulations are performed with GEOS-4 assimilated meteorology. $4^\circ \times 5^\circ$ simulations were performed with GISS GCM Model 3 meteorology.

	Tropospheric burden [Tg C]	Emission [Tg C/yr]	Wet Deposition [Tg C/yr]	Dry Deposition [Tg C/yr]	Tropospheric Lifetime [days]
$2^\circ \times 2.5^\circ$ Traditional Non-volatile POA Simulation					
Hydrophobic POA	0.042	15	0.3	0.7	15
Hydrophilic POA	0.40	15	25	3.3	5.2
Total POA	0.44	29	25	4	5.5
$4^\circ \times 5^\circ$ Traditional Non-volatile POA Simulation					
Hydrophobic POA	0.039	15	0.7	1.2	7.3
Hydrophilic POA	0.26	15	23	3.9	3.5
Total POA	0.30	29	24	5	3.7

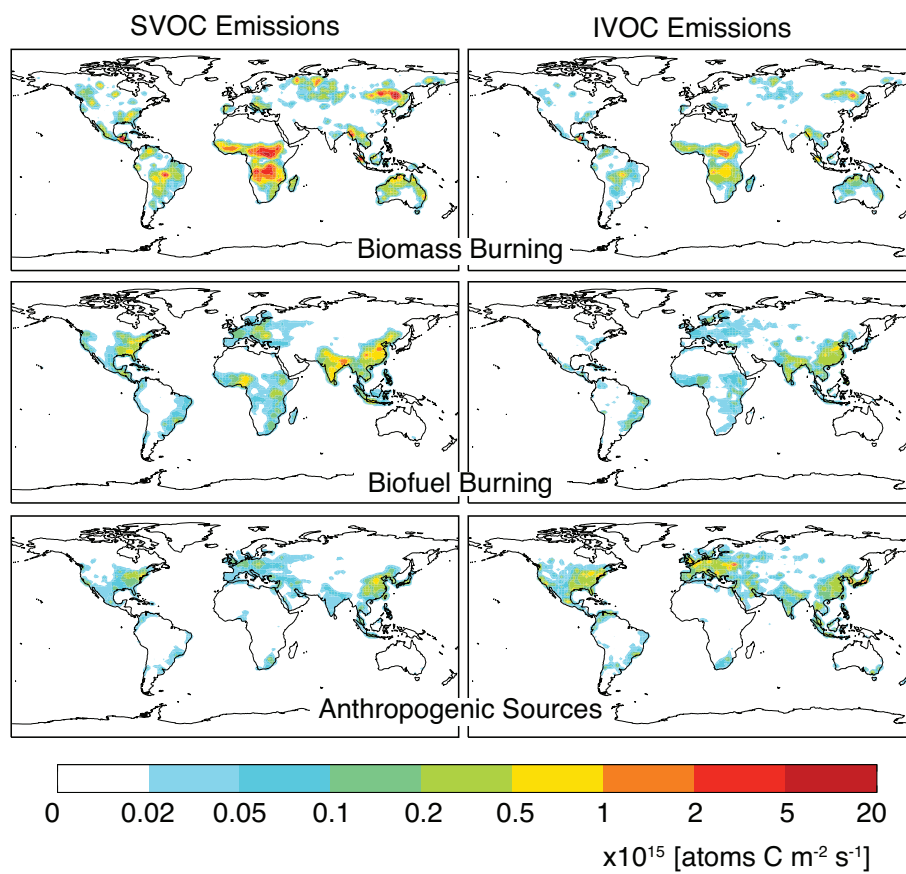


Figure 3.1: Emissions of SVOCs and IVOCs. SVOC emissions shown here are the baseline POA emission inventory. Plots are annual averages for year 2000. Note that the color scale is not linear.

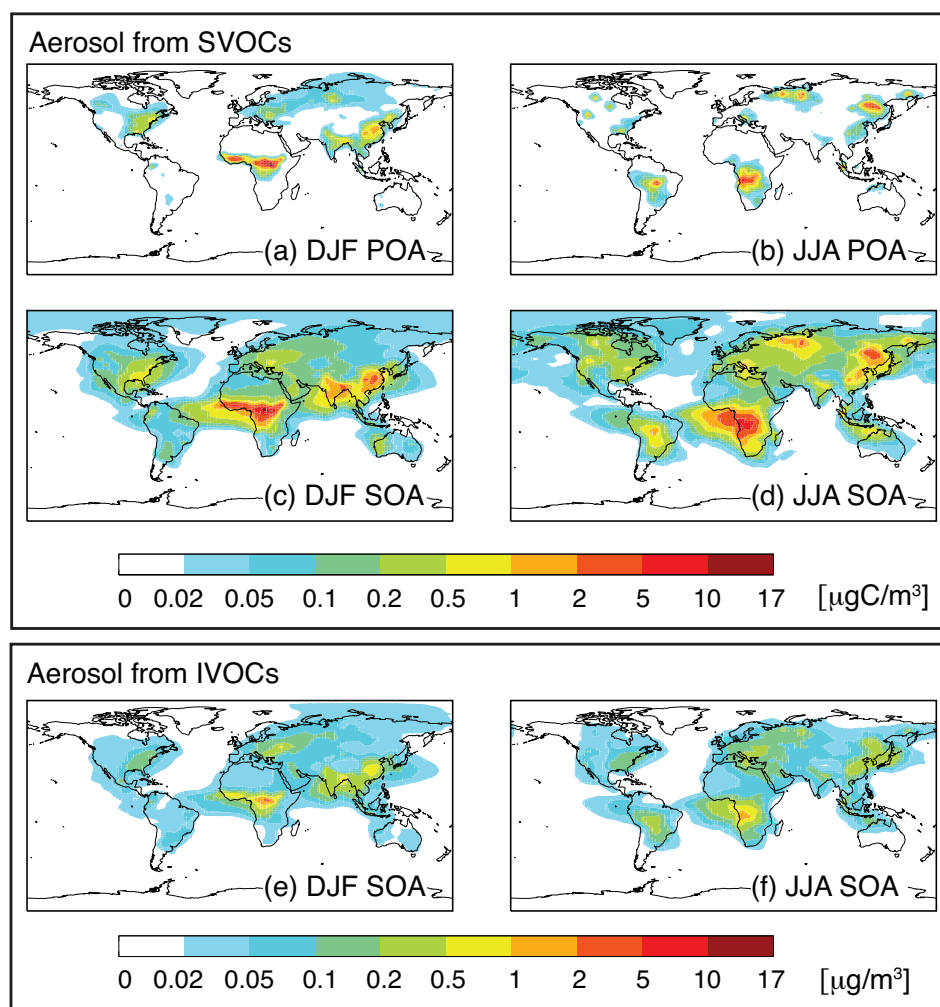


Figure 3.2: Predicted concentration of aerosol from SVOCs and IVOCs. Aerosol from SVOCs includes POA, (a and b), and SOA, (c and d), and is expressed in $\mu\text{gC}/\text{m}^3$. Aerosol from IVOCs is shown in panels (e and f) and is expressed in $\mu\text{g}/\text{m}^3$. Concentrations are shown at the surface for December-January-February (DJF) and June-July-August (JJA) for year 2000 (GEOS-4, $2^\circ \times 2.5^\circ$). Note that the color scale is not linear.

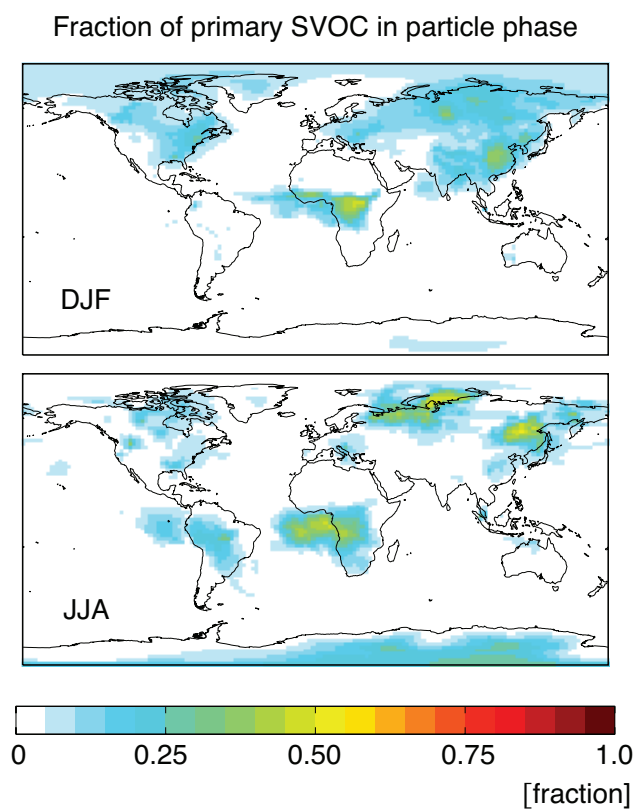


Figure 3.3: Fraction of primary semivolatile material in aerosol phase as POA at the surface, seasonally averaged for year 2000. Fraction is simply the aerosol-phase SVOC concentrations (in ppb) divided by the total SVOC (gas+aerosol) concentration (in ppb). Simulations performed with GEOS-4 at $2^\circ \times 2.5^\circ$.

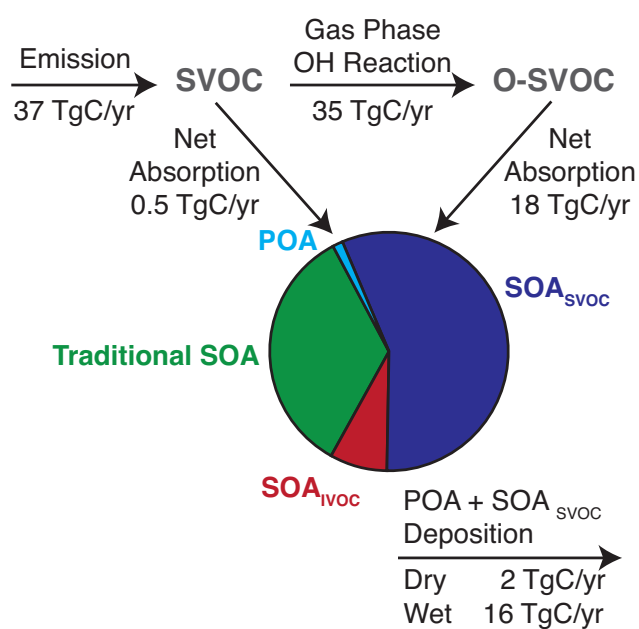


Figure 3.4: SVOC budget. Relative portions of pie indicate annual net production (32 TgC/yr total). SVOC and O-SVOC (oxidized SVOC) are also wet and dry deposited (not shown). All numbers are for year 2000. Simulation performed at $2^\circ \times 2.5^\circ$ with GEOS-4 meteorology.

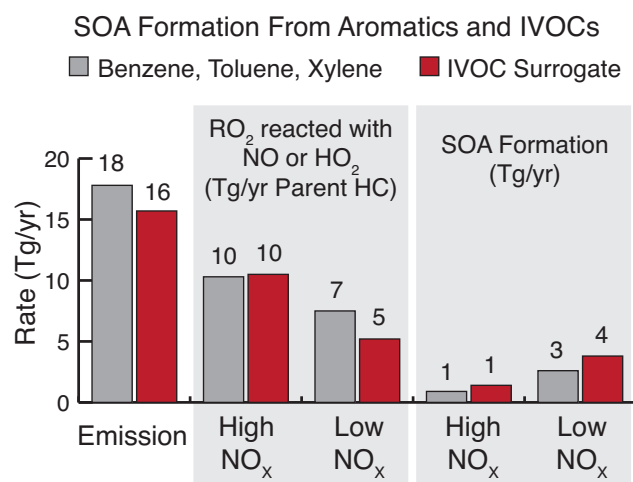


Figure 3.5: Emission, oxidation, and aerosol formation from aromatics and IVOCs. Simulation performed at $2^\circ \times 2.5^\circ$ with GEOS-4 meteorology.

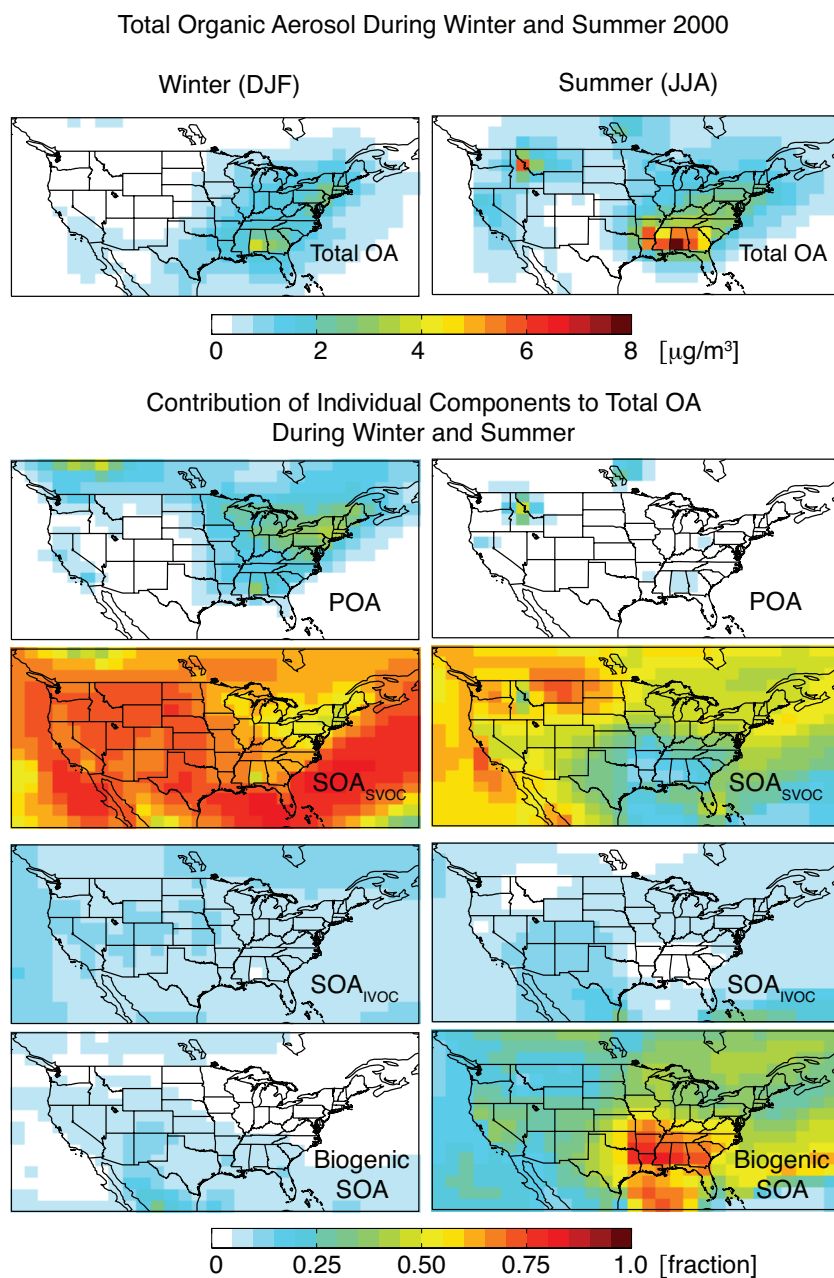


Figure 3.6: Total OA and contribution of each component to winter and summer concentrations over the US. Not shown is the contribution of aromatic SOA to total OA. Fraction is fraction of total OA. Simulations are $2^\circ \times 2.5^\circ$ with GEOS-4 meteorology.

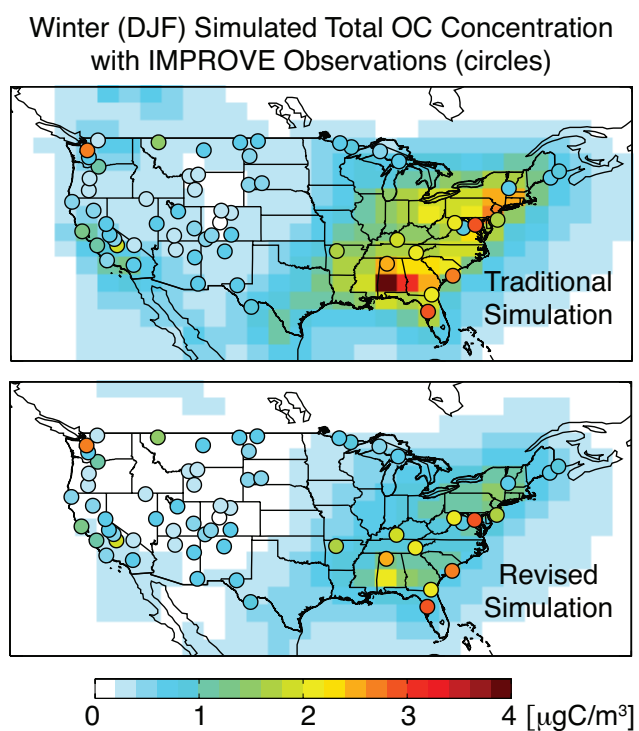


Figure 3.7: Winter (December-January-February 2000) surface total OC concentration from $2^\circ \times 2.5^\circ$ (GEOS-4) simulations for the traditional and revised frameworks. Total OC includes POA and SOA from traditional precursors, IVOCs, and SVOCs. IMPROVE observations (averaged over DJF for year 2000) are overlaid in circles. An outlier value of $>27 \mu\text{gC}/\text{m}^3$ has been removed from the IMPROVE observations. Only sites with valid data for at least half of the DJF 2000 season are shown.

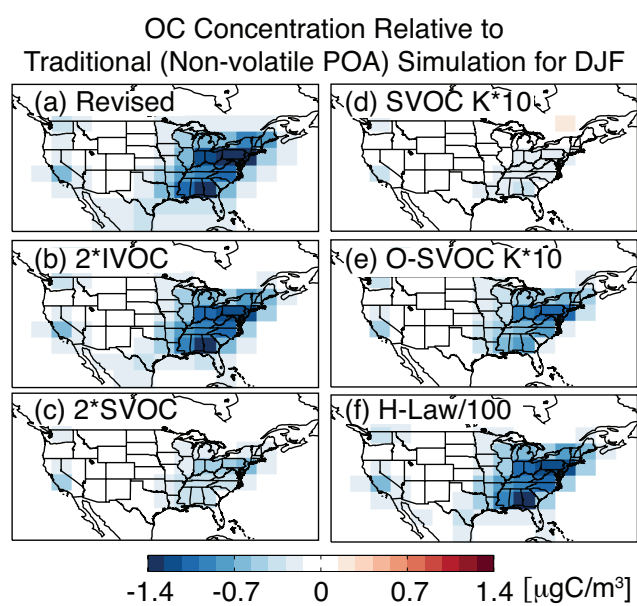


Figure 3.8: DJF surface total OC concentration (POA, SOA from SVOCs, SOA from IVOCs, and traditional SOA) relative to non-volatile POA simulation (POA and traditional SOA) using GISS meteorology at $4^\circ \times 5^\circ$. Sensitivity tests are given in Table 3.6.

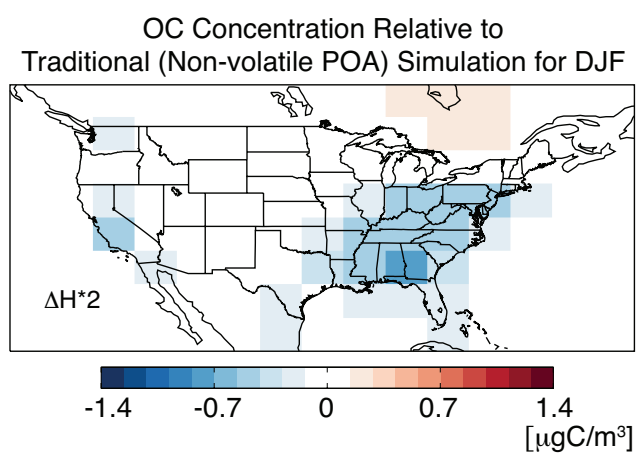


Figure 3.9: DJF surface total OC concentration (POA, SOA from SVOCs, SOA from IVOCs, and traditional SOA) from a revised simulation in which the enthalpy of vaporization is 83 kJ/mol relative to a non-volatile (traditional) POA simulation (POA and traditional SOA) using GISS meteorology at $4^\circ \times 5^\circ$.

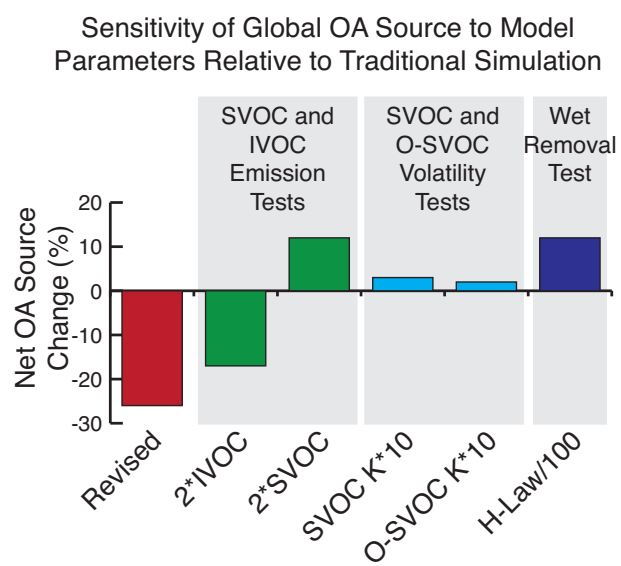


Figure 3.10: Change in global OA net source (from all types of organic aerosol) for sensitivity tests. Values are relative to traditional simulation at $4^\circ \times 5^\circ$ using GISS meteorology. Sensitivity tests are given in Table 3.6.

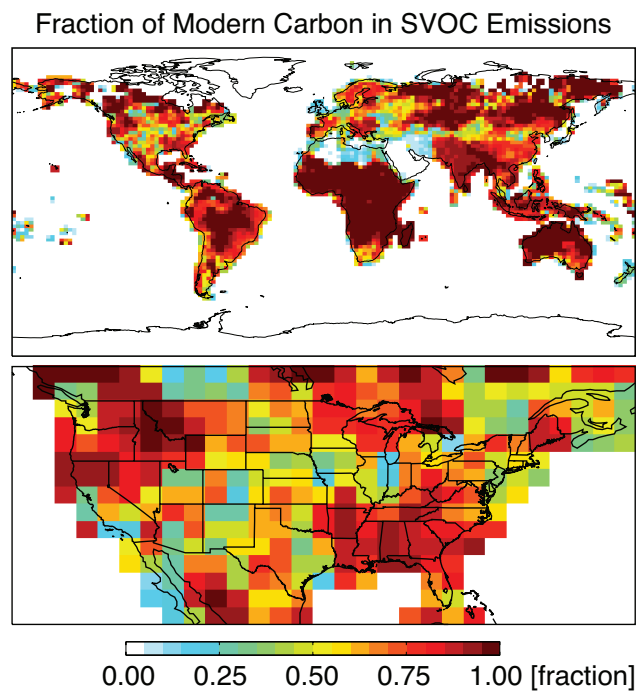


Figure 3.11: Fraction of SVOC emissions from modern carbon: $(\text{Biomass} + \text{Biofuel}) / (\text{Biomass} + \text{Biofuel} + \text{Anthropogenic})$.

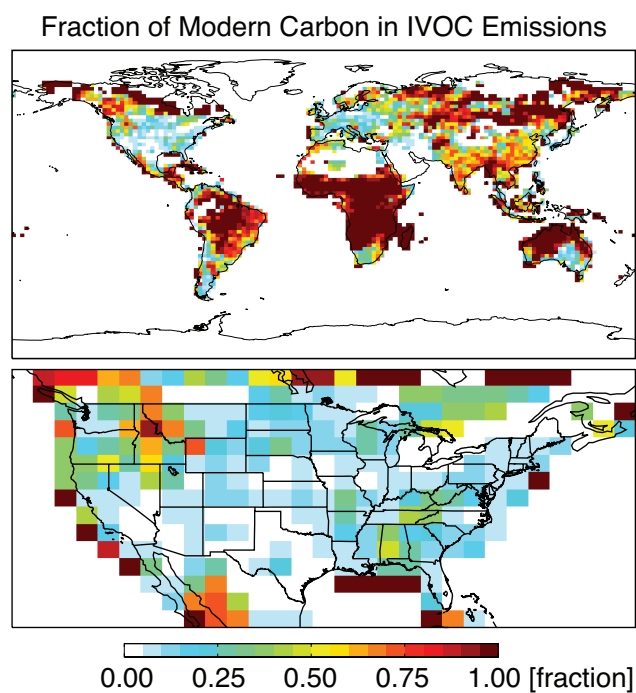


Figure 3.12: Fraction of IVOC emissions from modern carbon: $(\text{Biomass} + \text{Biofuel}) / (\text{Biomass} + \text{Biofuel} + \text{Anthropogenic})$. Note that the high contribution of modern carbon just off the coast of the US (such as over the Gulf of Mexico) results from small, but non-zero emissions from biofuel burning. Biofuel emissions occur in these locations as a result of degradation of the emission inventory as it is regridded from $0.25^\circ \times 0.25^\circ$ to $1^\circ \times 1^\circ$ and then $2^\circ \times 2.5^\circ$ or $4^\circ \times 5^\circ$ horizontal resolution for use in GEOS-Chem.

Chapter 4

Global modeling of organic aerosol: The importance of reactive nitrogen *

*Submitted to *Atmospheric Chemistry and Physics* as "Global modeling of organic aerosol: The importance of reactive nitrogen" by H. O. T. Pye, A. W. H. Chan, M. Barkley, and J. H. Seinfeld.

4.1 Abstract

Reactive nitrogen compounds, specifically NO_x and NO_3 , likely influence global organic aerosol levels. To assess these interactions, GEOS-Chem, a chemical transport model, is updated to include improved biogenic emissions (following MEGAN v2.1/2.04), a new organic aerosol tracer lumping scheme, aerosol from nitrate radical (NO_3) oxidation of isoprene, and NO_x -dependent terpene aerosol yields. As a result of significant nighttime terpene emissions, fast reaction of monoterpenes with the nitrate radical, and relatively high aerosol yields from NO_3 oxidation, biogenic hydrocarbon- NO_3 reactions are expected to be a major contributor to surface level aerosol concentrations in anthropogenically influenced areas such as the United States. By including aerosol from nitrate radical oxidation in GEOS-Chem, terpene aerosol approximately doubles and isoprene aerosol is enhanced by 30 to 40% in the Southeast United States. In terms of the global budget of organic aerosol, however, aerosol from nitrate radical oxidation is somewhat minor (slightly more than 3 Tg/yr) due to the relatively high volatility of organic- NO_3 oxidation products. Globally, 69 to 88 Tg/yr of organic aerosol is predicted to be produced annually, of which 14-15 Tg/yr is from oxidation of monoterpenes and sesquiterpenes and 8-9 Tg/yr from isoprene.

4.2 Introduction

The aerosol phase is an important intermediate or terminal form for many species in the atmosphere including volatile organic compounds (VOCs) (Goldstein and Galbally, 2007), and understanding aerosol is important for assessing the climate change and human health impacts of air pollution. Organic aerosol can result from direct emissions, producing primary organic aerosol (POA), or form in situ from chemical transformation, yielding secondary organic aerosol (SOA). Anthropogenic SOA contributors include light aromatics (Ng et al., 2007b), naphthalene (Chan et al., 2009), and alkanes (Lim and Ziemann, 2005). Low-volatility compounds emitted from sources including diesel combustion and biomass burning also lead to significant amounts of POA and SOA (Robinson et al., 2007). In addition to these hydrocarbons, biogenic compounds such as isoprene, monoterpenes, and

sesquiterpenes serve as SOA precursors (Hoffmann et al., 1997; Griffin et al., 1999a; Kroll et al., 2006). Chamber studies have provided the foundation for organic aerosol parameterizations in global models such as GEOS-Chem (Henze and Seinfeld, 2006; Liao et al., 2007; Henze et al., 2008; Pye and Seinfeld, 2010), NCAR Community Atmospheric Model (CAM3) (Heald et al., 2008), TM3 (Tsigaridis and Kanakidou, 2003), and GISS GCM II-prime (Chung and Seinfeld, 2002).

A number of issues related to organic aerosol remain unresolved. Models often predict organic aerosol levels that are much lower than those observed (Heald et al., 2005; Volkamer et al., 2006; Liao et al., 2007; Pye and Seinfeld, 2010). In addition, organic aerosol even in urban areas tends to contain significant “modern” carbon (Szidat, 2009; Marley et al., 2009; Schichtel et al., 2008) but correlates with anthropogenic tracers (de Gouw et al., 2005; Weber et al., 2007).

Emissions of NO_x represent a potential way for anthropogenic and biogenic systems to interact. NO_x ($\text{NO} + \text{NO}_2$) levels have been identified as an important SOA factor in photooxidation and ozonolysis (Presto et al., 2005; Ng et al., 2007a). Both modeling and experimental work indicate that the yield of aerosol is highly sensitive to NO_x , especially for low VOC/NO_x ratios ($\text{VOC}/\text{NO}_x < 1$ ppb/ppb) (Ng et al., 2007a; Capouet et al., 2008). Light aromatics (Ng et al., 2007b), polycyclic aromatic hydrocarbons (Chan et al., 2009), and monoterpenes (Presto et al., 2005) are expected to have lower yields under high- NO_x conditions ($\text{VOC}/\text{NO}_x < 0.1$ ppb/ppb), in which the peroxy radical reacts preferentially with NO instead of HO_2 . Ng et al. (2007a) examined the monoterpene, α -pinene, and the sesquiterpenes, longifolene and aromdendrene, and postulated that sesquiterpenes generally exhibit higher yields under high- NO_x conditions as a result of a higher probability of isomerization for $\text{RO}_2 + \text{NO}$ alkoxy radicals or higher yields of less volatile organic nitrates. For isoprene, yields under high- NO_x conditions are typically lower than under low NO_x conditions (Kroll et al., 2005, 2006). But, recent work indicates that high- NO_x isoprene oxidation can be just as effective as low- NO_x oxidation in producing SOA (Surratt et al., 2010; Chan et al., 2010). During the night, NO_2 reacts with O_3 to produce nitrate radicals (NO_3). Monoterpenes have a very short lifetime against reaction with NO_3 (Fry et al., 2009), and the yield of aerosol from reaction with NO_3 is generally higher than photooxidation yields (Griffin et al., 1999a; Ng et al., 2008).

In this work, updated biogenic emissions are incorporated with a new lumping scheme to simulate organic aerosol in the global chemical transport model GEOS-Chem. Possible interactions between anthropogenic and biogenic emissions in terms of SOA formation are investigated for the United States. New processes represented include aerosol from nitrate radical oxidation of isoprene and NO_x -dependent terpene aerosol yields. Section 4.3 describes the updated emissions and SOA parameterization. The Results section is devoted to examining the global organic aerosol (OA) budget and surface concentrations over the U.S.

4.3 Model Description

4.3.1 Global Model

Present-day (year 2000) organic aerosol is simulated in the global chemical transport model, GEOS-Chem (version 8-01-04, <http://acmg.seas.harvard.edu/geos/>). Simulations are performed at 2° latitude by 2.5° longitude horizontal resolution using GEOS-4 assimilated meteorology with 30 vertical layers up to 0.01 hPa. Simulations include fully-coupled ozone- NO_x -hydrocarbon chemistry (Bey et al., 2001). Updates to GEOS-Chem version 8-01-04 are discussed in the later sections.

A GEOS-Chem simulation using nonvolatile POA was found to have a mean bias of $-0.56 \mu\text{g}/\text{m}^3$ or -34% compared to the Interagency Monitoring of Protected Visual Environments (IMPROVE) observations over the United States (Liao et al., 2007). The bias tends to become even larger when semivolatile POA is implemented (Pye and Seinfeld, 2010). As a result, two types of simulations are performed in this work: a “traditional” POA simulation and a semivolatile POA simulation. The nonvolatile (traditional) POA simulation, which uses nonvolatile POA and does not consider SOA from intermediate volatility compounds, is used for some sensitivity simulations to compensate for the fact that the semivolatile POA model predicts aerosol levels that are too low. The traditional GEOS-Chem simulation has also been extensively compared to observations in the work of Park et al. (2003, 2006), Heald et al. (2005), and Liao et al. (2007). The semivolatile POA simulation (Pye and Seinfeld, 2010) replaces nonvolatile POA with a pool of primary semivolatile organic compounds

(SVOCs) that immediately partition between the gas and aerosol phases as well as react in the gas phase. The semivolatile POA simulation also includes intermediate volatility organic compounds (IVOCs, saturation concentration about $10^5 \mu\text{g}/\text{m}^3$) which are emitted entirely in the gas phase but are assumed to behave like naphthalene in terms of SOA yields (Pye and Seinfeld, 2010).

Semivolatile organic species are removed from the atmosphere by wet and dry deposition as in previous work (Chung and Seinfeld, 2002; Pye and Seinfeld, 2010). Dry deposition follows a resistance in series method (Wesely, 1989; Zhang et al., 2001), and gas-phase secondary organic species are assumed to be hydrophilic with a Henry's Law coefficient of $10^5 \text{ M}/\text{atm}$ (Chung and Seinfeld, 2002). Primary organic aerosol is treated as hydrophobic in the semivolatile POA simulation or emitted as half hydrophobic and half hydrophilic in the nonvolatile POA simulation.

4.3.2 Emissions

SOA precursor emissions include biogenic hydrocarbons, benzene, toluene, xylene, intermediate volatility compounds, and semivolatile organic compounds or primary organic aerosol. The light aromatic, IVOC, and POA/SVOC emissions are the same as in previous work (Henze et al., 2008; Pye and Seinfeld, 2010). Briefly, benzene, toluene, and xylene are emitted from biomass burning, biofuel burning, and other anthropogenic sources based on their emission ratios relative to CO (for biomass and biofuel burning) and emissions described by the Emission Database for Global Atmospheric Research (EDGAR V2.0). IVOCs are spatially distributed like naphthalene from biomass burning, biofuel burning, and other anthropogenic sources and scaled up to represent all intermediate volatility organic compounds as described by Pye and Seinfeld (2010). The traditional POA emission inventory is described by Park et al. (2003, 2006) and is used as a surrogate for SVOC emissions. When POA is treated as semivolatile (i.e. POA is replaced by SVOCs), the traditional POA inventory is scaled up 27% (Schauer et al., 2001; Pye and Seinfeld, 2010) to account for SVOCs that are emitted entirely in the gas-phase.

Biogenic emissions of isoprene and seven major monoterpenes (α -pinene, β -pinene, limonene, myrcene, sabinene, Δ 3-carene and ocimene), are updated to follow the Model of Emissions of

Gases and Aerosols from Nature (MEGAN) v2.1 (Guenther et al., 2006) as implemented in GEOS-Chem version 8-02-04. Other monoterpene and sesquiterpene (farnesene, β -caryophyllene, and other sesquiterpenes) emissions are added based on MEGAN v2.1 plant functional types and MEGAN v2.04 emission factors and parameters. Emissions are modeled as a species specific emission rate at standard conditions (ϵ) and corrected using emission activity factors for leaf age (γ_{Age}), temperature (γ_T), leaf area index (γ_{LAI}), and light (γ_P) (Guenther et al., 2006; Sakulyanontvittaya et al., 2008):

$$E = \epsilon \gamma_{Age} \gamma_T \gamma_{LAI} [\gamma_P \text{LDF} + (1 - \text{LDF})] \quad (4.1)$$

Included in the emissions updates (standard in GEOS-Chem version 8-02-04) are the use of monthly MODIS instead of AVHRR for the leaf area index used to calculate γ_{Age} and γ_{LAI} . The temperature adjustment (γ_T) is computed as a function both of the current temperature and the average temperature over the previous 10 days for isoprene (Guenther et al., 2006). For monoterpenes and sesquiterpenes, γ_T is computed as an exponential function of current temperature (Sakulyanontvittaya et al., 2008). Unlike isoprene emissions which are 100% light-dependent, only a fraction of the monoterpene and sesquiterpene emissions are light-dependent. The light-dependence fraction (LDF) is around 5 to 10% for most monoterpenes (except ocimene) and 50% for sesquiterpenes (Sakulyanontvittaya et al., 2008). The light activity factor (γ_P) uses the parameterized canopy environment emission activity (PCEEA) algorithm of Guenther et al. (2006). The effects of soil moisture and production or loss within the canopy are ignored.

Emissions of monoterpenes are grouped into three tracers: MTPA, LIMO, and MTPO (Fig. 4.1). MTPA (α -pinene and similar monoterpenes) consists of the bicyclic monoterpenes α -pinene, β -pinene, sabinene, and Δ^3 -carene. Limonene (LIMO) is not lumped with any other species since its aerosol yields tend to be much higher than other monoterpenes. MTPO (other monoterpenes) consists of myrcene, ocimene, terpinene, terpinolene, and other terpenoid compounds such as alcohols and ketones. MTPO is the equivalent of the MEGAN myrcene, ocimene, and other monoterpene categories.

4.3.3 SOA Parameterization

The yield of aerosol from a given hydrocarbon/oxidant pair can be parameterized using a volatility basis set (VBS) (Donahue et al., 2006) or an Odum 2-product approach (Odum et al., 1996). Both methods adequately describe most chamber conditions because of the limited range of organic loadings examined (on the order of one to several hundred $\mu\text{g}/\text{m}^3$). The Odum model is computationally advantageous since it requires only two (or one) surrogate species per parent hydrocarbon. However, lumping multiple parent hydrocarbon systems together requires approximation (Bian and Bowman, 2002). The VBS requires more semivolatile surrogates (generally four) (Pathak et al., 2007; Lane et al., 2008b) per parent hydrocarbon/oxidant system, but combining different systems is more straightforward.

The organic aerosols in this work are lumped into five aerosol systems based on the parent hydrocarbons treated: terpenes, isoprene, light aromatics and IVOCs, primary SVOCs, and oxidized SVOCs (Fig. 4.1). Each aerosol system is represented with either a unique VBS (for systems with multiple parent hydrocarbons and/or multiple aerosol forming pathways) or Odum 2-product fit (for systems in which there is essentially one parent hydrocarbon). The lumping was chosen to maximize the amount of parent hydrocarbon information while maintaining a limited number of tracers. The terpene system (TSOA/G) includes semivolatile aerosol formed from photooxidation, ozonolysis, and nitrate radical oxidation of monoterpenes and sesquiterpenes. The isoprene system (ISOA/G) contains semivolatile aerosol from photooxidation and nitrate radical oxidation. The photooxidation aerosol from light aromatics and the naphthalene-like IVOC surrogate (ASOA/G) are lumped together since they have similar behavior under high and low- NO_x conditions. SVOCs are emitted as two semivolatile species (POA/G1-2) in roughly equal amounts based on an Odum 2-product fit to wood burning emissions (Shrivastava et al., 2006), and each of the primary SVOCs can oxidize in the gas phase to form lower volatility species (OPOA/G) (Pye and Seinfeld, 2010). The aerosol treatment with semivolatile POA requires 14 semivolatile gas-phase species, 14 semivolatile aerosol-phase species, 1 nonvolatile species, and 7 gas-phase precursors (excluding isoprene) for a total of 36 tracers (indicated by red outlined boxes in Fig. 4.1) in addition to the standard gas-

phase simulation tracers. Except for isoprene and light aromatics, which are a part of the gas-phase chemical mechanism, SOA precursor chemistry is performed offline. The partitioning equations are the same as those in the work of Chung and Seinfeld (2002).

4.3.3.1 Aerosol Yields

Table 4.1 shows the VBS fits for the aerosol forming pathways. Following the work of Stanier et al. (2008), mass-based stoichiometric coefficients, α , for each parent hydrocarbon/oxidant system are obtained by minimizing the difference between modeled and observed yields. Most systems are fit with a VBS using saturation concentrations, C^* , of 1, 10, and 100 $\mu\text{g}/\text{m}^3$ at 298 K. If yields are not available at the reference temperature, an enthalpy of vaporization of 42 kJ/mol is used (Chung and Seinfeld, 2002). Figures showing the fits and data on which they were based is available as a supplement.

The terpene aerosol parameterization in GEOS-Chem based on the work of Chung and Seinfeld (2002) is updated to reflect NO_x -dependent yields, a more realistic aerosol density, and new experimental results. The behavior of the lumped monoterpenes, MTPA and MTPO, under low- NO_x conditions, is modeled based on the dark α -pinene ozonolysis fit by Shilling et al. (2008). Shilling et al. (2008) were able to obtain very low organic aerosol loading (less than 1 $\mu\text{g}/\text{m}^3$) and thus the saturation concentration of 0.1 $\mu\text{g}/\text{m}^3$ is included in the fit. Using α -pinene ozonolysis yields for all photooxidation and ozonolysis conditions for MTPO and MTPA is an approximation. This yield might overestimate the amount of aerosol formed since photooxidation pathways often have a lower yield than ozonolysis pathways (Griffin et al., 1999a), α -pinene has one of the highest ozonolysis aerosol yields of the bicyclic monoterpenes (Griffin et al., 1999a), and UV light should suppress SOA (Pathak et al., 2007). However, the Shilling et al. (2008) parameterization may underestimate yields since not all monoterpenes behave like α -pinene; for example, monoterpenes with two double bonds (like terpinene and to a certain extent myrcene) appear to have higher aerosol yields than those with one double bond under photooxidation (Griffin et al., 1999a). In addition, species like β -pinene and sabinene have higher yields under photooxidation than ozonolysis (Griffin et al., 1999a),

and investigations by Ng et al. (2007a) indicate that if NO_x is absent (or extremely low), α -pinene photooxidation can produce very high yields. The yield may also be underestimated since the fit from Shilling et al. (2008) was not corrected for wall loss, and as a result, the authors estimate the yields could be 30 to 60% higher than those captured by the fit. The MTPA/MTPO fit for high- NO_x photooxidation and ozonolysis is obtained by reducing the low- NO_x yield, and thus α , by 50% for a given loading based on work by Ng et al. (2007a) and Pathak et al. (2007). The yield of aerosol from limonene under high and low- NO_x conditions is based on data from Zhang et al. (2006) using a density of 1.3 g/cm^3 (Ng et al., 2007a). The Zhang et al. (2006) experiments show a very mild dependence on NO_x level with slightly higher yields under high- NO_x conditions at low loadings. The sesquiterpene yields are based on the same underlying data as previous GEOS-Chem simulations; the yield data for β -caryophyllene and α -humulene from Griffin et al. (1999a) with a $[\text{VOC}]/[\text{NO}_x]$ ratio greater than 3 ppbC/ppb are used to obtain a low- NO_x fit. The high- NO_x yield curve is obtained by doubling the yield for a given loading based on Ng et al. (2007a). All terpene (monoterpene and sesquiterpene) aerosol from the nitrate oxidation pathway is represented based on β -pinene experiments by Griffin et al. (1999a).

Aerosol from the isoprene + NO_3 pathway (Ng et al., 2008) is added to GEOS-Chem. SOA from photooxidation of isoprene (Henze and Seinfeld, 2006), light aromatics (Henze et al., 2008), and a naphthalene-like IVOC (Pye and Seinfeld, 2010) is essentially the same as previous work. The underlying data from previous GEOS-Chem aerosol studies for isoprene, light aromatics, and IVOCs are refit to a VBS with saturation concentrations of 1, 10, and $100 \mu\text{g/m}^3$. Although high- NO_x conditions have traditionally been thought to suppress isoprene aerosol (Carlton et al., 2009), recent work shows high- NO_x isoprene aerosol yields can be similar to the low- NO_x yields at atmospherically relevant NO_2/NO ratios (Chan et al., 2010). As in previous versions of GEOS-Chem, isoprene photooxidation aerosol follows low- NO_x behavior based on Kroll et al. (2006) regardless of the NO_x level (Henze and Seinfeld, 2006).

Primary SVOCs from biomass burning, biofuel burning, and other anthropogenic sources are represented using an Odum 2-product fit based on the work of Shrivastava et al. (2006), as implemented

by Pye and Seinfeld (2010). SVOCs are emitted as two species with saturation concentrations of 1600 and 20 $\mu\text{g}/\text{m}^3$ at 300 K. As the gas-phase SVOCs react with OH, the volatility of the reaction products decreases by a factor of 100 to form oxidized SVOCs (Grieshop et al., 2009). The oxidized SVOCs remain semivolatile but more efficiently partition to the aerosol phase than the primary SVOC emissions. More information about the SVOC and IVOC simulation can be found in the work of Pye and Seinfeld (2010).

4.3.3.2 Implementation of NO_x -Dependent Yields

The difference in yield between high- and low- NO_x conditions for photooxidation and ozonolysis is assumed to result from competition between the NO and HO_2 reactions of the peroxy radical (Presto et al., 2005). Following the approach used in GEOS-Chem for light aromatics and intermediate volatility compounds (Henze et al., 2008; Pye and Seinfeld, 2010), the amount of parent hydrocarbon reaction through each pathway is calculated. The amount of hydrocarbon reacting through the high- NO_x , $\text{RO}_2 + \text{NO}$ pathway, $(\Delta\text{HC}_{\text{NO},i,j})$ is computed as:

$$\Delta\text{HC}_{\text{NO},i,j} = \beta\Delta\text{HC}_{i,j} \quad (4.2)$$

where β is the fraction of peroxy radicals reacting with NO and ΔHC is the amount of parent hydrocarbon i reacted with oxidant j . The amount of hydrocarbon reacting through the low- NO_x , $\text{RO}_2 + \text{HO}_2$ pathway, $(\Delta\text{HC}_{\text{HO}_2,i,j})$ is computed as:

$$\Delta\text{HC}_{\text{HO}_2,i,j} = (1 - \beta)\Delta\text{HC}_{i,j} \quad (4.3)$$

Equations 4.2 and 4.3 assume $\text{RO}_2 + \text{RO}_2$ reactions are negligible in the atmosphere and reaction of the parent hydrocarbon with OH or ozone is the rate-limiting step for aerosol formation. The branching ratio, β , is computed from:

$$\beta = \frac{k_{\text{RO}_2+\text{NO}}[\text{NO}]}{k_{\text{RO}_2+\text{NO}}[\text{NO}] + k_{\text{RO}_2+\text{HO}_2}[\text{HO}_2]} \quad (4.4)$$

where k_{RO_2+NO} and $k_{RO_2+HO_2}$ are the rate constants for reaction of the peroxy radical with NO and HO₂, respectively. Due to limited information about reaction rates, all peroxy radicals resulting in SOA are assumed to have the same RO₂ + NO and RO₂ + HO₂ rate constants (Henze et al., 2008).

4.4 Results and Discussion

4.4.1 Emissions

Table 4.2 shows the global, annually averaged emission rates of POA and SOA precursors. Compared to standard GEOS-Chem version 8-01-04 (which uses MEGAN v2.0 and Griffin et al. (1999b) speciation), the bicyclic monoterpene (α -pinene, β -pinene, sabinene, and Δ 3-carene) emission rate is relatively unchanged. Ocimene emissions, however, are about a factor of 6 higher than previously estimated, and limonene emissions are about 60% lower. Global sesquiterpene emissions differ by less than 10% different from previous estimates based on the other reactive volatile organic compound (ORVOC) inventory of Guenther et al. (1995) and the speciation of Griffin et al. (1999b). Isoprene emissions are about 14% larger than MEGAN v2.0 as implemented in GEOS-Chem. One of the largest differences between previous GEOS-Chem studies (e.g. Henze and Seinfeld (2006) or Pye and Seinfeld (2010)) and this work is the significantly reduced terpenoid ketone and terpenoid alcohol emissions. All relevant terpenoid ketone and alcohol emissions (previously estimated at 43 Tg/yr) are assumed to be a subset of the MEGANv2.04 other monoterpene category which is predicted to have emissions of about 14 Tg/yr. The net result is that global terpene emissions are about 20% lower than previous model estimates. Regional differences may be much higher, and the diurnal variation is often significantly different (for example: sesquiterpenes were treated as 100% light dependent in previous work, but now are only 50% light dependent).

4.4.2 Global Budget

Figure 4.2 (a) shows the fraction of each lumped parent hydrocarbon reacting under high- NO_x ($\text{RO}_2 + \text{NO}$), low- NO_x ($\text{RO}_2 + \text{HO}_2$), and nitrate radical oxidation pathways. All pathways sum to one for each parent hydrocarbon except for isoprene which also reacts with ozone but does not produce aerosol from that pathway. All isoprene photooxidation is shown as “low NO_x ” since the aerosol yield is representative of those conditions. About 22, 52, and 26% of the lumped bicyclic monoterpenes, MTPA, react under high- NO_x , low- NO_x , and nitrate radical conditions, respectively. The rate constant for MTPO ozonolysis is slightly higher than the MTPA ozonolysis rate constant and consequently, the nitrate oxidation is less important, but still significant, for MTPO. In contrast, only 2% of the sesquiterpenes (SESQ), with their much stronger dependence on light and temperature for emission and relatively fast reaction with ozone, react with the nitrate radical. Isoprene is emitted only during the daytime, and less than 3% is predicted to react with the nitrate radical. Note that for all monoterpenes and sesquiterpenes, the low- NO_x pathway is globally dominant, reflecting where biogenic compounds are emitted and the branching ratio, β , in those locations (Fig. 4.3).

The bottom of Fig. 4.2 shows the predicted contribution of each reaction pathway to net aerosol production from a given biogenic parent hydrocarbon. These values were calculated using the yield at an organic loading of $1.5 \mu\text{g}/\text{m}^3$ which was found to approximately reproduce the lumped global net aerosol production rate in GEOS-Chem. For the lumped monoterpenes, MTPA and MTPO, the low- NO_x pathway is even more important relative to the high- NO_x pathways in terms of net aerosol production than would be estimated based on gas-phase oxidation since the low- NO_x yield is about double the yield under high- NO_x conditions. For limonene, the high- NO_x pathway becomes relatively more important for aerosol production. For sesquiterpenes, a similar amount of net aerosol production is predicted to result from the high and low- NO_x pathways since the yield is about double under high- NO_x conditions compared to low- NO_x conditions. For all monoterpenes and sesquiterpenes, the nitrate radical reaction contributes less to global net aerosol production than it contributes to gas-phase oxidation. Since very little isoprene reacts with nitrate, the majority of the isoprene aerosol comes from the photooxidation path, even though the yield of aerosol from the

nitrate radical path can be substantially higher.

Table 4.3 shows the predicted net production of SOA for year 2000. Despite the fact that the simulated monoterpene emissions have decreased substantially (about 20% globally) since the work of Pye and Seinfeld (2010), the amount of SOA predicted to form from terpenes has increased to 14–15 Tg/yr and isoprene SOA has decreased slightly to 8–9 Tg/yr. A traditional simulation in the work of Pye and Seinfeld (2010) (year 2000, GEOS-Chem v8-01-04, 2° by 2.5° horizontal resolution), predicted 10 Tg/yr of terpene SOA and 12 Tg/yr of isoprene SOA. Previous work by Henze et al. (2008) (year 2004, GEOS-Chem v7-04-11, 2° by 2.5° horizontal resolution), predicted 12 and 14 Tg/yr and work by Farina et al. (2010) (year 1980, Unified GISS-II', 4° by 5° horizontal resolution) predicted 21 and 6 Tg/yr from terpenes and isoprene, respectively. Increased terpene SOA production in the present work compared to Pye and Seinfeld (2010) is a result of higher aerosol yields from monoterpene and sesquiterpene oxidation. At low loadings (about 1 $\mu\text{g}/\text{m}^3$), the yield of aerosol from low- NO_x monoterpene (MTPA/O) oxidation is about 5x the yield using older parameterizations (Griffin et al., 1999a; Chung and Seinfeld, 2002). The high- NO_x sesquiterpene yield implemented in this work also results in significantly more aerosol from sesquiterpenes. Limonene yields (Zhang et al., 2006) at low loadings are about a factor of 10 higher than previous work using data from Griffin et al. (1999a), however limonene emissions are substantially lower. The nitrate radical oxidation yield is also slightly higher as a result of the density correction. At higher organic aerosol loadings, like those typical of summertime conditions in the southeast U.S. (about 10 $\mu\text{g}/\text{m}^3$), yields are generally higher than in previous work, but generally no more than about double (except for limonene). The yield of aerosol from isoprene photooxidation is within 10% of that using the Odum 2-product fit of Henze and Seinfeld (2006) at low loadings since it is based on the same underlying data (Kroll et al., 2006). The addition of isoprene from the NO_3 pathway contributes a small amount of aerosol since relatively little of the parent hydrocarbon reacts through that pathway. Changes in the estimated aerosol production rate from isoprene compared to previous work (Henze and Seinfeld, 2006; Henze et al., 2008; Pye and Seinfeld, 2010) are likely due to differences in the emissions and an improved tracer lumping scheme.

The preceding discussion focused on the global net aerosol production which is the sum of production and evaporation. Figure 4.4 shows the fraction of mass that partitions to the aerosol phase but later evaporates. Mass partitions to the aerosol phase in locations with high loadings (such as anthropogenic source regions) or low temperatures and evaporates when loadings becomes lower (such as in outflow regions) or temperatures increase (for example due to diurnal temperature variation). For the terpene SOA species with a saturation concentration of $0.1 \mu\text{g}/\text{m}^3$, about 24% of the mass that partitions to the aerosol phase eventually evaporates. For a species with a C^* of $10 \mu\text{g}/\text{m}^3$, about 80% eventually evaporates. The fit in Fig. 4.4 was obtained by modeling the fraction evaporated (F_E) for a species emitted in a location with an initial loading of $M_{o,i}$ and transported to an area with a loading of $M_{o,f}$:

$$F_E = 1 - \frac{1 + C^*/M_{o,i}}{1 + C^*/M_{o,f}}. \quad (4.5)$$

Equation 4.5 neglects losses in the gas or aerosol phases which leads to some of the discrepancy between the fitted curve and data. The fitted $M_{o,i}$ and $M_{o,f}$ were determined to be 2.56 and $0.33 \mu\text{g}/\text{m}^3$. Primary SVOCs are forced out of the particle phase to a greater degree than the other semivolatiles as a result of gas-phase reaction and are not included in the fit.

4.4.3 Surface Level Aerosol Over the United States

The global budget is heavily influenced by remote areas where biogenic emissions are high and NO levels are low (e.g. the Amazon basin). Biogenic hydrocarbons may behave differently when emitted in a location with significant anthropogenic emissions. In this section, the United States is used as a case study for aerosol formation in an anthropogenically influenced area.

4.4.3.1 Fate of the Peroxy Radical

NO_x levels influence the yield of aerosol through the rate of peroxy radical reaction with either NO or HO_2 . Over the U.S., the $\text{RO}_2 + \text{NO}$ reaction usually dominates over the $\text{RO}_2 + \text{HO}_2$ reaction, particularly in the Northeast (Fig. 4.3) and during the winter when HO_x levels are lower (Henze

et al., 2008). Even in the summer in the Southeast, more than 50% of the RO₂ is predicted to react with NO (Fig. 4.3). The effect of NO_x on light aromatic and IVOC SOA in a global model has been investigated previously (Henze et al., 2008; Pye and Seinfeld, 2010).

Figure 4.5 shows the predicted surface level organic aerosol from terpenes, isoprene, aromatics, and nonvolatile POA (a traditional simulation) during August 2000. The second panel shows the fraction of that organic aerosol from oxidation of a biogenic parent hydrocarbon (monoterpene, sesquiterpene, or isoprene). Compared to a semivolatile POA simulation in which a large fraction of the POA evaporates (Pye and Seinfeld, 2010), biogenic aerosol contributes less but still significant amounts of the aerosol in the southeast U.S. (about 50%). Compared to previous work, summertime aerosol is up to 2.6 μg/m³ lower in the Southeast and up to 0.66 μg/m³ lower in the Northeast.

Increased reaction of the peroxy radical with NO leads to both increased and decreased aerosol. More reaction through the high-NO_x pathway reduces the yield of aerosol from monoterpenes and light aromatics but increases the yield from sesquiterpenes. Figure 4.6 shows the effect on surface level organic aerosol (OA) of forcing the aerosol yield through the low-NO_x ($\beta=0$) or high-NO_x ($\beta=1$) path as compared to a simulation using the model calculated β for a traditional POA simulation (reference simulation is depicted in Figs. 4.3 and 4.5). The northeast U.S. is dominated by the response of monoterpenes and light aromatics which produce more aerosol in the low-NO_x simulation and less in the high-NO_x simulation. The difference between the standard simulation and the low-NO_x simulation is greater than the difference between the standard simulation and the high-NO_x simulation since model calculated NO_x levels are already sufficiently high to force most of the peroxy radical through the high-NO_x pathway. In the Southeast, the model response is dampened and shows an opposite trend for the high-NO_x simulation. This response occurs as a result of significant aerosol that is not dependent on the RO₂ branching ratio (POA, isoprene aerosol, and nitrate radical aerosol from terpenes) and sesquiterpene aerosol that has higher yields in the $\beta=1$ than in the $\beta=0$ simulation. While the branching of the peroxy radical reaction between high-NO_x and low-NO_x pathways has an influence on surface concentrations, the effect is generally small (OA levels are within about 10% of the levels using the model calculated β).

4.4.3.2 SOA from Nitrate Radical Oxidation

With roughly 30 to 40% of the monoterpene emissions and 20 to 30% of the sesquiterpene emissions occurring at night, aerosol from the nitrate oxidation pathway is predicted to be significant. Aerosol formed from nitrate radical oxidation of terpenes and isoprene contributes up to $3.35 \mu\text{g}/\text{m}^3$ of organic aerosol during August over the U.S. The nitrate pathway has the largest effect on terpene aerosol followed by isoprene. Aerosol production from the nitrate pathway increases terpene aerosol by up to $2.76 \mu\text{g}/\text{m}^3$ (generally $1.5 \mu\text{g}/\text{m}^3$ or more in the Southeast) and isoprene aerosol by about 0.4 to $0.6 \mu\text{g}/\text{m}^3$. Figure 4.7 shows the percent increase in aerosol from terpenes, isoprene, and all sources compared to a simulation in which the nitrate pathway does not produce aerosol (all simulations use traditional POA). An enhancement of 100%, as in the case for terpene OA, indicates that the aerosol level doubles when the nitrate pathway is included. Terpenes are predicted to be the largest contributor to biogenic aerosol in the Southeast, and total organic aerosol is enhanced slightly more than 30% over a wide area as a result of nitrate oxidation aerosol.

For nitrate aerosol to contribute to surface level OA, aerosol loadings must be significant. The yield of aerosol from the nitrate pathway for terpenes is 4% at $1 \mu\text{g}/\text{m}^3$ (less than the yield from photooxidation and ozonolysis of monoterpenes and sesquiterpenes) and 26% at $10 \mu\text{g}/\text{m}^3$ (more than the yield from photooxidation and ozonolysis of monoterpenes, see Table 4.1). So although nitrate oxidation enhances aerosol across the U.S., it is most pronounced in the Southeast where aerosol loadings are higher.

In terms of global budgets, the NO_3 pathway plays a modest role increasing net production of aerosol from terpenes (3 Tg/yr, 20% increase) and isoprene (1 Tg/yr, 10% increase). This lesser role in net global production compared to surface concentrations is due to the relatively low aerosol yield at low loadings and expected evaporation of 80% or more of the nitrate aerosol due to its relatively high volatility and the reduced importance of NO_3 reaction in the tropics where NO_x levels are low (see Table 4.1 for the volatility and Fig. 4.4 for the expected evaporation).

4.5 Considerations

In this section, we provide cautionary notes for the implications of our results in terms of emission controls, possible reasons results may be biased, the potential influences of errors in isoprene chemistry, and comments about extrapolating chamber data to the atmosphere.

4.5.1 Dependence of SOA Formation on NO_x Level

Simulations presented in Section 4.4.3.1 indicate that the $\text{RO}_2 + \text{NO}$ vs $\text{RO}_2 + \text{HO}_2$ branching of aromatic and terpene peroxy radicals does not exert a large control on organic aerosol concentrations. Caution should be used when extrapolating these results to implications for air quality management since there are other ways in which NO_x may influence organic aerosol concentrations that have not been examined or implemented in the model.

Another NO_x control on terpene SOA is through the gas-phase oxidants such as the hydroxyl radical, ozone, and nitrate radicals and previous modeling work indicates that changes in gas-phase oxidants may be the primary anthropogenic control on SOA. Simulations by Carlton et al. (2010) indicate that half of biogenic SOA can be controlled, and work by Lane et al. (2008a) indicates that reductions in NO_x emissions are likely to lead to decreased SOA concentrations as a result of lower oxidant concentrations, despite the fact that monoterpene SOA yields are predicted to be higher under low- NO_x conditions. However, the global α -pinene study of Capouet et al. (2008) indicates that the presence of NO_x increases OH and NO_3 levels relative to O_3 levels. As a result, the expected role of the high-yield terpene ozonolysis pathway is diminished and less aerosol results. Thus, a study looking at the implications of NO_x emission reductions may need to parameterize SOA based on gas-phase oxidant (OH vs. O_3) as well as NO_x level and examine the effects of NO_x reductions on oxidant levels.

Our simulations do indicate that the fate of the peroxy radical (reaction with NO or HO_2) is likely not the missing anthropogenic control on organic aerosol especially since increasing β tends to reduce OA concentrations (except in the southeast U.S.) based on current experimental results. Our simulations also indicate that NO_x -dependent monoterpene and sesquiterpene photooxidation and

ozonolysis yields may lead to a more accurate simulation in the northeast U.S. where concentrations are more sensitive to the branching ratio.

4.5.2 Modeled Importance of Nitrate Aerosol

Aerosol from nitrate radical oxidation of biogenic hydrocarbons has been included in previous global modeling work (Chung and Seinfeld, 2002; Farina et al., 2010) but its contribution to aerosol production not separately assessed. Experimental studies have been extrapolated to the global atmosphere and estimated 5 Tg/yr of aerosol from monoterpenes + NO₃ (Fry et al., 2009) and 2-3 Tg/yr from isoprene + NO₃ (Ng et al., 2008). Both of these estimates are about double the values presented in this work. However, our work highlights the potential for NO₃ produced aerosol to have a very large regional effect.

Observations indicate support for a large source of organic compounds from reaction of biogenic VOCs with nitrate radicals. Hennigan et al. (2009) monitored water soluble organic compounds (WSOC) in the gas and aerosol phases during summer in Atlanta and found a pronounced nighttime maximum in gas-phase WSOC likely due to products of nitrate oxidation but no similar maximum in nighttime particulate WSOC. Measurements near the northeast U.S. during the 2002 and 2004 New England Air Quality Studies also indicate a strong interaction between terpenes and nitrate. Isoprene emitted in the afternoon when OH levels are declining persists long enough to be oxidized by NO₃. The anticorrelation between α -pinene and NO₃ (Warneke et al., 2004) and isoprene and NO₃ (Brown et al., 2009) indicates that biogenic VOC + NO₃ reactions can be an important sink for both NO₃ and VOCs. Averaged over the entire 2002 campaign, terrestrial biogenic VOCs were estimated to be responsible for 19% of the combined NO₃ and N₂O₅ loss measured offshore (Aldener et al., 2006).

As a consequence of the offline oxidation, the current version of GEOS-Chem assumes oxidants such as OH, NO, HO₂, O₃, and NO₃ are 100% recycled when they react with monoterpenes and sesquiterpenes (i.e. NO₃ is not depleted when it reacts with monoterpenes or sesquiterpenes; isoprene, light aromatics, and IVOCs, however, are treated online). The offline treatment uses the

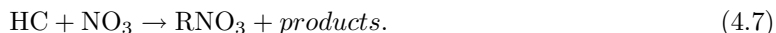
oxidant concentration at a given timestep to solve the differential equation for the depletion of the parent hydrocarbon. For constant oxidant concentrations, these equations generally have an analytical solution. Recycling of the oxidants is recommended when only a limited amount of the parent hydrocarbon gas-phase oxidation is represented and later generation products may release oxidants, but this approach may cause the model to overestimate the potential importance of aerosol from nitrate pathways.

The yield of organic nitrate can provide an estimate of how much nitrate may be removed from the system or sequestered for later release. Several studies have looked at the yield of organic nitrate from isoprene + NO₃ systems (treated online in the model). Isoprene + NO₃ is expected to yield 65 to 70% organic nitrate (Perring et al., 2009; Rollins et al., 2009), and first generation nitrate products may react with NO₃ again to produce secondary dinitrates (Rollins et al., 2009). The organic nitrates themselves may or may not release NO_x (Perring et al., 2009). This implies recycling no higher than 35% for the isoprene + NO₃ system. Recycling of reactive nitrogen may be higher in monoterpene systems than isoprene systems. The work of Fry et al. (2009) indicates that the yield of organic nitrates from β -pinene + NO₃ is about 40 to 45%, so 55 to 60% of the reacted NO₃ could be immediately recycled as NO₂ or some other reactive nitrogen species (Fry et al. (2009) were unable to detect the recycled species).

To gain insight into the potential role of monoterpene + nitrate reactions and possible depletion of nitrate, we examine one grid cell in the Southeast U.S. (85°W, 32°N) at the beginning of September using a coarse resolution simulation (4°x 5°). Based on the predicted NO₃ and monoterpene levels, Even for fairly aggressive levels of reactive nitrogen recycling, NO₃ will likely be tritrated in the early evening when isoprene is still present and NO₃ levels are lower. Later during the night, when NO₃ levels are higher, nitrate would likely be in excess. Following the analysis of Brown et al. (2009), we can assume nitrate radicals are at a pseudo steady state as they are formed from:



and removed by reaction with a hydrocarbon, HC:



Reaction with the hydrocarbon is shown to recycle a fraction of the NO_3 , R . The fractional loss of nitrate due to reaction 4.7, divided by all losses, including N_2O_5 hydrolysis, is:

$$\phi' = (1 - R) \frac{k_{\text{HC}+\text{NO}_3}[\text{NO}_3][\text{HC}]}{k_{\text{NO}_2+\text{O}_3}[\text{NO}_2][\text{O}_3]} = (1 - R)\phi \quad (4.8)$$

For a simulation with 100% recycling ($R=1$), ϕ for the lumped monoterpene MTPA is calculated to be approximately 1-2. Thus for any recycling less than 50 to 75%, reaction with the HC could be the dominant removal mechanism for NO_3 . Future work using online monoterpene and sesquiterpene oxidation can more carefully examine the interactions between biogenic VOCs and nitrate including the degree to which NO_3 may be titrated and aerosol concentrations lower than predicted in this work.

The amount of aerosol from the NO_3 pathway may also be underestimated by this work since NO_3 SOA-forming pathways of SVOCs and IVOCs have not yet been studied experimentally. SVOCs are globally the largest contributor to net aerosol production and since yields are generally higher for NO_3 oxidation compared to photooxidation and ozonolysis (for moderate loadings), SVOC reaction with NO_3 could be a substantial method of aerosol production on regional and/or global scales. However, a significant fraction of the SVOC and IVOC emissions are anthropogenic, and reaction with the nitrate radical is expected to be a minor removal process for many anthropogenic species such as alkanes and light aromatics (Warneke et al., 2004; Atkinson and Arey, 2003).

4.5.3 Uncertainties in Isoprene Chemistry

In remote areas with little anthropogenic influence (such as the Amazon basin), oxidation of isoprene as represented in the model tends to deplete OH levels to an extent greater than expected based on field measurements (Lelieveld et al., 2008; Butler et al., 2008; Archibald et al., 2010). This

falsely low OH can have several effects on organic aerosol levels. Reduced OH can lead to less isoprene, monoterpene, and sesquiterpene reaction with OH and therefore reduce the amount of photooxidation aerosol that forms. The isoprene (or terpene) that is not reacted may be transported to other regions where formation of aerosol is less favorable (for example due to low organic aerosol loadings) or more favorable (for example due to low temperatures and/or reduced deposition aloft), but in either case, the aerosol will be shifted away from where it would have normally formed. Depressed reaction of biogenic hydrocarbons with OH may also lead to an overestimate in the amount of hydrocarbon reacting with nitrate radicals. Isoprene and monoterpenes emitted during the daytime should react primarily with OH and ozone, but if OH levels are abnormally low, a large pool of biogenics may be left to react during the night. Fig. 4.2 indicates that 3% of the daytime isoprene is oxidized at night by NO_3 (isoprene is only emitted during the day), and coarse resolution simulations predict that 10% or less of the monoterpenes emitted during the daytime react with NO_3 . Observations do indicate that a certain amount of daytime emissions should be oxidized at night (Warneke et al., 2004). Even if the predicted amount of nitrate reaction is too high, it is likely to have only a small effect on net global production of aerosol since only about 3 Tg/yr of SOA (15% of the biogenic SOA production) is expected to come from nitrate oxidation. Aerosol levels over the Amazon, however, may be significantly overestimated. Issues related to isoprene-OH recycling are not expected to be as important for the simulations over the U.S. where NO_x levels are relatively high.

4.5.4 Extrapolation of Chamber Studies

The most representative chamber aerosol yields are those that occur when the fate of the RO_2 radical (reaction with RO_2 , HO_2 , NO , or NO_3) is the same in chamber studies and the atmosphere. Work by Ng et al. (2008) indicates that the aerosol from reaction of isoprene with NO_3 results from $\text{RO}_2 + \text{RO}_2$ reactions although aerosol from the $\text{RO}_2 + \text{NO}_3$ pathway may contribute as well (Ng et al., 2008; Rollins et al., 2009). This information raises the question of the applicability of the nitrate oxidation yields to the global atmosphere where parent hydrocarbon concentrations are much lower

and $\text{RO}_2 + \text{RO}_2$ should be less important.

Modeling errors can also result when chamber studies do not constrain yields at atmospherically relevant loadings. The SOA yields for terpene + NO_3 reactions are based on data collected by Griffin et al. (1999a). After correcting for density, the loadings in the chamber range from about 40 to $600 \mu\text{g}/\text{m}^3$. Although the fit shows a low root mean square error (RMSE, 5.7%, Table 4.1) the fit is unconstrained over the most atmospherically relevant loadings ($1\text{-}10 \mu\text{g}/\text{m}^3$) which could lead to over-predictions or under-predictions of the importance of terpene + NO_3 aerosol.

4.6 Conclusions

The global chemical transport model, GEOS-Chem, has been used to simulate global organic aerosol from monoterpenes, sesquiterpenes, isoprene, benzene, toluene, xylene, intermediate volatility compounds, and semivolatile organic compounds as well as traditional (nonvolatile) primary organic aerosol with a focus on biogenic aerosol. Models have historically under-predicted organic aerosol levels, and semivolatile POA causes even lower concentrations due to evaporation of a significant fraction of the emissions (Pye and Seinfeld, 2010). The semivolatile POA simulation should become more accurate as additional processes, such as partitioning into aerosol water (Pankow, 2010), are captured and new mechanisms of aerosol formation are elucidated. New terpene emissions used in this work are about 20% lower than previous GEOS-Chem estimates, potentially leading to even lower simulated aerosol concentrations.

Part of the expected decrease in surface concentrations and global production of aerosol in the model is offset by updating the SOA yields to some of the highest values currently supported by chamber experiments. A new lumping scheme is introduced that maintains a reasonable level of parent hydrocarbon identity while ensuring that species of different volatilities remain distinct. As part of the new framework, NO_x -dependent photooxidation and ozonolysis yields are implemented for monoterpene and sesquiterpene aerosol to complement those previously implemented for NO_x -dependent light aromatic SOA (Henze et al., 2008). The α -pinene dark ozonolysis experiments of Shilling et al. (2008) are used to represent low- NO_x monoterpene oxidation and form significant SOA,

particularly at low loadings. The yield of aerosol from sesquiterpenes under high- NO_x and limonene under high- and low- NO_x conditions is also significantly larger than in previous NO_x -independent implementations. Isoprene, light aromatic, and intermediate volatility compound aerosol is refit using a 3-product volatility basis set, and aerosol from nitrate oxidation of isoprene is added.

Changing the photooxidation and ozonolysis of terpenes and light aromatics to use high- NO_x ($\text{RO}_2 + \text{NO}$) vs low- NO_x ($\text{RO}_2 + \text{HO}_2$) yields leads to relatively small changes in surface concentrations as a result of competing effects of sesquiterpene aerosol (which is enhanced under high- NO_x conditions) and monoterpene/light aromatic aerosol (which is enhanced under low- NO_x conditions). Surface concentrations are more sensitive to the peroxy radical branching ratio ($\text{RO}_2 + \text{NO}$ vs $\text{RO}_2 + \text{HO}_2$) in the northeast than in the southeast U.S. where aerosol from isoprene, sesquiterpenes, primary emissions, and nitrate radical oxidation, which are independent of the RO_2 branching, dampen the model response.

Globally, 14-15 Tg/yr of SOA is predicted to form from terpenes and 8-9 Tg/yr from isoprene for 22-24 Tg/yr total of biogenic aerosol. Although nitrate radical generated aerosol contributes a small amount to the global burden as a result of its relatively high volatility, it can be very important on a regional level. Aerosol from NO_3 oxidation is predicted to be potentially very important in the Southeast U.S. where it enhances terpene SOA by about 100% or more and total aerosol concentrations by more than 30%. Model estimates of nitrate aerosol can be refined by better addressing recycling of nitrate for the terpene + nitrate reactions, and by obtaining better estimates (at low loadings and for multiple terpenes) of the nitrate + terpene SOA yield.

More work is needed to resolve the apparent contradiction that organic aerosol is dominated by modern carbon yet correlates with anthropogenic tracers. Simulations over the U.S. suggest that higher NO_x levels will generally suppress SOA since monoterpenes and light aromatics will generally have a lower yield of aerosol when NO levels are higher. However the impact of reduced NO_x emissions on OH and ozone oxidant levels was not examined and the effect of the RO_2 branching between NO and HO_2 on SOA levels is generally small. Thus far, GEOS-Chem model results have indicated two possible candidates for production of aerosol from modern carbon that would correlate

with anthropogenic tracers: the nitrate radical oxidation of terpenes and isoprene and oxidation of semivolatile organic compounds from biofuel burning (Pye and Seinfeld, 2010). Additional theories that need further examination are the possible implications of acidity, sulfate, or NO_2 enhanced production of biogenic aerosol (Surratt et al., 2007, 2010; Eddingsaas et al., 2010; Chan et al., 2010).

Supplemental material contains the SOA yield curves for the systems described in Table 4.1 (Appendix C).

4.7 Acknowledgements

The numerical simulations for this research were performed on Caltech's Division of Geological and Planetary Sciences Dell cluster. The authors would like to thank Dylan Millet for guidance linking MEGAN to GEOS-Chem. The authors would also like to thank Fabien Paulot, Nathan Eddingsaas, Jason Surratt, and Joseph Ensberg for useful discussions. The authors would also like to thank Paul Wennberg for feedback on the manuscript. This research has been supported by the Office of Science (BER), U.S. Department of Energy, Grant No. DE-FG02-05ER63983 and STAR Research Agreement No. RD-833749 awarded by the U.S. Environmental Protection Agency (EPA). It has not been formally reviewed by the EPA. The views expressed in this paper are solely those of the authors. MPB was supported by the Natural Environment Research Council (grant NE/D001471).

Bibliography

Aldener, M., Brown, S. S., Stark, H., Williams, E. J., Lerner, B. M., Kuster, W. C., Goldan, P. D., Quinn, P. K., Bates, T. S., Fehsenfeld, F. C., and Ravishankara, A. R.: Reactivity and loss mechanisms of NO_3 and N_2O_5 in a polluted marine environment: Results from in situ measurements during New England Air Quality Study 2002, *J. Geophys. Res.*, 111, D23S73, doi: 10.1029/2006JD007252, 2006.

- Archibald, A. T., Jenkin, M. E., and Shallcross, D. E.: An isoprene mechanism intercomparison, *Atmos. Environ.*, in press, doi:10.1016/J.ATMOSENV.2009.09.016, 2010.
- Atkinson, R. and Arey, J.: Atmospheric degradation of volatile organic compounds, *Chem Rev*, 103, 4605–4638, doi:10.1021/CR0206420, 2003.
- Bian, F. and Bowman, F. M.: Theoretical method for lumping multicomponent secondary organic aerosol mixtures, *Environ. Sci. Technol.*, 36, 2491–2497, doi:10.1021/Es015600s, 2002.
- Brown, S. S., Degouw, J. A., Warneke, C., Ryerson, T. B., Dube, W. P., Atlas, E., Weber, R. J., Peltier, R. E., Neuman, J. A., Roberts, J. M., Swanson, A., Flocke, F., McKeen, S. A., Brioude, J., Sommariva, R., Trainer, M., Fehsenfeld, F. C., and Ravishankara, A. R.: Nocturnal isoprene oxidation over the Northeast United States in summer and its impact on reactive nitrogen partitioning and secondary organic aerosol, *Atmos. Chem. Phys.*, 9, 3027–3042, 2009.
- Butler, T. M., Taraborrelli, D., Fischer, C. B. H., Harder, H., Martinez, M., Williams, J., Lawrence, M. G., and Lelieveld, J.: Improved simulation of isoprene oxidation chemistry with the ECHAM5/MESy chemistry-climate model: lessons from the GABRIEL airborne field campaign, *Atmos. Chem. Phys.*, 8, 4529–4546, 2008.
- Capouet, M., Mueller, J. F., Ceulemans, K., Compernelle, S., Vereecken, L., and Peeters, J.: Modeling aerosol formation in alpha-pinene photo-oxidation experiments, *J. Geophys. Res.*, 113, D02 308, doi:10.1029/2007JD008995, 2008.
- Carlton, A. G., Wiedinmyer, C., and Kroll, J. H.: A review of Secondary Organic Aerosol (SOA) formation from isoprene, *Atmos. Chem. Phys.*, 9, 4987–5005, 2009.
- Carlton, A. G., Pinder, R. W., Bhave, P. V., and Pouliot, G. A.: To what extent can biogenic SOA be controlled?, *Environ. Sci. Technol.*, 44, 3376–3380, doi:10.1021/Es903506b, 2010.
- Chan, A. W. H., Kautzman, K. E., Chhabra, P. S., Surratt, J. D., Chan, M. N., Crouse, J. D., Kurten, A., Wennberg, P. O., Flagan, R. C., and Seinfeld, J. H.: Secondary organic aerosol

- formation from photooxidation of naphthalene and alkylnaphthalenes: implications for oxidation of intermediate volatility organic compounds (IVOCs), *Atmos. Chem. Phys.*, 9, 3049–3060, 2009.
- Chan, A. W. H., Chan, M. N., Surratt, J. D., Chhabra, P. S., Loza, C. L., Crouse, J. D., Yee, L. D., Flagan, R. C., Wennberg, P. O., and Seinfeld, J. H.: Role of aldehyde chemistry and NO_x concentrations in secondary organic aerosol formation, *Atmos. Chem. Phys.*, 10, 7169–7188, doi:10.5194/acp-10-7169-2010, 2010.
- Chung, S. H. and Seinfeld, J. H.: Global distribution and climate forcing of carbonaceous aerosols, *J. Geophys. Res.*, 107, 4407, doi:10.1029/2001JD001397, 2002.
- de Gouw, J. A., Middlebrook, A. M., Warneke, C., Goldan, P. D., Kuster, W. C., Roberts, J. M., Fehsenfeld, F. C., Worsnop, D. R., Canagaratna, M. R., Pszenny, A. A. P., Keene, W. C., Marchewka, M., Bertman, S. B., and Bates, T. S.: Budget of organic carbon in a polluted atmosphere: Results from the New England Air Quality Study in 2002, *J. Geophys. Res.*, 110, D16 305, doi:10.1029/2004JD005623, 2005.
- Donahue, N. M., Robinson, A. L., Stanier, C. O., and Pandis, S. N.: Coupled partitioning, dilution, and chemical aging of semivolatile organics, *Environ. Sci. Technol.*, 40, 2635–2643, doi:10.1021/ES052297c, 2006.
- Eddingsaas, N. C., VanderVelde, D. G., and Wennberg, P. O.: Kinetics and products of the acid-catalyzed ring-opening of atmospherically relevant butyl epoxy alcohols, *J. Phys. Chem. A*, 114, 8106–8113, doi:10.1021/jp103907c, 2010.
- Farina, S. C., Adams, P. J., and Pandis, S. N.: Modeling global secondary organic aerosol formation and processing with the volatility basis set: Implications for anthropogenic secondary organic aerosol, *J. Geophys. Res.*, 115, D09 202, doi:10.1029/2009jd013046, 2010.
- Fry, J. L., Kiendler-Scharr, A., Rollins, A. W., Wooldridge, P. J., Brown, S. S., Fuchs, H., Dube, W., Mensah, A., dal Maso, M., Tillmann, R., Dorn, H. P., Brauers, T., and Cohen, R. C.: Organic

- nitrate and secondary organic aerosol yield from NO_3 oxidation of beta-pinene evaluated using a gas-phase kinetics/aerosol partitioning model, *Atmos. Chem. Phys.*, 9, 1431–1449, 2009.
- Goldstein, A. H. and Galbally, I. E.: Known and unexplored organic constituents in the earth's atmosphere, *Environ. Sci. Technol.*, 41, 1514–1521, doi:10.1021/ES072476p, 2007.
- Grieshop, A. P., Logue, J. M., Donahue, N. M., and Robinson, A. L.: Laboratory investigation of photochemical oxidation of organic aerosol from wood fires 1: measurement and simulation of organic aerosol evolution, *Atmos. Chem. Phys.*, 9, 1263–1277, 2009.
- Griffin, R. J., Cocker, D. R., Flagan, R. C., and Seinfeld, J. H.: Organic aerosol formation from the oxidation of biogenic hydrocarbons, *J. Geophys. Res.*, 104, 3555–3567, 1999a.
- Griffin, R. J., Cocker, D. R., Seinfeld, J. H., and Dabdub, D.: Estimate of global atmospheric organic aerosol from oxidation of biogenic hydrocarbons, *Geophys. Res. Lett.*, 26, 2721–2724, 1999b.
- Guenther, A., Hewitt, C. N., Erickson, D., Fall, R., Geron, C., Graedel, T., Harley, P., Klinger, L., Lerdau, M., McKay, W. A., Pierce, T., Scholes, B., Steinbrecher, R., Tallamraju, R., Taylor, J., and Zimmerman, P.: A global-model of natural volatile organic-compound emissions, *J. Geophys. Res.*, 100, 8873–8892, 1995.
- Guenther, A., Karl, T., Harley, P., Wiedinmyer, C., Palmer, P. I., and Geron, C.: Estimates of global terrestrial isoprene emissions using MEGAN (Model of Emissions of Gases and Aerosols from Nature), *Atmos. Chem. Phys.*, 6, 3181–3210, 2006.
- Heald, C. L., Jacob, D. J., Park, R. J., Russell, L. M., Huebert, B. J., Seinfeld, J. H., Liao, H., and Weber, R. J.: A large organic aerosol source in the free troposphere missing from current models, *Geophys. Res. Lett.*, 32, doi:10.1029/2005GL023831, 2005.
- Heald, C. L., Henze, D. K., Horowitz, L. W., Feddema, J., Lamarque, J. F., Guenther, A., Hess, P. G., Vitt, F., Seinfeld, J. H., Goldstein, A. H., and Fung, I.: Predicted change in global secondary organic aerosol concentrations in response to future climate, emissions, and land use change, *J. Geophys. Res.*, 113, D05 211, doi:10.1029/2007JD009092, 2008.

- Hennigan, C. J., Bergin, M. H., Russell, A. G., Nenes, A., and Weber, R. J.: Gas/particle partitioning of water-soluble organic aerosol in Atlanta, *Atmos. Chem. Phys.*, 9, 3613–3628, 2009.
- Henze, D. K. and Seinfeld, J. H.: Global secondary organic aerosol from isoprene oxidation, *Geophys. Res. Lett.*, 33, doi:10.1029/2006GL025976, 2006.
- Henze, D. K., Seinfeld, J. H., Ng, N. L., Kroll, J. H., Fu, T. M., Jacob, D. J., and Heald, C. L.: Global modeling of secondary organic aerosol formation from aromatic hydrocarbons: High- vs. low-yield pathways, *Atmos. Chem. Phys.*, 8, 2405–2420, 2008.
- Hoffmann, T., Odum, J. R., Bowman, F., Collins, D., Klockow, D., Flagan, R. C., and Seinfeld, J. H.: Formation of organic aerosols from the oxidation of biogenic hydrocarbons, *J Atmos Chem*, 26, 189–222, 1997.
- Kroll, J. H., Ng, N. L., Murphy, S. M., Flagan, R. C., and Seinfeld, J. H.: Secondary organic aerosol formation from isoprene photooxidation under high-NO_x conditions, *Geophys. Res. Lett.*, 32, L18 808, doi:10.1029/2005gl023637, 2005.
- Kroll, J. H., Ng, N. L., Murphy, S. M., Flagan, R. C., and Seinfeld, J. H.: Secondary organic aerosol formation from isoprene photooxidation, *Environ. Sci. Technol.*, 40, 1869–1877, doi:10.1021/Es0524301, 2006.
- Lane, T. E., Donahue, N. M., and Pandis, S. N.: Effect of NO_x on secondary organic aerosol concentrations, *Environ. Sci. Technol.*, 42, 6022–6027, doi:10.1021/Es703225a, 2008a.
- Lane, T. E., Donahue, N. M., and Pandis, S. N.: Simulating secondary organic aerosol formation using the volatility basis-set approach in a chemical transport model, *Atmos. Environ.*, 42, 7439–7451, doi:10.1016/J.ATMOENV.2008.06.026, 2008b.
- Lelieveld, J., Butler, T. M., Crowley, J. N., Dillon, T. J., Fischer, H., Ganzeveld, L., Harder, H., Lawrence, M. G., Martinez, M., Taraborrelli, D., and Williams, J.: Atmospheric oxidation capacity sustained by a tropical forest, *Nature*, 452, 737–740, doi:10.1038/NATURE06870, 2008.

- Liao, H., Henze, D. K., Seinfeld, J. H., Wu, S. L., and Mickley, L. J.: Biogenic secondary organic aerosol over the United States: Comparison of climatological simulations with observations, *J. Geophys. Res.*, 112, doi:10.1029/2006JD007813, 2007.
- Lim, Y. B. and Ziemann, P. J.: Products and mechanism of secondary organic aerosol formation from reactions of n-alkanes with OH radicals in the presence of NO_x, *Environ. Sci. Technol.*, 39, 9229–9236, doi:10.1021/Es051447g, 2005.
- Marley, N. A., Gaffney, J. S., Tackett, M., Sturchio, N. C., Heraty, L., Martinez, N., Hardy, K. D., Marchany-Rivera, A., Guilderson, T., MacMillan, A., and Steelman, K.: The impact of biogenic carbon sources on aerosol absorption in Mexico City, *Atmos. Chem. Phys.*, 9, 1537–1549, 2009.
- Ng, N. L., Chhabra, P. S., Chan, A. W. H., Surratt, J. D., Kroll, J. H., Kwan, A. J., McCabe, D. C., Wennberg, P. O., Sorooshian, A., Murphy, S. M., Dalleska, N. F., Flagan, R. C., and Seinfeld, J. H.: Effect of NO_x level on secondary organic aerosol (SOA) formation from the photooxidation of terpenes, *Atmos. Chem. Phys.*, 7, 5159–5174, 2007a.
- Ng, N. L., Kroll, J. H., Chan, A. W. H., Chhabra, P. S., Flagan, R. C., and Seinfeld, J. H.: Secondary organic aerosol formation from m-xylene, toluene, and benzene, *Atmos. Chem. Phys.*, 7, 3909–3922, 2007b.
- Ng, N. L., Kwan, A. J., Surratt, J. D., Chan, A. W. H., Chhabra, P. S., Sorooshian, A., Pye, H. O. T., Crouse, J. D., Wennberg, P. O., Flagan, R. C., and Seinfeld, J. H.: Secondary organic aerosol (SOA) formation from reaction of isoprene with nitrate radicals (NO₃), *Atmos. Chem. Phys.*, 8, 4117–4140, 2008.
- Odum, J. R., Hoffmann, T., Bowman, F., Collins, D., Flagan, R. C., and Seinfeld, J. H.: Gas/particle partitioning and secondary organic aerosol yields, *Environ. Sci. Technol.*, 30, 2580–2585, 1996.
- Pankow, J. F.: Organic particulate material levels in the atmosphere: Conditions favoring sensitivity to varying relative humidity and temperature, *Proc. Natl. Acad. Sci. U. S. A.*, 107, 6682–6686, doi:10.1073/Pnas.1001043107, 2010.

- Park, R. J., Jacob, D. J., Chin, M., and Martin, R. V.: Sources of carbonaceous aerosols over the United States and implications for natural visibility, *J. Geophys. Res.*, 108, doi:10.1029/2002JD003190, 2003.
- Park, R. J., Jacob, D. J., Kumar, N., and Yantosca, R. M.: Regional visibility statistics in the United States: Natural and transboundary pollution influences, and implications for the Regional Haze Rule, *Atmos. Environ.*, 40, 5405–5423, doi:10.1016/J.ATMOENV.2006.04.059, 2006.
- Pathak, R. K., Presto, A. A., Lane, T. E., Stanier, C. O., Donahue, N. M., and Pandis, S. N.: Ozonolysis of alpha-pinene: parameterization of secondary organic aerosol mass fraction, *Atmos. Chem. Phys.*, 7, 3811–3821, 2007.
- Perring, A. E., Wisthaler, A., Graus, M., Wooldridge, P. J., Lockwood, A. L., Mielke, L. H., Shepson, P. B., Hansel, A., and Cohen, R. C.: A product study of the isoprene+NO₃ reaction, *Atmos. Chem. Phys.*, 9, 4945–4956, 2009.
- Presto, A. A., Hartz, K. E. H., and Donahue, N. M.: Secondary organic aerosol production from terpene ozonolysis. 2. Effect of NO_x concentration, *Environ. Sci. Technol.*, 39, 7046–7054, doi:10.1021/Es050400s, 2005.
- Pye, H. O. T. and Seinfeld, J. H.: A global perspective on aerosol from low-volatility organic compounds, *Atmos. Chem. Phys.*, 10, 4377–4401, doi:10.5194/Acp-10-4377-2010, 2010.
- Robinson, A. L., Donahue, N. M., Shrivastava, M. K., Weitkamp, E. A., Sage, A. M., Grieshop, A. P., Lane, T. E., Pierce, J. R., and Pandis, S. N.: Rethinking organic aerosols: Semivolatile emissions and photochemical aging, *Science*, 315, 1259–1262, doi:10.1126/SCIENCE.1133061, 2007.
- Rollins, A. W., Kiendler-Scharr, A., Fry, J. L., Brauers, T., Brown, S. S., Dorn, H. P., Dube, W. P., Fuchs, H., Mensah, A., Mentel, T. F., Rohrer, F., Tillmann, R., Wegener, R., Wooldridge, P. J., and Cohen, R. C.: Isoprene oxidation by nitrate radical: alkyl nitrate and secondary organic aerosol yields, *Atmos. Chem. Phys.*, 9, 6685–6703, 2009.

- Sakulyanontvittaya, T., Duhl, T., Wiedinmyer, C., Helmig, D., Matsunaga, S., Potosnak, M., Milford, J., and Guenther, A.: Monoterpene and sesquiterpene emission estimates for the United States, *Environ. Sci. Technol.*, 42, 1623–1629, doi:10.1021/Es702274e, 2008.
- Schauer, J. J., Kleeman, M. J., Cass, G. R., and Simoneit, B. R. T.: Measurement of emissions from air pollution sources. 3. C-1-C-29 organic compounds from fireplace combustion of wood, *Environ. Sci. Technol.*, 35, 1716–1728, doi:10.1021/ES001331e, 2001.
- Schichtel, B. A., Malm, W. C., Bench, G., Fallon, S., McDade, C. E., Chow, J. C., and Watson, J. G.: Fossil and contemporary fine particulate carbon fractions at 12 rural and urban sites in the United States, *J. Geophys. Res.*, 113, doi:10.1029/2007JD008605, 2008.
- Shilling, J. E., Chen, Q., King, S. M., Rosenoern, T., Kroll, J. H., Worsnop, D. R., McKinney, K. A., and Martin, S. T.: Particle mass yield in secondary organic aerosol formed by the dark ozonolysis of alpha-pinene, *Atmos. Chem. Phys.*, 8, 2073–2088, 2008.
- Shrivastava, M. K., Lipsky, E. M., Stanier, C. O., and Robinson, A. L.: Modeling semivolatile organic aerosol mass emissions from combustion systems, *Environ. Sci. Technol.*, 40, 2671–2677, doi:10.1021/ES0522231, 2006.
- Stanier, C. O., Donahue, N., and Pandis, S. N.: Parameterization of secondary organic aerosol mass fractions from smog chamber data, *Atmos. Environ.*, 42, 2276–2299, 2008.
- Surratt, J. D., Lewandowski, M., Offenberg, J. H., Jaoui, M., Kleindienst, T. E., Edney, E. O., and Seinfeld, J. H.: Effect of acidity on secondary organic aerosol formation from isoprene, *Environ. Sci. Technol.*, 41, 5363–5369, doi:10.1021/Es0704176, 2007.
- Surratt, J. D., Chan, A. W. H., Eddingsaas, N. C., Chan, M. N., Loza, C. L., Kwan, A. J., Hersey, S. P., Flagan, R. C., Wennberg, P. O., and Seinfeld, J. H.: Reactive intermediates revealed in secondary organic aerosol formation from isoprene, *Proc. Natl. Acad. Sci. U. S. A.*, 107, 6640–6645, doi:10.1073/Pnas.0911114107, 2010.

- Szidat, S.: Radiocarbon analysis of carbonaceous aerosols: Recent developments, *Chimia*, **63**, 157–161, doi:10.2533/CHIMIA.2009.157, 2009.
- Tsigaridis, K. and Kanakidou, M.: Global modelling of secondary organic aerosol in the troposphere: a sensitivity analysis, *Atmos. Chem. Phys.*, **3**, 1849–1869, 2003.
- Volkamer, R., Jimenez, J. L., San Martini, F., Dzepina, K., Zhang, Q., Salcedo, D., Molina, L. T., Worsnop, D. R., and Molina, M. J.: Secondary organic aerosol formation from anthropogenic air pollution: Rapid and higher than expected, *Geophys. Res. Lett.*, **33**, L17811, doi:10.1029/2006GL026899, 2006.
- Warneke, C., de Gouw, J. A., Goldan, P. D., Kuster, W. C., Williams, E. J., Lerner, B. M., Jakoubek, R., Brown, S. S., Stark, H., Aldener, M., Ravishankara, A. R., Roberts, J. M., Marchewka, M., Bertman, S., Sueper, D. T., McKeen, S. A., Meagher, J. F., and Fehsenfeld, F. C.: Comparison of daytime and nighttime oxidation of biogenic and anthropogenic VOCs along the New England coast in summer during New England Air Quality Study 2002, *J. Geophys. Res.*, **109**, D10309, doi:10.1029/2003jd004424, 2004.
- Weber, R. J., Sullivan, A. P., Peltier, R. E., Russell, A., Yan, B., Zheng, M., de Gouw, J., Warneke, C., Brock, C., Holloway, J. S., Atlas, E. L., and Edgerton, E.: A study of secondary organic aerosol formation in the anthropogenic-influenced southeastern United States, *J. Geophys. Res.*, **112**, doi:10.1029/2007JD008408, 2007.
- Wesely, M. L.: Parameterization of surface resistances to gaseous dry deposition in regional-scale numerical-models, *Atmos. Environ.*, **23**, 1293–1304, 1989.
- Zhang, J. Y., Hartz, K. E. H., Pandis, S. N., and Donahue, N. M.: Secondary organic aerosol formation from limonene ozonolysis: Homogeneous and heterogeneous influences as a function of NO_x , *J. Phys. Chem. A*, **110**, 11053–11063, doi:10.1021/Jp06286f, 2006.
- Zhang, L. M., Gong, S. L., Padro, J., and Barrie, L.: A size-segregated particle dry deposition scheme for an atmospheric aerosol module, *Atmos. Environ.*, **35**, 549–560, 2001.

Table 4.1: SOA Yield Parameterizations at 298 K.

Parent HC	Oxidant	α for C* (C* in $\mu\text{g}/\text{m}^3$)						RMSE ^a [$\mu\text{g}/\mu\text{g}$]	Yield at 10 $\mu\text{g}/\text{m}^3$	Data
		nonvolatile	0.1	1	10	100	1000			
Monoterpenes and sesquiterpenes										
LIMO	OH, O ₃ ; NO	0	0	0.474	0.117	1.419	0.145	0.62	dark high-NO _x limonene ozonolysis (Zhang et al., 2006), refit using a density of 1.3 g/cm ³	
MTPA/O	OH, O ₃ ; NO	0	0.04	0.0095	0.09	0.015	NA	0.09	based on low-NO _x fit, adjusted for NO _x based on Ng et al. (2007a) and Pathak et al. (2007)	
SESQ	OH, O ₃ ; NO	0	0	0.000	1.146	2.981	NA	0.84	based on low-NO _x fit, adjusted for NO _x based on Ng et al. (2007a)	
LIMO	OH, O ₃ ; HO ₂	0	0	0.366	0.321	0.817	0.068	0.57	dark low-NO _x limonene ozonolysis (Zhang et al., 2006), refit using a density of 1.3 g/cm ³	
MTPA/O	OH, O ₃ ; HO ₂	0	0.08	0.019	0.18	0.03	0.016	0.19	dark α -pinene ozonolysis (Shilling et al., 2008), not wall loss corrected	
SESQ	OH, O ₃ ; HO ₂	0	0	0.000	0.574	1.489	0.037	0.42	β -caryophyllene and α -humulene [VOC/NO _x] > 3ppbC/ppb (Griffin et al., 1999a), fit using a density of 1.3 g/cm ³	
all terpenes	NO ₃	0	0	0.000	0.321	1.083	0.057	0.26	β -pinene+NO ₃ (Griffin et al., 1999a), fit using a density of 1.3 g/cm ³	
Isoprene										
ISOP	NO ₃	0	0	0.000	0.217	0.092	0.023	0.12	Ng et al. (2008)	
ISOP	OH	0	0	0.031	0.000	0.095	0.003	0.04	low-NO _x photooxidation (Kroll et al., 2006)	
Aromatics										
BENZ	OH; NO	0	0	0.078	0.000	0.793	0.005	0.14	benzene high-NO _x photooxidation (Ng et al., 2007b)	
TOLU	OH; NO	0	0	0.032	0.094	0.080	0.001	0.08	toluene high-NO _x photooxidation (Ng et al., 2007b)	
XYLE	OH; NO	0	0	0.025	0.036	0.090	0.002	0.05	xylylene high-NO _x photooxidation (Ng et al., 2007b)	
BENZ	OH; HO ₂	0.37	0	0	0	0	NA	0.37	benzene low-NO _x photooxidation (Ng et al., 2007b)	
TOLU	OH; HO ₂	0.36	0	0	0	0	NA	0.36	toluene low-NO _x photooxidation (Ng et al., 2007b)	
XYLE	OH; HO ₂	0.30	0	0	0	0	NA	0.30	xylylene low-NO _x photooxidation (Ng et al., 2007b)	
IVOCs										
NAP	OH; NO	0	0	0.039	0.296	0.235	0.036	0.20	naphthalene high-NO _x photooxidation (Chan et al., 2009)	
NAP	OH; HO ₂	0.73	0	0	0	0	NA	0.73	naphthalene low-NO _x photooxidation (Chan et al., 2009)	

^a Root mean square error in mass of SOA per mass of parent hydrocarbon reacted.

Table 4.2: SOA precursor emissions. Emissions are for year 2000 using GEOS-4 assimilated meteorology at 2° latitude by 2.5° longitude horizontal resolution.

Species	Global Emissions [Tg C/yr]
α -pinene	34
β -pinene	16
sabinene	8
Δ 3-carene	6
limonene	9
myrcene	3
ocimene	14
other monoterpenes	12
sesquiterpenes	12
isoprene	449
benzene	5
toluene	7
xylene	5
IVOCs ^a	15
traditional POA ^a	29
SVOCs ^a	37

^a Either POA is emitted as non-volatile at the rate specified (for traditional, non-volatile POA simulations) or IVOCs and SVOCs are emitted at the rates specified (for a semivolatile POA simulation). For more information on the IVOC and SVOC emissions, see Pye and Seinfeld (2010).

Table 4.3: Global net production of SOA (GEOS-Chem 2° latitude by 2.5° longitude horizontal resolution with GEOS-4 meteorology).

Precursor	Traditional Simulation [Tg/yr]	Semivolatile POA and IVOCs [Tg/yr]
Terpenes	15.1	13.7
Isoprene	8.6	7.9
Aromatics+IVOCs	3.2	8.5
SVOCs	61.2 ^a	0.7
Oxidized SVOCs	0.0	38.5
Total OA	88.2	69.3

^a POA emission rate in a traditional simulation with nonvolatile POA using an OM/OC ratio of 2.1.

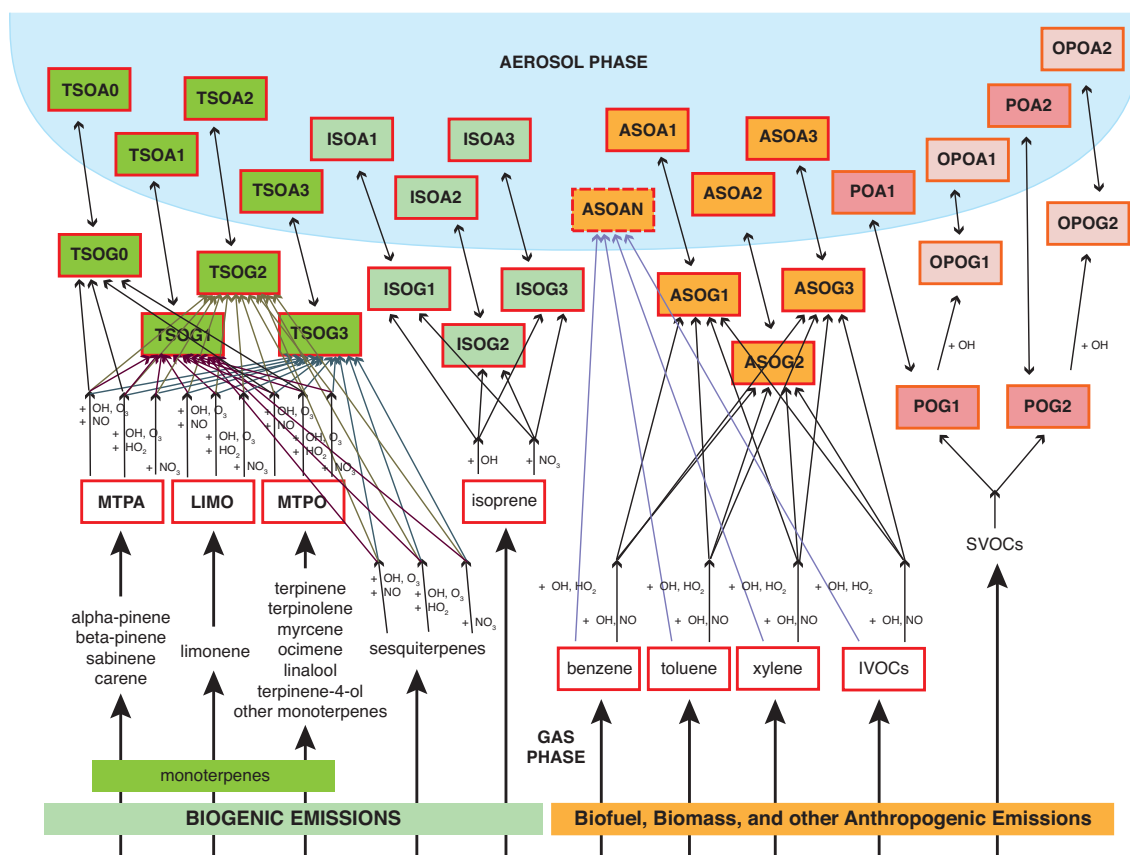


Figure 4.1: Schematic of SOA model. Species appearing in boxes are tracers. A bidirectional arrow across the aerosol/gas interface indicates a semivolatile species. ASOAN is nonvolatile. SOA/G0-3 species have saturation concentrations of 0.1, 1, 10, 100 $\mu\text{g}/\text{m}^3$. SVOCs are represented using an Odum 2-product fit. Yield parameters are shown in Table 4.1. For a traditional simulation, IVOCs are not emitted and nonvolatile POA replaces the SVOCs.

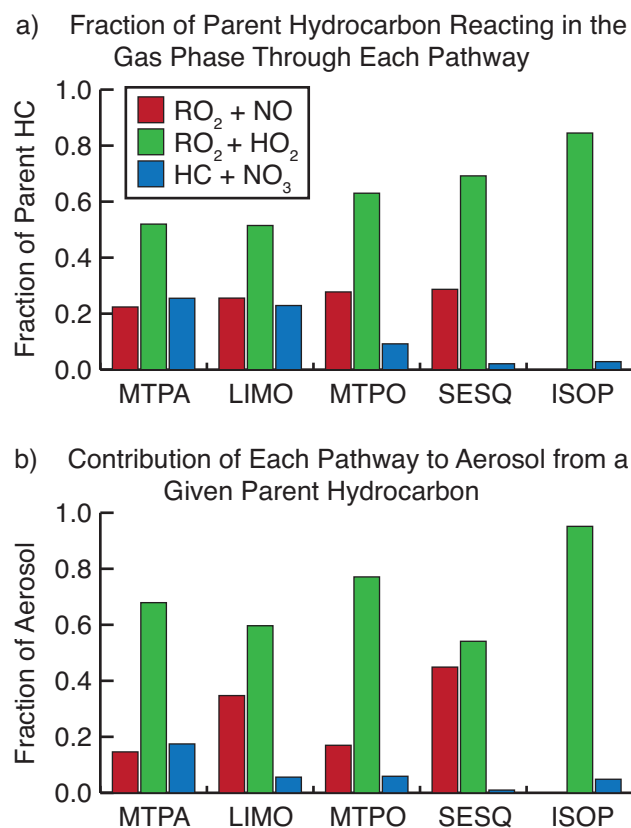


Figure 4.2: Fraction of parent hydrocarbon reacting through each SOA-forming pathway globally and annually averaged (a). Panel (b) shows the estimated contribution of each pathway to aerosol for each parent hydrocarbon. Panel (b) is estimated using the yield at an organic loading of $1.5 \mu\text{g}/\text{m}^3$. Isoprene reacting with ozone is not shown since it does not produce aerosol. Isoprene photooxidation is labeled as low- NO_x since yields are representative of those conditions.

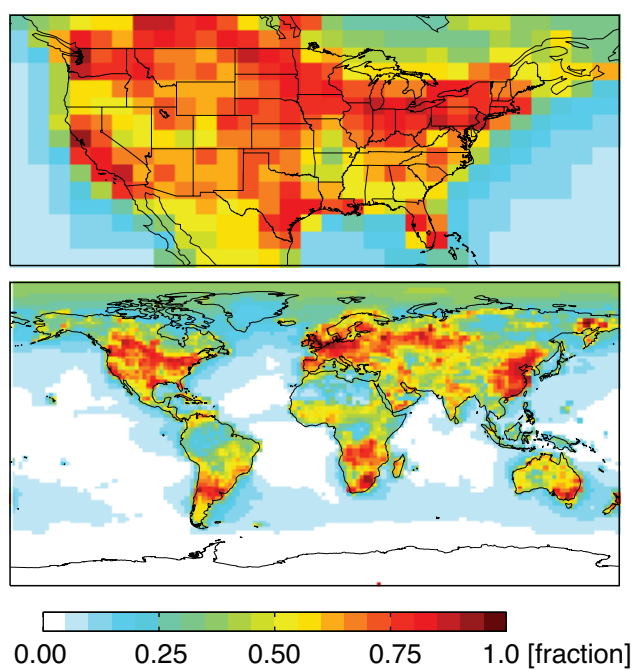


Figure 4.3: Fraction of peroxy radical species reacting with NO, β , averaged for the month of August 2000 at the surface (model level 1) for the United States and globally.

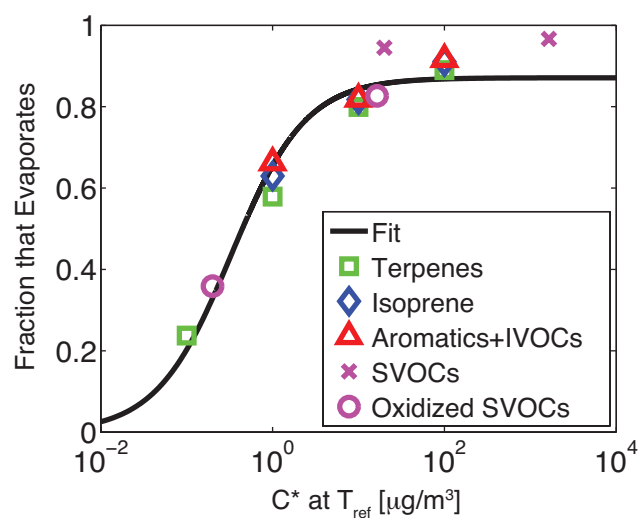


Figure 4.4: Fraction of semivolatile mass that partitions to the aerosol phase but later evaporates globally and annually averaged as a function of saturation concentration at the reference temperature. The fit corresponds to a semivolatile that is emitted in region with a loading of $2.6 \mu\text{g}/\text{m}^3$ and travels to a region with a loading of $0.3 \mu\text{g}/\text{m}^3$ without any losses.

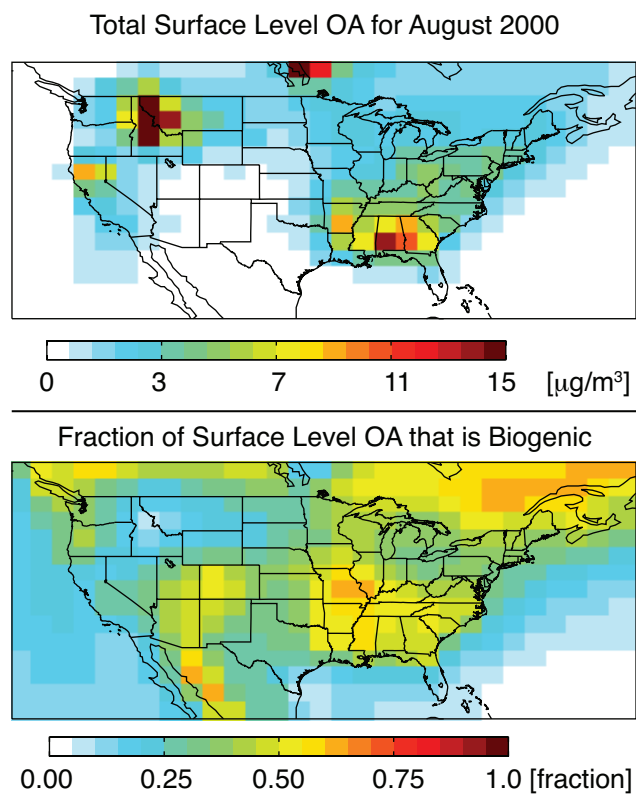


Figure 4.5: Surface level organic aerosol from monoterpenes, sesquiterpenes, isoprene, benzene, toluene, xylene, and primary organic aerosol from a traditional, non-volatile POA simulation during August 2000. The biomass burning event near Idaho is saturated on the colorbar. Bottom panel is the fraction of aerosol in the top panel that arises from monoterpenes, sesquiterpenes, and isoprene. POA is assumed to be non-volatile and IVOCs do not form aerosol.

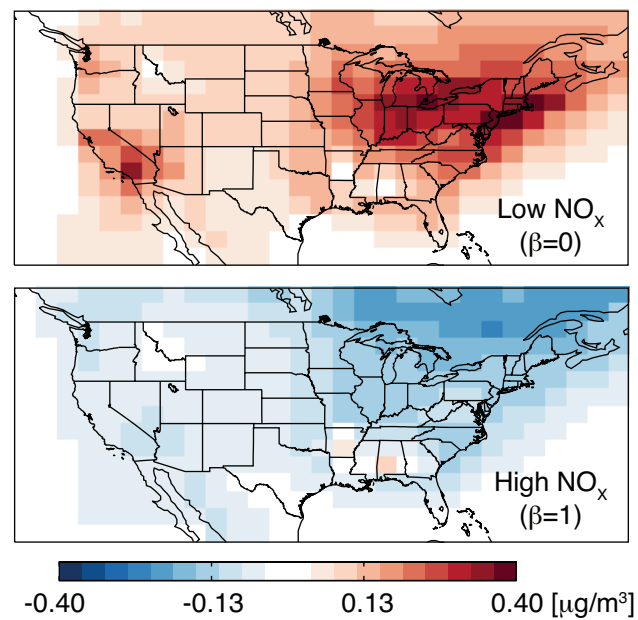


Figure 4.6: The change in surface concentration of total OA (August 2000) compared to concentrations in Fig. 4.5 as a result of forcing photooxidation and ozonolysis through either the low-NO_x ($\beta=0$) or high-NO_x ($\beta=1$) yields. POA is assumed to be non-volatile and IVOCs do not form aerosol (traditional simulation).

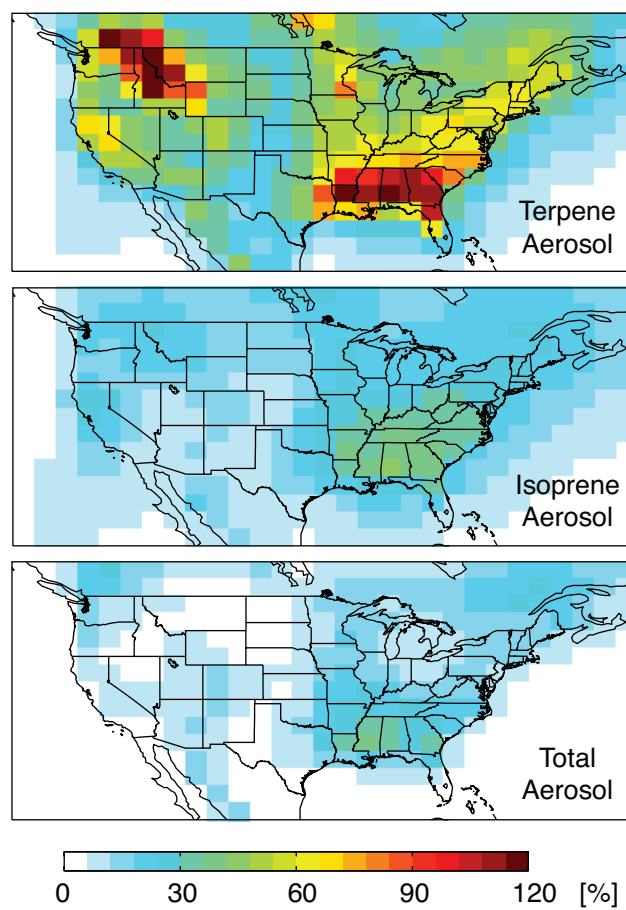


Figure 4.7: Enhancement in surface-level August 2000 aerosol from terpenes, isoprene, and all sources due to aerosol from the nitrate oxidation pathway. The change is relative to a simulation with yields set to zero for the nitrate oxidation pathway. POA is assumed to be non-volatile and IVOCs do not form aerosol (traditional simulation).

Chapter 5

Future Work

The present-day simulation of inorganic and organic aerosol in GEOS-Chem has been improved by adding ISORROPIA II and new pathways to organic aerosol formation. However, a number of processes leading to organic aerosol formation are still not included in models and projecting future concentrations requires an accurate representation of present-day aerosols. Chapters 3 and 4 identified a number of uncertainties in the organic aerosol simulation that should be addressed in future work. Addressing some of these uncertainties will require new experimental studies, while data is already available to start examining others.

1. Low-volatility organic compounds have traditionally been included in models as nonvolatile primary organic aerosol (POA). Although recent work has highlighted the fact that most POA is semivolatile and even provided fits that can be incorporated into atmospheric models, significant uncertainty still exists in terms of the emissions and atmospheric aging of these low-volatility compounds. New experimental studies can better constrain the emissions and provide information about how they age in the atmosphere.
2. Models need to represent the aging that occurs on time-scales longer than what has traditionally been examined in chamber studies. Chamber studies produce secondary organic aerosol (SOA) that is generally too volatile and not oxidized enough in comparison to ambient observations. New mechanisms and experimental support for aging traditional SOA in models is needed.
3. Much of the experimental work constraining the yields of organic aerosol from oxidation of monoterpenes and sesquiterpenes was performed in 1997 and 1999 in an outdoor chamber before the role of NO_x had been identified. This data is still extensively used in models. New experimental data from a variety of parent hydrocarbons oxidized by OH, ozone, and nitrate under atmospherically relevant temperatures and loadings would be helpful to confirm whether α -pinene ozonolysis yields are a reasonable representation of monoterpenes + OH, O_3 and whether the yield of aerosol from nitrate oxidation of terpenes used here is appropriate.
4. As mentioned in Chapter 4, monoterpenes have the potential to significantly influence night-

time oxidants. Future modeling work can refine estimates of monoterpene + NO_3 aerosol by accounting for titration of nitrate radicals.

5. A number of studies have indicated that organic aerosol contains a large amount of modern carbon but is correlated with anthropogenic tracers. Resolving this apparent contradiction is an important area of future work. Part of the conflict may be remedied by incorporating new information about the dependence of isoprene aerosol on NO_2 , sulfate, and particle acidity.

Appendix A

Secondary organic aerosol (SOA) formation from reaction of isoprene with nitrate radicals (NO_3) *

*Reproduced with permission from "Secondary organic aerosol (SOA) formation from reaction of isoprene with nitrate radicals (NO_3)" by N. L. Ng, A. J. Kwan, J. D. Surratt, A. W. H. Chan, P. S. Chhabra, A. Sorooshian, H. O. T. Pye, J. D. Crouse, P. O. Wennberg, R. C. Flagan, and J. H. Seinfeld, *Atmospheric Chemistry and Physics*, 8, 4117-4140. Copyright 2008 by the Authors. This work is distributed under the Creative Commons Attribution 3.0 License.

Secondary organic aerosol (SOA) formation from reaction of isoprene with nitrate radicals (NO₃)

N. L. Ng¹, A. J. Kwan², J. D. Surratt¹, A. W. H. Chan¹, P. S. Chhabra¹, A. Sorooshian¹, H. O. T. Pye¹, J. D. Crouse¹, P. O. Wennberg^{2,3}, R. C. Flagan^{1,2}, and J. H. Seinfeld^{1,2}

¹Division of Chemistry and Chemical Engineering, California Institute of Technology, Pasadena, CA 91125, USA

²Division of Engineering and Applied Science, California Institute of Technology, Pasadena, CA 91125, USA

³Division of Geological and Planetary Sciences, California Institute of Technology, Pasadena, CA 91125, USA

Received: 3 January 2008 – Published in Atmos. Chem. Phys. Discuss.: 15 February 2008

Revised: 3 July 2008 – Accepted: 3 July 2008 – Published: 1 August 2008

Abstract. Secondary organic aerosol (SOA) formation from the reaction of isoprene with nitrate radicals (NO₃) is investigated in the Caltech indoor chambers. Experiments are performed in the dark and under dry conditions (RH < 10%) using N₂O₅ as a source of NO₃ radicals. For an initial isoprene concentration of 18.4 to 101.6 ppb, the SOA yield (defined as the ratio of the mass of organic aerosol formed to the mass of parent hydrocarbon reacted) ranges from 4.3% to 23.8%. By examining the time evolutions of gas-phase intermediate products and aerosol volume in real time, we are able to constrain the chemistry that leads to the formation of low-volatility products. Although the formation of ROOR from the reaction of two peroxy radicals (RO₂) has generally been considered as a minor channel, based on the gas-phase and aerosol-phase data it appears that RO₂+RO₂ reaction (self reaction or cross-reaction) in the gas phase yielding ROOR products is a dominant SOA formation pathway. A wide array of organic nitrates and peroxides are identified in the aerosol formed and mechanisms for SOA formation are proposed. Using a uniform SOA yield of 10% (corresponding to M_o ≈ 10 μg m⁻³), it is estimated that ~2 to 3 Tg yr⁻¹ of SOA results from isoprene+NO₃. The extent to which the results from this study can be applied to conditions in the atmosphere depends on the fate of peroxy radicals in the nighttime troposphere.

1 Introduction

Isoprene is the most abundant non-methane hydrocarbon emitted into the atmosphere with a global emission of ~500 Tg yr⁻¹ (Guenther et al., 1995; Guenther et al., 2006). In the troposphere, isoprene reacts with hydroxyl radicals (OH), ozone (O₃), and nitrate radicals (NO₃). Owing to its high concentration and reactivity with OH radicals, isoprene plays an important role in the photochemistry occurring within the atmospheric boundary layer. Recently, it has been shown that the photooxidation of isoprene leads to the formation of low volatility species that condense to form SOA (Claeys et al., 2004; Edney et al., 2005; Kroll et al., 2005; Dommen et al., 2006; Kroll et al., 2006; Surratt et al., 2006); SOA yields as high as ~3% have been observed (Kroll et al., 2005; Kroll et al., 2006). Global SOA production from isoprene photooxidation has been estimated to be about 13 Tg yr⁻¹ (Henze et al., 2007).

Although emission of isoprene from vegetation is triggered by sunlight and increases with light intensity and temperature (e.g. Sharkey et al., 1996), the isoprene mixing ratio has been observed to peak in early evening in several field studies, with a measured mixing ratio up to a few ppb (Curren et al., 1998; Starn et al., 1998; Stroud et al., 2002; Steinbacher et al., 2005). After sunset, the isoprene mixing ratio drops rapidly, and it has been suggested that the reaction with nitrate radicals, NO₃, is a major contributor to isoprene decay at night (Curren et al., 1998; Starn et al., 1998; Stroud et al., 2002; Steinbacher et al., 2005). Typical NO₃ radical mixing ratios in boundary layer continental air masses range between ~10 to ~100 ppt (Platt and Janssen, 1995; Smith et al., 1995; Heintz et al., 1996; Carslaw et al., 1997). However, concentrations as high as



Correspondence to: J. H. Seinfeld
 (seinfeld@caltech.edu)

several hundred ppt have been observed over northeastern USA and Europe (Platt et al., 1981; von Friedeburg et al., 2002; Brown et al., 2006; Penkett et al., 2007). Given the rapid reaction rate between isoprene and NO₃ radicals ($k_{\text{NO}_3} = 7 \times 10^{-13} \text{ cm}^3 \text{ molecule}^{-1} \text{ s}^{-1}$ at $T = 298 \text{ K}$, IUPAC), it is likely that NO₃ radicals play a major role in the nighttime chemistry of isoprene.

The kinetics and gas-phase products of the isoprene-NO₃ reaction have been the subject of several laboratory and theoretical studies (Jay and Stieglitz, 1989; Barnes et al., 1990; Skov et al., 1992; Kwok et al., 1996; Berndt and Böge, 1997; Suh et al., 2001; Zhang et al., 2002; Fan et al., 2004). In many studies, C₅-nitrooxycarbonyl is identified as the major first-generation gas-phase reaction product (Jay and Stieglitz, 1989; Skov et al., 1992; Kwok et al., 1996; Berndt and Böge, 1997). Other compounds such as C₅-hydroxynitrate, C₅-nitrooxyhydroperoxide, and C₅-hydroxycarbonyl have also been identified (Kwok et al., 1996); C₅-hydroxynitrate has also been measured in ambient air with concentrations in the lower ppt range at a few ng m⁻³ (Werner et al., 1999). According to the experimental study by Barnes et al. (1990), the yield for nitrate-containing compounds from the reaction of isoprene and NO₃ radicals can be as high as 80%. A recent modeling study in conjunction with observations from the ICARTT field campaign suggests that ~50% of the total isoprene nitrates production occurs via reaction of isoprene and NO₃ radicals (Horowitz et al., 2007).

Little is known beyond the formation of the first-generation products of the reaction of NO₃ with isoprene. The isoprene nitrates and other first-generation products still contain a double bond, and it is likely that the further oxidation of these species will lead to low volatility products that can contribute to SOA formation at nighttime.

In this work, SOA formation from the reaction of isoprene with NO₃ radicals is investigated. Laboratory chamber experiments are performed in the dark using N₂O₅ as a source of NO₃ radicals. Aerosol yields are obtained over a range of initial isoprene concentrations (mixing ratios). By examining the time evolutions of aerosol volume and different intermediate gas-phase products, we are able to constrain the chemistry that leads to the formation of low-volatility products. Mechanisms for SOA formation are proposed and chemical composition data of the SOA formed are also presented.

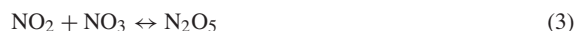
2 Experimental section

Experiments are carried out in the Caltech dual 28 m³ Teflon chambers. A detailed description of the facility is provided elsewhere (Cocker et al., 2001; Keywood et al., 2004). Before each experiment, the chambers are flushed continuously for over 24 h. Aerosol number concentration, size distribution, and volume concentration are measured by a Differential Mobility Analyzer (DMA, TSI model 3081) coupled with a condensation nucleus counter (TSI model 3760).

All aerosol growth data are corrected for wall loss, in which size-dependent particle loss coefficients are determined from inert particle wall loss experiments (Keywood et al., 2004). Temperature, relative humidity (RH), O₃, NO, and NO_x are continuously monitored. Experiments are performed in the dark at room temperature (20–21°C) and under dry conditions (RH < 10%).

In most experiments, seed aerosols are introduced into the chamber to act as a substrate onto which the gas-phase products may condense. Seed aerosols are generated by atomizing an aqueous solution with a constant-rate atomizer. The seed solution consists of 0.015 M (NH₄)₂SO₄. In a few experiments, acidic seed is used, consisting of 0.03 M MgSO₄ and 0.05 M H₂SO₄. The initial particle number concentration is ~20 000 particles cm⁻³, with a geometric mean diameter of ~50 nm. The initial seed volume is 10–12 μm³ cm⁻³. In some experiments, no seed particles are added and aerosols are formed via nucleation. After introduction of the seed aerosols (in seeded experiments), a known volume of isoprene (Aldrich, 99%) is injected into a glass bulb and introduced into the chamber by an air stream. The mixing ratio of isoprene is monitored with a gas chromatograph equipped with a flame ionization detector (GC-FID, Agilent model 6890N). The column used is a bonded polystyrene-divinylbenzene based column (HP-PLOT Q, 15 m × 0.53 mm, 40 μm thickness, J&W Scientific). The oven temperature is held at 60°C for 0.5 min, ramped at 35°C min⁻¹ to 200°C, and held constant for 3.5 min.

The thermal decomposition of N₂O₅ serves as a source of NO₃ radicals in these experiments. N₂O₅ is prepared and collected offline by mixing a stream of nitric oxide (≥99.5%, Matheson Tri Gas) with a stream of ozone in a glass bulb (Davidson et al., 1978):



Ozone is generated by flowing oxygen through an ozonizer (OREC model V10-0, Phoenix, AZ) at ~1 L min⁻¹. The mixing ratio of ozone is measured by a UV/VIS spectrometer (Hewlett Packard model 8453) to be ~2%. The flow rate of nitric oxide into the glass bulb is adjusted until the brown color in the bulb disappears. The N₂O₅ is trapped for 2 h in an acetone-dry ice bath (approximately at -80°C; cold enough to trap N₂O₅ but not O₃, as condensed O₃ can explode upon warming and is extremely dangerous) as a white solid, and stored between experiments under liquid nitrogen temperature. Once the seed and isoprene concentrations in the chamber stabilize, reaction is initiated by vaporizing N₂O₅ into an evacuated 500 mL glass bulb and introduced into the chamber with an air stream of 5 L min⁻¹.

The amount of N₂O₅ injected is estimated based on the vapor pressure in the glass bulb, which is measured using a capacitance manometer (MKS); this amount corresponds to an initial mixing ratio of ~1 ppm in the chamber. The thermal decomposition of N₂O₅ forms NO₂ and NO₃ radicals. Impurities in the N₂O₅ starting material are quantified by FTIR spectroscopy (Nicolet model Magna 550). N₂O₅ is vaporized into an evacuated pyrex cell (18 cm in length and 300 cm³) with CaF₂ windows. Spectra are collected immediately upon addition over the 1000 cm⁻¹ to 4000 cm⁻¹ window allowing for quantification of NO₂ (1616 cm⁻¹ band) and HNO₃ (3550 cm⁻¹ band) impurities.

A custom-modified Varian 1200 Chemical Ionization Mass Spectrometer (CIMS) is used to continuously monitor the concentrations of various gas-phase intermediates and products over the course of the experiments. The CIMS instrument is operated mainly in negative mode using CF₃O⁻ as a reagent ion, which selectively clusters with compounds having high fluorine affinity (e.g., acidic compounds and many hydroxy- and nitrooxy- carbonyls), forming ions at *m/z* MW+85. In some experiments, the CIMS instrument is also operated in the positive mode using H₂O as a reagent ion forming ions at *m/z* MW+1. The ionization schemes are as follows:

Negative chemical ionization: CF₃O⁻+HB→CF₃O⁻·HB
 Positive chemical ionization: H₃O⁺+D→D·H⁺+H₂O
 (where D has a proton affinity >H₂O)

The term “product ion” is used throughout this manuscript to describe the ionized products formed through the above chemical reaction schemes. Typically, we scan from *m/z* 50 to 400. More details about the CIMS technique are given in Crouse et al. (2006) and Ng et al. (2007a). Because authentic standards are not available for the major products, sensitivities are not experimentally determined. We estimate the collision rate of CF₃O⁻ with these products (which determines the sensitivity) with the empirical method of Su and Chesnavich (1982), which bases its predictions on an analyte’s dipole moment and polarizability. Dipole moments and polarizabilities are calculated with the Spartan06 quantum package, and are based on molecular structures optimized with the B3LYP/6-31G(d) method. Further details on estimating CIMS sensitivities based on quantum calculations are described in Paulot et al. (2008). As isomers would have different polarities and hence different sensitivities, in estimating the concentrations it is assumed that the NO₃ attack at C₁-position to C₄-position is 5.5:1 (See Sect. 4.1).

Aerosol physical and chemical properties are monitored by many instruments. Real-time particle mass spectra are obtained with an Aerodyne quadrupole Aerosol Mass Spectrometer (Q-AMS) (Jayne et al., 2000). A Particle-Into-Liquid Sampler (PILS, Brechtel Manufacturing, Inc.) coupled with ion chromatography (IC) is employed for quantitative measurements of water-soluble ions in the aerosol phase

(Sorooshian et al., 2006). Duplicate Teflon filters (PALL Life Sciences, 47-mm diameter, 1.0-μm pore size, teflo membrane) are collected from a selected number of experiments for offline chemical analysis. Filter sampling is initiated when the aerosol volume reaches its maximum value. Depending on the total volume concentration of aerosol in the chamber, the filter sampling time is 2–4 h, which results in ~2–5 m³ of total chamber air sampled. Teflon filters used for high-resolution electrospray ionization-time-of-flight mass spectrometry (ESI-TOFMS) analysis are extracted in 5 mL of high-purity methanol (LC-MS CHROMASOLV-Grade, Sigma-Aldrich) by 45 min of sonication. Methanol sample extracts are then blown dry under a gentle N₂ stream (without added heat) once the filters are removed and archived at -20°C. Dried residues are then reconstituted with 500 mL of a 1:1 (v/v) solvent mixture of 0.1% acetic acid in water (LC-MS CHROMASOLV-Grade, Sigma-Aldrich) and 0.1% acetic acid in methanol (LC-MS CHROMASOLV-Grade, Sigma Aldrich). All resultant filter extracts are analyzed by a Waters ACQUITY ultra performance liquid chromatography (UPLC) system, coupled to a Waters LCT Premier XT time-of-flight mass spectrometer (TOFMS) equipped with an ESI source that is operated in the negative (-) ionization mode. Detailed operating conditions for the UPLC/(-)ESI-TOFMS instrument have been described previously (Ng et al., 2007a). A Waters ACQUITY UPLC HSS column is selected to separate the SOA components because of its increased retention of water-soluble polar organics; separation is achieved as a result of trifunctionally-bonded (T3) C₁₈ alkyl residues on this column, which prevent stationary phase collapse when a 100% aqueous mobile phase is used and result in better retention of water-soluble polar organic compounds. In addition to the UPLC/(-)ESI-TOFMS analysis, all remaining Teflon filters are extracted and analyzed for total peroxide content (sum of ROOR and ROOH) by using an iodometric-spectroscopic method (Docherty et al., 2005; Surratt et al., 2006).

To study the mechanism of SOA formation, in several experiments the experimental protocols are slightly modified: (1) An excess amount of isoprene (relative to N₂O₅ concentration) is injected into the chamber to prevent the further reaction of first-generation gas-phase products, allowing these products to be detected more readily; (2) After the addition of isoprene, pulses of N₂O₅ are introduced into the chamber to study the evolution of different intermediate gas-phase products; (3) With isoprene well mixed in the chamber, N₂O₅ is introduced slowly to maximize the self-reaction of peroxy radicals (see Sect. 4.2). This is achieved by first injecting N₂O₅ into a 65 L Teflon bag; then an air stream of 1 L min⁻¹ is passed through the Teflon bag to introduce N₂O₅ into the chamber over a 7 h period. We refer to this as the “slow N₂O₅ injection experiment”; and (4) With N₂O₅ well mixed in the chamber, isoprene is introduced slowly to maximize the reaction between peroxy radicals and nitrate radicals (see Sect. 4.2). This is achieved by first injecting isoprene into a

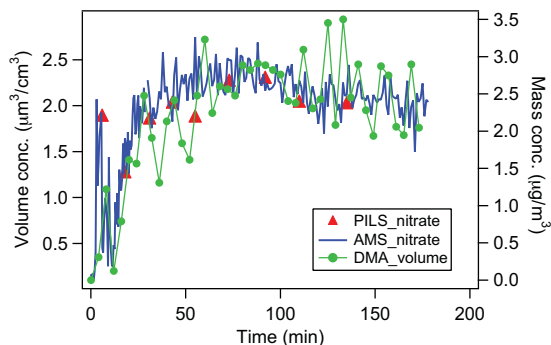


Fig. 1. Time profiles of aerosol volume, inorganic nitrate measured by PILS/IC, and nitrate signals from Q-AMS in a blank experiment (~ 1 ppm N_2O_5 , ammonium sulfate seed, no isoprene).

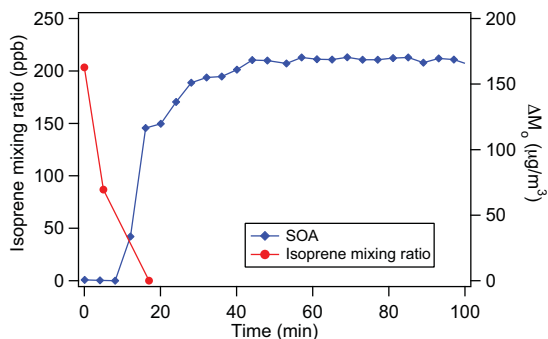


Fig. 2. Reaction profile of the oxidation of an initial mixture containing 203.4 ppb isoprene ($573 \mu\text{g}/\text{m}^3$).

65 L Teflon bag, and then introduced into the chamber with an air stream of 1 L min^{-1} for 7 h. We refer to this as the “slow isoprene injection experiment”.

Experimental conditions and results are given in Table 1. In calculating SOA yield (defined as the ratio of the organic aerosol mass formed to the mass of parent hydrocarbon reacted), knowledge of the SOA density is required. By comparing volume distributions from the DMA and mass distributions from the Q-AMS, the effective density for the SOA formed can be estimated (Bahreini et al., 2005; Alfarrá et al., 2006).

3 Results

3.1 Blank experiments

Blank experiments are performed to ensure that the aerosol growth observed is from the reaction of isoprene with NO_3 radicals. In these experiments, ~ 1 ppm N_2O_5 is introduced

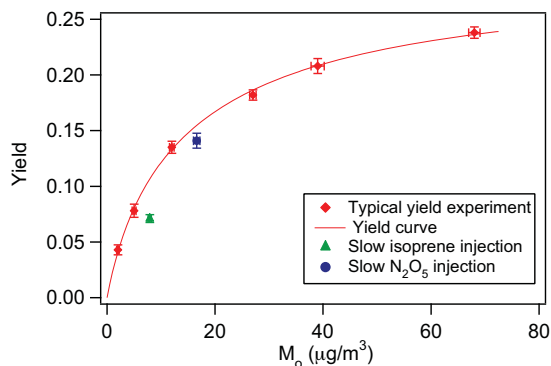


Fig. 3. SOA yield data and yield curve for isoprene- NO_3 reaction. Also shown are SOA yields from the slow N_2O_5 injection experiment and slow isoprene injection experiment.

into chamber after the addition of ammonium sulfate seed aerosol (with no isoprene present). As shown in Fig. 1, aerosol volume increases by $\sim 2 \mu\text{m}^3 \text{ cm}^{-3}$ within an hour after the introduction of N_2O_5 . About $2.5 \mu\text{g m}^{-3}$ of inorganic nitrate is measured by PILS/IC, which agrees well with the amount of nitrates detected by Q-AMS. FTIR analysis indicates the presence of $\sim 10\%$ HNO_3 and 4% NO_2 impurity in the N_2O_5 prepared, thus the nitrates measured by PILS/IC and Q-AMS likely arise from the partitioning or reactive uptake of gas-phase HNO_3 into the aerosol phase, or HNO_3 produced from heterogeneous hydrolysis of N_2O_5 . As in the Q-AMS analysis, no organic species are detected in the filter samples collected from these blank experiments.

3.2 Aerosol yields

A series of experiments with different initial isoprene concentrations are carried out (these are referred to as “typical yield experiments” hereafter). The initial isoprene concentration ranged from 18.4 to 203.4 ppb. Figure 2 shows the reaction profile of the oxidation of an initial mixture containing 203.4 ppb isoprene. Since the chamber is NO_x -free at the beginning of the experiment, once N_2O_5 is introduced into the chamber the equilibrium in Reaction (3) favors the formation of NO_3 . This generates a relatively high concentration of NO_3 radicals and results in rapid isoprene decay. Aerosol growth is observed and aerosol volume continues to increase even after all the isoprene is consumed. Owing to the rapid isoprene decay and the relatively long time between each GC measurement (12 min), the isoprene decay over time is captured only in experiments in which the initial isoprene concentration is > 100 ppb. Based on the observed isoprene decay in these experiments and the isoprene- NO_3 rate constant k_{NO_3} , the average NO_3 concentration in the chamber is estimated to be ~ 140 ppt.

Table 1. Initial conditions and results for yield experiments.

Date	T (K)	RH (%)	ΔHC (ppb) ^a	ΔM_o ($\mu\text{g}/\text{m}^3$) ^b	SOA Yield (%)
8/9/07	294	5.1	101.6 \pm 0.6	68.1 \pm 1.1	23.8 \pm 0.5
8/10/07	293	4.7	30.2 \pm 0.1	11.5 \pm 0.4	13.5 \pm 0.5
8/11/07	294	5.4	67.1 \pm 0.1	39.3 \pm 1.2	20.8 \pm 0.7
8/12/07	293	6.0	51.7 \pm 0.2	26.7 \pm 0.6	18.2 \pm 0.5
8/13/07	294	5.7	18.4 \pm 0.1	2.2 \pm 0.2	4.3 \pm 0.5
8/14/07	294	5.5	21.8 \pm 0.1	4.8 \pm 0.4	7.8 \pm 0.6
10/4/2007 ^c	293	5.5	39.5 \pm 0.1 ^d	7.9 \pm 0.3	7.1 \pm 0.6
10/25/2007 ^e	294	6.4	42.0 \pm 0.1	16.6 \pm 0.6	14.1 \pm 0.7

^a Stated uncertainties (1σ) are from scatter in isoprene measurements.

^b Stated uncertainties (1σ) are from scatter in particle volume measurements.

^c Slow isoprene injection experiment.

^d Concentration estimated based on a separate calibration experiment (see Sect. 3.2); the uncertainty in the measured isoprene concentration is assumed to be the same as in the slow N₂O₅ injection experiment.

^e Slow N₂O₅ injection experiment.

The SOA yield of each experiment (Table 1) is shown in Fig. 3. The density of the SOA is determined to be 1.42 g cm⁻³. The amount of inorganic nitrate detected by PILS/IC in each experiment ranges from 1.6 to 2.6 $\mu\text{g m}^{-3}$, which is approximately equal to that measured in the blank experiments. In calculating SOA yield, the organic aerosol mass is corrected for the amount of inorganic nitrate measured in each experiment. For convenience, SOA yields can be parameterized by a semi-empirical model based on absorptive gas-particle partitioning of two semivolatile products (Odum et al., 1996, 1997a,b):

$$Y = \Delta M_o \left[\frac{\alpha_1 K_{om,1}}{1 + K_{om,1} M_o} + \frac{\alpha_2 K_{om,2}}{1 + K_{om,2} M_o} \right] \quad (4)$$

in which Y is the aerosol yield, ΔM_o is the organic aerosol mass produced, M_o is the organic aerosol mass present (equal to ΔM_o in chamber experiments with no absorbing organic mass present initially), α_i is the mass-based gas-phase stoichiometric fraction for semivolatile species i , and $K_{om,i}$ is the gas-particle partitioning coefficient for species i . With this two-product model, Eq. (4) is fit to the experimental yield data (data with $\Delta M_o < 100 \mu\text{g m}^{-3}$) and the yield parameters obtained are: $\alpha_1=0.089$, $\alpha_2=0.203$, $K_{om,1}=0.182 \text{ m}^3 \mu\text{g}^{-1}$, and $K_{om,2}=0.046 \text{ m}^3 \mu\text{g}^{-1}$. For an organic aerosol mass of $\sim 10 \mu\text{g m}^{-3}$, the aerosol yield is $\sim 10\%$.

Also shown in Fig. 3 are aerosol yields from the slow isoprene/N₂O₅ injection experiments. Since the PILS/IC is not employed in these experiments, in calculating SOA yields it is assumed that the amount of inorganic nitrate formed in these slow injection experiments is roughly the same as that in other experiments. For the slow isoprene injection experiment, no isoprene is observed by GC-FID, indicating that once the isoprene enters the chamber, it is quickly consumed by reaction with NO₃. The time profile of isoprene

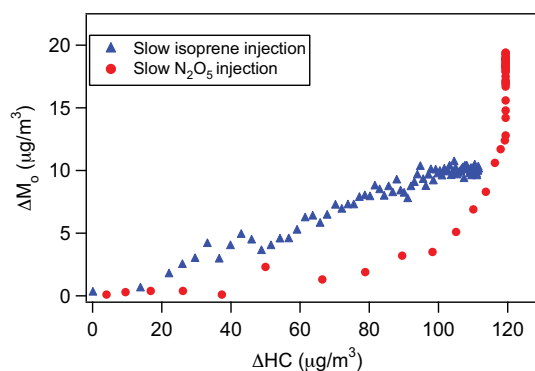


Fig. 4. Time-dependent growth curves for the slow N₂O₅ injection experiment and slow isoprene injection experiment (last two experiments in Table 1).

injection is obtained in a separate experiment, in which the same amount of isoprene is added into the chamber without N₂O₅ present. Assuming the amount of isoprene injected into the chamber is the same as the isoprene reacted, the amount of isoprene reacted over the course of the slow isoprene experiment can be deduced. As seen in Fig. 3, the SOA yield from the slow N₂O₅ injection experiment is roughly the same as those in the other yield experiments; the yield from the slow isoprene injection experiment, however, is lower.

The time-dependent “growth curves” (organic aerosol, ΔM_o , as a function of hydrocarbon reacted, ΔHC) over the course of the slow N₂O₅ injection experiment and the slow isoprene injection experiment are shown in Fig. 4. As hydrocarbon measurements are made with a lower frequency than particle volume, the isoprene concentrations shown are obtained by interpolating GC-FID measurements. In both

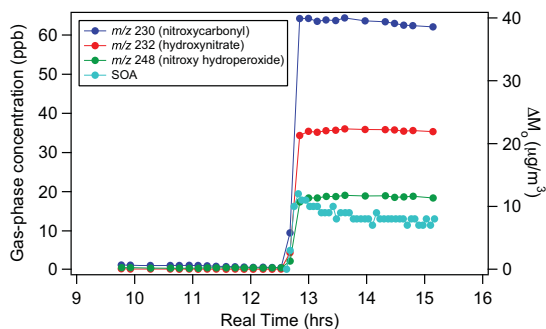


Fig. 5. Time profiles of the major gas-phase products (m/z 230, 232, and 248) and the corresponding aerosol growth from the excess isoprene experiment.

experiments about 40 ppb of isoprene is consumed, the only difference being the order of isoprene/ N_2O_5 injection. From Fig. 4 it is clear that as the reaction proceeds, more aerosol is formed in the slow isoprene injection experiment for the same amount of isoprene reacted. However, the final SOA yield under the slow N_2O_5 injection conditions is higher due to continued aerosol formation even after the complete consumption of isoprene. The presence of a “hook” at the end of the growth curve for the slow N_2O_5 injection experiment indicates that further reactions are contributing to aerosol growth after isoprene is consumed (Ng et al., 2006). Higher generation products also contribute to the aerosols formed in the slow isoprene injection experiment; however, their contributions are not readily observed in the growth curve owing to the way the experiment is conducted. This is further discussed in Sect. 4.3.

3.3 Gas-phase measurements

The CIMS technique measures the concentrations of different gas-phase products over the course of the experiments. A series of experiments is carried out to study the mechanisms of SOA formation by varying the relative amount of isoprene and N_2O_5 injected and monitoring the time evolution of the intermediate products. Shown in Fig. 5 are the time profiles of three major gas-phase products and the corresponding aerosol growth from the excess isoprene experiment. In this experiment, ~ 120 ppb of N_2O_5 is first injected into the chamber, followed by the introduction of ~ 800 ppb isoprene. The initial concentration of isoprene is estimated based on the volume of the isoprene injected and the chamber volume. Once isoprene is injected, a number of product ions are formed immediately, with m/z 230, 232, and 248 being the most dominant ones. Several minor product ions at m/z 185, 377, and 393 are also observed (not shown). With the presence of excess isoprene, it is expected that the three major products detected are first-generation products.

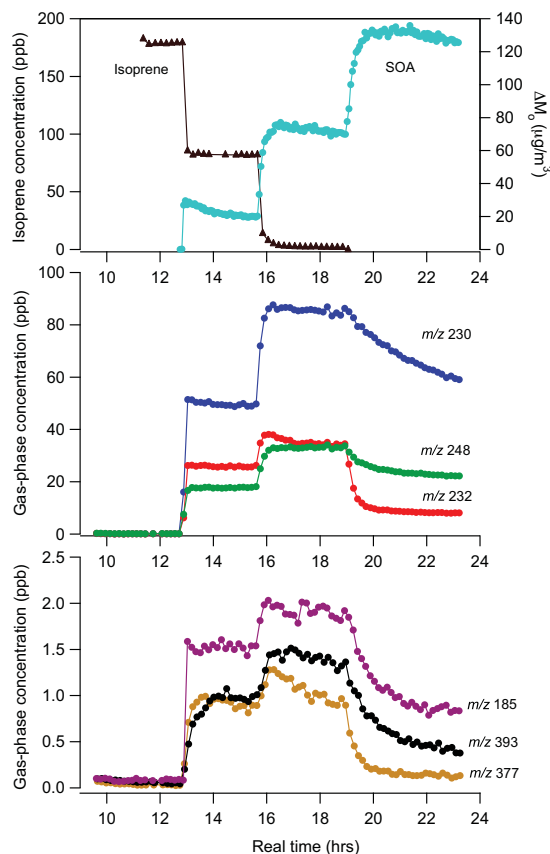


Fig. 6. Time evolution of various gas-phase products in the staggered N_2O_5 injection experiment (Isoprene is first injected into the chamber, followed by the addition of 3 pulses of N_2O_5 : ~ 120 , 50, and 210 ppb). The top panel shows the isoprene decay and aerosol formation; the middle panel shows the time profiles of the three major first-generation products (m/z 230, 232, and 248); the bottom panel shows the time profiles of three minor products (m/z 185, 377, and 393). (The likely identities for these products are shown in Fig. 11).

Their further reaction is suppressed, as indicated by the relatively constant concentrations of the product ions once they are formed. At the end of the experiment, 725 ppb of isoprene is measured by GC-FID. A small amount of aerosol is formed instantaneously, likely from the condensation of relatively nonvolatile first-generation products, or from further generation products that are formed at a relatively rapid rate.

To study further the evolution of the gas-phase products, an experiment is performed in which pulses of N_2O_5 are introduced into the chamber (with isoprene present) (Fig. 6). The top panel shows the isoprene decay and aerosol formation; the middle panel shows the time profiles of the three major first-generation products (m/z 230, 232, and 248); the

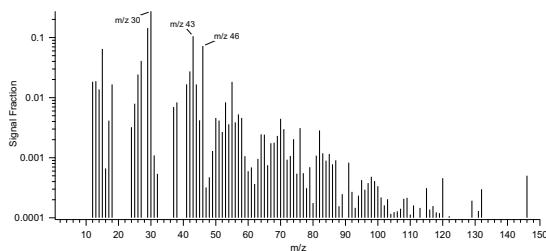


Fig. 7. A typical AMS spectrum for SOA formed in typical yield experiments.

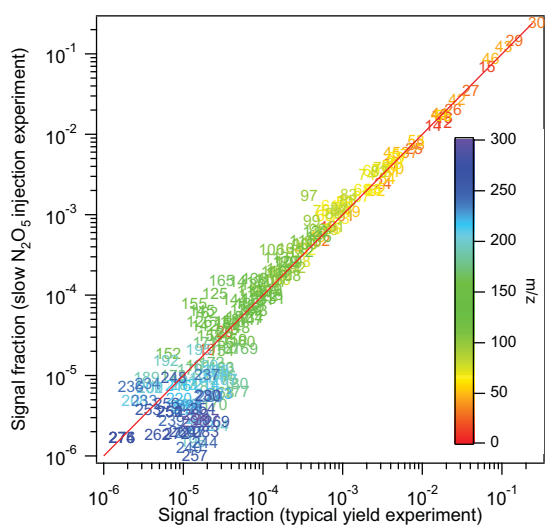


Fig. 8. AMS spectra signal from the slow N₂O₅ injection experiment versus a typical yield experiment. Each mass fragment is normalized by the total signal. The solid red line is the 1:1 line. Note that the higher masses ($m/z > 165$) are dominated by noise.

bottom panel shows the time profiles of three minor products (m/z 185, 377, and 393). In this experiment, 179 ppb of isoprene is first injected into the chamber, followed by the addition of 3 pulses of N₂O₅ (~120, 50, 210 ppb). The observations after the addition of the first pulse of N₂O₅ are similar to the excess isoprene experiment described above. With the addition of ~120 ppb N₂O₅, 97 ppb of isoprene is reacted away, m/z 230, 232, and 248 are formed with concentrations of 49.8 ppb, 26.1 ppb, and 17.3 ppb, respectively. Because of the lack of authentic standards, the concentrations are uncertain. Similar to the data in Fig. 5, the concentrations of these product ions stay relatively constant owing to the presence of excess isoprene. The minor products at m/z 185, 377, and 393, are formed with the concentrations 1.4 ppb, 0.9 ppb, and 0.9 ppb, respectively. Because the sum of the ion concentra-

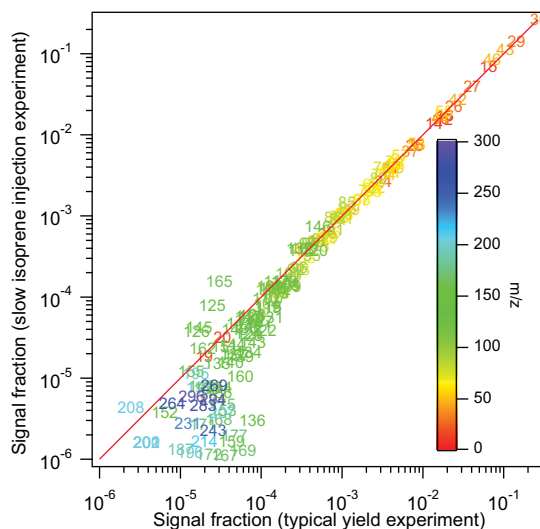


Fig. 9. AMS spectra signal from the slow isoprene injection experiment versus a typical yield experiment. Each mass fragment is normalized by the total signal. The solid red line is the 1:1 line. Note that the higher masses ($m/z > 165$) are dominated by noise.

tions derived from our estimated sensitivities is equal to the reacted isoprene, our estimated sensitivity must represent a lower limit for the actual sensitivity of the CIMS technique to these compounds. It is noted that the m/z 393 ion is formed with a relatively slower rate than all other product ions. A small amount of aerosol is observed. At $t=15:40$, a second pulse of N₂O₅ (~50 ppb) is introduced into the chamber and the remaining 82 ppb isoprene is completely consumed. As seen from Fig. 6, the concentrations of all intermediate products increase accordingly and more aerosol is produced. The last pulse of N₂O₅ (~210 ppb) is added at $t=19:00$. Since all isoprene has been consumed, the additional NO₃ radicals react mainly with the first-generation products, as indicated by the decay of m/z 230, 232, and 248, 185, 377, and 393 ions. Of all of the observed products, it appears that m/z 232 and 377 ions are the most reactive with NO₃ radicals, and their decays in excess NO₃ are strongly correlated with aerosol growth. The rest of the product ions display relatively slower decay kinetics. The decay of the major product ion at m/z 230 does not appear to correlate with aerosol growth, as the concentration of the m/z 230 ion continues to decrease throughout the experiment but there is no further aerosol growth. Since the CIMS instrument has only 0.5 AMU resolution and it cannot distinguish products of similar or identical molecular weight, it is likely that many of observed ions comprise isomers formed from the NO₃ attack at different positions. The fact that many of the observed product ions show two distinct decay time scales indicates that these isomers have substantially different reactivity towards NO₃ radicals.

3.4 Chemical composition of SOA

3.4.1 Aerosol Mass Spectrometer (Q-AMS) measurements

Figure 7 shows the AMS spectrum of SOA formed in the typical yield experiments. Each mass fragment is normalized by the total signal. The SOA exhibits relatively high signals at m/z 30, 43, and 46. The signals at m/z 30 and 46 likely correspond to NO^+ (30) and NO_2^+ (46) fragments from the nitrates in the aerosol. The spectrum shown in Fig. 7 is obtained when aerosol volume reaches its maximum value; the spectrum obtained several hours after aerosol volume peaks shows minimal changes in the mass fractions of different fragments, indicating that the aerosol composition is not changing significantly over time.

Figure 8 shows the mass spectrum of the slow N_2O_5 injection experiment versus a typical yield experiment; Fig. 9 shows the mass spectrum of the slow isoprene injection experiment versus a typical yield experiment. As shown in both figures, the mass fragments fall on the 1:1 line, suggesting a similar SOA composition under the three different experimental conditions. At higher mass to charge ratios the plots drift below the one-to-one line and it appears that the typical experiments have stronger signals at higher m/z 's. However, the signals at these masses (>165) are strongly dominated by noise and cannot be interpreted as differences between the spectra.

3.4.2 Offline chemical analysis

Figure 10 shows the representative UPLC/(–)ESI-TOFMS base peak ion chromatograms (BPCs) for different types of experiments conducted. The numbers denoted above the selected chromatographic peaks correspond to the most abundant negative ions observed in their respective mass spectra. Comparison of the BPCs shown in Fig. 10 indicates that the compositions of the SOA are quite similar for the typical yield experiment, slow isoprene injection experiment, and the acid seed experiment, suggesting a common SOA formation pathway. The SOA composition from the excess isoprene experiment, however, is different from these experiments. This will be discussed further in Sect. 4.4.

Accurate mass measurements for all ions observed by the UPLC/(–)ESI-TOFMS technique for a typical yield experiment are listed in Table 2. The error between the measured mass and theoretical mass is reported in two different ways, ppm and mDa. Overall, the error between the measured and theoretical masses is found to be less than ± 2 mDa and ± 5 ppm, allowing for generally unambiguous identification of molecular formulae. None of the listed ions is observed in solvent blanks and control filters. By combining the elemental SOA composition (i.e. TOFMS suggested ion formula) data and the gas-phase data from CIMS, structures for each of the SOA components are also proposed. As shown in Table 2, the types of compounds formed included

nitrooxy-organic acids, hydroxynitrates, nitrooxy-organic peroxides (e.g. nitrooxy-hydroxyperoxides), and nitrooxy-organosulfates. It should be noted that the data presented in Table 2 are also applicable to all other types of experiments conducted in this study; however, none of the organosulfates are observed in the nucleation experiments, consistent with previous work (Liggio et al., 2005; Liggio et al., 2006; Surratt et al., 2007a,b; Iinuma et al., 2007a,b). Surprisingly, previously characterized organosulfates of the 2-methyltetrols and the 2-methyltetrol mono-nitrates detected at m/z 215 and m/z 260 (not listed in Table 2), respectively, which are produced from the photooxidation of isoprene in the presence of acidified sulfate seed aerosol (Surratt et al., 2007a,b; Gómez-González et al., 2007), are also observed in the acid seed experiment shown in Fig. 10, suggesting that nighttime oxidation of isoprene in the presence of acidic seed may also be a viable pathway for these known ambient tracer compounds.

Owing to the implementation of reverse-phase chromatography, the SOA components that are more hydrophilic elute from the column the earliest, while the more hydrophobic components elute the latest. It is clear from Table 2 that compounds with the same carbon number and general functionality (i.e. carboxylic acid, alcohol, or organosulfate), but differing number of nitrooxy groups, exhibit distinctly different chromatographic behaviors. The presence of more nitrooxy groups appears to increase the retention time of the SOA compound. For example, it is found that m/z 194 organic acid compound ($\text{C}_5\text{H}_8\text{NO}_7^-$) containing one nitrooxy group elutes earlier than that of the m/z 239 organic acid compounds ($\text{C}_5\text{H}_7\text{N}_2\text{O}_9^-$) containing two nitrooxy groups. Similarly, the m/z 305 organosulfate ($\text{C}_5\text{H}_9\text{N}_2\text{O}_{11}\text{S}^-$) elutes earlier than that of the m/z 349 organosulfate ($\text{C}_5\text{H}_8\text{N}_3\text{O}_{13}\text{S}^-$).

SOA components that are either nitrooxy-organic acids or nitrooxy-organosulfates are detected strongly as the $[\text{M}-\text{H}]^-$ ion, consistent with previous work (Surratt et al., 2006; Surratt et al., 2007a,b; Gao et al., 2004a,b; Gao et al., 2006), whereas the hydroxynitrates and nitrooxy-hydroxyperoxides are detected as both the $[\text{M}-\text{H}]^-$ and $[\text{M}-\text{H} + \text{C}_2\text{H}_4\text{O}_2]^-$ ions, with the latter acetic acid adduct ion, in most cases, being the base peak ion (i.e. dominant ion). The acetic acid adduct ions for the hydroxynitrates and the nitrooxy-hydroxyperoxides are formed owing to the presence of acetic acid in the UPLC mobile phase. Previous studies have shown that non-acidic hydroxylated species (such as the 2-methyltetrols) and organic peroxides formed from the photooxidation of isoprene (Claeys et al., 2004; Edney et al., 2005; Surratt et al., 2006) are either undetectable or yield weak negative ions when using (–)ESI-MS techniques. However, it appears that the co-presence of nitrooxy groups in the hydroxylated SOA components allow for these compounds to become acidic enough to be detected by the UPLC/(–)ESI-TOFMS technique, or allow for adduction with acetic acid. Further confirmation for the presence of organic peroxides in the isoprene SOA produced from NO_3 oxidation is provided by the iodometric-spectroscopic measurements shown

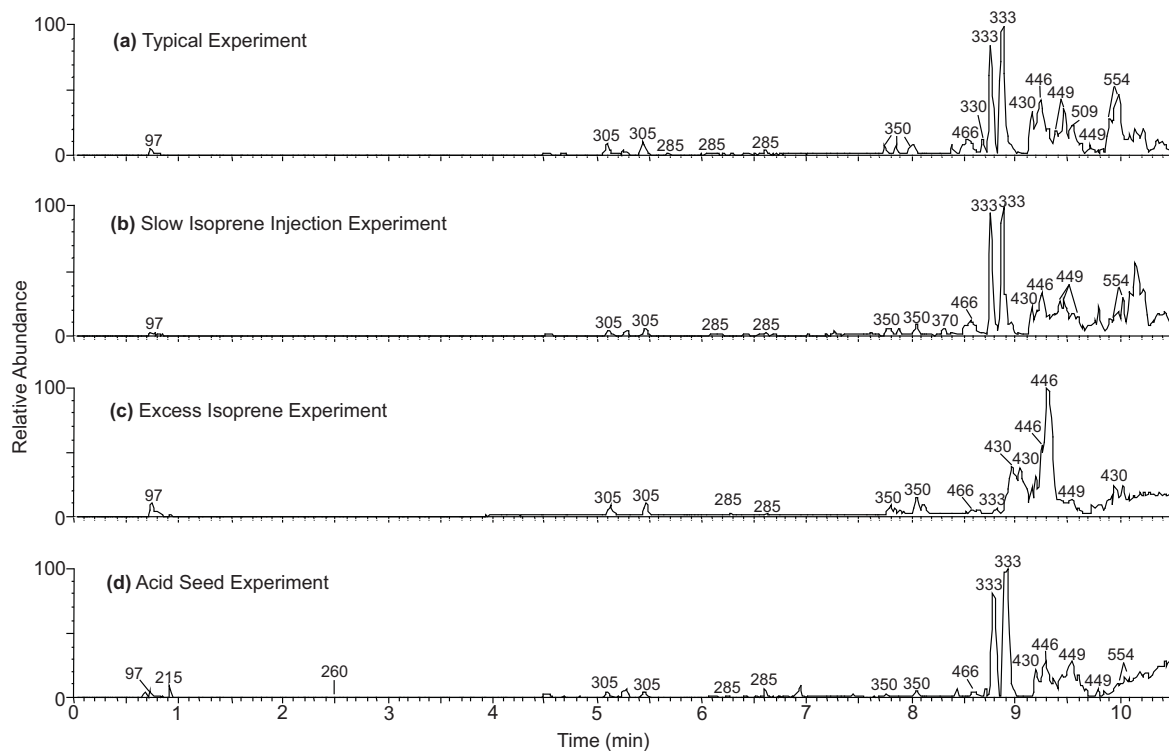


Fig. 10. UPLC/(-)ESI-TOFMS base peak ion chromatograms (BPCs) for the following isoprene-NO₃ oxidation experiments: (a) 200 ppb isoprene+1 ppm N₂O₅+seed aerosol generated from 15 mM (NH₄)₂SO₄ atomizing solution; (b) 300 ppb isoprene+1 ppm N₂O₅+seed aerosol generated from 15 mM (NH₄)₂SO₄ atomizing solution; (c) 1.2 ppm isoprene+700 ppb N₂O₅+seed aerosol generated from 15 mM (NH₄)₂SO₄ atomizing solution; (d) 200 ppb isoprene+1 ppm N₂O₅+seed aerosol generated from 30 mM MgSO₄+50 mM H₂SO₄ atomizing solution. The numbers indicated above the selected chromatographic peaks correspond to the most abundant negative ion, which is either the [M-H]⁻ or [M-H+C₂H₄O₂]⁻ ion.

in Table 3. Based upon the UPLC/(-)ESI-TOFMS measurements shown in Table 2, an average molecular weight of 433 for the organic peroxides is assumed for the calculations shown in Table 3. The contribution of organic peroxides to the SOA mass concentration is found to be fairly reproducible for duplicate typical experiments (i.e., 8/22/07 and 10/24/07). The amount of organic peroxides in the excess isoprene experiment is below detection limits. Owing to the lack of authentic standards, there are large uncertainties associated with the quantification of these products in the aerosol phase. This is further discussed in Sect. 4.4.

4 Gas-phase chemistry and SOA formation

4.1 Formation of various gas-phase products

As seen from Figs. 5 and 6, the three major first-generation products formed from isoprene-NO₃ reaction are the *m/z* 230, 232, and 248 ions. Since the CIMS technique uses

CF₃O⁻ (anionic mass 85 Da) as the reagent ion, compounds are detected at a *m/z* value of their molecular weight (MW) plus 85. The product ions at *m/z* 230, 232, and 248 likely correspond to C₅-nitrooxycarbonyl (MW 145), C₅-hydroxynitrate (MW 147), and C₅-nitrooxyhydroperoxide (MW 163). These products have been observed in previous studies (Jay and Stieglitz, 1989; Skov et al., 1992; Kwok et al., 1996; Berndt and Böge, 1997) and their formation from the isoprene-NO₃ reaction is relatively straightforward (Fig. 11). The reaction proceeds by NO₃ addition to the C=C double bond, forming four possible nitrooxyalkyl radicals depending the position of the NO₃ attack. Previous studies suggest that NO₃ radicals predominantly attack isoprene in the 1-position, with a branching ratio (C₁-position/C₄-position) varying between 3.5 and 7.4 (Skov et al., 1992; Berndt and Boge, 1997; Suh et al., 2001). As mentioned before, the average branching ratio (5.5:1) is used in estimating the sensitivities of the compounds measured by CIMS. In Fig. 11, only the nitrooxyalkyl radical formed from the C1

Table 2. SOA products identified using UPLC/(–)ESI-TOFMS.

Retention Time (min)	Measured [M–H] [–] Ion (<i>m/z</i>)	TOFMS Suggested [M–H] [–] Ion Formula	Error (mDa, ppm)	Measured [M–H+C ₂ H ₄ O ₂] [–] Ion (<i>m/z</i>)	TOFMS Suggested [M–H+C ₂ H ₄ O ₂] [–] Ion Formula	Error (mDa, ppm)	Proposed Structure ^a
3.68 ^b	194.0310	C ₅ H ₈ NO ₇ [–]	0.9, 4.6	^c			
4.52 ^b	239.0137	C ₅ H ₇ N ₂ O ₉ [–]	–1.5, –6.3				
5.09 ^d	304.9946	C ₅ H ₉ N ₂ O ₁₁ S [–]	1.9, 6.2				
5.24 ^b	239.0152	C ₅ H ₇ N ₂ O ₉ [–]	0.0, 0.0				
5.43 ^d	304.9944	C ₅ H ₉ N ₂ O ₁₁ S [–]	1.7, 5.6				
6.07	225.0350	C ₅ H ₉ N ₂ O ₈ [–]	–0.9, –4.0				
6.12	225.0342	C ₅ H ₉ N ₂ O ₈ [–]	–1.7, –7.6				
6.60	225.0375	C ₅ H ₉ N ₂ O ₈ [–]	1.6, 7.1	285.0676	C ₇ H ₁₃ N ₂ O ₁₀ [–]	0.6, 2.1	
7.75 ^d	349.9775	C ₅ H ₈ N ₃ O ₁₃ S [–]	–0.3, –0.9				
7.85 ^d	349.9764	C ₅ H ₈ N ₃ O ₁₃ S [–]	0.2, 0.6				
8.00 ^d	349.9784	C ₅ H ₈ N ₃ O ₁₃ S [–]	–0.4, –1.1				
8.48 ^d	466.0268	C ₁₀ H ₁₆ N ₃ O ₁₆ S [–]	1.7, 3.6				
8.54 ^d	466.0264	C ₁₀ H ₁₆ N ₃ O ₁₆ S [–]	1.3, 2.8				
8.72 ^d	466.0237	C ₁₀ H ₁₆ N ₃ O ₁₆ S [–]	–1.4, –3.0				
8.76 ^e	270.0199	C ₅ H ₈ N ₃ O ₁₀ [–]	–1.1, –4.1	330.0393	C ₇ H ₁₂ N ₃ O ₁₂ [–]	–2.8, –8.5	
8.81 ^d	466.0237	C ₁₀ H ₁₆ N ₃ O ₁₆ S [–]	–1.4, –3.0				
8.85 ^e	270.0204	C ₅ H ₈ N ₃ O ₁₀ [–]	–0.6, –2.2	330.0379	C ₇ H ₁₂ N ₃ O ₁₂ [–]	–4.2, –12.7	
9.15	370.0734	C ₁₀ H ₁₆ N ₃ O ₁₂ [–]	0.9, 2.4	430.0940	C ₁₂ H ₂₀ N ₃ O ₁₄ [–]	–0.5, –1.2	
9.19	386.0678	C ₁₀ H ₁₆ N ₃ O ₁₃ [–]	–0.5, –1.3	446.0888	C ₁₂ H ₂₀ N ₃ O ₁₅ [–]	–0.6, –1.3	
9.24	370.0732	C ₁₀ H ₁₆ N ₃ O ₁₂ [–]	–0.2, –0.5	430.0937	C ₁₂ H ₂₀ N ₃ O ₁₄ [–]	–0.8, –1.9	
9.25	386.0683	C ₁₀ H ₁₆ N ₃ O ₁₃ [–]	–0.2, –0.5	446.0893	C ₁₂ H ₂₀ N ₃ O ₁₅ [–]	–0.1, –0.2	
9.37	449.0637	C ₁₀ H ₁₇ N ₄ O ₁₆ [–]	–0.3, –0.7	509.0854	C ₁₂ H ₂₁ N ₄ O ₁₈ [–]	0.3, 0.6	
9.41	386.0684	C ₁₀ H ₁₆ N ₃ O ₁₃ [–]	0.1, 0.3	446.0903	C ₁₂ H ₂₀ N ₃ O ₁₅ [–]	0.9, 2.0	
9.45	449.0653	C ₁₀ H ₁₇ N ₄ O ₁₆ [–]	1.3, 2.9	509.0853	C ₁₂ H ₂₁ N ₄ O ₁₈ [–]	0.2, 0.4	
9.90 ^f	494.0537	C ₁₀ H ₁₆ N ₅ O ₁₈ [–]	4.7, 9.5	554.0669	C ₁₂ H ₂₀ N ₅ O ₂₀ [–]	–3.3, –6.0	
9.98 ^f	494.0518	C ₁₀ H ₁₆ N ₅ O ₁₈ [–]	2.8, 5.7	554.0676	C ₁₂ H ₂₀ N ₅ O ₂₀ [–]	–2.6, –4.7	

^a Structural isomers containing nitrate, sulfate, or hydroxyl groups at other positions are likely; for simplicity, only one isomer is shown.

^b These compounds appear to be very minor SOA products due to very small chromatographic peak areas, confirming that the further oxidation of the nitrooxycarbonyl and hydroxycarbonyl first-generation gas-phase products do not yield significant quantities of SOA.

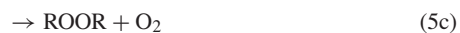
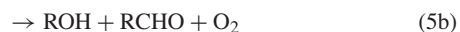
^c A blank cell indicates that the detected SOA product had no observable acetic acid adduct ion (i.e. [M–H+C₂H₄O₂][–]).

^d These organosulfate SOA products were observed only in experiments employing either (NH₄)₂SO₄ (i.e. neutral) or MgSO₄ + H₂SO₄ (i.e. acidic) seed aerosol. These organosulfate SOA products were also observed in the excess isoprene experiments.

^e In addition to the acetic acid adduct ion, these compounds also had a significant adduct ion at [M–H+HNO₃][–] (*m/z* 333), indicating that these compounds are likely not very stable due to the fragmentation of one of the NO₃ groups during the MS analysis.

^f These compounds were only weakly detected in the excess isoprene experiments.

attack is shown. The nitrooxyalkyl radicals then react with O₂ to form RO₂ radicals, which react further with HO₂, RO₂, or NO₃ radicals under the experimental conditions in this study. The reaction of RO₂ radicals and HO₂ radicals leads to the formation of C₅-nitrooxyhydroperoxide (*m/z* 248). The reaction of two RO₂ radicals (self reaction or cross reaction) has three different possible channels:



The second channel results in the formation of C₅-nitrooxycarbonyl (*m/z* 230) and C₅-hydroxynitrate (*m/z* 232). According to channel (5b), these two products should be formed with a 1:1 ratio; however, C₅-nitrooxycarbonyl can also be formed from alkoxy radicals (alkoxy radicals formed through RO₂+RO₂ reaction or RO₂+NO₃ reaction). In Fig. 6, 49.8 ppb of C₅-nitrooxycarbonyl and 26.1 ppb of C₅-hydroxynitrate are formed after the addition of the first pulse of N₂O₅, indicating ~24 ppb of C₅-nitrooxycarbonyl is formed from the reaction of alkoxy radicals. The branching ratios for the reaction of small peroxy radicals have been investigated in previous studies. It is found that the branching ratio for channel (5a) for methylperoxy and ethylperoxy radicals is ~0.3–0.4 and ~0.6, respectively (Lightfoot et al., 1992; Wallington et al., 1992; Tyndall et al., 1998). It is

Table 3. Peroxide content of SOA formed by NO₃ oxidation of isoprene.

Experiment Date	Seeded ^a / Nucleation	[Isoprene] (ppb)	[N ₂ O ₅] (ppm)	SOA Volume Growth Observed ^b (μm ³ /cm ³)	Total SOA Mass Concentration ^c (μg/m ³)	Peroxide Aerosol Mass Concentration (μg/m ³)	Contribution of Peroxides to the SOA Mass Concentration Observed (%)
8/22/07	AS	200	1	102	145	46	32
8/30/07	AMS	200	1	123	174	40	23
10/22/07 ^d	AS	1200	0.7	70	100	b.d.l. ^e	f
10/23/07	nucleation	200	1	125	177	31	17
10/24/07	AS	200	1	111	158	47	30
10/27/07 ^g	AS	300	1	110	156	47	30

^a AS=ammonium sulfate seed, AMS=acidified magnesium sulfate seed.

^b Averaged over the course of filter sampling.

^c Assuming a SOA density of 1.42 g/cm³. This was based on DMA and Q-AMS measurements.

^d Excess isoprene experiment.

^e Below detection limits.

^f No observable contribution of organic peroxides to the SOA mass concentration.

^g Slow injection of isoprene in this experiment to enhance the RO₂+NO₃ reaction pathway.

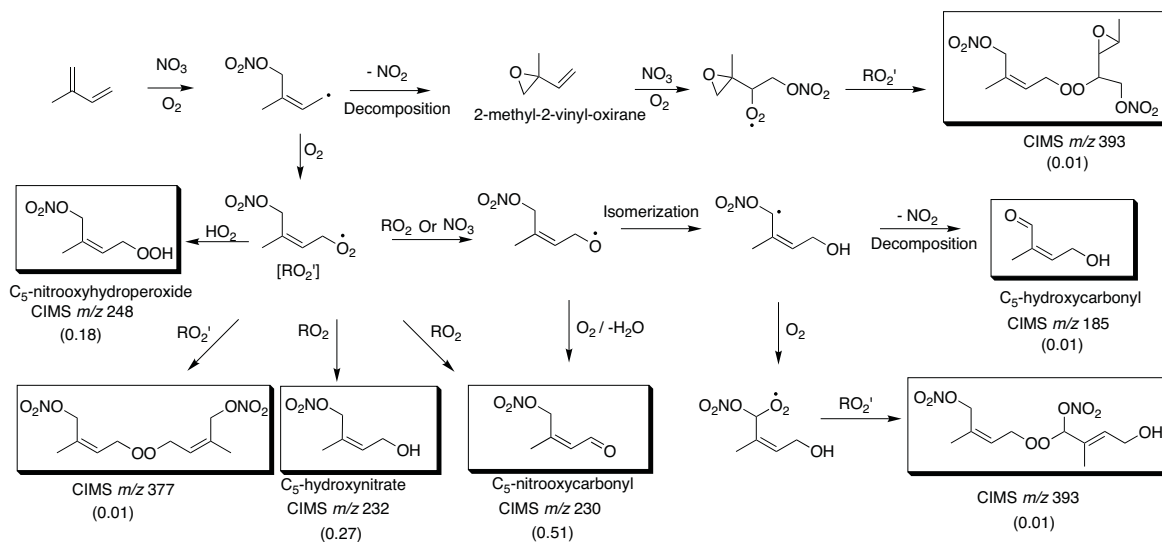


Fig. 11. Proposed mechanisms for the formation of various gas-phase intermediate product ions observed by CIMS. Multiple structural isomers are possible. In this figure, RO₂' refers to the isoprene peroxy radical (nitrooxyperoxy radical), RO₂ refer to a generic peroxy radical. The numbers in the parentheses refer to the molar yields of the products. It is noted that the sensitivity for *m/z* 393 is not calculated; instead, it is assumed that the sensitivity (and hence the sum of the molar yields of the two isomers shown, since *m/z* 377 and *m/z* 393 are formed with the same concentration) to be the same as that for *m/z* 377.

likely that the isoprene peroxy radicals react via this pathway to form alkoxy radicals and contribute to the "extra" 24 ppb of C₅-nitrooxycarbonyl. This observation is indicative that most RO₂ radicals react with other RO₂ radicals instead with NO₃ or HO₂ radicals.

Other than C₅-nitrooxycarbonyl, C₅-hydroxynitrate, and C₅-nitrooxyhydroperoxide, three other minor products (*m/z* 185, 377 and 393 ions) are also observed as intermediate products. The proposed mechanisms for the formation of

these gas-phase products are also shown in Fig. 11. Although channel (5c) in the RO₂+RO₂ reaction is found to be minor for small peroxy radicals such as methylperoxy and ethylperoxy radicals (Kan et al., 1980; Niki et al., 1981, 1982; Wallington et al., 1989; Tyndall et al., 1998; Tyndall et al., 2001), the product ion at *m/z* 377 could be the corresponding ROOR product formed from the self reaction of isoprene peroxy radicals. The product ion at *m/z* 185 likely corresponds to the C₅-hydroxycarbonyl. It has been observed

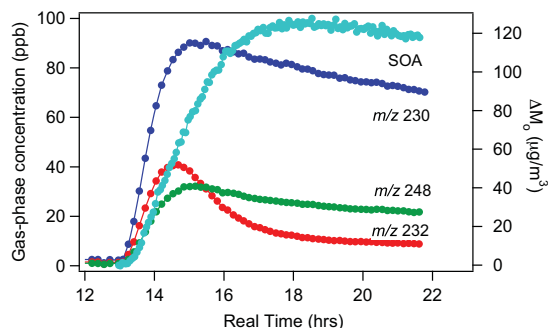


Fig. 12. Time profiles of the major gas-phase products (m/z 230, 232, and 248) and the corresponding aerosol growth from the slow N_2O_5 injection experiment. Note that this experiment has a higher initial isoprene concentration (~ 200 ppb) compared to the one shown in Fig. 4.

in previous studies and it likely arises from the isomerization of nitroxyalkoxy radicals through a 6-member transition state to form a hydroxynitroxy alkyl radical, which then decomposes to form NO_2 and C_5 -hydroxycarbonyl (Kwok et al., 1996). Such isomerization has also been proposed to occur in the photooxidation of isoprene (Paulson and Seinfeld, 1992; Carter and Atkinson, 1996; Dibble, 2002). It is possible that the hydroxynitroxy alkyl radical formed proceeds to react with O_2 to form a peroxy radical, which then reacts with the isoprene peroxy radical to form the product ion at m/z 393. The product ion at m/z 393 shows a slower rate of formation (Fig. 6) compared to other product ions suggesting that it might also be formed from the further oxidation of a first-generation product. 2-methyl-2-vinyl-oxirane has been observed from isoprene- NO_3 reaction in previous studies at 20 mbar in helium (Berndt and Böge, 1997) and 20 Torr in argon (Skov et al., 1994), respectively. When operated in positive mode with H_3O^+ as the reagent ion (products are observed at $m/z = MW + 1$), CIMS shows a protonated molecule at m/z 85. Although the epoxide yield is found to be $< 1\%$ of the total reacted isoprene at atmospheric pressure (Skov et al., 1994), the signal at m/z 85 can arise in part from the epoxide. The further oxidation of the epoxide results in the formation of an epoxide peroxy radical, which can react with the isoprene peroxy radical to form the peroxide at m/z 393. It is noted that a product ion at m/z 246 is detected in CIMS, which could arise from the corresponding carbonyl product formed from the reactions of two epoxide peroxy radicals, or from the fragmentation of the epoxide alkoxy radicals. Unlike m/z 393, which decays after the addition of the last pulse of N_2O_5 , m/z 246 stays relatively constant suggesting that it is not being further oxidized by NO_3 radicals. To examine further the possibility of peroxide formation (m/z 377 and 393) in the gas phase, an experiment is conducted using 1,3-butadiene as the parent hydrocarbon. The analogous

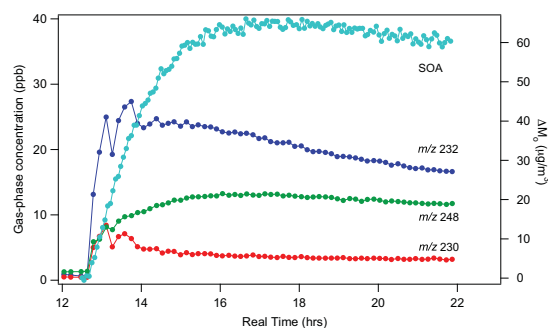


Fig. 13. Time profiles of the major gas-phase products (m/z 230, 232, and 248) and the corresponding aerosol growth from the slow isoprene injection experiment. Note that this experiment has a higher initial isoprene concentration (~ 200 ppb) compared to the one shown in Fig. 4.

product ions for the 1,3-butadiene system, i.e. m/z 349 and 365, are observed in CIMS, providing further indication that the formation of ROOR products from two RO_2 radicals is occurring in the gas phase. Further details of the gas-phase chemistry of isoprene and 1,3-butadiene will be forthcoming in a future manuscript.

4.2 Effect of peroxy radical chemistry on SOA yield

The SOA yield ranges from 4.3% to 23.8% for an initial isoprene concentration of 18.4 to 101.6 ppb in the typical yield experiments. While the SOA yield from the slow N_2O_5 injection experiment is roughly the same as that in the typical yield experiments, the SOA yield from the slow isoprene injection experiment is lower (Fig. 3). In both cases, ~ 40 ppb of isoprene is consumed, the main difference being the relative importance of $RO_2 + RO_2$ reaction versus $RO_2 + NO_3$ reaction in each system. In the slow N_2O_5 injection experiment, a relatively small amount of NO_3 is available in the chamber. Once RO_2 radicals are formed, it is expected that they would react primarily with other RO_2 radicals instead of NO_3 radicals owing to the presence of a relatively higher isoprene concentration in the chamber. On the other hand, the slow isoprene injection experiment favors $RO_2 + NO_3$ reaction owing to the presence of excess N_2O_5 in the chamber. Thus the higher SOA yield observed in the slow N_2O_5 injection experiment suggests the products formed via $RO_2 + RO_2$ reaction partition more readily into the aerosol phase, or the $RO_2 + RO_2$ reaction forms products that further react and contribute significantly to aerosol growth. The fact that the SOA yield from the slow N_2O_5 injection experiment is roughly the same as in the typical yield experiments implies that $RO_2 + RO_2$ reaction dominates in typical yield experiments.

The time profile for the three major first-generation gas phase products and SOA growth from the slow N_2O_5 injection experiment and slow isoprene injection experiment are

shown in Figs. 12 and 13, respectively. It is noted that this pair of experiments has a higher initial isoprene concentration (~200 ppb) compared to the pair of experiments shown in Fig. 4. In both cases, once the first-generation products are formed they can react further with NO₃ radicals, making it difficult to estimate the formation yields of these products based on the measured concentrations. The extent to which these products react further is expected to be higher in the slow isoprene injection experiment owing to the presence of excess NO₃ in chamber; this is consistent with the relatively lower concentrations of first-generation products observed. As mentioned before, it is possible that the CIMS signal at the observed *m/z* comprises isomers formed from the NO₃ attack at positions other than the C1 carbon. Such isomers have slightly different structures but they could exhibit a very different reaction rate towards NO₃ radicals. For instance, studies have shown that the reaction rates of NO₃ radicals with unsaturated alcohols and unsaturated carbonyl compounds can vary by several orders of magnitude depending on the position of the substituted methyl group (Noda et al., 2002; Canosa-Mas et al., 2005). It is possible that the minor products formed from NO₃ attack at other positions react much slower with NO₃ radicals, hence the concentrations of the observed product ions do not decay to zero towards the end of the experiment. At the end of the experiment, about 8 ppb and 3 ppb of C₅-hydroxynitrate is left in the slow N₂O₅ injection experiment and slow isoprene injection experiment, respectively. Assuming the amount of reactive isomers and unreactive (or relatively slow reacting) isomers are formed in the same ratio in the slow N₂O₅ injection experiment and the slow isoprene injection experiment, we can deduce that a relatively higher concentration of reactive C₅-hydroxynitrate (as well as the two other first-generation products) is formed in the slow N₂O₅ injection experiment. This is consistent with the larger extent of RO₂+RO₂ reaction (which forms C₅-hydroxynitrate) and the higher SOA yield observed in the slow N₂O₅ injection experiment, as it appears that C₅-hydroxynitrate is an effective SOA precursor (Fig. 6).

4.3 Growth curves: multiple steps in SOA formation

By examining the time-dependent growth curves (organic aerosol, ΔM_o , as a function of hydrocarbon reacted, $\Delta H C$) we can gain insights into the general mechanisms of SOA formation (Ng et al., 2006, 2007a,b). Figure 4 shows the time-dependent growth curves for the slow N₂O₅ injection experiment and the slow isoprene injection experiment, respectively. For the slow N₂O₅ injection experiment, the initial aerosol growth likely arises from the condensation of first-generation products as the presence of excess isoprene in the chamber suppresses their further oxidation. If higher generation products do contribute to SOA formation, they would have to be formed at relatively fast rates. After isoprene is consumed, aerosol mass continue to increase and results in a “hook” in the growth curve. This indicates that

secondary products (or higher generation products) also contribute significantly to SOA formation. The same observation can be made if we examine the reaction profile of a typical yield experiment (Fig. 2): there is further SOA growth after all isoprene is reacted away, indicating that the further oxidation of first generation products are contributing to SOA formed. These observations are consistent with the fact that the decay of first-generation products observed in CIMS (especially the *m/z* 232 and *m/z* 377 ions) is strongly anticorrelated with further SOA growth (Fig. 6). On the other hand, the slow isoprene injection experiment does not allow us to differentiate the contribution of first- and second-generation products to SOA formation. With the presence of excess NO₃ radicals in the chamber, the first-generation products formed in the slow isoprene injection experiment would be further oxidized once they are formed. The SOA growth observed throughout this experiment is from the partitioning of these highly oxidized and nonvolatile products. Hence, at the beginning of the experiment, for the same amount of $\Delta H C$, the amount of SOA formed in this experiment is higher than that in the slow N₂O₅ injection experiment, in which the aerosol growth is probably from the condensation of relatively more volatile first-generation products. Both the AMS data and filter sample data (Figs. 8, 9, and 10) show a very similar composition for the final SOA formed in slow N₂O₅ injection experiment and the slow isoprene injection experiment, suggesting a common SOA forming channel. Based on the previous discussion on the effect of peroxy radical chemistry on SOA yields, it is likely that the RO₂+RO₂ reaction is the SOA-forming channel in both cases; such a reaction occurs to a large extent in the slow N₂O₅ injection experiments and results in the formation of more SOA.

4.4 Proposed mechanisms of SOA formation

The combination of CIMS gas-phase data and elemental SOA composition data provides substantial insights into the mechanisms of SOA formation. Shown in Figs. 14–17 are the proposed SOA formation mechanisms from the further oxidation of the various gas-phase products measured by CIMS. The compounds in the boxes are the SOA products detected by UPLC/(–)ESI-TOFMS. Owing to multiple chromatographic peaks observed in the UPLC/(–)ESI-TOFMS extracted ion chromatograms (EICs) for the negative ions of the proposed SOA products, structural isomers are likely; however, for simplicity we show only one possible isomer for each product formed from a particular reaction pathway. Many of the SOA products detected are formed from the further oxidation of first- or higher-generation products, which is consistent with the observation of continual SOA growth after the complete consumption of isoprene (hence a “hook” in the growth curve). With the large number of nitrate-substituted compounds detected by UPLC/(–)ESI-TOFMS technique, it is also not surprising that AMS shows strong signals at *m/z* 30 (NO⁺) and *m/z* 46 (NO₂⁺).

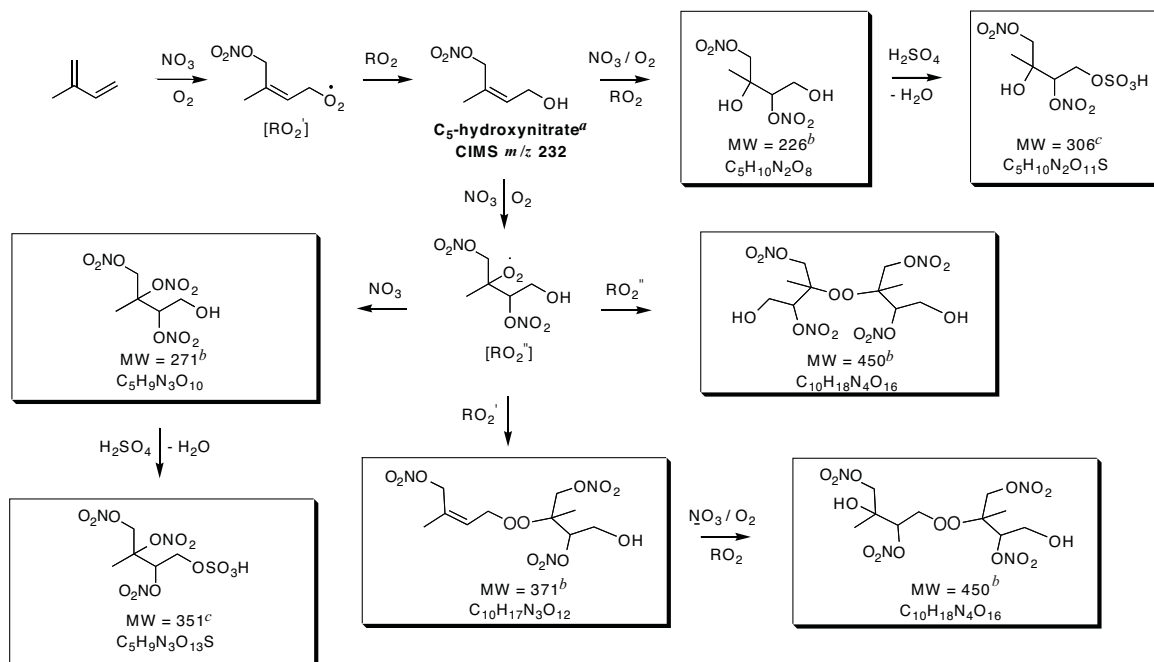


Fig. 14. Proposed mechanism for SOA formation from the formation and decay of the C₅-hydroxynitrate gas-phase product formed from the isoprene + NO₃ reaction. Boxes indicate UPLC/(–)ESI-TOFMS detected SOA products; molecular formulas were confirmed by the accurate mass data provided by the UPLC/(–)ESI-TOFMS. Multiple structural isomers are possible, consistent with the multiple chromatographic peaks observed in the extracted ion chromatograms; however, only one structural isomer is shown for simplicity. ^a This first-generation gas-phase product was previously observed by Jay and Stieglitz (1989), Skov et al. (1992), Kwok et al. (1996), and Berndt and Böge (1997); this gas-phase product was detected as the [M+CF₃O][–] ion by the CIMS instrument. ^b These particle-phase compounds were detected as both their [M–H][–] and [M–H+C₂H₄O₂][–] ions; the acetic acid adduct ([M–H+C₂H₄O₂][–]) ion was, in most cases, the molecular ion (i.e. dominant ion). ^c These organosulfate compounds were detected as their [M–H][–] ions and were observed only in ammonium sulfate and acidified magnesium sulfate seeded experiments.

Shown in Figs. 14 and 15 are the proposed SOA formation pathways from the further oxidation of the *m/z* 232 (i.e. C₅-hydroxynitrate) and 377 gas-phase product ions (as detected by CIMS). The decay of these two products has been found to be strongly correlated with aerosol growth (Fig. 6), which is consistent with the large number of SOA products formed from their further oxidation. The further oxidation of these two gas-phase products also yields SOA compounds of the same molecular weight (compounds of MW 371 and 450). Although *m/z* 393 is a minor gas-phase product, the further oxidation of this compound leads to formation of several SOA products (Fig. 16). As mentioned before, there are two possible formation routes for *m/z* 393, and the further oxidation of both products is shown in Fig. 16. The further oxidation of the *m/z* 393 ion appears to yield SOA products that are specific only to this gas-phase product: these include the SOA products of MW 387 and 467.

Figure 17 shows the proposed SOA formation mechanisms from three other gas-phase products (*m/z* 185, *m/z* 230, and *m/z* 277); the further oxidation of these product ions leads to relatively minor SOA products. Although C₅-nitrooxycarbonyl (*m/z* 230) is the most abundant gas-phase product detected by CIMS, its further oxidation is not well correlated with aerosol growth (Fig. 6). The further oxidation of *m/z* 230 yields an SOA product at MW 240. This organic acid product is found to be quite minor when examining the peak area in its corresponding extracted ion chromatogram (EIC). It is noted that no SOA products are detected from the further oxidation of the C₅-nitrooxyhydroperoxide (*m/z* 248) (also a major gas-phase product); it is possible that these hydroperoxide products are not acidic enough to be detected by the UPLC/(–)ESI-TOFMS technique, or degrade during sample workup and/or analysis procedures. It has been shown that hydroxycarbonyl

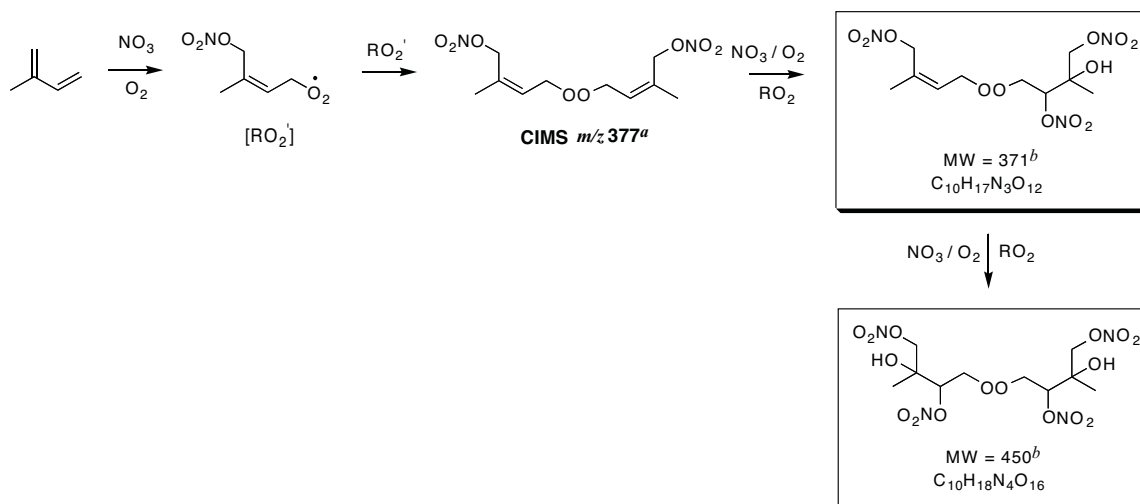


Fig. 15. Proposed mechanism for SOA formation from the formation and decay of the CIMS *m/z* 377 gas-phase product formed from the isoprene+NO₃ reaction. Boxes indicate UPLC/(–)ESI-TOFMS detected SOA products; molecular formulas were confirmed by the accurate mass data provided by the UPLC/(–)ESI-TOFMS. Multiple structural isomers are possible, consistent with the multiple chromatographic peaks observed in the extracted ion chromatograms; however, only one structural isomer is shown for simplicity. ^a This first-generation gas-phase product was detected as the [M + CF₃O][–] ion by the CIMS instrument. ^b These particle-phase compounds were detected as both their [M–H][–] and [M–H+C₂H₄O₂][–] ions; the acetic acid adduct ([M–H+C₂H₄O₂][–]) ion was, in most cases, the molecular ion (i.e. dominant ion).

plays a key role in SOA formation from the reaction of linear alkenes with NO₃ radicals (Gong et al., 2005), however, in the isoprene-NO₃ system, the further oxidation of the minor gas-phase product C₅-hydroxycarbonyl (*m/z* 185) leads to the formation of only one minor aerosol product at MW 195. Some evidence for the formation of a C₅-dinitrate first-generation gas-phase product is indicated from the CIMS and UPLC/(–)ESI-TOFMS data. This first-generation gas-phase product has been observed previously by Werner et al. (1997). The CIMS shows a weak signal at *m/z* 277, which could be associated to the dinitrate product; we do not know, however, whether the negative ion efficiently clusters with such compounds. Further evidence for the dinitrate gas-phase product is provided by the UPLC/(–)ESI-TOFMS detection of an SOA product at MW 495, which could result from the further oxidation of a C₅-dinitrate precursor. The precursor compound before the last oxidation step shown in this mechanism in Fig. 17 may exist in the particle phase; however, this compound is not likely to be detected by the UPLC/(–)ESI-TOFMS technique owing to the lack of acidic hydrogens from neighboring hydroxyl and/or carboxyl groups.

The SOA products highlighted in Figs. 14–17 are observed in all major experiments conducted; however, not all of these products are strongly detected in the excess isoprene experiment (Fig. 10c). With the presence of excess isoprene, further oxidations of first-generation products should be minimal and no significant SOA formation is expected. The reaction rate of isoprene and NO₃ radicals is $k_{\text{NO}_3} = 7 \times 10^{-13} \text{ cm}^3 \text{ molecule}^{-1} \text{ s}^{-1}$. To our knowledge, the reaction rate of the first-generation products and NO₃ radicals has not been studied. The structure of *m/z* 232 (C₅-hydroxynitrate) is similar to 3-methyl-2-buten-1-ol (MBO321), except that the γ -carbon has one nitro group and one methyl group substitution instead of two methyl group substitutions. The reaction rate coefficient of MBO321 and NO₃ radicals is $k_{\text{NO}_3} = 1 \times 10^{-12} \text{ cm}^3 \text{ molecule}^{-1} \text{ s}^{-1}$. It is found that the reaction rate with NO₃ radicals increases with increasing number of methyl groups at the γ -carbon (Noda et al., 2002), which is in accordance with the stabilization theory for leaving groups discussed in Atkinson (1997) and Noda et al. (2000). With reference to this, we would expect the reaction rate of C₅-hydroxynitrate and NO₃ radicals to be slower than that of MBO321 due to the presence of the electron withdrawing nitro group. Hence, it is likely that the reaction rate of isoprene and NO₃ radicals and C₅-hydroxynitrate and NO₃ radicals are roughly in the same range. The relative production rate of first- and second-generation products will then be the ratio of the

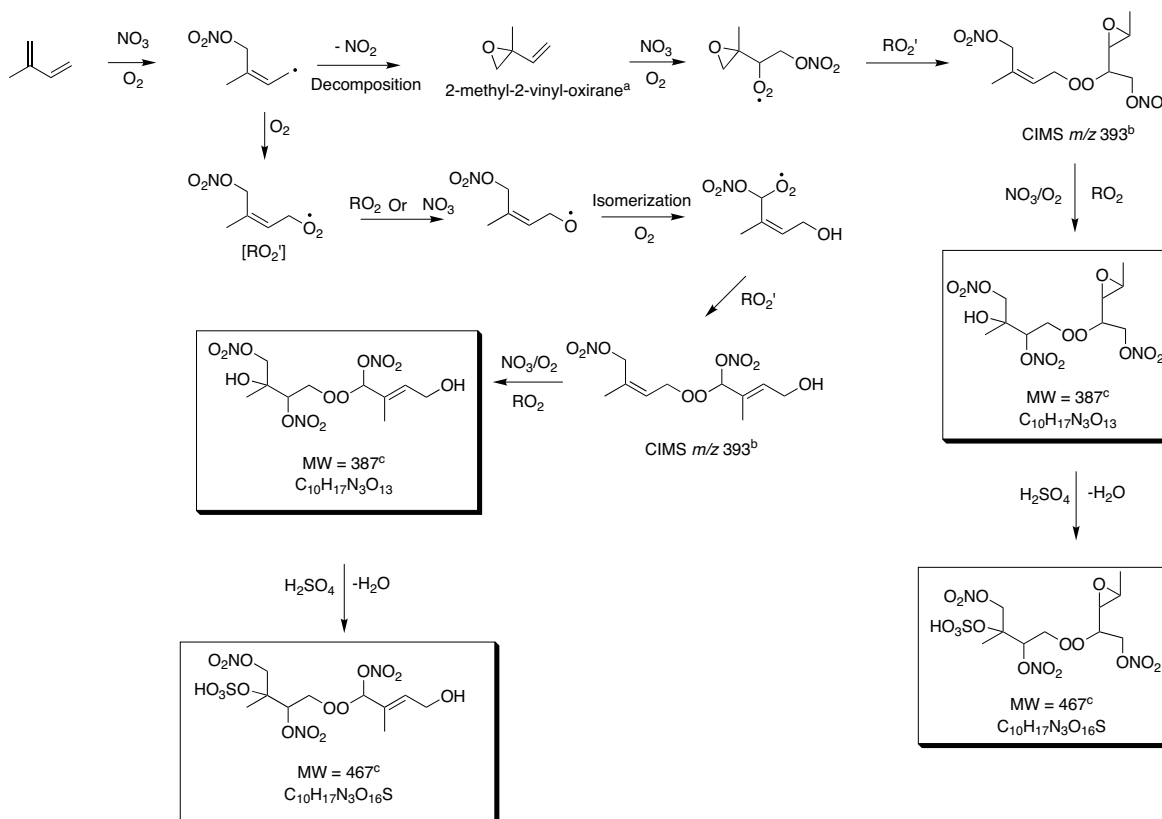


Fig. 16. Proposed mechanism for SOA formation and decay of the CIMS *m/z* 393 gas-phase product formed from the isoprene+NO₃ reaction. Boxes indicate UPLC/(–)ESI-TOFMS detected SOA products; molecular formulas were confirmed by the accurate mass data provided by the UPLC/(–)ESI-TOFMS. Multiple structural isomers are possible, consistent with the multiple chromatographic peaks observed in the extracted ion chromatograms; however, only one structural isomer is shown for simplicity. ^a This first-generation gas-phase product was detected as the [M+H]⁺ ion by the CIMS instrument; this gas-phase product was previously observed by Berndt and Böge (1997) and could also be 2-(1-methyl-vinyl)oxirane. ^b This gas-phase product was detected as the [M+CF₃O][–] ion. ^c These particle-phase compounds were detected as both their [M–H][–] and [M–H+C₂H₄O₂][–] ions; the acetic acid adduct ([M–H+C₂H₄O₂][–]) ion was, in most cases, the molecular ion (i.e. dominant ion). ^d This organosulfate compound was detected as its [M–H][–] ion and was observed only in the ammonium sulfate and acidified magnesium sulfate seeded experiments.

concentrations of isoprene and first-generation products, and aerosol can be formed either from the condensation of relatively non-volatile first-generation products (e.g. *m/z* 393) or higher generation products that are formed relatively fast in the gas-phase. It appears from the UPLC/(–)ESI-TOFMS data that enough RO₂+RO₂ chemistry is occurring to yield many of the products shown in Figs. 14–17. When comparing the UPLC/(–)ESI-TOFMS BPCs (Fig. 10) of all experiments, it is clear that the *m/z* 430 and *m/z* 446 are the dominant ions in the excess isoprene experiment, while *m/z* 333 is the dominant chromatographic peak in other experiments. The chromatographic peak at *m/z* 430 corresponds to the acetic acid cluster ion for the compound at MW 371, which can be formed from the further oxidation of CIMS *m/z* 232

and 377 ions (Figs. 14 and 15). The chromatographic peak at *m/z* 446 corresponds to the acetic acid cluster ion for the compound at MW 387, which is formed from the further oxidation of CIMS *m/z* 393 (Fig. 16). The detection of these two SOA products (MW 371 and MW 387) suggests that further oxidation of *m/z* 232, 377, and 393 is occurring in the excess isoprene experiment and contributing to SOA growth. Studies have shown that NO₃ uptake on organic surfaces (even to saturated organic surfaces) be quite rapid (Moise et al., 2002; Knopf et al., 2006; Rudich et al., 2007). Hence, it is also possible that CIMS *m/z* 393 (a first-generation product according to one of the formation routes) is nonvolatile enough that it partitions into the aerosol phase and its further oxidation proceeds heterogeneously. Chromatographic peaks

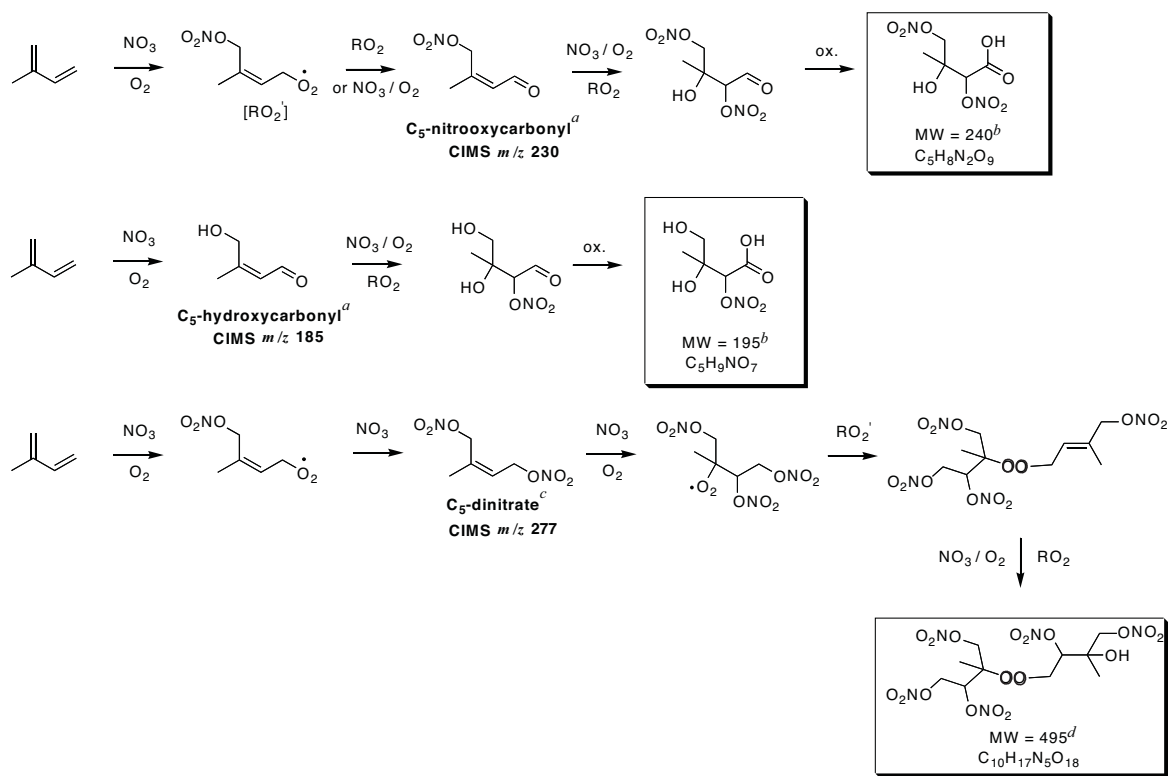


Fig. 17. Proposed mechanism for SOA formation from the formation and decay of the C₅-nitrooxycarbonyl, C₅-hydroxycarbonyl, and C₅-dinitrate first-generation products formed from the isoprene+NO₃ reaction. Boxes indicate UPLC/(–)ESI-TOFMS detected SOA products; molecular formulas were confirmed by the accurate mass data provided by the UPLC/(–)ESI-TOFMS. Multiple structural isomers are possible, consistent with the multiple chromatographic peaks observed in the extracted ion chromatograms; however, only one structural isomer is shown for simplicity. ^a These first-generation gas-phase products were previously observed by Skov et al. (1994) and Kwok et al. (1996); these gas-phase products were detected as the [M+CF₃O][–] ion by the CIMS instrument. ^b These are minor SOA products, confirming that the further oxidation of the C₅-nitrooxycarbonyl and C₅-hydroxycarbonyl first-generation products do not yield significant amounts of SOA. ^c This first-generation gas-phase product was previously observed by Werner et al. (1999); this gas-phase product was also detected as the [M+CF₃O][–] ion by the CIMS instrument. ^d This particle-phase compound was detected as both its [M–H][–] and [M–H+C₂H₄O₂][–] ions; the acetic acid adduct ([M–H+C₂H₄O₂][–]) ion was the molecular ion (i.e. dominant ion).

such as *m/z* 333 (associated with MW 271 compound), 449 (MW 450 compound) and 554 (MW 495 compound) are not as strong in the excess isoprene experiment owing to the fact there is not enough NO₃ in the system to allow for the formation of these highly oxidized compounds.

From the UPLC/(–)ESI-TOFMS (Table 2) and PILS/IC measurements, it appears that organic acids are not a major contributor to SOA formation from the oxidation of isoprene by NO₃ radicals. The UPLC/(–)ESI-TOFMS technique detects only two minor organic acids at MW 195 and 240. Additionally, the PILS/IC technique does not detect large quantities of any small organic acids. The sum of formate, acetate, glycolate, lactate, oxalate, and pyruvate are usually be-

tween 0.01–0.50 μg m^{–3}. These observations are different from the SOA produced in the photooxidation of isoprene (under high- and low-NO_x conditions), in which a large number of organic acids, such as 2-methylglyceric, formic, and acetic acid, are observed (Surratt et al., 2006; Szmigielski et al., 2007). In the photooxidation experiments, the level of organic acids detected under low-NO_x conditions is lower than under high-NO_x conditions. The low-NO_x isoprene SOA was previously found to also have a significant amount of organic peroxides, as detected in the current study (Table 3); however, organic peroxides detected previously in low-NO_x isoprene SOA were not structurally elucidated through MS techniques performed in the present study (Table 2, Figs. 14–

17), possibly owing to the lack of nitrooxy groups which seem to induce acidity and/or increase the adductive abilities of organic peroxides with acetic acid during the ESI-MS analysis. Overall, it appears that the isoprene-NO₃ SOA is much more similar to the previously studied low-NO_x isoprene SOA. More specifically, it appears that both contain a large amount of organic peroxides, organosulfates (if conducted in the presence of sulfate seed aerosol), and neutral hydroxylated compounds, such as the hydroxynitrates observed in Fig. 14 (e.g. MW 226 and 271 products).

As discussed earlier, the formation yields of ROOR from the reaction of two peroxy radicals is very low for small peroxy radicals (Kan et al., 1980; Niki et al., 1981, 1982; Wallington et al., 1989; Tyndall et al., 1998, 2001). However, according to both gas-phase and aerosol-phase data in this study, it appears that the RO₂+RO₂ reaction (self reaction or cross-reaction) in the gas phase yielding ROOR products is an important SOA formation pathway. Such reaction has been proposed to form low-volatility diacyl peroxides in the SOA formed from cyclohexene ozonolysis (Ziemann, 2002). In the case of self-reaction of peroxy radicals, the molecular weight of the product is essentially doubled, providing an efficient way to form products of low volatility. Based on the iodometric spectroscopic method the contributions of peroxides (ROOH+ROOR) to the total SOA formed is 17–32% (Table 3). We can estimate the mass yield of peroxides based on their percentage contribution to total SOA and the SOA yield for each of the experiments in Table 3. It is found that the mass yield of peroxides range from ~6–10%. For the two experiments (i.e., 8/22/07 and 10/24/07) that are carried out under similar conditions as those in the yield experiments, the mass yield of peroxide is 8%.

Based on the shape of the Odum yield curve (Fig. 3), it is expected that the products are semivolatile. Hence, the relatively large contribution of nonvolatile peroxides in the aerosol phase appears to be inconsistent with the observed yield curve behavior. It is evident from the UPLC/(–)ESI-TOFMS data that there exists a wide array of peroxides in the aerosol composition, however, we need to caution that there are large uncertainties associated with the quantification of peroxides owing to the lack of authentic standards. Based on the standard deviations of the measurements, the uncertainty is at least 10%, yet if we take into account the following factors it is expected that the true uncertainty would be larger. In estimating the percentage contribution of peroxides, an average molecular weight of 433 for peroxides is used. The peroxides formed would largely depend on the branching ratio of various reactions and this number may not reflect the molecular weights of the wide array of peroxides formed. Also, the iodometric spectroscopic method does not allow the distinction between ROOH and ROOR products. Hence, the contribution of the low volatility ROOR products may not be as high as estimated. ROOH standards were run in the ESI-TOFMS to examine the possibility of ROOH further reacting in the mass spectrometer to form ROOR and no ROOR

products were detected. As mentioned before, it appears that the presence of nitrooxy groups in ROOR products aids their detection in the MS. Since the ROOH standards used do not have a nitrooxy group, unfortunately we cannot rule out the possibility that ROOR products are formed but just not being detected. Finally, it is worth noting that the initial isoprene concentrations in the yield experiments are much lower than those experiments in which SOA composition is measured. In performing the yield experiments, the initial isoprene concentrations are kept relatively low so as to be closer to atmospheric levels. Because of the lower initial isoprene concentration (hence lower aerosol loading), the partitioning of various products would be different and it is likely that level of peroxides would be lower in the yield experiments. Nevertheless, the higher concentration experiments are necessary to produce enough aerosols for filter analysis and to map out the complete spectrum of oxidation products.

To fully elucidate the relationship between the actual products identified and those inferred from fitting the yield data would require a modeling study that is beyond the scope of this work. However, we emphasize that there are large uncertainties associated with the quantification of peroxides and it is likely that their contributions to total SOA can be overestimated. Indeed, if the mass yield for these nonvolatile peroxides were lower (for instance, ~2%), this would agree well with the observed yield curve behavior. The measurement of peroxides certainly warrants further study. This work serves as a good example in showing that caution must be taken when interpreting experiments with low aerosol yields, especially when a relatively minor pathway may be responsible for forming the aerosols.

5 Approximate estimate of global production of SOA from isoprene+NO₃

The global chemical transport model GEOS-Chem (v. 7-04-11) (<http://www-as.harvard.edu/chemistry/trop/geos/>) is used to estimate, roughly, global SOA formation from the isoprene+NO₃ reaction. The current version of GEOS-Chem treats mechanistically SOA formation from isoprene+OH, monoterpenes and sesquiterpenes, and aromatics; here we will estimate SOA formation from isoprene+NO₃ by using an approximate, uniform SOA yield of 10% (corresponding to $M_o \cong 10 \mu\text{g m}^{-3}$ in Fig. 3). It is noted that this yield is quite uncertain and the importance of peroxy radical self reactions in this study suggest that the SOA yield in the atmosphere will be highly sensitive to the nature of the nighttime peroxy radical chemistry. Here, we seek to obtain only a “back-of-the-envelope” estimate.

Two global isoprene emissions are available in GEOS-Chem: GEIA (Global Emission Inventory Activity) (Guenther et al., 1995) and MEGAN (Model of Emissions and Gases from Nature) (Guenther et al., 2006). Both models require, as input, meteorological data such as temperature

to calculate the amount isoprene emitted. For the present estimate, the meteorological fields employed by Wu et al. (2007), generated by the Goddard Institute for Space Studies (GISS) General Circulation Model III, are used. Meteorological conditions correspond approximately to those of year 2000.

Table 4 presents the annual emissions of isoprene as predicted by each of the emission models, together with the amount of isoprene predicted to react via OH, O₃, and NO₃, the global burden, and lifetime. We note that there is a significant difference between the annual isoprene emissions predicted by the earlier and newer emission models. Isoprene+OH accounts for 300 to 400 Tg yr⁻¹ of isoprene consumption. Henze et al. (2007) predict that annual SOA production from isoprene+OH is about 13 Tg yr⁻¹ (based on the MEGAN inventory and GEOS-4 meteorological fields, which are assimilated fields from actual year 2004). Note that SOA production from isoprene+OH, or any other pathway for that matter, is sensitive to the production of SOA from other hydrocarbon precursors since gas-aerosol partitioning depends on the total organic aerosol mass.

If we take as a rough estimate a 10% SOA yield from the isoprene+NO₃ pathway from the results in Table 4, 2 to 3 Tg yr⁻¹ of SOA results from isoprene+NO₃. This rate of production would make SOA from isoprene+NO₃ as significant as that from sesquiterpenes, biogenic alcohols, and aromatics, each of which is estimated to produce about 2 to 4 Tg yr⁻¹ of SOA based on yields measured in chamber studies (Henze et al., 2007). As a reference, the global SOA production is estimated to be 10–70 Tg yr⁻¹ (Kanakidou et al., 2005). Recently, Goldstein et al. (2007) provided several alternative approaches to estimate global SOA production: 510–910 Tg C yr⁻¹ based on the global mass balance of VOC removal, 225–575 Tg C yr⁻¹ based on SOA deposition plus oxidation, 140–540 Tg C yr⁻¹ based on comparison with the sulfate budget, and 223–615 Tg C yr⁻¹ required to maintain the assumed global mean vertical SOA distribution. If we assume mass carbon/mass organics=0.5, the lower limit for SOA production from these estimates would be 280 Tg yr⁻¹, which is much larger than that estimated from chamber SOA yields. Still, the 3 Tg yr⁻¹ of SOA estimated for the isoprene + NO₃ system is worth noticing. Owing to efficient photodissociation, NO₃ achieves its highest concentrations at night. By contrast, isoprene emissions are assumed to be zero at night in both emission models. Consequently, the isoprene+NO₃ reaction occurs only at night, involving isoprene that remains unreacted after each daytime period.

We caution that the estimates above are obtained at the crudest level of approximation, in which a globally uniform SOA yield of 10% from isoprene+NO₃ is applied. As we note from Table 4, there is also a substantial difference between predictions of the two available isoprene emission models; the more recent MEGAN model represents an improved level of understanding over the earlier GEIA model. Predictions of SOA formation from the isoprene+NO₃ path-

Table 4. Global estimation of isoprene using GEOS-Chem.

	Emission Model	
	GEIA ^a	MEGAN ^b
Isoprene emission (Tg/y)	507	389
Global isoprene burden (Tg)	1.7	1.7
Isoprene lifetime (days)	1.2	1.6
Isoprene reacted (Tg/y) by		
Isoprene+OH	407	304
Isoprene+O ₃	69	62
Isoprene+NO ₃	29	21

^a Modification of GEIA for GEOS-Chem are described at Bey et al. (2001c). Original GEIA reference is Guenther et al. (1995).

^b Guenther et al. (2006).

way are, of course, highly dependent on ambient NO₃ radical concentrations. Nitrate radical concentrations predicted in the current simulations vary from about 0.1 ppt in remote regions of South America to 20 ppt or more in the southeastern USA (in August). Future work will address the simulation of SOA formation from isoprene+NO₃ following the microphysical treatment in GEOS-Chem.

6 Implications

We report a series of chamber experiments investigating the formation of secondary organic aerosols from the reaction of isoprene with nitrate radicals. For an initial isoprene concentration of 18.4 to 101.6 ppb, the SOA yield ranges from 4.3% to 23.8% (typical yield experiments). The SOA yield from the slow N₂O₅ injection experiment (RO₂+RO₂ reaction dominates) is much higher than that from the slow isoprene injection experiment (RO₂+NO₃ dominates), implying that RO₂+RO₂ is a more effective channel of forming SOA. The SOA yield from the slow N₂O₅ experiment is roughly the same as that in the typical yield experiments, suggesting that SOA yields obtained in this study likely represent conditions in which peroxy-peroxy radical reactions are favored. Using a uniform SOA yield of 10% (corresponding to M_o≅10 μg m⁻³), ~2 to 3 Tg yr⁻¹ of SOA results from isoprene+NO₃, which is about 1/4 of the amount of SOA estimated to be formed from isoprene+OH (~13 Tg yr⁻¹) (Henze et al., 2007).

The extent to which the results from this study can be applied to conditions in the atmosphere depends on the relative importance of the various reaction pathways of peroxy radicals in the nighttime atmosphere: RO₂+RO₂, RO₂+NO₃, RO₂+NO, and RO₂+HO₂. However, the fate of peroxy radicals in the atmosphere is uncertain owing to the large uncertainties in the reaction rate constants and ambient concentrations of the radicals (Skov et al., 1992; Kirchner and Stockwell, 1996; Bey et al., 2001a, b; Vaughan et al., 2006). For

instance, a modeling study by Kirchner and Stockwell (1996) suggests that the RO_2+NO_3 reaction is the dominant pathway at night; 77% and 90% of the total RO_2 at night is predicted to react with NO_3 in polluted atmosphere and rural air (mixed with aged air), respectively. The other pathways are not as important; while RO_2+RO_2 can account for about 8–23% of the total RO_2 reaction, RO_2+HO_2 only accounts for 6–10%, and RO_2+NO is minimal (0–1%) (Kirchner and Stockwell, 1996). These results are at odds with the study by Bey et al. (2001a,b), which suggests that NO_3 radicals are not involved significantly in the propagation of RO_2 radicals (<5%). Instead, RO_2+NO (77%) and RO_2+RO_2 (40%) are dominant in the mixed layer in the urban and rural areas, respectively. Although there is no definite conclusion as which reaction pathway dominates in the nighttime atmosphere, both studies seem to suggest that RO_2+HO_2 is relatively not as important. In this work, we investigated situations in which either RO_2+RO_2 or RO_2+NO_3 dominates. In both cases the RO_2+HO_2 reaction is expected to be a minor channel and thus this is in line with the modeling studies. Although RO_2+NO is not considered in this study, this reaction produces the same alkoxy radical as in the RO_2+NO_3 reaction. It is likely that it would result in similar products as those in the case where the RO_2+NO_3 reaction dominates. Currently, only the reaction rate constants for small, relatively simple RO_2 radicals with NO_3 radicals have been reported (e.g. Biggs et al., 1994; Daele et al., 1995; Canosa-Mas et al., 1996; Vaughan et al., 2006) and they are roughly in the range of $(1-3)\times 10^{-12} \text{ cm}^3 \text{ molecule}^{-1} \text{ s}^{-1}$. With the oxidation of various volatile organic compounds by O_3 and NO_3 under nighttime conditions, it is expected that multifunctional peroxy radicals would be prevalent; the reaction rates of these complex peroxy radicals warrant future study. Furthermore, more field measurements on the concentrations of various radicals would also help to constrain the relative importance of the different reaction pathways.

In this study, we have shown that the formation of ROOR from the reaction of two peroxy radicals is an effective SOA-forming channel based on gas-phase data and elemental SOA composition data. If the results from this study can be applied to other systems (i.e., the reaction of NO_3 radicals with other volatile organic compounds), the organic peroxides could possibly be formed in all systems; they may not have been identified previously owing to the lack of suitable analytical techniques such as accurate mass measurements from high resolution MS. Since the formation of ROOR from two peroxy radicals has always been considered as a minor channel, the reaction has not been widely studied. Ghigo et al. (2003) ruled out the direct formation of products (RO, ROH, RCHO) from the tetroxide intermediate ROOOOR. Instead, they proposed that the tetroxide breaks up into a weakly bound complex of two RO radicals and O_2 , which then fall apart or undergoes intersystem crossing to form the corresponding alcohol and carbonyl products. The formation of ROOR was not discussed in Ghigo et al. (2003)

owing to little experimental evidence for the production of ROOR. However, the observation of ROOR formation in this study suggests that this reaction does occur and is potentially important for aerosol formation. As pointed out by Dibble (2008), the mechanism proposed by Ghigo (2003) would seem to allow for easy production of ROOR from the RO-RO- O_2 complex. Therefore, it appears that there are at least two possible pathways for ROOR formation: it can either be formed through the RO-RO- O_2 complex as suggested by Dibble (2008), or there may exist a direct pathway for ROOR formation from ROO+ROO. Certainly more work is needed regarding the formation, detection, and quantification of ROOR products.

It is also worth noting that while most NO_3 chemistry occurs at night, it can also be important during the day at specific locations. Recently, a study by Fuentes et al. (2007) suggested substantial formation of NO_3 radicals can take place in forested environments with moderate to high levels of BVOC production, resulting in a significant oxidation of isoprene and terpenes by NO_3 radicals. For instance, approximately 60% of the terpenes react with NO_3 radicals within the canopy. Clearly, more study is needed to evaluate the importance of NO_3 chemistry of biogenic hydrocarbons under different environments and time of the day.

Acknowledgements. This research was funded by US Department of Energy Biological and Environmental Research Program DE-FG02-05ER63983. This material is based in part on work supported by the National Science Foundation (NSF) under grant ATM-0432377. The Waters LCT Premier XT time-of-flight mass spectrometer interfaced to a Waters UPLC system was purchased in 2006 with a grant from the National Science Foundation, Chemistry Research Instrumentation and Facilities Program (CHE-0541745). The LCQ Ion Trap mass spectrometer was purchased in 1997 with funds from the National Science Foundation through the CRIF program (CHE-9709233). J. D. Surratt is supported in part by the US EPA under the STAR Graduate Fellowship Program. A. J. Kwan and H. O. T. Pye acknowledge the support of NSF graduate research fellowships. The authors would like to thank C. D. Vecitis, J. Cheng, and M. R. Hoffmann for use of and aid with their ozonizer and UV-VIS spectrometer; to K. Takematsu and M. Okumura for helpful advice on preparing N_2O_5 ; to J. H. Kroll and M. Claeys for helpful discussions and suggestions; to M. N. Chan for assistance with filter sample collection; to H. G. Kjaergaard and F. Paulot for performing the quantum calculations and estimating the sensitivities of CIMS to various gas-phase products; and to Y. Yu and the reviewers for helpful comments on the manuscript.

Edited by: S. Martin

References

- Alfarra, M. R., Paulsen, D., Gysel, M., Garforth, A. A., Dommen, J., Prevot, A. S. H., Worsnop, D. R., Baltensperger, U., and Coe, H.: A mass spectrometric study of secondary organic aerosols formed from the photooxidation of anthropogenic and biogenic precursors in a reaction chamber, *Atmos. Chem. Phys.*, 6, 5279–5293, 2006, <http://www.atmos-chem-phys.net/6/5279/2006/>.
- Bahreini, R., Keywood, M. D., Ng, N. L., Varutbangkul, V., Gao, S., Flagan, R. C., and Seinfeld, J. H.: Measurements of secondary organic aerosol (SOA) from oxidation of cycloalkenes, terpenes, and m-xylene using an Aerodyne aerosol mass spectrometer. *Environ. Sci. Technol.*, 39, 5674–5688, 2005.
- Barnes, I., Bastian, V., Becker, K. H., and Tong, Z.: Kinetics and products of the reactions of NO₃ with monoalkenes, dialkenes, and monoterpenes, *J. Phys. Chem.*, 94, 2413–2419, 1990.
- Berndt, T. and Böge, O.: Gas-Phase reaction of NO₃ radicals with isoprene: A kinetic and mechanistic study, *Inter. J. Chem. Kinet.*, 29, 755–765, 1997.
- Bey, I., Aumont, B., and Toupance, G.: A modeling study of the nighttime radical chemistry in the lower continental troposphere. 1. Development of a detailed chemical mechanism including nighttime chemistry, *J. Geophys. Res.*, 106(D9), 9959–9990, 2001a.
- Bey, I., Aumont, B., and Toupance, G.: A modeling study of the nighttime radical chemistry in the lower continental troposphere. 2. Origin and evolution of HO_x, *J. Geophys. Res.*, 106(D9), 9991–10001, 2001b.
- Bey, I., Jacob, D. J., Yantosca, R. M., Logan, J. A., Field, B. D., Fiore, A. M., Li, Q. B., Liu, H. G. Y., Mickley, L. J., and Schultz, M. G.: Global modeling of tropospheric chemistry with assimilated meteorology: Model description and evaluation, *J. Geophys. Res.*, 106(D19), 23 073–23 095, 2001c.
- Biggs, P., Canosa-Mas, C. E., Fracheboud, J. M., Shallcross, D. E., and Wayne, R. P.: Investigation into the kinetics and mechanisms of the reaction of NO₃ with CH₃ and CH₃O at 298K between 0.6 Torr and 8.5 Torr – is there a chain decomposition mechanism in operation, *J. Chem. Soc., Faraday Trans.*, 90, 1197–1204, 1994.
- Brown, S. S., Ryerson, T. B., Wollny, A. G., Brock, C. A., Peltier, R., Sullivan, A. P., Weber, R. J., Dube, W. P., Trainer, M., Meagher, J. F., Fehsenfeld, F. C., and Ravishankara, A. R.: Variability in nocturnal nitrogen oxide processing and its role in regional air quality, *Science*, 311, 5757, 67–70, 2006.
- Canosa-Mas, C. E., Flugge, M. L., King, M. D., and Wayne, R. P.: An experimental study of the gas-phase reaction of the NO₃ radical with α s β unsaturated carbonyl compounds, *Phys. Chem. Chem. Phys.*, 7, 643–650, 2005.
- Canosa-Mas, C. E., King, M. D., Lopez, R., Percival, C. J., Wayne, R. P., Shallcross, D. E., Pyle, J. A., and Daele, V.: Is the reaction CH₃C(O)O₂ and NO₃ important in the night-time troposphere? *J. Chem. Soc., Faraday Trans.*, 92, 2211–2222, 1996.
- Carshaw, N., Carpenter, L. J., Plane, J. M. C., Allan, B. J., Burgess, R. A., Clemitshaw, K. C., Coe, H., and Penkett, S. A.: Simultaneous measurements of nitrate and peroxy radicals in the marine boundary layer, *J. Geophys. Res.*, 102, 18 917–18 933, 1997.
- Carter, W. P. L. and Atkinson, R.: Development and evaluation of a detailed mechanism for the atmospheric reactions of isoprene and NO_x, *Int. J. Chem. Kinet.*, 28, 497–530, 1996.
- Claeys, M., Graham, B., Vas, G., Wang, W., Vermeylen, R., Pashynska, V., Cafmeyer, J., Guyon, P., Andreae, M. O., Artaxo, P., and Maenhaut, W.: Formation of secondary organic aerosols through photooxidation of isoprene, *Science*, 303, 1173–1176, 2004.
- Cocker III, D. R., Flagan, R. C., and Seinfeld, J. H.: State-of-the-art chamber facility for studying atmospheric aerosol chemistry, *Environ. Sci. Technol.*, 35, 2594–2601, 2001.
- Crouse, J. D., McKinney, K. A., Kwan, A. J., and Wennberg, P. O.: Measurements of gas-phase hydroperoxides by chemical ionization mass spectrometry, *Anal. Chem.*, 78, 6726–6732, 2006.
- Curren, K., Gillespie, T., Steyn, D., Dann, T., and Wang, D.: Biogenic isoprene in the Lower Fraser Valley, British Columbia, *J. Geophys. Res.*, 103, D19, 25467–25477, 1998.
- Daele, V., Laverdet, G., Lebras, G., and Poulet, G.: Kinetics of the reactions of CH₃O+NO, CH₃O+NO₃, and CH₃O₂+NO₃, *J. Phys. Chem.*, 99, 1470–1477, 1995.
- Davidson, J. A., Viggiano, A. A., Howard, C. J., Fehsenfeld, F. C., Albritton, D. L., and Ferguson, E. E.: Rate constants for the reaction of O₂⁺, NO₂⁺, NO⁺, H₃O⁺, CO₃⁻, NO₂⁻, and halide ions with N₂O₅ at 300 K, *J. Chem. Phys.*, 68, 2085–2087, 1978.
- Dibble, T. S.: Isomerization of OH-isoprene adducts and hydroxylalkoxy isoprene radicals, *J. Phys. Chem.*, 106(28), 6643–6650, 2002.
- Dibbe T. S.: Failures and limitations of quantum chemistry for two key problems in the atmospheric chemistry of peroxy radicals, *Atmos. Environ.*, in press, 2008.
- Docherty, K., Wu, W., Lim, Y., and Ziemann, P.: Contributions of Organic Peroxides to Secondary Aerosol Formed from Reactions of Monoterpenes with O₃, *Environ. Sci. Technol.*, 39, 4049–4059, 2005.
- Dommen, J., Metzger, A., Duplissy, J., Kalberer, M., Alfarra, M. R., Gascho, A., Weingartner, E., Prevot, A. S. H., Verheggen, B., and Baltensperger, U.: Laboratory observation of oligomers in the aerosol from isoprene/NO_x photooxidation, *Geophys. Res. Lett.*, 33, L13805, doi:10.1029/2006GL026523, 2006.
- Edney, E. O., Kleindienst, T. E., Jaoui, M., Lewandowski, M., Offenberg, J. H., Wang, W., and Claeys, M.: Formation of 2-methyl tetrols and 2-methylglyceric acid in secondary organic aerosol from laboratory irradiated isoprene/NO_x/SO₂/air mixtures and their detection in ambient PM_{2.5} samples collected in the eastern United States, *Atmos. Environ.*, 39, 5281–5289, 2005.
- Fan, J. and Zhang, R.: Atmospheric oxidation mechanism of isoprene, *Environ. Chem.*, 1, 140–149, doi:10.1071/EN04045, 2004.
- Fuentes, J. D., Wang, D., Rowling, D. R., Potosnak, M., Monson, R. K., Goliff, W. S., and Stockwell, W. R.: Biogenic hydrocarbon chemistry within and above a mixed deciduous forest, *J. Atmos. Chem.*, 56, 165–185, 2007.
- Gao, S., Keywood, M. D., Ng, N. L., Surratt, J. D., Varutbangkul, V., Bahreini, R., Flagan, R. C., and Seinfeld, J. H.: Low molecular weight and oligomeric components in secondary organic aerosol from the ozonolysis of cycloalkenes and α -pinene, *J. Phys. Chem. A*, 108, 10 147–10 164, 2004a.
- Gao, S., Ng, N. L., Keywood, M. D., Varutbangkul, V., Bahreini, R., Nenes, A., He, J., Yoo, K. Y., Beauchamp, J. L., Hodyss, R. P., Flagan, R. C., and Seinfeld, J. H.: Particle phase acidity and oligomer formation in secondary organic aerosol, *Environ. Sci. Technol.*, 38, 6582–6589, 2004b.
- Gao, S., Surratt, J. D., Knipping, E. M., Edgerton, E. S., Shahgholi, M., and Seinfeld, J. H.: Characterization of polar organic com-

- ponents in fine aerosols in the southeastern United States: Identity, origin, and evolution, *J. Geophys. Res.*, 111, D14314, doi:10.1029/2005JD006601, 2006.
- Ghigo, G., Maranzana, A., and Tonachini, G.: Combustion and atmospheric oxidation of hydrocarbons: Theoretical study of the methyl peroxy self-reaction, *J. Chem. Phys.*, 118, 23, 2003.
- Goldstein, A. H. and Galbally, I. E.: Known and unexplored organic constituents in the earth's atmosphere, *Environ. Sci. Technol.*, 41, 1514–1521, 2007.
- Gong, H., Matsunaga, A., and Ziemann, P.: Products and mechanism of secondary organic aerosol formation from reactions of linear alkenes with NO₃ radicals, *J. Phys. Chem.*, 109, 4312–4324, 2005.
- Gómez-González, Y., Surratt, J. D., Cuyckens, F., Szmigielski, R., Vermeylen, R., Jaoui, M., Lewandowski, M., Offenberg, J. H., Kleindienst, T. E., Edney, E. O., Blockhuys, F., Van Alsenoy, C., Maenhaut, W. and Claeys, M.: Characterization of organosulfates from the photooxidation of isoprene and unsaturated fatty acids in ambient aerosol using liquid chromatography/(–) electrospray ionization mass spectrometry, *J. Mass Spectrom.*, 43(3), 371–382, doi:10.1002/jms.1329, 2007.
- Guenther, A., Hewitt, C. N., Erickson, D., Fall, R., Geron, C., Graedel, T., Harley, P., Klinger, L., Lerdau, M., McKay, W. A., Pierce, T., Scholes, B., Steinbrecher, R., Tallamraju, R., Taylor, J., and Zimmerman, P.: A global-model of natural volatile organic compound emissions, *J. Geophys. Res.*, 100(D5), 8873–8892, 1995.
- Guenther, A., Karl, T., Harley, P., Wiedinmyer, C., Palmer, P. I., and Geron, C.: Estimates of global terrestrial isoprene emissions using MEGAN (Model of Emissions of Gases and Aerosols from Nature), *Atmos. Chem. Phys.*, 6, 3181–3210, 2006, <http://www.atmos-chem-phys.net/6/3181/2006/>.
- Heintz, F., Platt, U., Flentje, H., and Dubois, R.: Long-term observation of nitrate radicals at the tor station, Kap Arkona (Rugen), *J. Geophys. Res.*, 101(D17), 22 891–22 910, 1996.
- Henze, D. K., Seinfeld, J. H., Ng, N. L., Kroll, J. H., Fu, T.-M., Jacob, D. J., and Heald, C. L.: Global modeling of secondary organic aerosol formation from aromatic hydrocarbons: high- vs. low-yield pathways, *Atmos. Chem. Phys.*, 8, 2405–2420, 2008, <http://www.atmos-chem-phys.net/8/2405/2008/>.
- Horowitz, L. W., Fiore, A. M., Milly, G. P., Cohen, R. C., Perring, A., Wooldridge, P. J., Hess, P. G., Emmons, L. K., and Lamarque, J.: Observational constraints on the chemistry of isoprene nitrates over the eastern United States, *J. Geophys. Res.*, 112, D12S08, doi:10.1029/2006JD007747, 2007.
- Inuma, Y., Müller, C., Berndt, T., Böge, O., Claeys, M., and Herrmann, H.: Evidence for the existence of organosulfates from β -pinene ozonolysis in ambient secondary organic aerosol, *Environ. Sci. Technol.*, 41, 6678–6683, 2007b.
- Inuma, Y., Müller, C., Böge, O., Gnauk, T., and Herrmann, H.: The formation of organic sulfate esters in the limonene ozonolysis secondary organic aerosol (SOA) under acidic conditions, *Atmos. Environ.*, 41, 5571–5583, 2007a.
- Jay, K. and Stieglitz, L.: The gas phase addition of NO_x to olefins, *Chemosphere*, 19, 1939–1950, 1989.
- Jayne, J. T., Leard, D. C., Zhang, X., Davidovits, P., Smith, K. A., Kolb, C. E., and Worsnop, D. W.: Development of an Aerosol Mass Spectrometer for size and composition analysis of submicron particles, *Aerosol Sci. Technol.*, 33, 49–70, 2000.
- Kan, C. S., Calvert, J. G., and Shaw, J. H.: Reactive channels of the CH₃O₂-CH₃O₂ reaction, *J. Phys. Chem.*, 84, 3411–3417, 1980.
- Kanakidou, M., Seinfeld, J. H., Pandis, S. N., Barnes, I., Dentener, F. J., Facchini, M. C., Van Dingenen, R., Ervens, B., Nenes, A., Nielsen, C. J., Swietlicki, E., Putaud, J. P., Balkanski, Y., Fuzzi, S., Horth, J., Moortgat, G. K., Winterhalter, R., Myhre, C. E. L., Tsigaridis, K., Vignati, E., Stephanou, E. G., and Wilson, J.: Organic aerosol and global climate modelling: a review, *Atmos. Chem. Phys.*, 5, 1053–1123, 2005, <http://www.atmos-chem-phys.net/5/1053/2005/>.
- Keywood, M. D., Varutbangkul, V., Bahreini, R., Flagan, R. C., and Seinfeld, J. H.: Secondary organic aerosol formation from the ozonolysis of cycloalkenes and related compounds, *Environ. Sci. Technol.*, 38, 4157–4164, 2004.
- Kirchner, F. and Stockwell, W. R.: Effect of peroxy radical reactions on the predicted concentrations of ozone, nitrogenous compounds, and radicals, *J. Geophys. Res.*, 101(D15), 21 007–21 022, 1996.
- Knopf, D. A., Mak, J., Gross, S., and Bertram, A. K.: Does atmospheric processing of saturated hydrocarbon surfaces by NO₃ lead to volatilization?, *Geophys. Res. Lett.*, 33, L17816, doi:10.1029/2006GL026884, 2006.
- Kroll, J. H., Ng, N. L., Murphy, S. M., Flagan, R. C., and Seinfeld, J. H.: Secondary organic aerosol formation from isoprene photooxidation under high-NO_x conditions, *J. Geophys. Res.*, 32, L18808, doi:10.1029/2005GL023637, 2005.
- Kroll, J. H., Ng, N. L., Murphy, S. M., Flagan, R. C., and Seinfeld, J. H.: Secondary organic aerosol formation from isoprene photooxidation, *Environ. Sci. Technol.*, 40, 1869–1877, 2006.
- Kwok, E. S. C., Aschmann, S. M., Arey, J., and Atkinson, R.: Product formation from the reaction of the NO₃ radical with isoprene and rate constants for the reactions of methacrolein and methyl vinyl ketone with the NO₃ radical, *Inter. J. Chem. Kinet.* 28, 925–934, 1996.
- Liggio, J. and Li, S. M.: Organosulfate formation during the uptake of pinonaldehyde on acidic sulfate aerosols, *Geophys. Res. Lett.*, 33, L13808, doi:10.1029/2006GL026079, 2006.
- Liggio, J., Li, S. M., and McLaren, R.: Heterogeneous reactions of glyoxal on particulate matter: Identification of acetals and sulfate esters, *Environ. Sci. Technol.*, 39, 1532–1541, 2005.
- Lightfoot, P. D., Cox, R. A., Crowley, J. N., Destriau, M. Hayman, G. D., Jenkin, M. E., Moortgat G. K., and Zabel, F.: Organic peroxy radicals – kinetics, spectroscopy and tropospheric chemistry, *Atmos. Environ.*, 26, 1805–1961, 1992.
- Moise, T., Talukdar, R. K., Frost, G. J., Fox, R. W., and Rudich, Y.: Reactive uptake of NO₃ by liquid and frozen organics, *J. Geophys. Res.*, 107(D2), 4014, doi:10.1029/2001JD000334, 2002.
- Ng, N. L., Chhabra, P. S., Chan, A. W. H., Surratt, J. D., Kroll, J. H., Kwan, A. J., McCabe, D. C., Wennberg, P. O., Sorooshian, A., Murphy, S. M., Dalleska, N. F., Flagan, R. C., and Seinfeld, J. H.: Effect of NO_x level on secondary organic aerosol (SOA) formation from the photooxidation of terpenes, *Atmos. Chem. Phys.*, 7, 5159–5174, 2007a, <http://www.atmos-chem-phys.net/7/5159/2007/>.
- Ng, N. L., Kroll, J. H., Chan, A. W. H., Chhabra, P. S., Flagan, R. C., and Seinfeld, J. H.: Secondary organic aerosol formation from *m*-xylene, toluene, and benzene, *Atmos. Chem. Phys.*, 7, 3909–3922, 2007b, <http://www.atmos-chem-phys.net/7/3909/2007/>.

- Ng, N. L., Kroll, J. H., Keywood, M. D., Bahreini, R., Varutbangkul, V., Flagan, R. C., Seinfeld, J. H., Lee, A., and Goldstein, A. H.: Contribution of first- versus second-generation products to secondary organic aerosols formed in the oxidation of biogenic hydrocarbons, *Environ. Sci. Technol.*, 40, 2283–2297, 2006.
- Niki, H., Maker, P. D., Savage, C. M., and Breitenbach L.P.: Fourier Transform Infrared studies of the self-reaction of CH₃O₂ radicals, *J. Phys. Chem.*, 85, 877–881, 1981.
- Niki, H., Maker, P. D., Savage, C. M., and Breitenbach L.P.: Fourier Transform Infrared studies of the self-reaction of C₂H₅O₂ radicals, *J. Phys. Chem.*, 86, 3825–3829, 1982.
- Noda, J., Nyman, G., and Langer S.: Kinetics of the gas-phase reaction of some unsaturated alcohols with the nitrate radical, *J. Phys. Chem.*, 106, 945–951, 2002.
- Odum, J. R., Hoffmann, T., Bowman, F., Collins, D., R. C. Flagan, R. C., and Seinfeld, J. H.: Gas/particle partitioning and secondary organic aerosol yields, *Environ. Sci. Technol.*, 30, 2580–2585, 1996.
- Odum, J. R., Jungkamp, T. P. W., Griffin, R. J., Flagan, R. C., and Seinfeld, J. H.: The atmospheric aerosol-forming potential of whole gasoline vapor, *Science*, 276, 96–99, 1997a.
- Odum, J. R., Jungkamp, T. P. W., Griffin, R. J., Forstner, H. J. L., Flagan, R. C., and Seinfeld, J. H.: Aromatics, reformulated gasoline and atmospheric organic aerosol formation, *Environ. Sci. Technol.*, 31, 1890–1897, 1997b.
- Paulot, F., Crouse, J. D., Kjaergaard, H. G., Kroll, J. H., Seinfeld, J. H., and Wennberg, P. O.: Isoprene photooxidation mechanism: resonance channels and implications for the production of nitrates and acids, accepted, *Atmos. Chem. Phys. Discuss.*, 2008.
- Paulson, S. E. and Seinfeld, J. H.: Development and evaluation of a photooxidation mechanism for isoprene, *J. Geophys. Res.*, 97(D18), 20 703–20 715, 1992.
- Penkett, S. A., Burgess, R. A., Coe, H., Coll, I., Hov, Ø., Lindskog, A., Schmidbauer, N., Solberg, S., Roemer, M., Thijssse, T., Beck, J., and Reeves C. E.: Evidence for large average concentrations of the nitrate radical (NO₃) in Western Europe from the HANSA hydrocarbon database, *Atmos. Environ.*, 41, 3465–3478, 2007.
- Platt, U. and Janssen, C.: Observation and role of the free radicals NO₃, ClO, BrO and IO in the troposphere, *Faraday Discuss.*, 100, 175–198, 1995.
- Platt, U., Perner, D., Schroder, J., Kessler, C., and Toennissen, A.: The diurnal variation of NO₃, *J. Geophys. Res.*, 86, 11 965–11 970, 1981.
- Rudich, Y., Donahue, N. M., and Mentel, T. F.: Aging of organic aerosol: Bridging the gap between laboratory and field studies, *Annu. Rev. Phys. Chem.*, 58, 321–352, 2007.
- Sharkey, T. D., Singsaas, E. L., Vanderveer, P. J., and Geron, C.: Field measurements of isoprene emission from trees in response to temperature and light, *Tree Physiol.*, 16, 649–654, 1996.
- Skov, H., Benter, Th., Schindler, R. N., Hjorth, J., and Restelli, G.: Epoxide formation in the reactions of the nitrate radical with 2,3-dimethyl-2-butene, cis- and trans-2-butene and isoprene, *Atmos. Environ.*, 28, 1583–1592, 1994.
- Skov, H., Hjorth, J., Lohse, C., Jensen, N. R. and Restelli, G.: Products and mechanisms of the reactions of the nitrate radical (NO₃) with isoprene, 1,3-butadiene and 2,3-dimethyl-1,3-butadiene in air, *Atmos. Environ.*, 26A(15), 2771–2783, 1992.
- Smith, N., Plane, J. M. C., Nien, C. F., and Solomon, P. A.: Night-time radical chemistry in the San-Joaquin Valley, *Atmos. Environ.*, 29, 2887–2897, 1995.
- Sorooshian, A., Brechtel F. J., Ma, Y. L., Weber R. J., Corless, A., Flagan, R. C., and Seinfeld, J. H.: Modeling and characterization of a particle-into-liquid sampler (PILS), *Aerosol Sci. Technol.*, 40, 396–409, 2006.
- Starn, T. K., Shepson, P. B., Bertman, S. B., Riemer, D. D., Zika, R. G. and Olszyna, K.: Nighttime isoprene chemistry at an urban-impacted forest site, *J. Geophys. Res.*, 103(D17), 22 437–22 447, 1998.
- Steinbacher, M., Dommen, J., Ordenez, C., Reimann, S., Gruebler, F. C., Staehelin, J., Andreani-Aksoyoglu, S., and Prevot, A. S. H.: Volatile organic compounds in the Po Basin. Part B: Biogenic VOCs, *J. Atmos. Chem.*, 51, 293–315, 2005.
- Stroud, C. A., Roberts, J. M., Williams E. J., Hereid, D., Angevine, W. M., Fehsenfeld, F. C., Wisthaler, A., Hansel, A., Martinez-Harder, M., Harder, H., Brune, W. H., Hoenninger, G., Stutz, J., and White, A. B.: Nighttime isoprene trends at an urban forested site during the 1999 Southern Oxidant Study, *J. Geophys. Res.*, 107(D16), 4291, doi:10.1029/2001JD000959, 2002.
- Su, T. and Chesnavich, W. J.: Parametrization of the ion-polar molecule collision rate constant by trajectory calculations, *The Journal of Chemical Physics*, 76, 5183, 1982.
- Suh, I., Lei, W., and Zhang, R.: Experimental and theoretical studies of isoprene reaction with NO₃, *J. Phys. Chem.*, 105, 6471–6478, 2001.
- Surratt, J. D., Kroll, J. H., Kleindienst, T. E., Edney, E. O., Claeys, M., Sorooshian, A., Ng, N. L., Offenberg, J. H., Lewandowski, M., Jaoui, M., Flagan, R. C., and Seinfeld, J. H.: Evidence for organosulfates in secondary organic aerosol, *Environ. Sci. Technol.*, 41, 517–527, 2007a.
- Surratt, J. D., Lewandowski, M., Offenberg, J. H., Jaoui, M., Kleindienst, T. E., Edney, E. O., and Seinfeld, J. H.: Effect of acidity on secondary organic aerosol formation from isoprene, *Environ. Sci. Technol.*, 41, 5363–5369, 2007b.
- Surratt, J. D., Murphy, S. M., Kroll, J. H., Ng, N. L., Hildebrandt, L., Sorooshian, A., Szmigielski, R., Vermeylen, R., Maenhaut, W., Claeys, M., Flagan, R. C., and Seinfeld, J. H.: Chemical composition of secondary organic aerosol formed from the photooxidation of isoprene, *J. Phys. Chem. A*, 110, 9665–9690, 2006.
- Szmigielski, R., Surratt, J. D., Vermeylen, R., Szmigielska, K., Kroll, J. H., Ng, N. L., Murphy, S. M., Sorooshian, A., Seinfeld, J. H., and Claeys, M.: Characterization of 2-methylglyceric acid oligomers in secondary organic aerosol formed from the photooxidation of isoprene using trimethylsilylation and gas chromatography/ion trap mass spectrometry, *J. Mass Spectrom.*, 42, 101–116, 2007.
- Tyndall, G. S., Cox, R. A., Granier, C., Lesclaux, R., Moortgat, G. K., Pilling, M. J., Ravishankara, A. R., and Wallington, T. J.: Atmospheric chemistry of small peroxy radicals, *J. Geophys. Res.*, 106(D11), 12 157–12 182, 2001.
- Tyndall, G. S., Wallington, T. J., and Ball, J. C.: FTIR product study of the reactions of CH₃O₂+CH₃O₂ and CH₃O₂+O₃, *J. Phys. Chem.*, 102, 2547–2554, 1998.
- Vaughan, S. Canosa-Mas, C. E., Pfrang, C., Shallcross, D. E., Watson, L., and Wayne, R. P.: Kinetic studies of reactions of the nitrate radical (NO₃) with peroxy radicals (RO₂): an indirect

4140

- source of OH at night? *Phys. Chem. Chem. Phys.*, 8, 3749–3760, 2006.
- von Friedeburg, C., Wagner, T., Geyer, A., Kaiser, N., Platt, U., Vogel, B. and Vogel, H.: Derivation of tropospheric NO₃ profiles using off-axis differential optical absorption spectroscopy measurements during sunrise and comparison with simulations, *J. Geophys. Res.*, 107(D13), 4168, doi:10.1029/2001JD000481, 2002.
- Wallington, T. J., Dagaut, P., and Kurylo, M. J.: Ultraviolet absorption cross-sections and reaction kinetics and mechanisms for peroxy radicals in the gas phase, *Chem. Rev.*, 92, 667–710, 1992.
- Wallington, T. J., Gierczak, C. A., Ball, J. C., and Japar, S. M.: Fourier Transform Infrared studies of the self-reaction of C₂H₅O₂ radicals in air at 295 K, *Int. J. Chem. Kinet.*, 21, 1077–1089, 1989.
- N. L. Ng et al.: SOA formation from isoprene-NO₃ reaction
- Werner, G., Kastler, J., Looser, R., and Ballschmiter, K.: Organic nitrates of isoprene as atmospheric trace compounds, *Angew. Chem. Int. Ed.*, 38(11), 1634–1637, 1999.
- Wu, S. L., Mickley, L. J., Jacob, D. J., Logan, J. A., Yantosca, R. M., and Rind, D.: Why are there large differences between models in global budgets of tropospheric ozone? *J. Geophys. Res.*, 112(D5), D05302, doi:10.1029/2006JD007801, 2007.
- Zhang, D. and Zhang, R.: Unimolecular decomposition of nitrooxyalkyl radicals from NO₃-isoprene reaction, *J. Chem. Phys.*, 116(22), 9721–9728, 2002.
- Ziemann, P.: Evidence for low-volatility diacyl peroxides as a nucleating agent and major component of aerosol formed from reactions of O₃ with cyclohexene and homologous compounds, *J. Phys. Chem.*, 106, 4390–4402, 2002.

Appendix B

Supplement to: A global perspective on aerosol from low-volatility organic compounds *

*Reproduced with permission from Supplement to “A global perspective on aerosol from low-volatility organic compounds” by H. O. T. Pye and J. H. Seinfeld, *Atmospheric Chemistry and Physics*, 10, 4377-4401.

SUPPLEMENT TO: A GLOBAL PERSPECTIVE ON AEROSOL FROM LOW VOLATILITY COMPONENTS

H. O. T. PYE AND J. H. SEINFELD
CALIFORNIA INSTITUTE OF TECHNOLOGY

Figure S1: Traditional simulation organic aerosol concentration and change in total OA from traditional to revised simulation. Total OA includes POA and all forms of SOA. Level 1 is closest to the surface. Level 7 is approximately 4 km in altitude and 600 hPa at the center. Note that the color bars use different scales. Simulated concentrations for the present day traditional simulation show the maximum seasonally averaged concentration in the lower right corner of each panel. Simulations use GEOS-4 meteorology at $2^\circ \times 2.5^\circ$ for year 2000. See Section 3.1 of main manuscript for discussion.

Figure S2: June-July-August 2000 surface total OC concentration relative to traditional (non-volatile POA) simulation using GISS meteorology at $4^\circ \times 5^\circ$ horizontal resolution. Tests are outlined in Table 6 (main manuscript).

Figure S3: December-January-February 2001 surface total OC concentration relative to traditional (non-volatile POA) simulation. OC includes POA and all forms of SOA. Sensitivity simulations are outlined in Table 6 (main manuscript). Simulations use year 2001 meteorology from the GISS GCM III at $4^\circ \times 5^\circ$ resolution. Figure S.2 is the same as Figure 8 in the main manuscript with the only exception being that Figure S3 uses year 2001 and Figure 8 uses year 2000.

Figure S4: December-January-February 2000 surface total OC concentration relative to traditional (non-volatile POA) simulation using GEOS-4 meteorology at $2^\circ \times 2.5^\circ$ horizontal resolution. Tests are outlined in Table 6 (main manuscript). Panel (a) shows the difference between the traditional simulation and the revised simulation. Panel (b) shows the difference between the traditional simulation and a simulation in which POA emissions are doubled to obtain the SVOC emissions (compare to panel (c) of Figure 8 in the main manuscript).

Date: May 5, 2010.

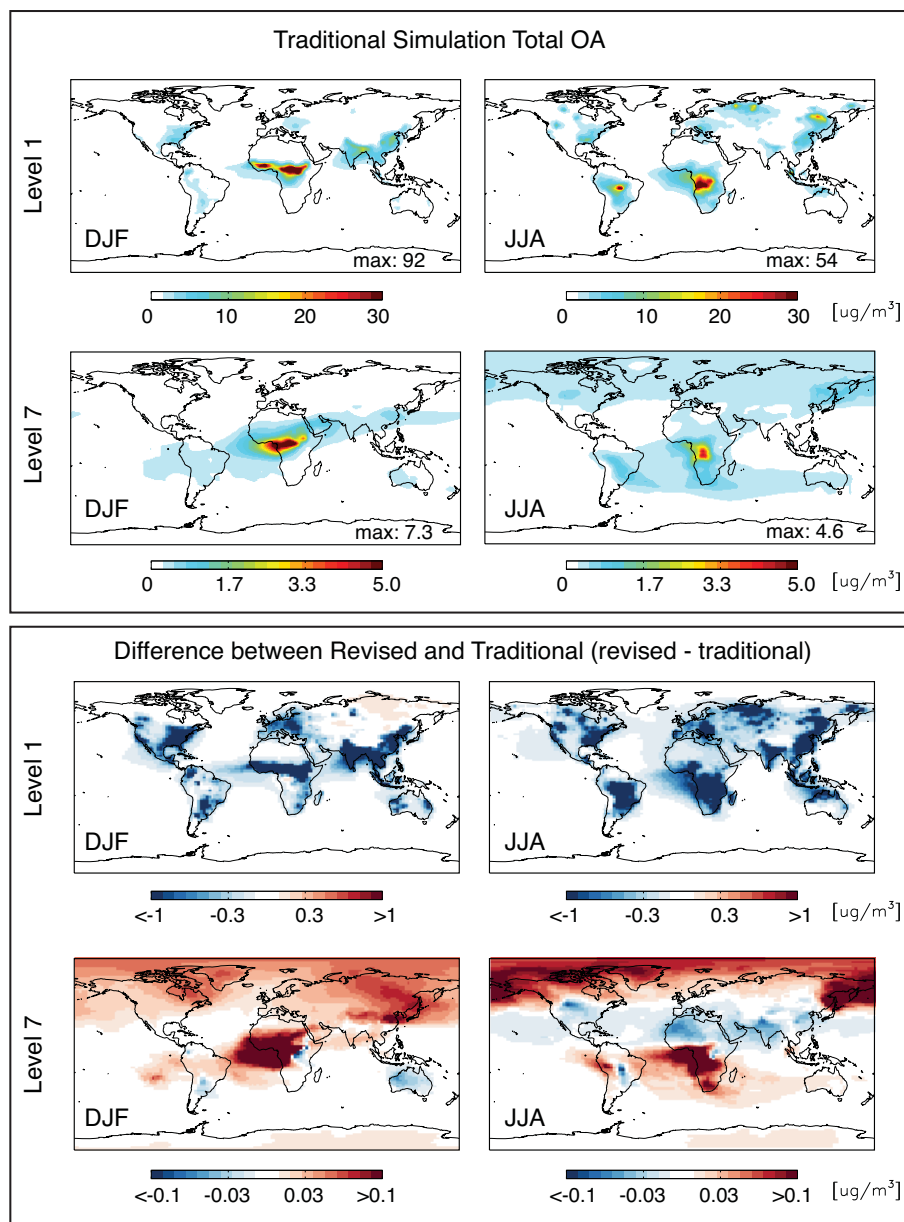


FIGURE S1. Traditional simulation organic aerosol concentration and change in total OA from traditional to revised simulation. Total OA includes POA and all forms of SOA. Level 1 is closest to the surface. Level 7 is approximately 4 km in altitude and 600 hPa at the center. Note that the color bars use different scales. Simulated concentrations for the present day traditional simulation show the maximum seasonally averaged concentration in the lower right corner of each panel. Simulations use GEOS-4 meteorology at $2^\circ \times 2.5^\circ$ for year 2000. See Section 3.1 of main manuscript for discussion.

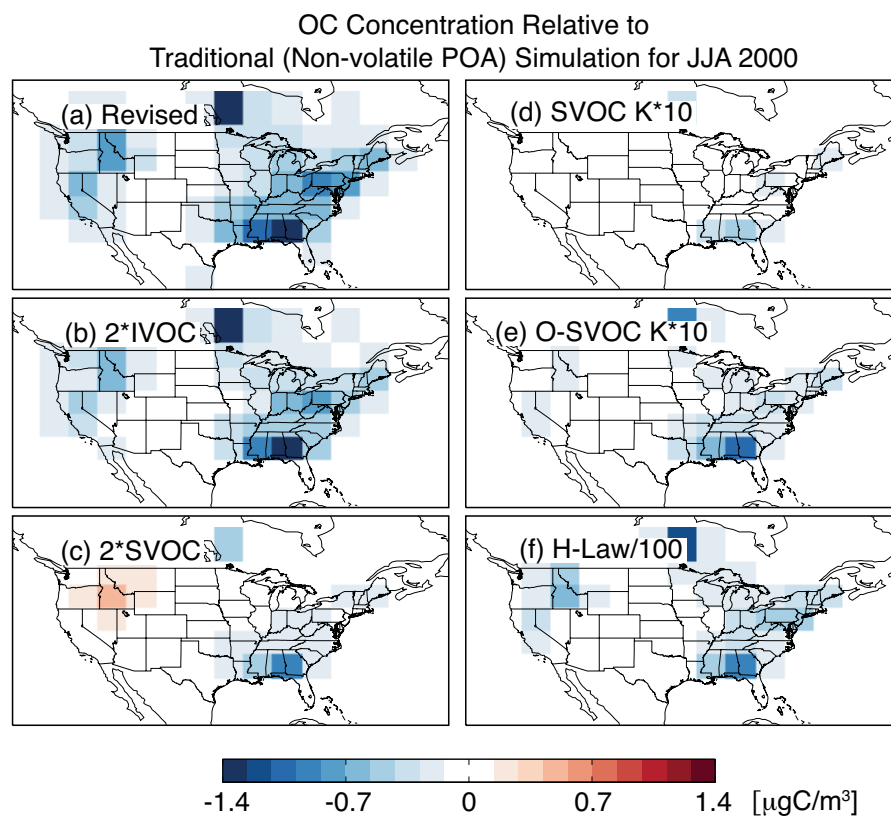


FIGURE S2. June-July-August 2000 surface total OC concentration relative to traditional (non-volatile POA) simulation using GISS meteorology at $4^\circ \times 5^\circ$ horizontal resolution. Tests are outlined in Table 6 (main manuscript).

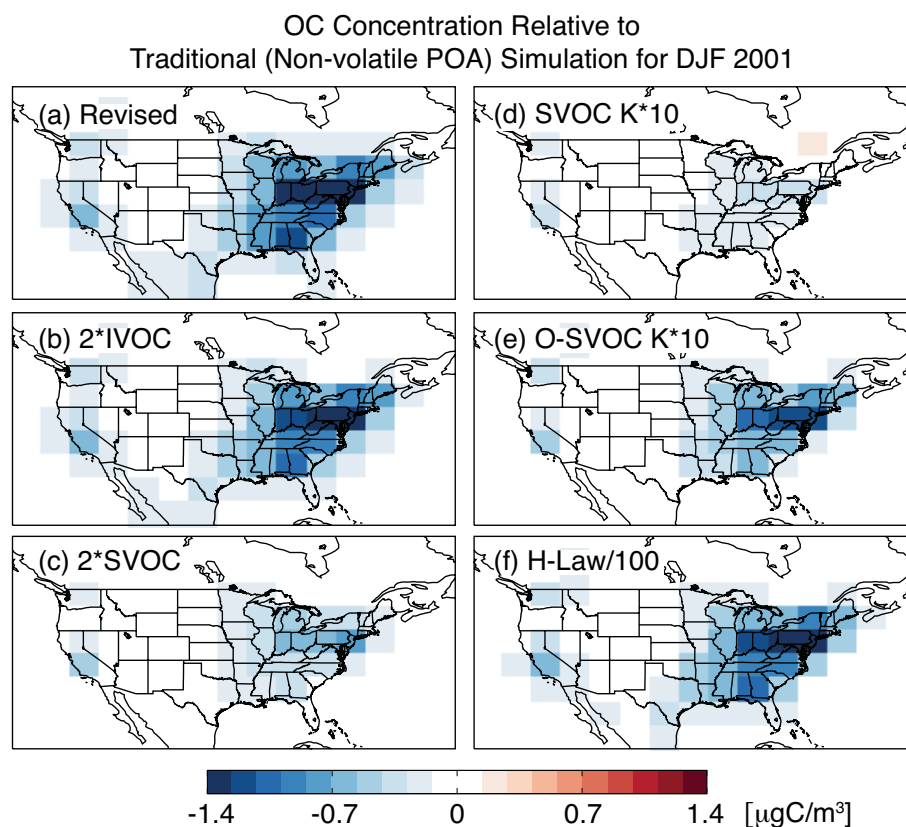


FIGURE S3. December-January-February 2001 surface total OC concentration relative to traditional (non-volatile POA) simulation. OC includes POA and all forms of SOA. Sensitivity simulations are outlined in Table 6 (main manuscript). Simulations use year 2001 meteorology from the GISS GCM III at $4^\circ \times 5^\circ$ resolution. Figure S.2 is the same as Figure 8 in the main manuscript with the only exception being that Figure S.2 uses year 2001 and Figure 8 uses year 2000.

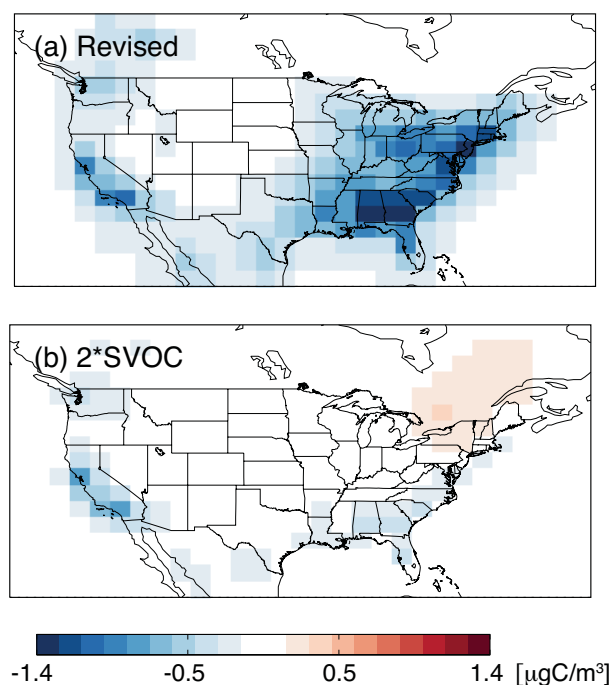
OC Concentration Relative to Traditional
(Non-volatile POA) Simulation for DJF

FIGURE S4. December-January-February 2000 surface total OC concentration relative to traditional (non-volatile POA) simulation using GEOS-4 meteorology at $2^\circ \times 2.5^\circ$ horizontal resolution. Tests are outlined in Table 6 (main manuscript). Panel (a) shows the difference between the traditional simulation and the revised simulation. Panel (b) shows the difference between the traditional simulation and a simulation in which POA emissions are doubled to obtain the SVOC emissions (compare to panel (c) of Figure 8 in the main manuscript).

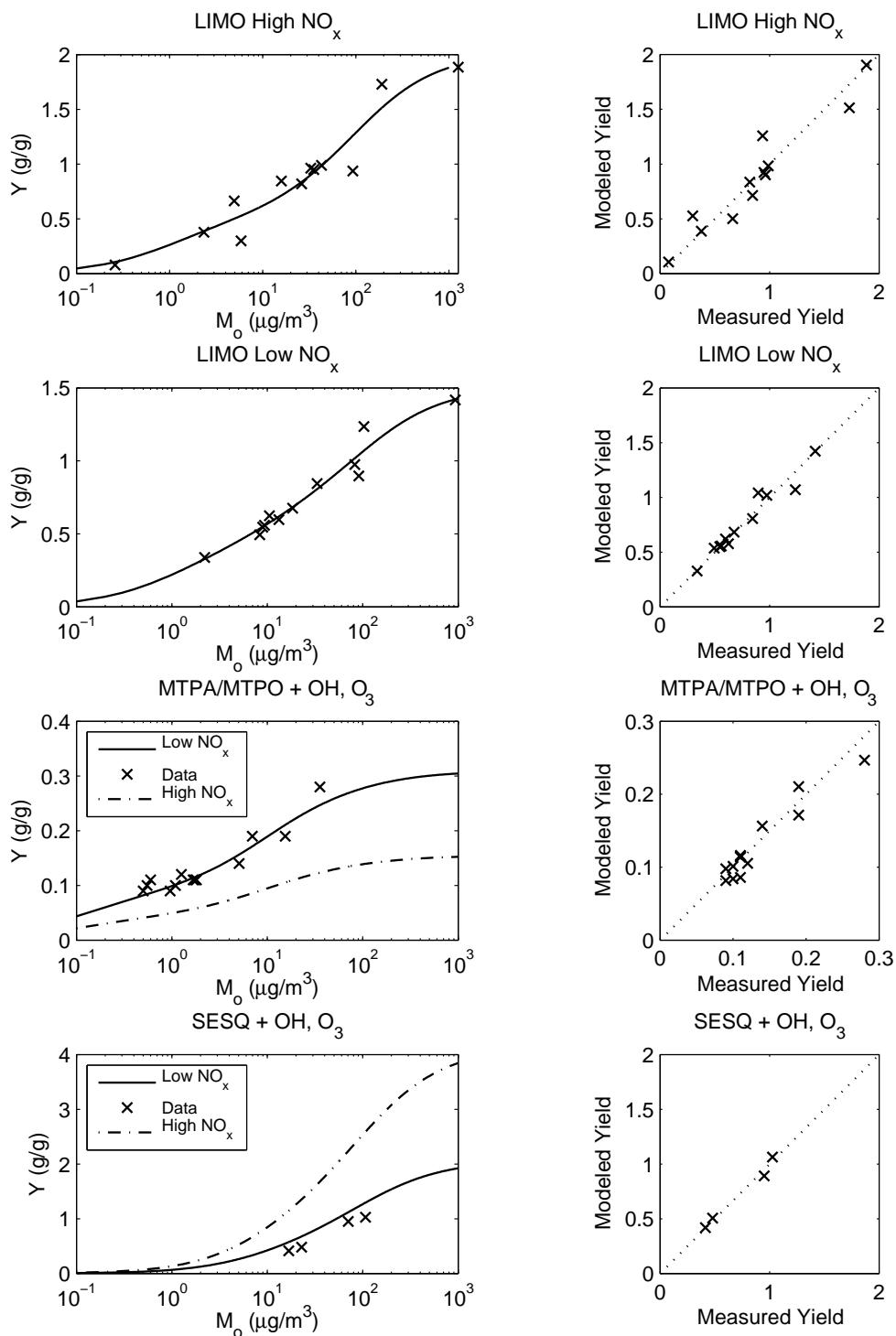
Appendix C

Supplement to: Global modeling of organic aerosol: The importance of reactive nitrogen*

*Submitted to *Atmospheric Chemistry and Physics* as a supplement to "Global modeling of organic aerosol: The importance of reactive nitrogen" by H. O. T. Pye, A. W. H. Chan, M. P. Barkley, and J. H. Seinfeld

**SUPPLEMENT TO: GLOBAL MODELING OF ORGANIC
AEROSOL: THE IMPORTANCE OF REACTIVE NITROGEN**H. O. T. PYE¹, A. W. H. CHAN¹, M. BARKLEY², AND J. H. SEINFELD¹¹Division of Chemistry and Chemical Engineering, California Institute of
Technology, Pasadena, California, USA²School of GeoSciences, University of Edinburgh, Edinburgh, Scotland, UK

The supplemental information (Fig. S1–S3) shows the chamber data and fits based on those data described in Table 1 (main manuscript). The first column shows the data plotted as yield (mass of aerosol formed divided by mass of parent hydrocarbon reacted) vs. organic aerosol loading (mass of aerosol formed in $\mu\text{g}/\text{m}^3$). Fits are shown at the reference temperature (298 K) and data are shown at the experimental temperature (usually around 298 K, but about 310 K for sesquiterpenes and β -pinene + NO_3). The right column shows the modeled yield based on the fit (corrected for temperature using an enthalpy of vaporization of 42 kJ/mol) vs. the measured yield from the chamber experiment. The dotted line is the 1:1 line.

FIGURE S1. Aerosol yields from high- and low- NO_x terpene oxidation.

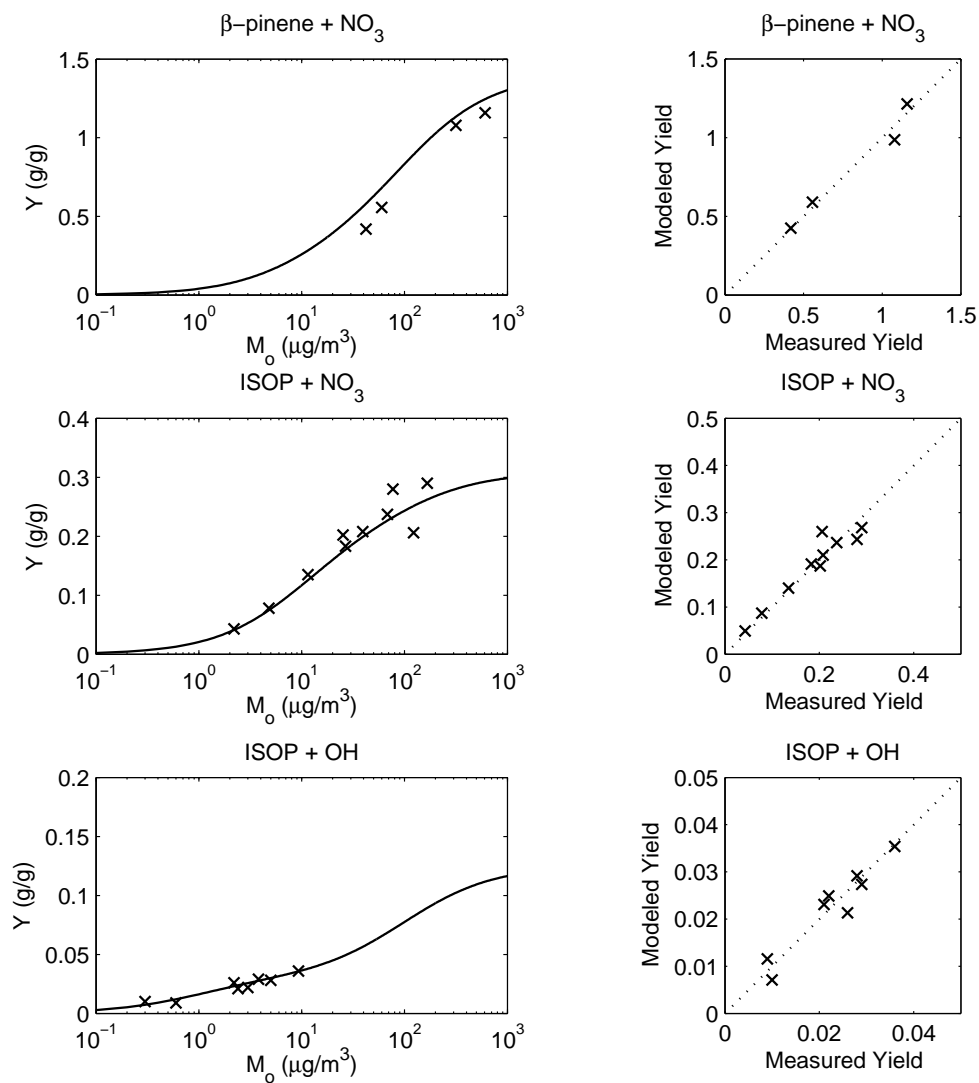


FIGURE S2. Aerosol yields from nitrate radical oxidation (of terpenes and isoprene) and isoprene photooxidation.

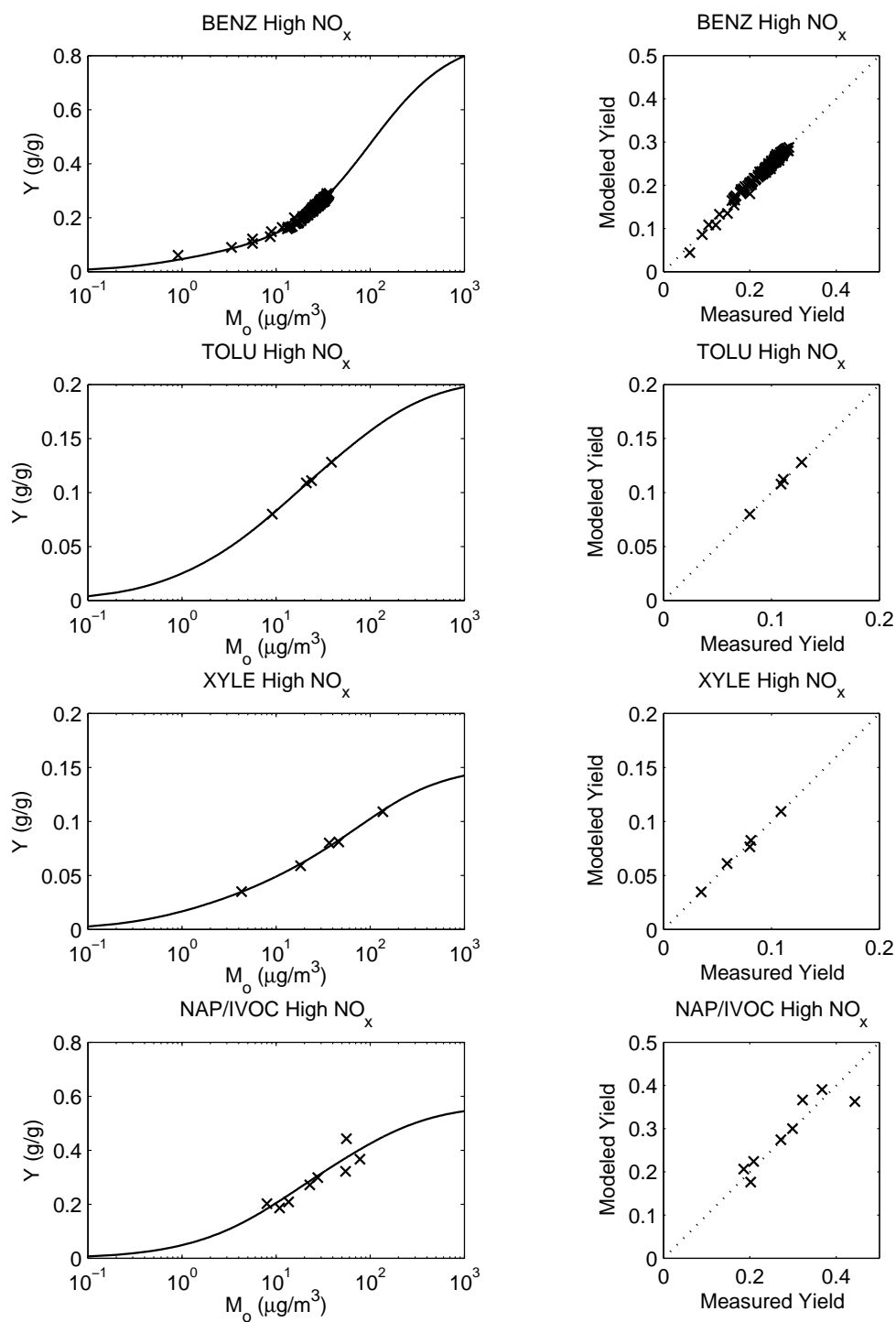


FIGURE S3. Aerosol yields from light aromatic and naphthalene high- NO_x photooxidation.